Genetics, Evolution and Environment
University College London

EXPERIMENTAL AND COMPUTATIONAL APPROACHES REVEAL MECHANISMS OF EVOLUTION OF GENE REGULATORY NETWORKS UNDERLYING ECHINODERM SKELETOGENESIS

David Viktor Dylus

Research Project submitted in partial fulfillment of the requirements for the degree of PhD in Systems Biology.

Supervisor: Dr. Paola Oliveri
Second supervisor: Dr. Eugene Schuster

London, June 2015

I, David Viktor Dylus, confirm that the work presented in this thesis is my own. Where information has been derived from other sources, I confirm that this has been indicated in the thesis.

ABSTRACT

The evolutionary mechanisms in distantly related animals involved in shaping complex gene regulatory networks (GRN) that encode morphologically similar structures remain elusive. In this context, echinoderm larval skeletons found only in brittle stars and sea urchins out of the five classes provide an ideal system. Here, we characterise for the first time the development of the larval skeleton in the poorly described class of echinoderms, the ophiuroid *Amphiura filiformis*, and we compare it systematically with the well-established sea urchin.

In the first part of this study, we show that ophiuroids and euechinoids, that split at least 480 Million years ago (Mya), have remarkable similarities in tempo and mode of skeletal development. Despite morphological and ontological similarities, our high-resolution study of the dynamics of regulatory states using 24 sea urchin candidates highlights that gene duplication, protein function diversification and cis-regulatory element evolution all contributed to shape the regulatory program for larval skeletogenesis in different branches of echinoderms. Our data allows to comment on the independent or homologous evolution of the larval skeleton in light of the recently established phylogeny of echinoderm classes.

In the second part of this study, we employ mRNA sequencing to establish a transcriptome and analyse its content quantitatively and qualitatively. We identify a core set of skeletogenic genes that is highly conserved using various comparative genomic analyses including other three classes of echinoderms. Additionally, from a differential screen on samples with inhibited skeleton we obtain a list of candidates specific for brittle star skeleton development and analyse their expression using experimental techniques. Finally, we provide access to all transcriptomic and

expression data via a customised web interface.

In conclusion, we establish the brittle star *A. filiformis* as new developmental model system and provide novel insights into evolution of GRNs.

ACKNOWLEDGMENTS

In this thesis I am summarising nearly 4 years of work in echinoderm biology. Throughout this years, I have learned so much personally and professionally that when reflecting on it, my mind seems incapable of comprehending all the things I have experienced. I am extremely grateful to CoMPLEX/UCL, to have been given the opportunity to work in science, to think without any concern of economical value about theories and enjoy the liberty of my own thoughts. On this journey I was accompanied by many people and it seem impossible for me to thank all of them in the way they would deserve to be thanked. Surely, only due to their companionship, whether relaxing after a day of struggle or exciting with an intense scientific discussion, I was able to reach this point. Nevertheless, some people have to be thanked because their contribution is directly linked to this adventure. First, I would like to thank Jack Paget and Monica Marinescu for supporting me when I first applied here in London and Ruggero Cortini and Francessco Massucci for spending a first real ”gentleman's” year with me in London. Then I would like to thank all my friends here in London that had to endure my various moods and gave support in good and bad times. Especially, I am grateful to everyone from the Roberto Mayor Lab and the Max Telford Lab throughout the years 2010 to 2015. Additionally, I am very thankful to everyone from the Kentish Town community.

Throughout my PhD, I was given the opportunity to teach several students, with whom I formed a symbiotic relationship. They helped me and I tried to support their projects in the best possible way. For this I am very thankful to Matt Pilgrim, Yan-kay Ho, Thomas Mullan, Alun Jones, Pantelis Nicola and Luisana Carballo. Moreover, at this point I would also like to thank Patrick Toolan-Kerr and Helen Robertson for valuable comments on the manuscript.

Experimental work is performed alone, but a laboratory needs team work. I am, especially, thankful to Anna Czarkwiani and Libero Petrone. We struggled, we laughed, we learned, we enjoyed and we worked together. I am more than thankful that you two were my two ”Lab-mates” throughout these years. I also would like to thank at this point Avi Lerner for struggling to teach an engineer in basic experimental techniques.

Most importantly, I would like to thank my supervisor Dr. Paola Oliveri for the patience in my first attempts in experimental biology, the addicting enthusiasm and the always open mind for questions of any kind, which allowed me to grow quickly into the exciting field of developmental biology and especially gene regulatory networks. I truly hope, that our professional and personal collaboration will never end. Furthermore, I would like to thank also Dr. Eugene Schuster who pointed me always at the right moment into the right direction helping me to never loose my aims out of sight.

Finally, I would like to thank the one person that was always there, kept me stable when I was insecure, pushed me when needed, put me back on track when I was flying and never gave up believing in me, Maria Kotini. I owe you the most for these years and there are no words that are able to express the gratitude I feel. Thank you.

David Dylus

Für meine Eltern und meinen Bruder.

CONTENTS

LIST OF FIGURES

Figure Page

LIST OF TABLES

ABBREVIATIONS

GRN	Gene regulatory network
TF	Transcription factor
CRE	*cis*-regulatory elements
ODE	Ordinary differential equation
Mya	Million years ago
SM	Skeletogenic mesoderm
DNG	Double negative gate
CNE	Conserved non-coding element
PMC	Primary mesenchyme cell
NSM	Non-skeletogenic mesoderm
IL	Interlocking loop
EMT	Epithelical to mesenchyme transition
EST	Expressed sequence tag
SW	Sea water
FSW	Filtered sea water
FASW	Filtered artificial sea water
PABA	Para Amino Benzoic Acid
PCR	Polymerase chain reaction
QPCR	Quantitative polymerase chain reaction
RACE	Rapid amplification of cDNA ends
nr	non-redundant

OMA Orthology matrix approach

WMISH Whole mount *in situ* hybridisation

HB Hybridisation buffer

FISH Fluorescent whole mount *in situ* hybridisation

hpf Hours post fertilisation

aa Amino acid

HD Homeodomain

eh1 Engrailed homology domain

ORF Open reading frame

CEG Core eukaryotic genes

ZNF Zinc finger genes

Afi *Amphiura filiformis*

Ame *Antedon mediterranea*

Spu *Strongyloncentrotus purpuratus*

Pmi *Patiria miniata*

EC Expression cluster

RIN RNA integrity number

IT Initial transcriptome

RT Reference transcriptome

CEGMA Core eukaryotic gene mapping approach

GO Gene ontology

Chapter 1

INTRODUCTION

1.1 Networks in biology

All organisms throughout the tree of life share one common feature: the genome. The genome is the sum of all genetic material of an organism and includes coding and non-coding sequences of DNA. Coding sequences are templates for mRNA transcription that themselves largely form templates for translation to proteins, which ultimately are involved in all chemical and physical activities within an organism. Proteins are the ”workhorse” of life. On the other hand, within non-coding regions are short regulatory stretches of DNA that regulate whether and how much of a gene is transcribed. Both, coding and non-coding DNA, are linked and dependent on each other. Between organisms, the number of genes and complexity of gene regulation varies (Alberts et al., 2002; Ponting et al., 2011). For example, the smallest genome of the eubacteria *Mycoplasma genitalium* contains 524 genes[1], compared with ∼20,000 genes in the human genome, up to the largest genome found to date in the loblolly pine tree *Pinus taeda* with ∼60,000 genes (Zimin et al., 2014). In addition, in a recent study a comparison of functional sequences between human and fly genomes found that a higher proportion of non-coding sequence than coding sequence is under positive selection, and that this proportion is increased with the complexity of the organism (Ponting et al., 2011). In order to understand the complexity of interactions between biological components, theoretical approaches led to the establishment of biological networks. Biological networks consist of nodes, *i.e.* genes, proteins or metabolites and linkages that describe interac-

[1] UCSC Genome Browser `http://archaea.ucsc.edu/cgi-bin/hgGateway?db=mycoGeni`

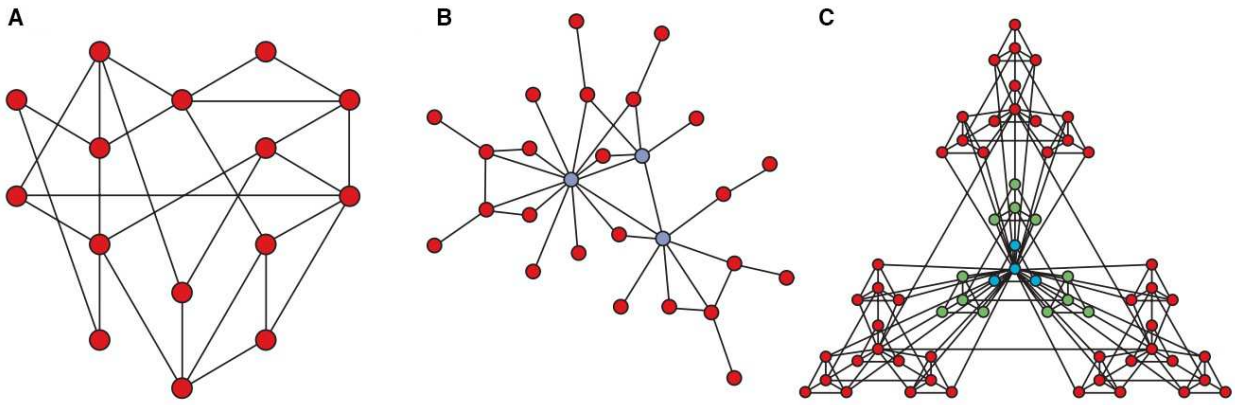

Figure 1.1: **Types of networks.** (A) Random network. (B) Scale free network showing hubs in blue. (C) Hierarchical network of different modules (triangles with different colours). Figure was taken from Barabási and Oltvai (2004).

tions between two nodes that are of physical and/or regulatory nature (addressed below in detail). These networks allow to comprehend biological processes on a systems level, and are especially important where looking just at a single component will not be sufficient to draw conclusions about the observed changes. Therefore, they are applied in development, immunity, cancer and plant biology to give some examples (reviewed in Krouk et al. (2013); Madhamshettiwar et al. (2012); Singh et al. (2014); Davidson (2011)).

1.1.1 Types of biological networks

Various types of interactions exist in biology and thus various types of networks can be modelled. Examples of these include metabolic networks describing irreversible chemical reactions (Jeong et al., 2000); protein interaction networks describing binding of protein complexes (Li et al., 2004); and genetic networks (Featherstone and Broadie, 2002) in which the nodes are individual genes and links are derived from correlations of expression data (reviewed in Barabási and Oltvai (2004)). In network theoretical terms they can all be considered as scale-free networks (Figure 1.1). ”Scale-free” means that the connectivity of each node does not follow a uniform distribution (similar number of connections on each node), but more a power-law distribution, which means that most nodes have only a few linkages and a few nodes have many linkages. In lit-

erature, nodes with many linkages are often referred to as hubs. Examples of different types of networks are shown in Figure 1.1. The only network type that does not follow a ”scale free” notion are transcription factor networks. While outgoing links show that a few transcription factors regulate most genes and many only a few (a characteristic for ”scale free”), incoming links show that most genes are regulated by one to three transcription factors (reviewed in Barabási and Oltvai (2004)). The main focus in this thesis will be on transcriptional regulatory networks which are here referred to as gene regulatory networks (GRN; see below). Interestingly, it was hypothesised that throughout evolution, new nodes are added to hubs rather than to low connected nodes (Barabasi and Albert, 1999). This was shown to be true in protein interaction networks, where gene duplications produce novel proteins with similar ancestral binding properties and thus, add novel linkages with higher probability to their previous binding partners (Pastor-Satorras et al., 2003). Additionally, this finding is consistent with cross genome comparative studies, which revealed that hubs are highly conserved throughout evolution (Eisenberg and Levanon, 2003). These results provide an explanation for the existence and maintenance of the ”scale-free” nature of biological networks throughout evolution (reviewed in Barabási and Oltvai (2004)).

In order to be able to analyse large complex networks, structural properties of different types of networks have been investigated. In a comparison of networks originating from world wide web, ecological food webs and gene interactions from yeast and bacteria, Milo et al. (2002) found that within each of these networks some sub-circuits with a few nodes are overrepresented. This discovery led to the definition of a motif (Shen-Orr et al., 2002; Alon, 2007; Davidson, 2010). A network motif is a sub-graph that occurs more frequently than would be expected at random. Importantly, the overrepresentation of different motifs within different types of networks varies. Milo et al. (2002) showed that in gene regulatory networks of yeast or bacteria, three node feed-forward loop motifs were found more often, whereas ecological food webs contained more three node chain motifs. Feed-forward loops are where one node controls another and both, the first and second node, control a third one. Three node chains are when a first node inputs to a second

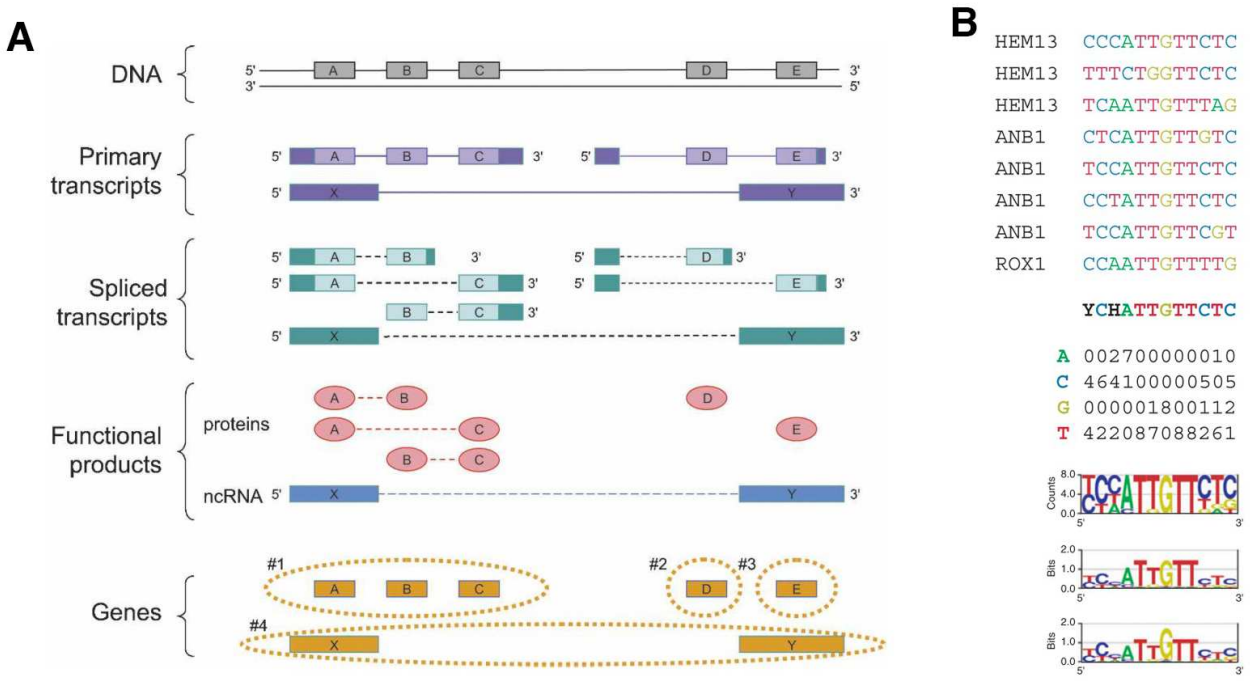

Figure 1.2: **Definition of a gene and DNA binding motif.** (A) Description of how to define a gene. Figure was taken from Gerstein et al. (2007). (B) Example of a conserved *cis*-regulatory element or DNA binding motif. Figure was taken from D'haeseleer (2006).

which inputs to a third (reviewed in Macneil and Walhout (2011)). Interestingly, while many motifs have been found to be evolutionary conserved in yeast protein interaction networks (Wuchty et al., 2003), convergent evolution was determined as the main mechanism for the formation of motifs in transcription regulatory networks (Conant and Wagner, 2003). In conclusion, biological networks offer a systems approach in understanding various biological phenomena.

1.1.2 The regulatory genome

Before starting with a clear description of GRNs in development, I need to define the individual parts of a regulatory genome. Within a genome the definition of a gene is not trivial and Pearson (2006) claimed that with the increase of genome knowledge a clear definition becomes a more and more complex task. One possible definition of a gene was given by Gerstein et al. (2007): "A gene is a union of genomic sequences encoding a coherent set of potentially overlapping functional products." This implies that a gene encodes for a protein or an RNA and that for several protein products sharing overlapping regions the union is taken for all overlaps coding for them.

Moreover, the union must be logical, which implies that it must be done separately for final protein and RNA products, thus allowing the existence of multiple genes on the same overlapping stretch of DNA (Figure 1.2 A). Importantly, regulatory regions are not included in this definition, because they can be shared between multiple genes (Gerstein et al., 2007).

What about gene content of a genome? Due to the high variation of genes throughout evolution it is better to think about gene content in terms of gene families. These are sets of several genes with similar biochemical functions that are formed by the duplication of a single original gene. Recently published work on three spiralian genomes revealed that the common ancestor of all bilatarians likely contained at least 8,756 gene families and that through subsequent gene duplication within bilatarians these families conservatively account for 47 to 85% of genes in extant organisms (70% of human genes) (Simakov et al., 2013). Interestingly, humans retain 7,553 of these gene families and evolved 2,796 new ones (Demuth et al., 2006). A well-studied example for this is the C2H2 family of zinc finger genes. A comparative study of *Drosophila melanogaster*, *Caenorhabditis elegans*, and humans revealed that at least one gene of each C2H2 subfamily was present in all of them. However, differences were observable within each subfamily (variations in paralogous number) (Knight and Shimeld, 2001). Moreover, the conservation of these subclasses was recently expanded to include all eukaryotes (Seetharam and Stuart, 2013). Other examples of conserved gene families are Ets and Forkhead transcription factors (Wang and Zhang, 2008; Carlsson and Mahlapuu, 2002) and Fgf signalling molecules (Oulion et al., 2012). Due to the high level of conservation of gene families across the Bilataria, Erwin and Davidson (2002) postulated that bilaterians share a similar regulatory ”toolkit”, which was found to be particularly true for genes participating in development (Carroll, 2008). As a consequence, the individual differences in expansion and reduction of genes within one family were associated with being responsible for the differences in body plans throughout the bilaterians (Davidson, 2006; Degnan et al., 2009).

The other part of the genome consists of non-coding sequence motifs, which are short stretches of DNA that exhibit some sort of biological function (Figure 1.2 B). They can be binding sites for

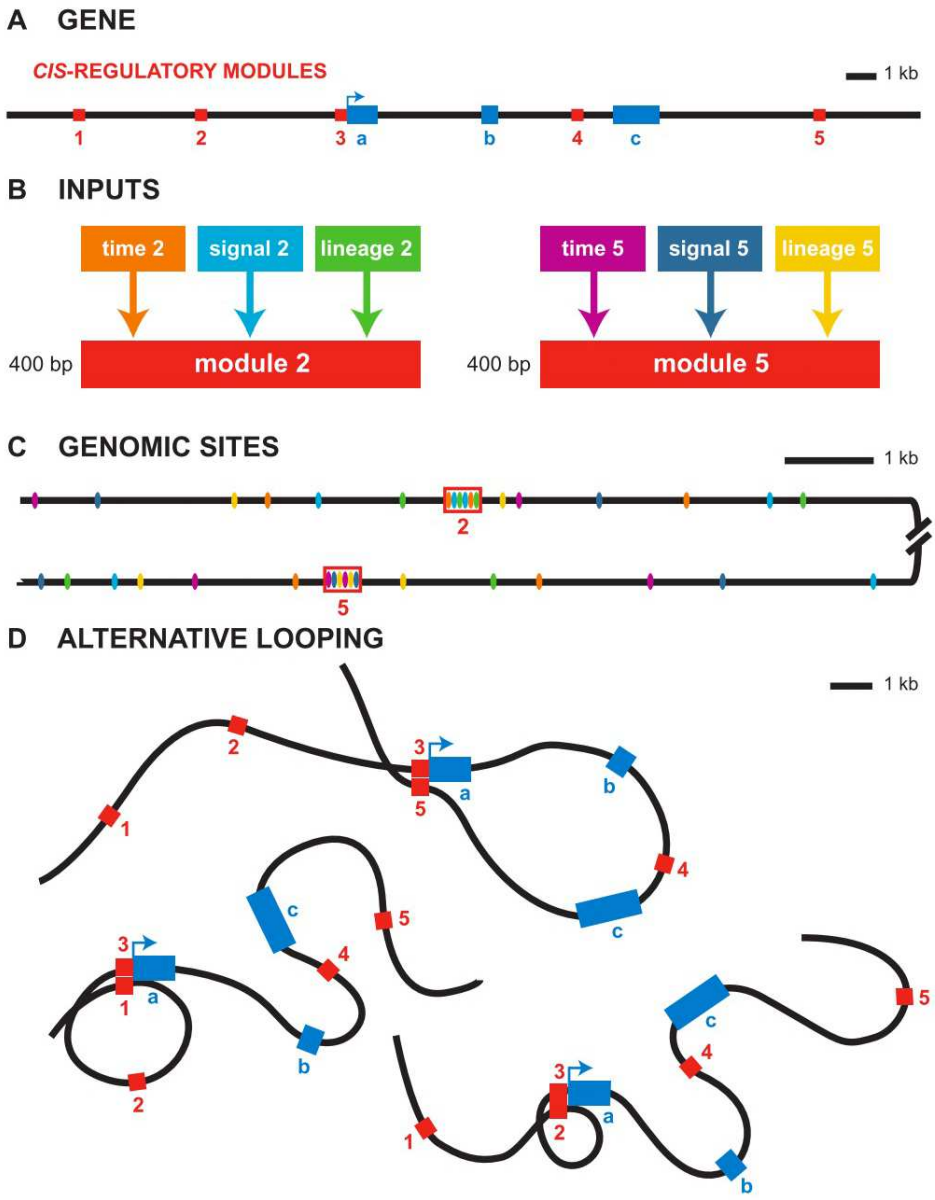

Figure 1.3: **Genomic cis-regulatory modules.** (A) A generic gene with exons (blue blocks) and five *cis*-regulatory modules (red blocks). (B) Two examples of inputs that define regulatory modules. (C) Distribution of transcription factor binding motifs within *cis*-regulatory blocks and randomly on the genome. (D) Alternative looping, used to deploy different modules for regulatory function. The three diagrams show, respectively, the conformations when module 1, module 5, or module 2 are in action. For transcription the proximal module (3) is always required, in that the distal modules (i.e., 1, 5, or 2) must interact with elements within the proximal module for function (for real examples of this, see Chapter 2). Figure was taken from Davidson (2006).

transcription factors (here referred to as *cis*-regulatory motifs) at the DNA level, or recognition sites for the splicing machinery on RNA level (reviewed in Matlin et al. (2005) or others). In this thesis, I will focus specifically on DNA binding motifs. One way to identify computationally DNA binding motifs is by phylogenetic foot-printing, in which large portions of genomes of evolutionary related species are aligned to each-other and the sequences of interest identified as highly conserved stretches of non-coding sequence (Ganley et al., 2008). Once identified, they can then be experimentally validated by point mutations on reporter constructs. Generally, the main function of DNA motifs is to regulate gene expression. Regulation of gene expression requires two components: first are *cis*-regulatory modules that conditionally control spatial and temporal gene expression. They are usually within the vicinity (but not always) of a gene to be regulated. The second components are the *trans*-regulatory elements, which are sequence specifc DNA-binding proteins and collectively constitute the regulatory states, *i.e.* the sum of active transcription factors within a cell at a given time. *cis*-regulatory modules can be further divided into enhancers and silencers and represent inputs that provide an instruction for the basal transcription of a gene. These instructions define whether a gene should be active, silenced and can also specify the rate of transcription. All three factors depend on the occupancy of a given *cis*-regulatory module and type of *trans*-regulatory elements. An example of such is provided in Figure 1.3. In functional terms *cis*-regulatory modules can be thought of as processing functions for transcription of a gene that follow logical operators (Bolouri and Davidson, 2002; Istrail and Davidson, 2005). Depending on the input, *i.e.* regulatory state, concentrations of transcription factors and the physical state of the chromosome, occupancy of a *cis*-regulatory module defines the state of transcription of a gene. Therefore, if the initial state, including all the processing functions and the time delay created between transcription to translation is known, it should be theoretically possible to predict all the states of a cell throughout time. This was shown in developmental context by Peter et al. (2012) and is described in more detail below. In summary, a genome is composed of many parts, each of which has some functional meaning. Historically, everything that was non-coding for pro-

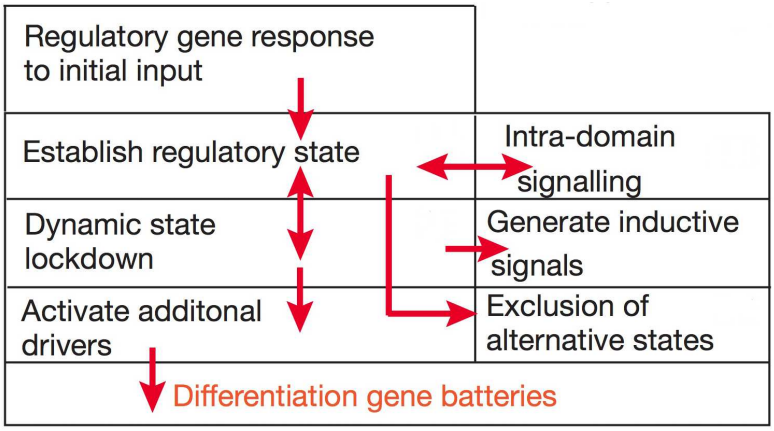

Figure 1.4: **Schematic of a GRN.** Diagram explaining the different parts and their interactions of a developmental GRN. This figure was taken from Davidson (2006).

teins was considered ”junk” DNA. But with the accumulation of data, recently it was estimated that around 80% of the genome suits some functional purpose (Pennisi, 2012).

Now that I have described the individual components of a GRN, I will address the structure and construction of GRNs in a developmental context.

1.1.3 Gene regulatory networks

Developmental GRNs are maps of gene interactions that logically describe the formation of various morphological features throughout development. They explain the generation of regulatory states within different territories and link causally the genome with the developmental process. The nodes in a GRN are genes and their *cis*-regulatory apparatuses. The activity of a gene (enhanced or silenced) is controlled by the *cis*-regulatory sequence and is thus determined by the presence of a set of transcription factors with the ability to recognise it in the nucleus. In this way the linkages of the individual nodes are established. Development is a dynamic process in which multiple cell types are formed from a single cell. Davidson (2006) described this increase of complexity by the continuing generation of new regulatory states in individual spatial domains of the embryo produced by their underlying genetic subprogram. Thus, once it is know, which part of the embryo will give rise to which final cell type, a single GRN for this cell-type can be constructed.

This implies that for the whole embryo, different territories (sub-GRNs) are connected through signalling. During development individual parts are employed in an hierarchical manner. Firstly, a cascade of transcription factors (TF) is activated by maternal factors in order to specify precisely the position and attributes of cells that will later form various body parts. Feedback loops stabilise the regulatory states (set of expressed genes in a specific cell type) and increase robustness of the developmental process. In this way a specific cell fate is ”locked-down”. Signalling pathways link the individual sub-GRNs for specific cell types throughout the embryo and ensure their correct placement. Once the specification is completed, a group of differentiation genes is activated at the periphery of the GRN. The composition of these genes decides the final cell type and thus its function in an organism. Moreover, differentiation genes are the final output of the GRN and have no regulatory capabilities, *i.e.* do not bind any *cis*-regulatory elements (CRE), and thus do not effect transcription of other genes. Moreover, they are large in number and consistent with the partially ”scale-free” architecture described above. A schematic representation of this process in presented in Figure 1.4. In this way GRNs have the ability to link the process of development directly to the genome. The most complete GRN described so far is for the endomesoderm development in the sea urchin *Strongyloncentrotus purpuratus* and in particular for the formation of the larval skeleton (Oliveri et al., 2008; Rafiq et al., 2012, 2014). Since this is fundamental for the comparative analysis of this study, later it will be described in detail. One key characteristic of GRNs in development is their modular structure and the re-usability of specific sub-circuits. These are not the same as previously described motifs (*e.g.* feed-forward loops), because a sub-circuit has to have a clearly definable function for a developmental process. This, however, is not the case for all generally known motifs. Examples for such functions are the separation of a space or the ”lock-down” of a cell fate (reviewed Davidson (2010)).

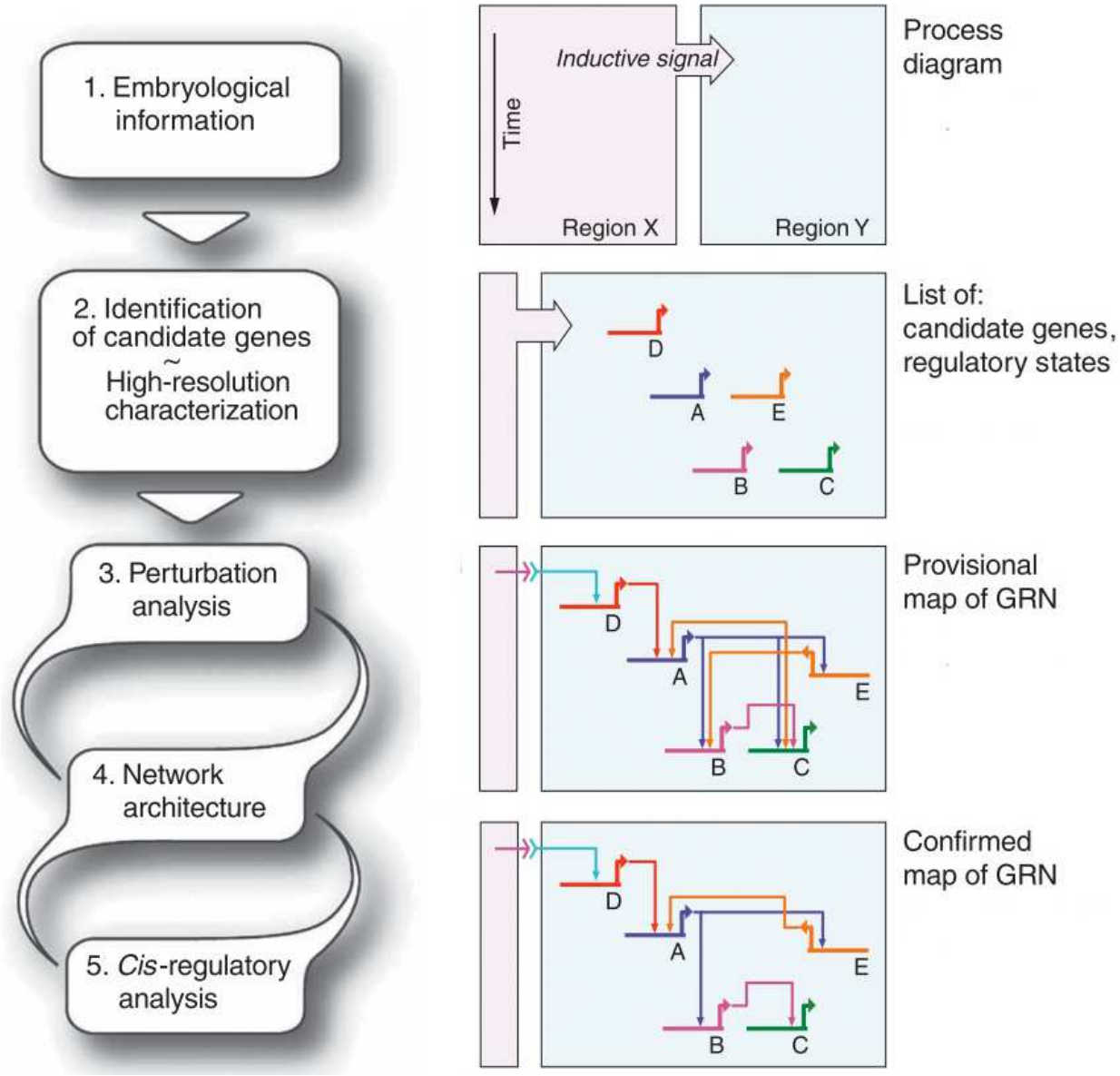

Figure 1.5: **Experimental procedure to construct a gene regulatory network.** On the left are the individual steps and on the right the assembly of GRN. This figure was taken from Materna and Oliveri (2008).

1.1.4 Construction of GRNs

In order to establish a GRN Materna and Oliveri (2008) laid out a protocol describing the individual steps. This protocol generally follows five steps and is schematically presented in Figure 1.5. First, all embryological information are collected and laid out in a process diagram. This includes knowledge about cell lineages, cell specification, divisions and morphological features. Then, a territory or cell type is chosen and all genes expressed within a timeframe of interest are identified. This identification can occur through candidate approach, by compiling a list of orthologs that are used in a close relative species in a similar territory, or identified using genome wide screens, *e.g.* next generation sequencing approaches. Once a list of candidates is compiled, the spatial and temporal expression details have to be resolved in high resolution. All genes that are found to be active and expressed in the territory, then form the nodes of the network. Third, identified candidates are perturbed in their expression and function by antisense morpholino, RNAi, genome editing, overexpression or other methodologies. Fourth, the perturbed samples are screened for differential expression of other genes analysed and affected genes are connected, thus forming the functional linkages and establishing the network architecture. Finally, *cis*-regulatory analysis is performed on affected genes in order to confirm the direct or the indirect effect of perturbation.

In order to represent and to integrate all of this type of data, Longabaugh et al. (2005) developed a methodology for computational representation. The software BioTapestry[2] (Longabaugh et al., 2005), allows the integration of all the collected data and the formation of a GRN that is capable of representing the activity of individual nodes in individual embryonic cell types in time (Longabaugh, 2012). In order to be able to incorporate the fact that the same gene can participate for the specification of multiple territories Arnone et al. (1997) introduced the concept of view from the nucleus and view from the genome. The view from the nucleus provides a way of incorporating the pleiotropy of a single gene (Figure 1.6). In contrast the view from the genome

[2] http://www.biotapestry.org

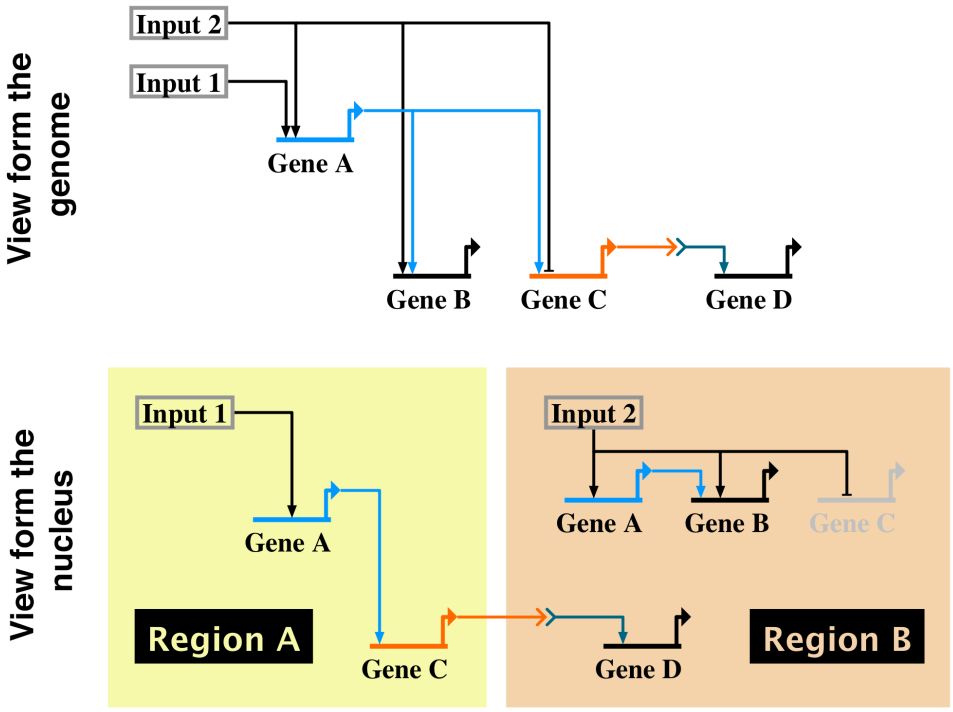

Figure 1.6: **GRN modelling using BioTapestry.** On the top is depict the view from the genome, incorporating every gene only once thus neglecting the expression in different spatial domains (*i.e.* different cells). On the bottom is the view from the nucleus with two regions A and B. As seen gene A is part of both regions, due to expression in multiple regions. Inputs are modelled as constants and different regions can only communicate through signalling as depict by the linkage between regions with two arrows. This figure was taken from Longabaugh (2012).

contains a single representation of each gene and neglects the spatiality within an embryo.

1.1.5 Modelling of GRNs

GRNs are a useful tool for understanding the cause and effect of developmental complexity. As described above, they are formed by the integration of various types of experimental evidence. Once such a network is obtained, mathematical models can be applied for analysis and prediction of network behaviour. Various modelling approaches for biological networks exist and I will briefly discus continuous modelling using ordinary differential equations (ODE) and in more detail modelling using boolean approaches (reviewed in (Karlebach and Shamir, 2008; Tomlin and Axelrod, 2007; Vijesh, 2013)). Stochastic modelling represents a third type, but will not be discussed further (for review in a developmental context (Raj and van Oudenaarden, 2008)). In the context of modelling, I am discussing the application of continuous and boolean approaches assuming the network structure is already given. This is different from using statistical modelling to infer network structure, *e.g.* from time series expression and/or perturbation data. Usually, ODE models have one equation for each gene that describes the temporal behaviour caused by incoming and outgoing inputs of other genes. The rate of input and output is defined by chemical kinetics (Figure 1.7 A). This approach was used to model the whole endomesoderm development in the sea urchin (Kühn et al., 2009). Neglecting changes in space (embryo divides and creates new territories in time) and assuming static signalling, the authors constructed a model where each equation represented the dynamical change of expression of a single gene. Using *in silico* perturbations, Kühn et al. (2009) were capable of recapitulating less than half of experimental perturbations with their model (48%). Although it was stated in (Kühn et al., 2009) that a lot of measurements - especially to determine the kinetic constants - were missing, and that for only one gene (Endo16 (Bolouri and Davidson, 2002)) a detailed *cis*-regulatory logic analysis exists, it was concluded that the current endomesoderm GRN is incomplete. On the contrary, it was shown for other models, *e.g.* cell-cycle in the bacterium *Caulobacter crescentus* (Li et al., 2008c) that

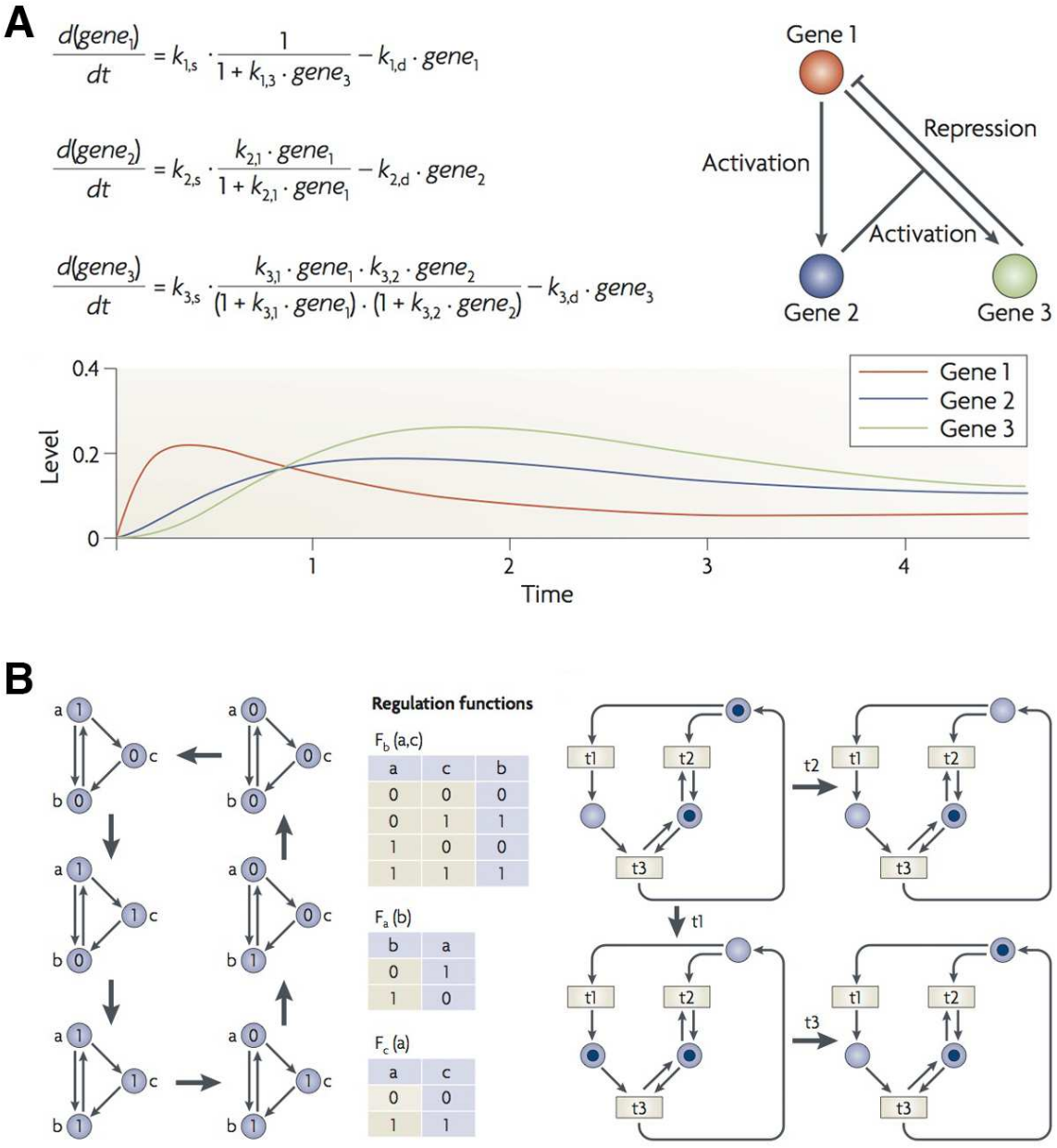

Figure 1.7: **Different approaches of GRN modelling.** (A) Modelling using differential equations. Each node is represented by one equation. k_x are the kinetic rate constants. Incoming connections are added and outgoing are subtracted. Repression is modelled using Michaelis Menten kinetics. (B) Boolean network model of three genes a,b and c. The circles represent the individual state and the squares represent the regulation functions. This figure was taken from Karlebach and Shamir (2008).

when enough data is available, the experimentally obtained gene expression patterns are consistent with the model (reviewed in (Karlebach and Shamir, 2008)). Therefore, whether the GRN topology is actually correct, but not enough data is available to support it, or the GRN topology is wrong remained open.

A more simplified approach of modelling is through boolean approaches, also called logic models (Figure 1.7 B). Boolean logic has only two states, which can be defined as 1 (active) and 0 (inactive). For GRNs each gene can have only one of such states in a specific territory at a specific time, and thus the state of a specific territory can be summarised in a vector in which each element represents the activity of a single gene in a specific territory. It follows that the state of a whole embryo at all time points can be represented as a matrix. In this way, changes in time are assumed to occur synchronously in discrete time steps. The update of this model occurs through functions that are defined by logical operations, *e.g.* AND, OR, NOR (reviewed in (Karlebach and Shamir, 2008)). In the context of development a specific cell type is defined by the current regulatory state. The regulatory state is equivalent to a boolean vector of 1's and 0's describing the activity of a gene in a cell type. Maternal inputs provide the first input into the model and once all the regulatory functions are defined the model should accurately predict the regulatory states in different territories. Such a model is thus similar to an automaton. One argument for use of boolean models in developmental biology is that one embryonic space defines the future cell type and this embryonic space is defined by a regulatory state, thus being boolean in nature (Peter et al., 2012). Recently, this approach was applied to the endomesoderm development of the sea urchin (Peter et al., 2012; Faure et al., 2013). This model used the GRN for endomesoderm development as a basis for modelling (Peter and Davidson, 2009). The logical functions were derived from perturbation experiments and *cis*-regulatory analysis. Additionally, conditions for signalling between adjacent cells were included. The time step was defined as 3 hours (based on the delay between transcription to translation (Bolouri and Davidson, 2003)). With minor exceptions the model was capable of reproducing the individual regulatory state activity in the embryo throughout

time. Additionally, *in silico* perturbations were consistent with experimentally observed changes of spatial expression. However, these results are not very surprising since the logical regulatory functions for each gene were derived from perturbation experiments in the first place. Although it is quite remarkable that spatial regulatory states can be captured using such a simplified model, some transcription factors that have two different types of regulatory output depending on the concentrations of their inputs (Damle and Davidson, 2011), cannot be incorporated with such an approach. Since binary logic works with ON and OFF states it cannot incorporate dependencies of TF concentrations.

1.2 Evolution of gene regulatory networks

GRNs provide a causal explanation for the development of an embryo. Assuming that this is true, it follows that the mechanism that shapes GRNs in order to produce a viable and fit organism is evolution itself. Thus, changes throughout the animal kingdom should be found as changes in the nodes and wiring of a network and the architectural properties of different species should be reflected along the phylogenetic tree. Remarkably, without clear evidence on *cis*-regulation, this hypothesis was already postulated over 40 years ago (Britten and Davidson, 1969).

1.2.1 Towards a theory of GRN evolution

One of the first studies addressing this process in echinoderms was presented by Hinman et al. (2003), where the GRN for endomesoderm formation was compared between star fish *Patiria miniata* and sea urchin *Strongyloncentrotus purpuratus*, species that shared a last common ancestor at least 480 million years ago (Mya) (Pisani et al., 2012). A five-gene feedback loop for endoderm specification was found to be highly conserved in both species (Figure 1.8). However, whereas in star fish the gene *Pmi-tbr* receives inputs from the feedback loop leading to endoderm specification, in sea urchin the gene *Spu-tbr* is restricted to skeletogenic mesoderm (SM) specification. The conservation of this feedback loop and the differences in the *tbr* gene led to the theory that GRNs are modular, and that certain parts are under different selective pressure than others. Parts that are highly conserved between species - and even families - were defined as kernels (Figure 1.8). Furthermore, it raised the hypothesis that individual parts of the network can be linked to different strengths of selection (Davidson, 2006). Kernels are believed to be responsible for Phylum to Superphylum characters, while more evolutionary liable plug-ins and input/output switches are thought to define the animal class, order or family and are shown through size or morphological patterning. Alterations and deployment of differentiation genes should define the functional abilities of a body and can give rise to speciation. Examples of each class are presented for the sea urchin dGRN in Chapter 5 in (Davidson, 2006) and are summarized

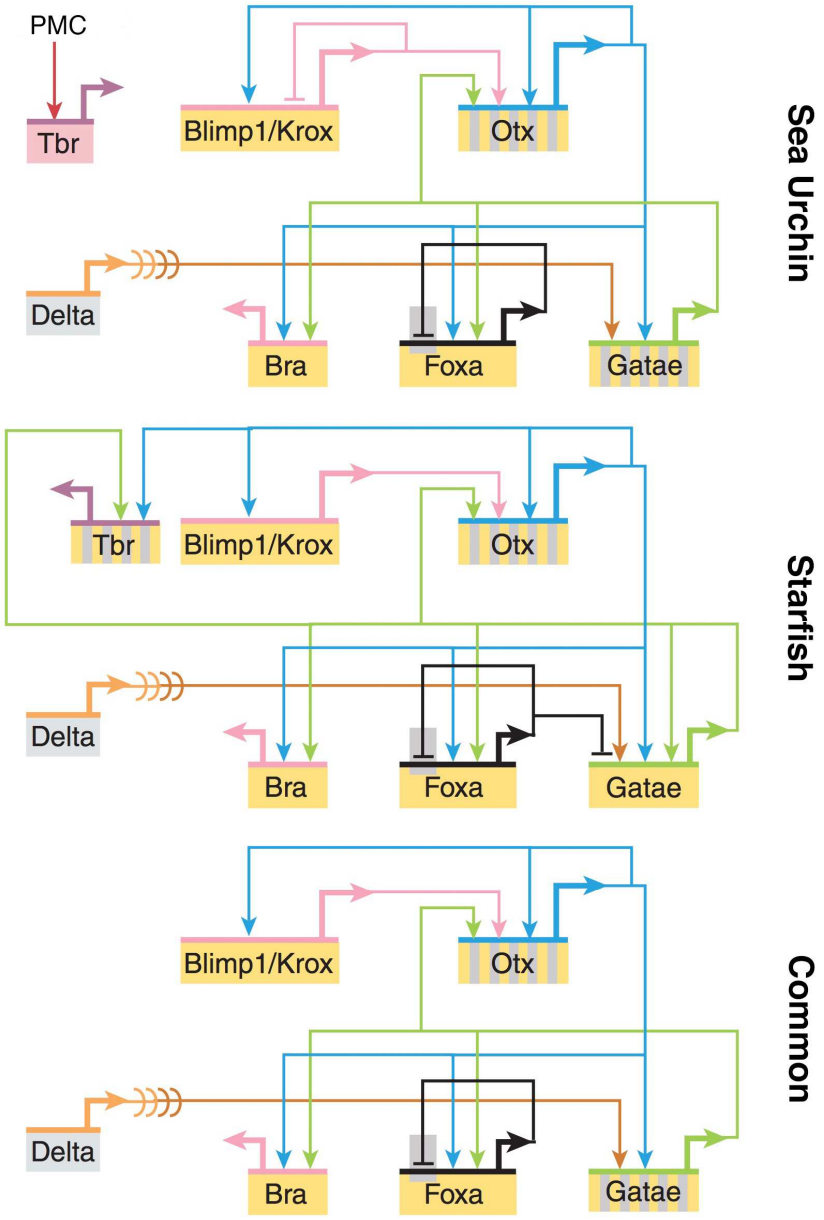

Figure 1.8: **Example of a kernel.** On top the GRN for endoderm formation in the sea urchin. In the centre the GRN for endoderm formation in the starfish and at the bottom the GRN showing commonalities between the sea urchin and starfish. This image was adapted from Davidson and Erwin (2006).

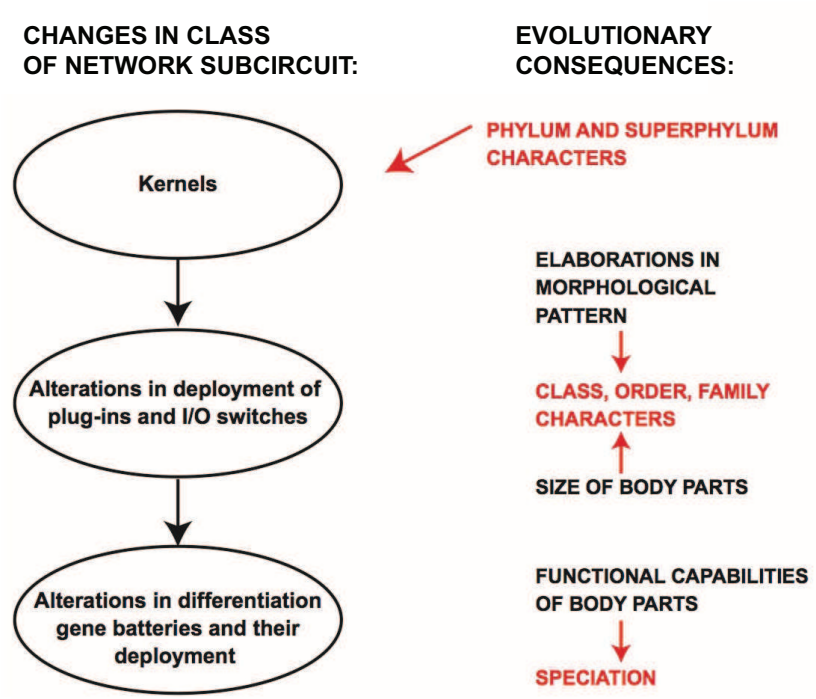

Figure 1.9: **Theory of GRN evolution.** Diagram showing how changes in different parts of a GRN can be linked to evolutionary events along a phylogenetic tree. This figure was taken from Davidson (2006).

in Figure 1.10. Interestingly, several years later a study in the annelid *Capitella teleta* found the conservation of expression of orthologous genes to *foxA*, *otx*, *bra*, *blimp1* and *gataE* in endoderm formation (Boyle et al., 2014) as in the development of the sea urchin. This study thus provided further evidence for this feedback loop to be an ancient module or kernel.

In order to explore whether certain characteristics are under less selective constraints, Hinman et al. (2007) investigated what is happening up- and down-stream of the conserved module of the endoderm network (Hinman et al., 2003). She showed that the employment of Delta-Notch signalling in starfish is different from sea urchin and that different downstream genes are targeted by the kernel described above. The gene *Spu-tbr* is completely uninvolved in endoderm specification in sea urchin and investigations showed that a change in a regulatory motif for the transcription factor *Spu-otx* made a co-option of *Spu-tbr* into the SM lineage possible (Hinman et al., 2007). On the other side, in sand dollar *tbr* was found to participate in endoderm and SM

lineage (Minemura et al., 2009). This observation lead to the conclusion that very recently the evolution of the regular sea urchin re-deployed this gene into the SM lineage and lost its endodermal function. In a comparative study between sea urchin juvenile and embryo *Spu-tbr* was found to participate only in embryo skeletogenesis (Gao and Davidson, 2008). More detailed studies on the regulation of this gene revealed two distinct modes of expression (Wahl et al., 2009). *Spu-tbr* is first repressed by *Spu-hesC*, and maintained at stable levels by a positive input of *Spu-ets1/2* following ingression (Wahl et al., 2009). *ets1/2* is present in embryonic development of all studied echinoderms, but only in echinoids and ophiuroids it is expressed in the SM lineage (Koga et al., 2010), and thus likely to participate in the GRN for this cell type. Spatial expression data of *ets1/2* alone, however, are not enough to discriminate the functional difference of endomesoderm to skeletogenic mesoderm (Koga et al., 2010). Other three regulatory genes of sea urchin larval skeleton development -*Spu-tel*, *Spu-foxB*, and *Spu-foxO*- were not found to participate in the juvenile (Gao and Davidson, 2008). On the contrary, other SM genes were expressed in cells of skeletal elements in both sea urchin juvenile and embryo (Killian and Wilt, 2008; Gao and Davidson, 2008). This observation along with the fact that orthologs of these genes are also expressed in cells associated with spines and other skeletal elements of juvenile star fish led to the hypothesis that the whole GRN responsible for development of the skeleton was co-opted from the adult into the embryo in sea urchin (Gao and Davidson, 2008) and this process included the addition of *Spu-tel*, *Spu-foxB*, *Spu-foxO* and *Spu-tbr* (Gao and Davidson, 2008). Strikingly, it is theoretically possible to co-opt the adult GRN for skeletegoenes in only two steps. First, a CRE for the repressor *Spu-hesC* has to be added on *Spu-alx1*, *Spu-ets1/2* and *Spu-tbr* and second *Spu-hesC* has to be put under the control of another repressor *Spu-pmar1*, thus creating the double negative gate (DNG; xplained below in detail). Using a modelling approach, it was shown that few beneficial mutations can lead to an orchestrated gene-expression change and produce a viable phenotype (Crombach and Hogeweg, 2008). In order for this change to happen, work on *alx1* in holothuroids showed that first the mesoderm had to be separated into distinct territories

(McCauley et al., 2012). Once mutations in CRE changed these territories the adult skeleton was then able to be co-opted into the embryo. In this context the evolution of micromeres remains unanswered but it was hypothesized that it evolved in parallel to the DNG in sea urchin (Ettensohn, 2009). The network part downstream of the DNG, containing *Spu-hex*, *Spu-erg* and *Spu-tgif*, is conserved between star fish and sea urchin, even though the input is likely to a completely different set of genes (McCauley et al., 2010). This recursively wired feedback loop seems to be ancestrally derived (McCauley et al., 2010), and is a good example of how in evolutionary time some linkages are more conserved than others. Furthermore, it shows how a complete module can be recruited to participate in a different cellular context.

Downstream of this specification part of the network are the bio-mineralisation genes. They are part of the differentiation tier and are assumed to be under fewer selective constraints (Erwin and Davidson, 2009). Sea urchin seems to use a unique set of genes for skeletogenesis, with no counterparts found in vertebrates (Livingston et al., 2006). Only hemichordates have a very small number of sea urchin bio-mineralisation orthologs, but their molecular involvement in skeletogenesis remains still to be addressed (Cameron and Bishop, 2012). Depending on the network hierarchy changes in linkages are under different selective pressures and the differentiation tier is considered fast evolving (Erwin and Davidson, 2009; Hinman et al., 2009). Whilst a lot of evidence across echinoderms has been accumulated to make the theory of evolution on a GRN level plausible, up to now very little work has been done on brittle stars, the only other class of echinoderm that develops an elaborate skeleton in the larva.

1.2.2 Mechanisms of GRN evolution

Although many studies in different organisms analyzed the complex developmental GRNs (reviewed in (Levine and Davidson, 2005)), little is known about the mechanisms of successful rewiring during evolution and most studies, with few exceptions (McCauley et al., 2012; Garfield et al., 2013), remain at the level of single nodes. Comparative developmental and genomic studies

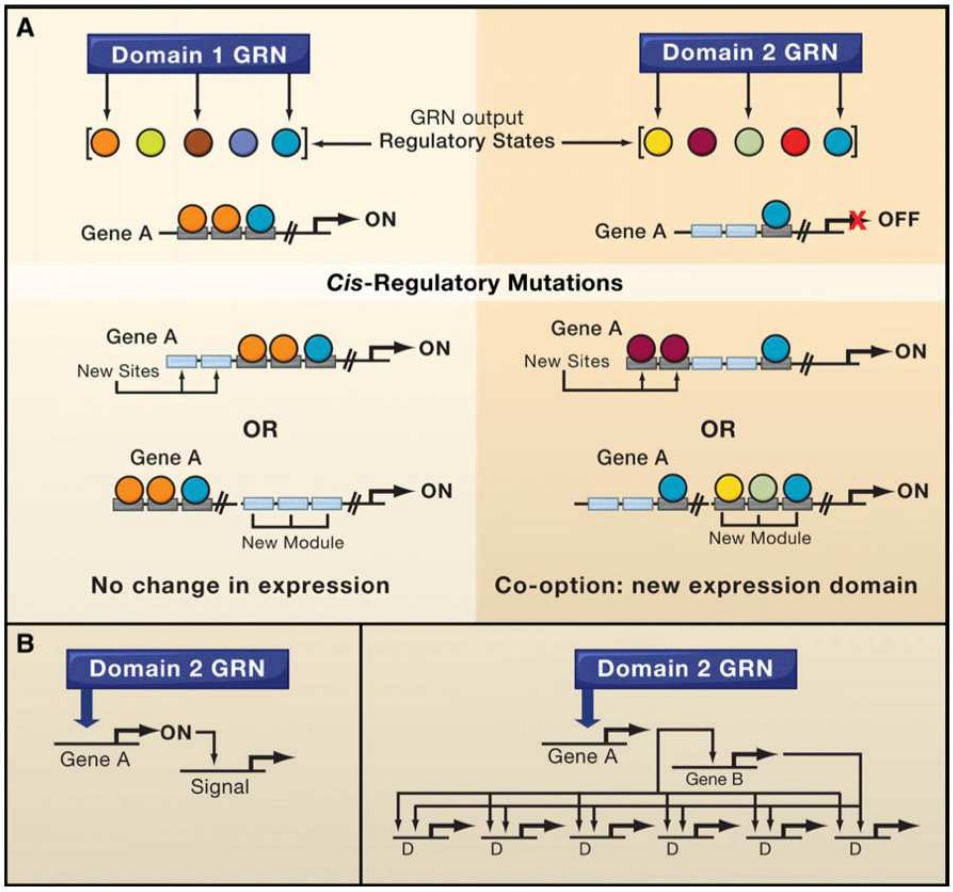

Figure 1.10: ***Cis*-regulatory module evolution.** (A) Domain 1 and 2, which have different regulatory states, drive the expression of gene A differently. Expression of gene A is dependent on occupancy of the *cis*-regulatory module. Gene A is here expressed in domain 1 but not 2. Two possible scenarios of *cis*-regulatory mutations are shown: 1) appearance of new sites within the module by internal nucleotide sequence change. 2) a module from elsewhere is transposed into the DNA near gene A with new sites. While in both cases the output in domain 1 is not effected, the new sites allow expression of gene A in domain 2. (B) Possible effects of activity of gene A in a new context. This figure was taken from Peter and Davidson (2011).

over the past two decades clearly showed that developmental regulatory genes are remarkably conserved among animal phyla, suggesting that phenotypic differences between organisms are achieved through variation of gene expression and thus, GRN architecture (Peter and Davidson, 2011).

1.2.2.1 Re-wiring by cis-regulatory element evolution

Changes in GRN architecture are mostly obtained through modifications in expression of regulatory genes, thus putting changes in the cis-regulatory apparatuses of regulatory genes as

the main mechanisms of GRN evolution (Davidson, 2006; Peter and Davidson, 2011; McLean et al., 2011; Wray, 2007). The highly evolutionary conserved kernels, likely rely on conservation of cis-regulatory control of the genes they are formed of. The finding of conserved non-coding elements (CNE) in the regulatory apparatus of several developmental genes encoding for transcription factors supports the existence of such kernels (Royo et al., 2011; Parker et al., 2011; Nelson and Wardle, 2013). On the other hand, fast evolving network linkages were identified when comparing closely related species. A study of five closely related vertebrate species using ChipSeq of two transcription factors gave support to both claims (Schmidt et al., 2010). Whereas only a small fraction of *cis*-regulatory sequence was found to be conserved, the majority exhibited a high turnover rate. Changes in *cis*-regulatory sequence have been also been confirmed to be responsible for morphological variation. For example, it has been shown that changes in the expression of the Drosophila yellow gene cause differences in wing pigmentation (Prud'homme et al., 2006), and recently the evolutionary path for these differences has been resolved. First, a novel *cis*-regulatory module for pigmentation differentiation genes evolved downstream of the *distaless* (*Dll*) gene, and then species-specific diversification occurred changing the spatial expression of *Dll* in different species and thus changing the wing pigmentation (Arnoult et al., 2013). In another study, specific deletion in the cis-regulatory sequence of the human androgen receptor gene was linked with the loss of sensory vibrissae and penile spine (McLean et al., 2011; Reno et al., 2013). Moreover, it has been shown that novel, more complex morphological features, can originate by co-option of an existing regulatory circuit into a new developmental time or location, as in the before mentioned echinoderm larval skeleton (Gao and Davidson, 2008). Thus, cis-regulatory changes in developmental regulatory genes have been considered the major driving force of GRNs evolution.

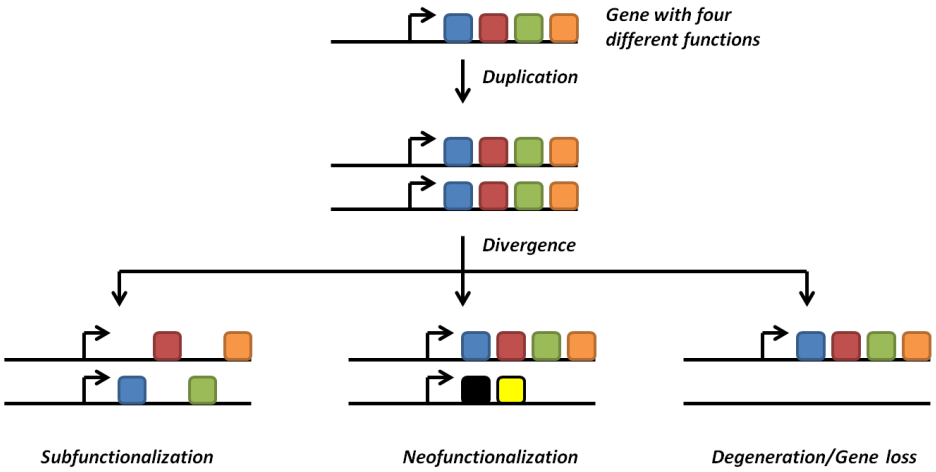

Figure 1.11: **Protein evolution by gene duplication.** Diagram shows different evolutionary scenarios after gene duplication. The coloured blocks represent different protein domains. This figure was taken from `wikipedia.org`.

1.2.2.2 Re-wiring by protein evolution

Alteration on CRE represent only one side of GRN evolution; important evolutionary changes have also been reported at the protein level, where non-synonymous variation or the variation of short linear domains can be clearly linked to the evolution of new function or specificity of interaction (for review Wagner and Lynch (2008)). The simplest way of protein evolution is by mutations on non-synonymous sites. An example of this is the Drosophila ubx gene, which specifically evolved a repressor domain that is absent in other athropods but important for the evolutionary transition of limb patterning (Grenier and Carroll, 2000; Galant and Carroll, 2002; Ronshaugen et al., 2002). Another possibility of protein evolution is through gene duplication. Once duplication occurs, the relaxed selective pressure on the gene duplicate allows for evolutionary changes by mutations Figure 1.11. In the most common scenario the duplicate becomes non-functional. However, two possibilities exist that can create a functional protein out of the duplicate: neo-functionalisation and sub-functionalisation. In neo-functionalisation the gene duplicate receives a novel function, whereas the template retains its ancestral role. An example of neo-functionalisation is found in the bicoid gene that evolved as duplication of the hox3 para-

log gene zen. Whereas zen maintained its ancestral function, relaxed selective pressure on bcd allowed protein changes responsible for recognition of new DNA motifs and consequently regulation of new target genes, facilitating the evolution of a new role as morphogen in anterior-posterior patterning (reviewed in McGregor (2005)).

On the other hand, in sub-functionalisation, following gene duplication both copies undergo changes to give rise to two novel proteins. One example for this process is the B-Myb gene in vertebrates, which underwent two rounds of gene duplication. The first round of duplication gave rise to A/C-Myb through neo-functionalisation (Davidson et al., 2005), shown using a functional equivalence assay where only the vertebrate B-Myb could rescue the phenotype in *Drosophila melanogaster* lacking its endogenous Myb gene. The second duplication event gave rise to A-Myb and C-Myb, both having differences in protein domains and both not being able to rescue the *D. melanogastor* lacking Myb phenotype (Davidson et al., 2013; Ganter and Lipsick, 1999) exemplifying sub-functionalisation. Importantly, Jarvela and Hinman (2015) argued that transcription factor evolution occurs mostly due to the modularity of a protein having different domains that are responsible for different functions. Other examples for mechanisms of neo- or sub-functionalisations are exon shuffling, where different exons are exchanged to create hybrid proteins, and changes in binding domains allowing the duplicate to bind to a different *cis*-regulatory sequence (reviewed in Jarvela and Hinman (2015)). While both these mechanisms have been shown as participating in GRN evolution, (Carroll, 2008) argues that gene duplications generating a new node in a GRN are rare, especially for genes that play crucial roles in development.

Nevertheless, protein evolution does not always have to be preceded by gene duplication as shown for the CEBPB gene in mammals (Lynch et al., 2011). In a study comparing the CEBPB gene from mammals with and without a placenta, three amino acid substitutions were found to be responsible for reversing the response of CEBP to GSK-3b-mediated phosphorylation from repression to activation, and thus changing its response to this signalling pathway (Lynch et al., 2011).

Despite claims that protein evolution is less important for evolution of the animal body plan several examples demonstrate showing how novelty has arisen using this mechanism.

1.3 Phylogeny of echinoderms

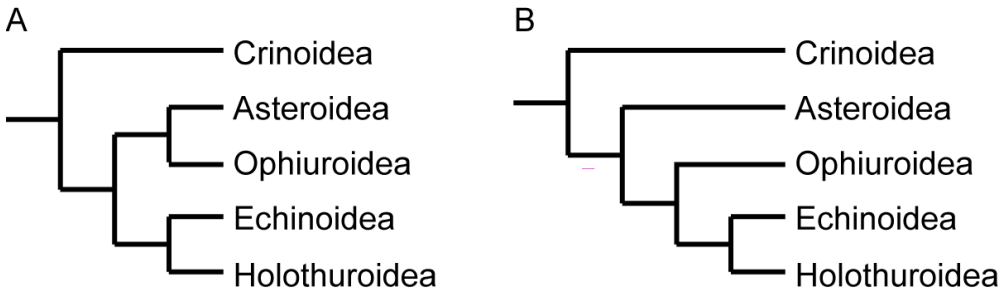

Figure 1.12: **Schematic representation of the two major phylogenetic propositions for the echinodermata group.** (A) Asterozoan hypothesis. The Asteroidea and the Ophiuroidea share a common ancestor and the Echinoidea and the Holothuroidea share another. These two subgroups evolved from one common ancestor. (B) Cryptosyringid hypothesis. The Echinoidea and the Holothuroidea share a common ancestor. This group evolved from the same ancestor as the Ophiuroidea. Figure was taken from (Littlewood et al., 1997).

To address questions about evolution in development it is important to understand the phylogenetic context of the animals of choice. In this thesis I am making use of the class of Echinodermata. Echinoderms belong to the deuterostomes and, along with the hemichordates, form a sister-group to the chordates[3]. Due to their distinct morphology and their mineralized skeletal elements, echinoderms have an excellent fossil record. This, in combination with other type of data, *i.e.* molecular phylogenies and clock estimates, have allowed the exact moment of divergence from hemichordates to be pinpointed to around 570 Mya (Erwin et al., 2011; Smith et al., 2013; Pisani et al., 2012). Within the Echinodermata, the criniods are the basal out-group (Paul and Smith, 1984). The asteroids, ophiuroids, holothuroids and echinoids form a monophyletic group called Eleutherozoa. Echinoids are further divided in euechinoids and cidaroids, that latter is commonly known as pencil urchin. In phylogeny, the grouping between the holothuroids and echinoids is widely accepted in the science community and is based on concurrent results in all studies described below. More prevalent is the question of how to place the ophiuroids and asteroids in the Eleutherozoa. The two main hypothesis that have been discussed over the years are the Asterzoan hypothesis (Figure 1.12 A) and the Cryptosingrid hypothesis (Figure 1.12 B). In the

[3] http://www.tolweb.org/

Asterzoan hypothesis, asteroids and ophiuroids form together an sister-group to echinoids and holothuroids, whereas in the Cryptosingrid hypothesis asteroids from an out-group to ophioroids that form an out-group to echinoids and holothuroids. In the earliest work morphological studies strongly supported the Cryptosingrid hypothesis (Hyman, 1955). First molecular analysis using ribosomal RNA, on the other hand, were inconclusive owing to strong phylogenetic signal in favour for both hypothesis (Littlewood et al., 1997). An analysis based on 13 protein coding sequences of 23 Eleutherozoan mitochondrial genomes gave equal support for the two mentioned hypotheses and also for an adapted cryptosingrid hypothesis where ophiuroids and asteroids exchange their position (Perseke et al., 2010). Other work on protein-coding genes and ribosomal sequences (Smith, 1997) and additional morphological characteristics (Janies, 2001) gave support for both hypothesis and were unable to resolve the dispute regarding the correct phylogeny of the echinodermata. The difficulties in establishing a unifying phylogeny were due to the choice of analytical method and the fact that the early split of the different species was causing long branch attraction errors (Felsenstein, 1978; Pisani et al., 2012; Janies et al., 2011). With the rise of next generation sequencing methodologies new approaches, as well as more complete sampling of the phylogenetic tree, could be used to address this problems. The first analysis that was able to account for these errors and provided a clear solution strongly supporting the Asterozoa hypothesis was reported by Telford et al. (2014). A probabilistic Bayesian phylogenetics approach was used on 219 genes in 15 species including all four groups. The Asterozoa grouping was further supported in a recent study of 185 genes that included data on 14 hemichordates and 19 echinoderms (Cannon et al., 2014) and another study incorporating fossil records and 61 different taxa (O'Hara et al., 2014), and a study including 23 *de novo* transcriptomes from every echinoderm class (Reich et al., 2015).

Most echinoderms undergo metamorphosis and develop the adult animal within a self-sustained larva. Interestingly, the types of larva vary between the individual classes. Ophiuroids and echinoids both develop into a pluteus type larvae (Hyman, 1955). The pluteus larvae is charac-

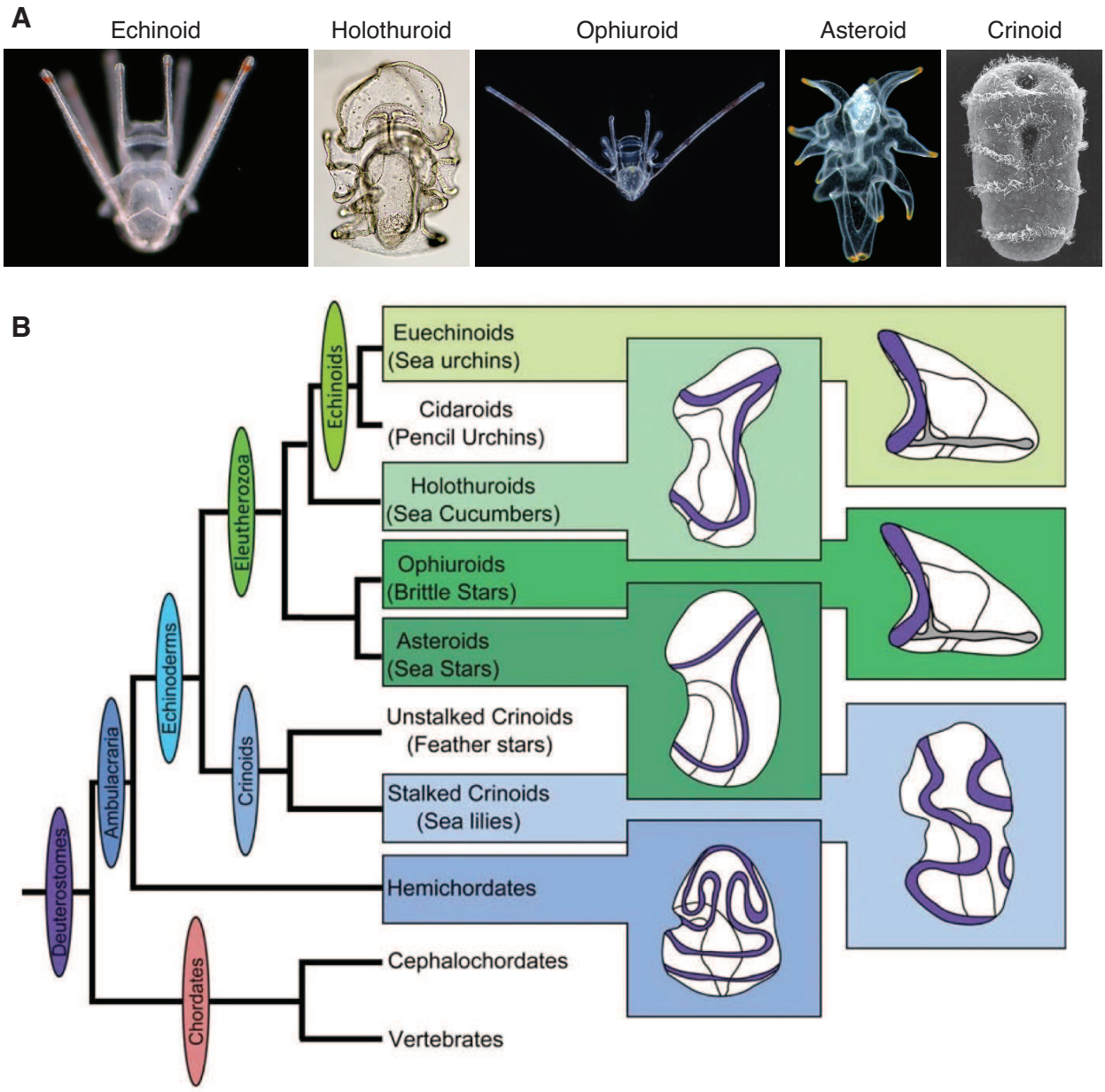

Figure 1.13: **Larval types in echinoderms.** (A) Asteroids, holothuroids and crinoids have a dipleurula type larvea without a skeleton, whereas ophiuroids and echinoids have a pluteus type larvae with skeleton. (B) Phylogeny based on Asterzoan hypothesis and variations of larval types in echinoderms. Image of ophiuroid larvae was taken from `http://arkive.org`. Image of crinoid larvae was taken from `http://scaa.usask.ca`. Images of asteroid and echinoid larvae were taken from `http://cifonauta.cebimar.usp.br`. Image of holothuroid larvae was taken from `http://commons.wikimedia.org`. Figure B was taken from Hinman and Cheatle Jarvela (2014)

terised by a mesodermally derived skeleton that supports feeding and cilia mediated swimming behaviour. Asteroids develop into a bipinnaria larvae with two ciliated bands: one in front of the mouth, and the other behind it and around the edge of the body. The larva of holothuroids is known as an auricularia larva, because the ciliated band of the dipleurula larva of holothuroids becomes sinuous and lobed, thus resembling a human ear. Both these types of larvae can be characterized as dipleurula type larvae, owing to their bilateral symmetry (Figure 1.13) (Hyman, 1955). Additionally, in contrast to asteroids that do not form any skeleton in the larva, holothuroids do form small spicules that do not aggregate to extend into a full skeleton. In the out-group to the Eleutherozoa, the crinoids, some species also develop a dipleurula type larva, whereas others a doliolaria larva (Nakano et al., 2003, 2009). A doliolaria larva is characterized by large quantities of yolk and several ciliated bands arranged in hoops around the body. The occurrence of an auricularia larva in crinoids suggests that the plutei forms of echinoids and ophiuroids are derived features. This is supported by the fact that hemichordates develop through a tornaria larvae that is similar to the dipleurula type (Tagawa et al., 1998). Thus, one of the main differences within the echinoderms is the development of the larval skeleton. Importantly, all echinoderms have an adult skeleton. This posses the question as to when exactly the larval skeleton evolved within the Eleutherozoa. The two possibilities are convergent evolution, where echinoids and ophiuroids evolved a skeleton independently, or ancestral evolution, where holothuroids reduced the skeleton and asteroids lost it. This unique phylogenetic arrangement of larval forms that are well studied and described offers, thus, an ideal opportunity to investigate differences between convergent and ancestral evolution.

1.4 Echinoderm development as model for GRN evolution

Although echinoderms develop into two main types of larva, they all have conserved patterns of early development with only a few distinct differences (Figure 1.14). As mentioned above, only ophiuroids, echinoids and holothuroids give rise to spicules, whereas asteroids do not. The spicules are formed from a subpopulation of cells derived from the mesoderm (McCauley et al., 2012). While the mesoderm is the most well studied part of the embryo in echinoderms excluding ophiuroids (McCauley et al., 2012; Oliveri et al., 2008; Rafiq et al., 2012, 2014), it is not yet possible to answer the question about convergent or derived evolution of the larval skeleton. In order to be able to address the question about its evolution, I will first describe in detail the development and GRN for this cell type in echinoids and complete this description on occasions where studies exist in other classes of echinoderms.

1.4.1 Morphological observations

Already prior to fertilization the animal-vegetal axis is established in the sea urchin embryo by a gradual accumulation of β-catenin at the vegetal side (Angerer and Angerer, 2003; Hörstadius, 1973). Following fertilization, after three rounds of equal cleavages the cells at the animal side of the embryo divide meriodinally to produce a ring of 8 mesomeres. In contrast, the blastomeres at the vegetal side divide asymmetrically, producing 4 macromeres and 4 micromeres. This unequal division pattern is found only in euechinoids. Starfish, sea cucumbers and brittle stars, on the other hand, divide equally. During the 5th cleavage another asymmetric division of micromeres gives rise to 4 small micromeres at the vegetal pole and 4 large micromeres above them. A fate map exists for all 4 tiers that are present at the 60-cell stage (Logan and McClay, 1997). While the 4 small micromeres will divide only once more and will give rise to the germ cells, the large micromeres will give rise to the skeleton. These are often referred to as SM or primary mesenchyme cells (PMCs). Descendants from the macromeres (veg2 cells) will give rise to the endoderm and non-skeletogenic mesoderm (NSM), including pigment cells, blastocoelar cells,

muscle cells, and coelomic pouch cells. Above the cells part of veg2 is the veg1 territory, which gives rise to endoderm and some ectoderm. The animal half of the embryo gives rise to the ectodermal territories and is not the subject of this study, but I refer the interested reader to (Duboc and Lepage, 2008; Lapraz et al., 2009). Arguably, the micromeres/PMCs represent the best-studied cell type in any species. Within the echinoderms, micromeres are found only in the echinoids, and although the ophiuroid develops an extended larval skeleton it does so without the formation of micromeres (Yamashita, 1985). In sea urchin, specification of these cells happens before ingression in 16 to 32 progenitor cells. Once specified, the PMC undergo epithelial to mesenchymal transition and ingress into the blastocoel. The PMCs then divide once more and migrate towards two ventro-lateral clusters next to the location of archenteron invagination. This is the position where the cells are fused (Hodor and Ettensohn, 1998) and give rise to tri-radiate spicules that extend to give the larvae its pluteus shape (reviewed in Lyons et al. (2012)). This is similarly observed in brittle stars. Although holothuroids have PMCs that ingress and give rise to spicules, these do not secrete biomineralized rods and thus do not form an extended skeleton (McCauley et al., 2012). Asteroids do not have cells that ingress at blastula stage from the vegetal pole of the embryo and as mentioned earlier do not form any skeleton in the larva (Figure 1.14).

1.4.2 Early specification and the double negative gate

Throughout the first cleavages in sea urchin the three genes *Spu-otx*, *Spu-wnt8* and *Spu-blimp1* are initiated through a gradual enrichment of nuclearised β-catenin at the vegetal side of the embryo (Logan et al., 1999). At the same time, the gene *Spu-soxB1* - an antagonist of β-catenin - enters the nuclei of all blastomeres but the micromeres (Kenny et al., 1999) and *Spu-otx* is initially nuclearised only in the micromeres (Chuang et al., 1996). By fifth cleavage nuclearised β-catenin is bound to Spu-TCF where it activates, along with maternal Spu-Blimp1, the expression of *Spu-wnt8* using an AND promoter logic (Smith et al., 2007). After the next division *Spu-wnt8* feedbacks and enhances the levels of β-catenin/TCF. Additionally, maternally abundant Spu-Otx

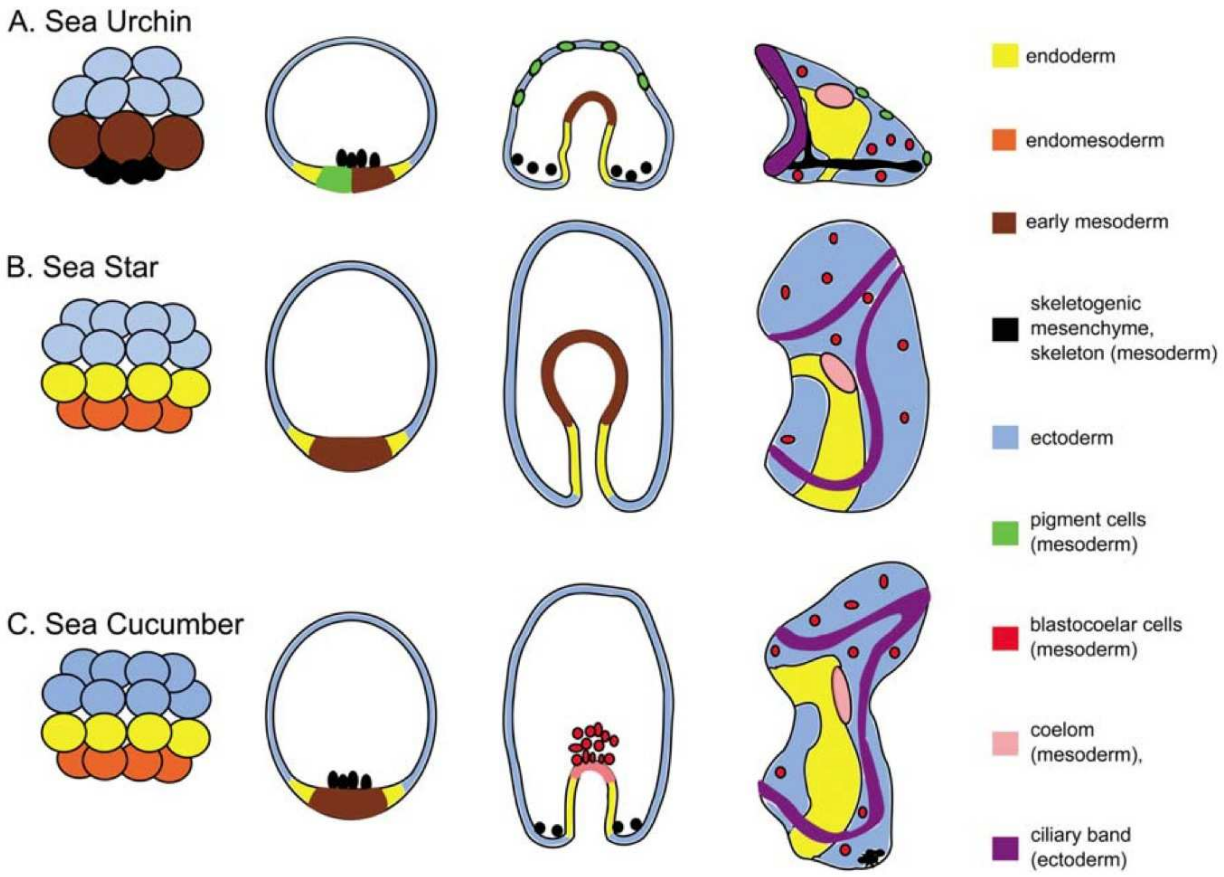

Figure 1.14: **Schematic development of three classes of echinoderms.** Figure was taken from Hinman and Cheatle Jarvela (2014).

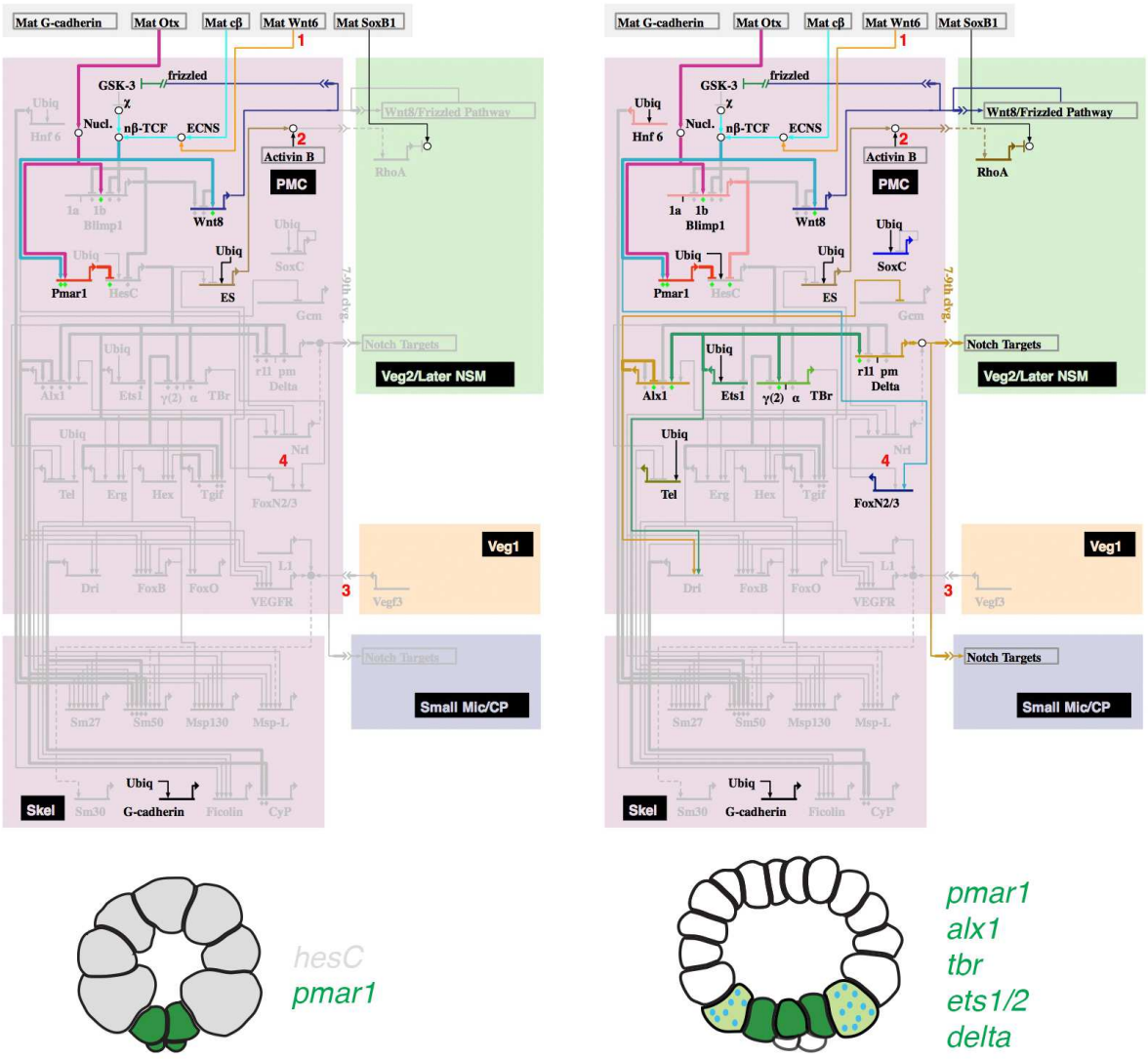

Figure 1.15: **GRN for larval skeletogenesis in sea urchin 6hpf and 10hpf.** Left the GRN for 6hpf with according expression patters and to the right GRN for 10hpf with according expression patterns. Snapshots of GRNs were obtained from `http://biotapestry.org`

starts zygotic expression of *Spu-blimp1* (Li et al., 1997). These events establish the distinction of endomesoderm from ectoderm along the animal-vegetal axis. Additionally, three distinct territoiris are formed: the micromeres, other mesoderm and endoderm. Interestingly, in starfish a gradual enrichment of nuclearised β-catenin has also been shown to be involved in the separation of embryonic territories in a dose-dependent manner (McCauley et al., 2014).

In order to specify the micromeres in sea urchin to become skeletogenic, nuclearised β-catenin/TCF and *Spu-blimp1* activate the expression of *Spu-pmar1*. Once translated, *Spu-blimp1* and *Spu-pmar1* repress the expression of *Spu-hesC* in these cells. Thus, *Spu-hesC* is expressed everywhere but in the micromeres. Overexpression of *Spu-pmar1* or knock-down of *Spu-hesC* transforms all cells to a skeletogenic fate (Oliveri et al., 2002; Revilla-i Domingo et al., 2007) and thus confirms the repressive action. This is consistent with an upregulation of all genes downstream of *Spu-hesC*. These genes are *Spu-alx1* (Ettensohn et al., 2003), *Spu-ets1/2* (Oliveri and Davidson, 2004; Kurokawa et al., 1999), *Spu-tbr* (Croce et al., 2001; Fuchikami et al., 2002), *Spu-delta* (Oliveri and Davidson, 2004), *Spu-tel* (Rizzo et al., 2006) and the transiently active *Spu-soxC* (Howard-Ashby et al., 2006). All of them are expressed at this stage in the micromeres and most provide direct inputs into the differentiation cascade. Importantly, knock-down of *Spu-pmar1* causes upregulation of *Spu-hesC* (Smith and Davidson, 2009). Therefore, these two genes plus the intermediate targets of *Spu-hesC* form a double negative gate. This mechanism puts the skeletogenic fate into the micromeres and is a logical mechanism for space separation (Davidson, 2010). The GRN and expression pattern are shown in Figure 1.15.

Interestingly, so far the *pmar1* gene has only been reported in euechinoids, and the expression pattern of orthologs to *hesC* show a lot of variation in echinoderms (McCauley et al., 2010; Yamazaki et al., 2014). In the asteroid *Patiria miniata Pmi-hesC* is co-expressed with orthologous of sea urchin downstream genes in the mesoderm. Functional studies additionally confirmed the absence of a repressive function for *Pmi-ets1/2* and *Pmi-erg* even though its function as a repressor was confirmed in ecotodermal territories (McCauley et al., 2010). This makes a similar

repression mechanism downstream of nuclearised β-catenin unlikely. Similarly, in the cidaroid *Prionocidaris baculosa Pba-hesC* is co-expressed with its downstream genes and knock-down experiments show no repressive effect on *Pba-alx1*, *Pba-ets1/2* and *Pba-tbr* (Yamazaki et al., 2014). Interestingly, only knock-down of *Pba-alx1* showed a phenotype with abolished skeletogenesis in this class of euechinoids (Yamazaki et al., 2014).

In order to repress an alternative fate of the SM lineage in echinoids, Alx1 is repressing *Spu-gcm*. Downstream of the DNG, Delta signals to the adjacent cells through Notch and activates *Spu-gcm* in NSM lineage. *Spu-gcm* is one of the major drivers in the non-skeletogenic mesoderm (NSM) lineage and targets downstream *Spu-pks* a gene encoding for an enzyme involved in the formation of pigment cells in sea urchin (Ransick and Davidson, 2006; Calestani et al., 2003). Knock-down of *Spu-alx1* transfates the SM-lineage into the NSM-lineage and causes upregulation of *Spu-gcm*, whereas mRNA overexpression of *Spu-alx1* causes a reduction of gcm (Oliveri et al., 2008). Many genes directly regulated by the double negative gate have been further verified by *cis*-regulatory anlaysis (Damle and Davidson, 2011). Interestingly, *Spu-alx1* shows a very steep increase of mRNA levels once it is activated and Damle and Davidson (2011) showed that stabilization of mRNA levels of this gene are achieved by self-regulation through a concentration dependent dimerization mechanism.

1.4.3 Stabilization of skeletogenic fate

Once initiated, the skeltogenic program progress to a stabilization step, where Spu-Ets1/2 inputs into *Spu-erg* the first gene of an interlocking loop (IL). Spu-Erg activates expression of *Spu-tgif* and *Spu-hex*. Spu-Tgif inputs into *Spu-hex* that once translated inputs into *Spu-erg*, thus closing the loop (Oliveri et al., 2008). The role of this highly connected feedback loop is to ”lock down” the skeletogenic fate of these cells. In total there are 4 feedback-loops between these three genes: One between *Spu-erg* and *Spu-hex*, another one between *Spu-hex* and *Spu-tgif*, one between the three of them and a final self feedback for *Spu-tgif*. Thus, this intertwined

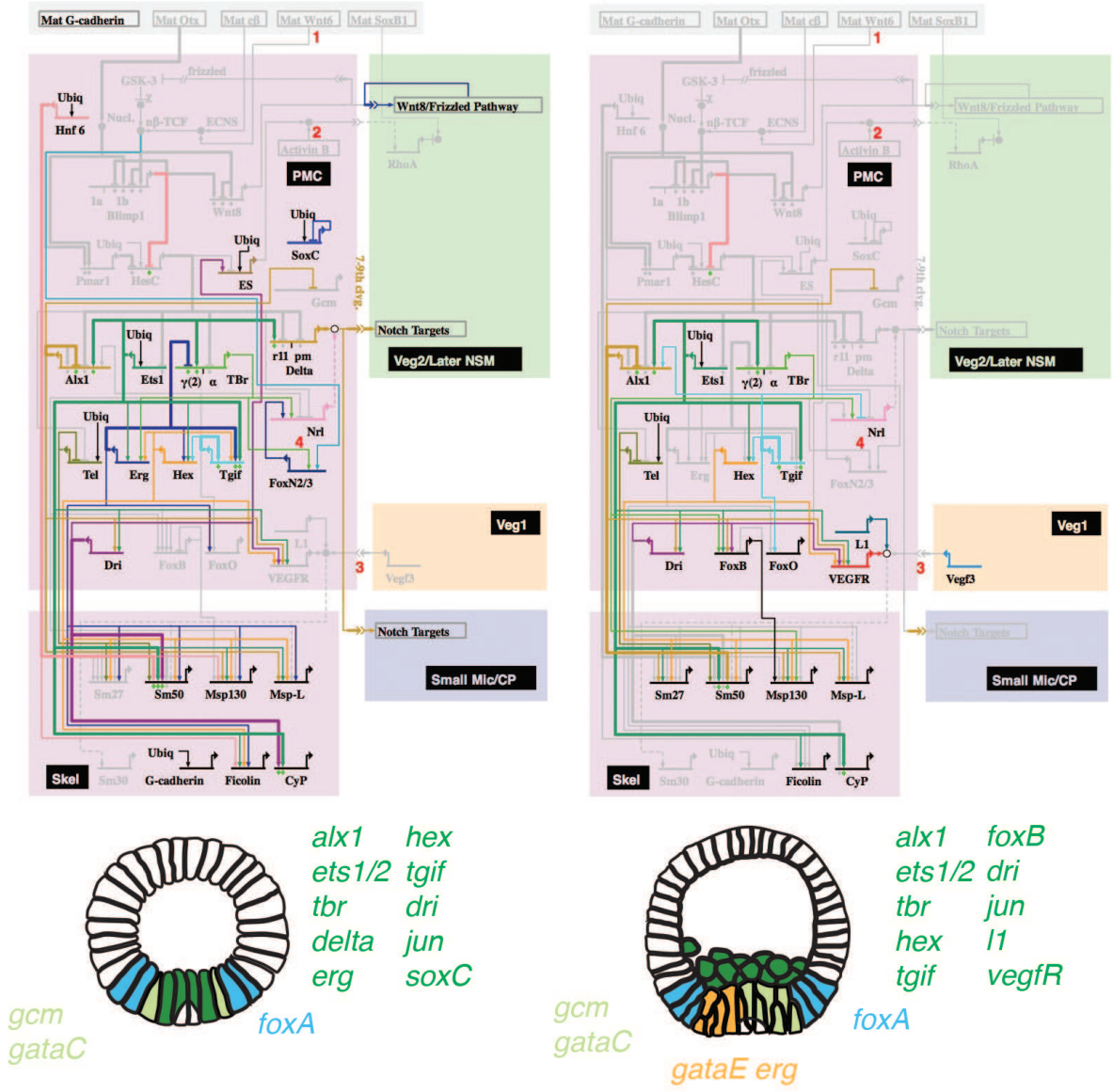

Figure 1.16: **GRN for larval skeletogenesis in sea urchin 15hpf and 24hpf.** Left the GRN for 15hpf with according expression patters and to the right GRN for 24hpf with according expression patterns. Snapshots of GRNs were obtained from `http://biotapestry.org`

nature of this sub-circuit has the ability to dynamically stabilise the regulatory state downstream of themselves. Knock-down experiments on any of these three genes show a drastic down-regulation on the other two (Oliveri et al., 2008). Moreover, knock-down experiments of *Spu-tbr*, *Spu-hex* and *Spu-tgif* show no effect on ingression but an effect on bio-mineralisation (Oliveri et al., 2008). Interestingly, the order of activation of these genes is reflected in their time-courses (Materna et al., 2010). Expression pattern in an holothuroids and additional functional studies in an asteroid suggest a conservation of these IL in the mesoderm (McCauley et al., 2010, 2012) of these classes.

Spu-tgif and *Spu-erg* not only participate in this IL, but also have effects on genes upstream. *cis*-regulatory analysis using bacterial artificial chromosomes for the *Spu-tbr* locus showed that late in development (mesenchym blastula) Spu-Erg, now expressed only in the NSM lineage, has a repressive effect on this gene, ensuring expression of *Spu-tbr* only in the SM lineage (Wahl et al., 2009). Spu-Tgif with Spu-Ets1/2 on the other hand, both drive the expression of *Spu-alx1* in the SM lineage, which directly drives expression of downstream bio-mineralisation genes.

Additionally, Spu-Alx1 and Spu-Tbr provide inputs into two further transcription factors, *Spu-dri* and *Spu-foxB*, that themselves input into the differentiation gene batteries. Oliveri et al. (2008) showed with a high-throughput knock-down study that most of these genes produce a phenotype with inhibited skeleton and are thus essential for this developmental process. Consistently, genes active at the top of the GRN hierarchy showed a more severe phenotype than other genes (Oliveri et al., 2008). In this way it is possible to determine the individual roles in morphological changes, *e.g* knock-down of *Spu-alx1* disrupts ingression of PMCs, whereas knock-down of *Spu-hex* effects only the bio-mineralisation process. Two recent studies extended this network. A nanostring analysis of embryos with and without PMCs revealed the involvement of two other TF in skeletogenesis (Rafiq et al., 2014; Barsi et al., 2014). These are *Spu-nk7*, *Spu-mitf* and *Spu-alx4*, which are first expressed just prior to mesenchyme blastula stage in SM cells and are all affected by knock-down of either *Spu-ets1/2* or *Spu-alx1*. Their late expression suggests, an involvement

as drivers of epithelical to mesenchyme transition (EMT) or the skeletogenic downstream genes. In another sea urchin *Lytechinus varigatus* the canonical EMT genes *Lva-twi* and *Lva-sna* were found to be involved in this process (Saunders and McClay, 2014). However, no detectable expression of *Spu-twi* mRNA levels in *S. purpuratus* suggests no involvement in this species (Tu et al., 2014), and therefore have not been included into *S. purpuratus* GRN model (Figures 1.15 and 1.16).

1.4.4 Cell movements and skeletogenic differentiation genes

Once specification and stabilisation of fate of the PMCs are completed, the cells ingress into the blastocoel through EMT. The ingressed cells extend long filopodia that touch all the surrounding cells and migrate towards two ventro-lateral clusters next to the archenteron. At this moment, both *vegf* and *fgf* ligands are expressed in the ectoderm in cells close to these clusters shown in the sea urchin *Paracentrotus lividus* and *Lytechinus varigatus* (Duloquin et al., 2007; Röttinger et al., 2008; Adomako-Ankomah and Ettensohn, 2013). Whereas the receptors *vegfR* and *fgfR2* are expressed in the PMCs, experiments inhibiting either the fgf/fgfR2 or the vegf/vegfR pathway showed incorrect positioning of the PMCs and thus abnormalities in skeleton development. Furthermore, the extension of the skeleton towards the animal pole was shown also to be dependent on vegf/vegfR signalling (Adomako-Ankomah and Ettensohn, 2013). Inhibition of vegfR in sea urchin does not down-regulate all differentiation genes (Duloquin et al., 2007), but sufficient to inhibit skeleton formation. This signalling, can thus be understood as a sort of checkpoint. If the cells are in the right positions, then an additional signalling input will trigger the activation of some bio-mineralisation components such that a correct skeleton can be formed.

Interestingly, many downstream genes are already transcribed before ingression of PMCs, *e.g. msp130r1* (Illies et al., 2002), *p19* (Costa et al., 2012), *sm50* (Oliveri and Davidson, 2004) and more; while others such as *sm30* (Wilt et al., 2013) will only be express late when bio-mineralisation is formed. This indicates that transcription of these genes in the correct proportions

is needed in order to physically assemble the skeleton. As mentioned earlier, this is the final tier of the hierarchical GRN. Consistent with the scale-free nature of such networks, recently, the differentiation cascade has been extensively enlarged. Whereas the regulatory part consists of roughly 24 genes (based on Oliveri et al. (2008); Barsi et al. (2014)), studies using proteomic or next generation sequencing approaches identified around $\sim$1000 genes expressed or involved in this process (Rafiq et al., 2012; Mann et al., 2010a,b) and for many of those a linkage of was detected by inhibition of either *alx1* or *ets1/2* (Rafiq et al., 2014).

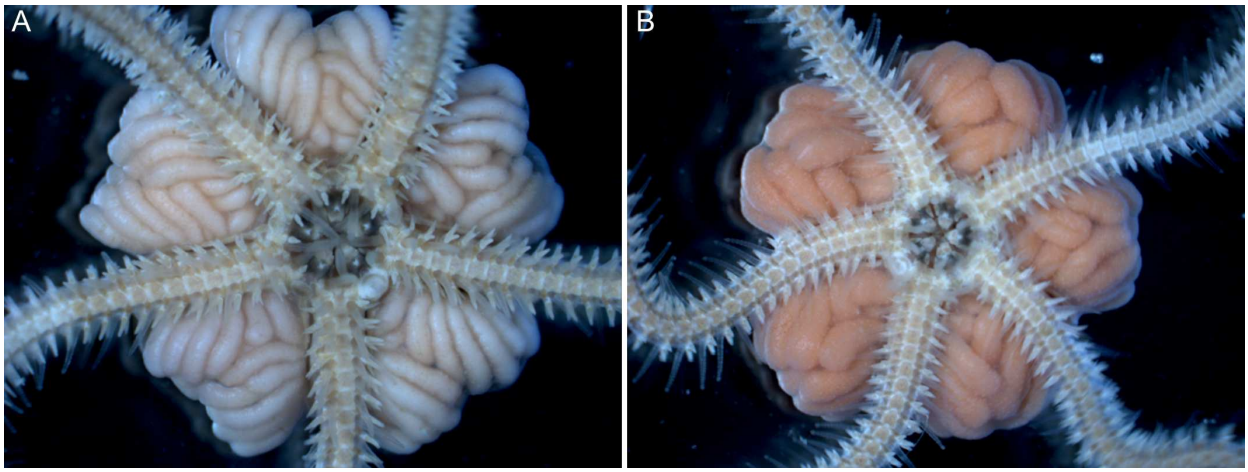

Figure 1.17: **Adult Brittle Stars.** Oral view of (A) male and (B) female *A. filiformis* adults. (B) The gametes of different color are produced in the trophic gonads within the bursae.

1.5 The brittle star *Amphiura filiformis*

The brittle star *Amphiura filiformis* (Müller, 1776) is part of the Ophiuroidea taxon and belongs to the burrowing brittle stars, described by (Buchanan, 1964). *A. filiformis* is radially symmetric, a characteristic shared by all the echinoderms. Male and female adults exhibit sexual dimorphism only during the reproductive seasons when their gonads are present at the oral side (Peterson et al., 2000) of the animal, shown in Figure 1.17. They are otherwise indistinguishable between each other. This type of brittle stars are suspension feeders and collect food in the sea by exposing one arm out of the mud and transporting sea particles along the arm into the mouth located at the central disk of the animal (Buchanan, 1964; Loo et al., 1996). *A. filiformis* has its reproductive season from mid summer to beginning of autumn in the North Western European waters (Bowmer, 1982). In Sweden the reproductive peak is reached between June to August (Skold et al., 1994). During this period the brittle star rises from the mud and lift up from the surface contracting its five arms. The central disk is lifted and the gonads on the oral part of the body are released into the water.

Very little is known about development of brittle stars and all studies performed are scattered among various species. Cell lineage studies were performed in *Ophiopholis aculuata*, showing

that brittle stars do not form micromeres and that at 8 cell stage their skeletogenic lineage is not yet segregated from other endomesodermal lineages (Primus, 2005). Despite their very similar appearance, the pluteus larvae of these two echinoderm classes show several differences: specifically their calcified structures have different sensitivity to ocean acidification (reviewed in (Dupont et al., 2010)). On the other side, a transcriptome analysis of a *Ophiocoma wendtii* gastrula stage identified several genes orthologous to sea urchin skeletogenic genes suggesting a similar molecular make up of these structures (Vaughn et al., 2012). Furthermore, the only embryonic gene expression studies reported so far have been carried out in the brittle star species *Amphipholis kochii* on a transcription factor, *ets1/2*, and two signalling molecules, *vegf* and *vegfR*. The expression patterns in the brittle star and in sea urchin embryos are remarkably similar, supporting the similarities of larval skeleton development between brittle stars and sea urchins (Hirokawa et al., 2007; Koga et al., 2010).

1.6 Modern approaches in new organisms

As seen in the last section, in comparison to sea urchin developmental biology, information about brittle stars is very sparse. In order to establish molecular tools and quickly advance the knowledge about brittle star developmental biology, next generation mRNA sequencing provides a fast method to obtain information about whole organism genes and expression. In this section, I will describe the general principles behind mRNA sequencing with focus on the Illumina platform that was also used for this study. I will briefly discuss various bio-informatics strategies for *de novo* assembly and quantification.

1.6.1 mRNA sequencing

RNA sequencing allows the measurement of gene content and expression of all RNA in a sample of interest. Samples can be whole organism or different cell types. For next generation sequencing the general experimental procedure can be summarised as follows. A library of cDNAs, with attached adapters on both ends is prepared from extracted mRNA. To sequence this library in a high-throughput manner the individual cDNAs are fragmented into shorter pieces. This library is then sequenced, either amplified or not amplified. In Illumina sequencing the fragmented sequences with adapters are then processed on a flow cell. The basepair composition is detected by primer ligation on the free end and extension of the fragment, for which a distinct fluorescent signal is released during the addition of each basepair onto the fragment. Sequences are obtained either from one end (single-end sequencing) or from both ends (paired-end sequencing). Depending on sequencing technology and experimental set up the reads are usually 30-400bp long (reviewed in (Wang et al., 2009)). In general, RNA-seq is a powerful approach to obtain data at a whole transcriptome level with unprecedented sensitivity and accuracy (Ozsolak and Milos, 2011; Wang et al., 2009; Marguerat and Bähler, 2010; Wilhelm and Landry, 2009). Compared with expressed sequence tag (EST) sequencing and microarray chips, RNA-seq has a substantially higher dynamic range, has single-nucleotide resolution and allows reliable identification of

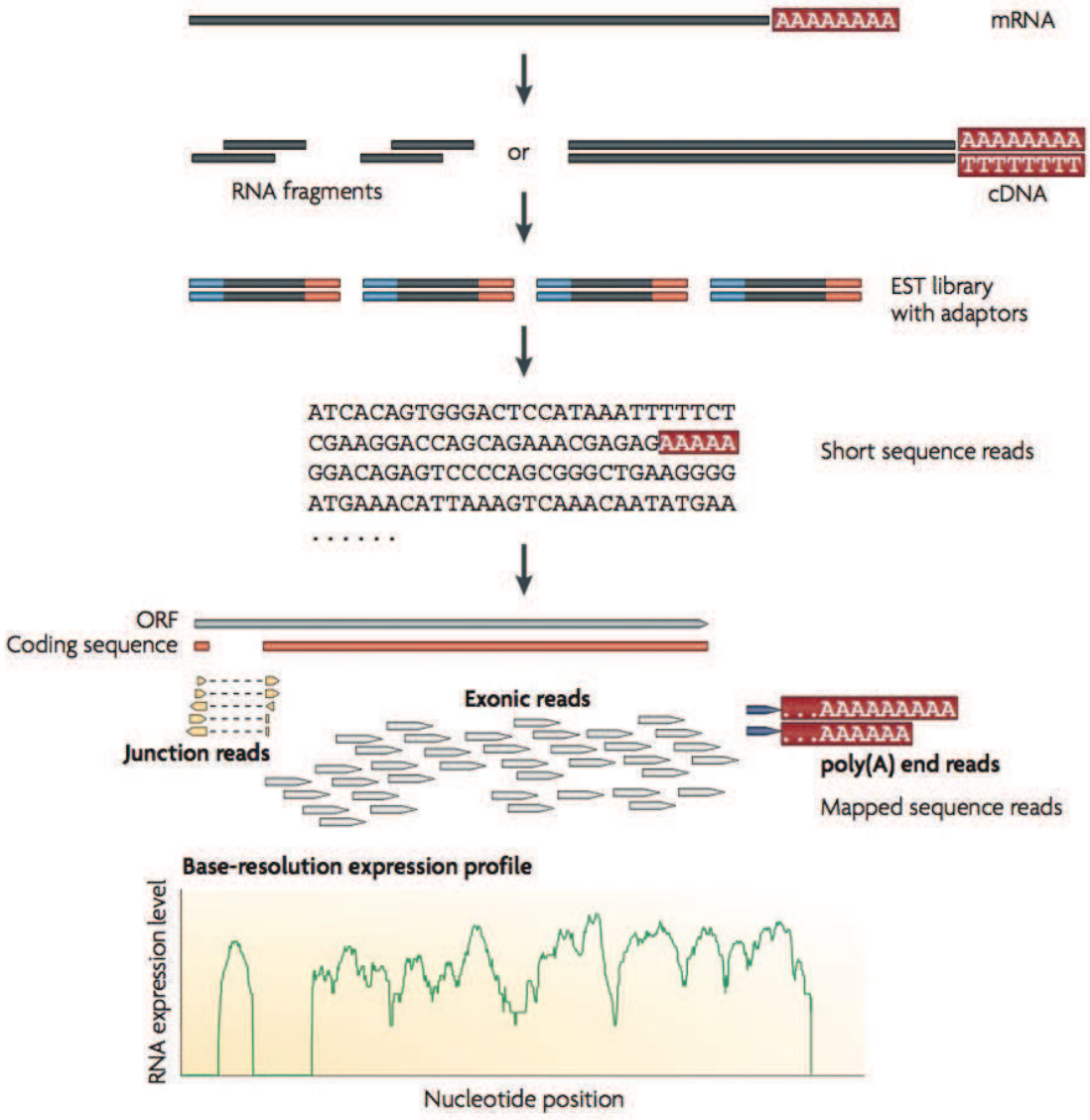

Figure 1.18: **RNA sequencing.** Figure displays procedure for RNA sequencing. ORF stands for open reading frame. Figure was taken from Wang et al. (2009).

rare transcripts and alternative splicing (Wang et al., 2009; Marguerat and Bähler, 2010; Wilhelm and Landry, 2009; Marioni et al., 2008).

1.6.2 Bio-informatics for transcriptomics

1.6.2.1 Assembly

The purpose of RNA-seq for organisms lacking a genome is two fold. First, one wants to obtain information about sequences of the RNA molecules, and second, about their quantity in the sample. The starting point of any transcriptome analysis are the reads. Reads are sequences with single-letter base calls and their numeric quality value for each base call (Ewing and Green, 1998). Before starting the assembly, reads are usually pre-processed (low quality basepairs are removed and adapters are trimmed). There are several tools available facilitating this process, *i.e.* Trimmomatic (Bolger et al., 2014), CutAdapt (Martin and Wang, 2011) and more (comparison in (Chen et al., 2014)). Importantly, it has been shown that this pre-processing step improves the assembly and re-alignment rate (Del Fabbro et al., 2013; Bolger et al., 2014).

In order to find what genes are expressed in a sample the processed reads can be either re-aligned to a genome, if available, or assembled *de novo*. In general, an assembly groups reads into contigs. Due to their short read length, full-length assembly of transcripts is computationally challenging. As such, assembly of a transcriptome cannot be compared to the assembly of a genome due to the following reasons: 1) The abundance of different transcripts varies in mRNA samples causing variation in transcript sequencing depth (Martin and Wang, 2011). DNA sequencing depth, on the other hand, is expected to be the same across a genome. 2) Genome assembly does not have to deal with splice variants as does transcriptome assembly. Thus, transcriptome assembly requires several transcripts to be assembled for the same locus (Chang et al., 2015).

Before the development of assembly programs specifically designed for *de novo* transcriptomes, genome derived assemblers were applied *i.e.* ABySS (Birol et al., 2009), SOAPdenovo (Li

et al., 2009a), Oases (Schulz et al., 2012), and SOAPdenovo-Trans (Xie et al., 2014). However, these performed poorly due to the different assumptions underlying a genome versus a transcriptome. In cases where a closely related species is available, Vijay et al. (2013) showed in an *in silico* study that direct re-alignment of reads performs better than *de novo* assembly. Nevertheless, for cases where a reference genome is available other approaches are better suited, but are not discussed further here (reviewed in (Martin and Wang, 2011)). Grabherr et al. (2011) released the first assembly software specifically designed for a transcriptome problem called Trinity. Trinity first assembles large contigs directly from the reads, then it builds many de Brujin graphs from these contigs and finally searches for all the paths in these graphs that represent splicing isoforms (Grabherr et al., 2011). In de Brujin graphs a node represents a word and is connected to other nodes that shares the same word but differ in one letter either at the beginning or the end of the word. These words are also called k-mers, where k defines the length of the word. A drawback of Trinity is its false-positive rate that is generated due to its sensitivity to detect splice-variants. This has been shown to be dependent on the length of k. Generally, smaller k values perform better for transcripts that are lowly expressed or are shorter and higher k values for transcripts that are highly expressed or are longer. Therefore, novel assembly strategies have been released incorporating different lengths of k-mers in the assembly, *i.e.* Trans-ABySS (Robertson et al., 2010), Oases-M (Schulz et al., 2012) (multiple-k version of Oases), IDBA-Tran (Peng et al., 2013) and Bridger (Chang et al., 2015). Recently, Chang et al. (2015) compared several of these assemblers in terms of accuracy and number of full length reconstructed references on three mammalian datasets (dog, human and mouse). For accuracy Bridger outperformed the other assemblers and for full length reconstructed sequences Bridger performed comparably to Trinity.

Another approach to circumvent non-uniformity of RNA-seq reads is to normalise the processed reads *in silico* before assembly. Brown et al. (2012) developed such an approach to *in silico* to normalise the reads, called digital normalisation. This method organises the coverage of transcripts by removal of highly redundant reads, thereby removing the majority of errors and

decreasing sampling variation. Additionally, Lowe et al. (2014) showed that the reduced amount of reads decreases the assembly time. In conclusion, many strategies exist for *de novo* transcriptome assembly that get continuously updated and extended with new software, ultimately improving the transcript recovery in terms of accuracy and completeness.

1.6.2.2 Quantification

Once the contigs are successfully assembled, it is possible to quantify the transcriptome by re-alignment of the processed reads. Due to fact that *de novo* assemblers produce much more isoforms of a gene than actually exist, mapping of reads is not an easy task if no reference genome is available. Generally, quantification involves two steps: first, the reads are re-aligned on the reference and second, abundance is estimated for isoforms and genes based on the mapping.

For the alignment of reads, the two major approaches are spliced and unspliced aligning. The first will not be discussed here any further because it only applies when a reference genome is available (reviewed in Garber et al. (2011)). Unspliced aligners can be grouped into two categories. The first are based on Burrows-Wheeler transformations. This transformation compacts the transcriptome in a data structure that is very efficient when searching for perfect matches (Burrows and Wheeler, 1994; Ferragina and Manzini, 2001). Examples for such aligners are BOWTIE (Langmead et al., 2009) and BWA (Li and Durbin, 2009). Unfortunately, the performance of this method decreases exponentially with the number of mismatches. This exponential decrease is caused by its iterative search for perfect matches (Langmead et al., 2009; Li et al., 2009b; Li and Durbin, 2009). Thus, it is as reliable as the quality of the reference. The other alignment procedure is based on ”seed methods” (Homer et al., 2009; Jiang and Wong, 2008; Li et al., 2008a,b; Lunter and Goodson, 2011; Smith and Davidson, 2008). This method finds matches for short subsequences, termed ”seeds”, under the assumption that at least one seed in a read will perfectly match the reference. Each seed is then used to narrow candidate regions

where more sensitive methods (such as Smith-Waterman) can be applied to extend seeds to full alignments. This type of unspliced aligner are perfectly suited to map reads against a reference from a distant species (Garber et al., 2011). On the other hand, if an ideal reference is available, Burrow-Wheeler methods outperform seed-based methods (Garber et al., 2011).

Once the reads are successfully aligned onto a reference, in a next step the abundance is calculated. The simplest way of calculating abundance is by counting the number of reads that map uniquely to each contig (Marioni et al., 2008; Nagalakshmi et al., 2008), and by taking into account how well a contig can be aligned to (Morin et al., 2008). This approach, however, comes with several drawbacks. For example, the count can be incorrectly estimated for individual isoforms (Wang et al., 2010) because the same read can be mapped onto several contigs and others. In order to compensate for this problem several methods have been developed, but most of them rely on a genome as reference. However, two methods exist that have the ability to work only with a reference transcriptome. They are RSEM (Li and Dewey, 2011) and CORSET (Davidson and Oshlack, 2014). Both use BOWTIE as an aligner for the reads before calculating expression values. RSEM uses a maximum likelihood approach to address read-mapping uncertainty and estimates the number of fragments that are derived from a given contig (Li et al., 2009a). Thus, RSEM is compensating for the ability of a read to be aligned to multiple genes or isoforms. Especially, reliable results are obtained for the gene count (sum of isoform counts) and it has been shown that RSEM performs equally or better to other quantification methods (Li and Dewey, 2011). However, the RSEM gene counts rely on a pre-computed list of which isoforms belong to which genes. Trinity by default, outputs each contig (isoform) with an identifier as to which cluster of contigs (gene) it belongs to. More precisely, a gene is all paths with overlaps from the de Brujin graph. Other ways of clustering exist and can also be applied, *e.g.* UCLUST (Edgar, 2010) or CD-HIT (Fu et al., 2012). These clustering approaches group genes by a user defined sequence similarity and do not perform well with splice variants. An implementation for transcriptome quantification, including the clustering of contigs into genes before estimation of count values, is included in the CORSET

procedure. Corsets hierarchically clusters the contigs based on the proportion of shared reads and expression patterns if mutliple samples are available. In this way expression pattern clustering allows discrimination between paralogs. Corset was shown to outperform other clustering approaches in terms of recall (the ratio of true positives over true positives plus false negatives) and precision (the ratio of true positives over true positives plus false positives) for assemblies of yeast, chicken and human using either Trinity or Oases assemblies (Davidson and Oshlack, 2014). In particular, for differential expression analysis Corset showed much more reliable results than other approaches.

Chapter 2

HYPOTHESIS

In development, a single cell divides and creates new territories that communicate with each other through signalling and get specified by a unique combination of active regulatory genes until their final fate is reached. These events are observed in changes of quantitative and spatial expression of genes in time but also in the spatial arrangement of the embryo. As I have introduced, one way to incorporate changes in space and time is by modelling development with GRNs. Because GRNs provide a system level understanding of development they provide a unique opportunity to study evolution in terms of re-wiring.

The general aim of this study consists in understanding mechanisms of GRN re-wiring during evolution. In order to study evolutionary changes in body plan, two points are of major importance. First a well-established GRN is needed and second a class of animals that develop similarly but have maintained, lost or acquired a morphological character. Echinoderms fulfil both conditions: 1) The GRN for *S. purpuratus* development is the most extensively studied in all developmental systems (Oliveri et al., 2008; Rafiq et al., 2012, 2014; Barsi et al., 2014) and particular attention has been given to endomesoderm formation for which other echinoderm classes (star fish and sea cucumber) have been included. 2) The extended larval skeleton that forms from a subset of mesodermal cells is only to be found in two out of the four classes of the Eleutherozoa. Compared to other studies in closely related species, echinoderms allow to study the evolution of GRNs throughout the whole phylum.

To complete the picture a detailed molecular characterisation of brittle stars was missing.

Therefore, in this thesis, I am filling an important gap in echinoderm comparative GRN studies. More specifically, in this study I am introducing the brittle star *Amphiura filiformis* as novel developmental system and I am dissecting for the first time the cellular events and molecules involved in mesoderm development. I then analyse the results in context of echinoderm evolution and general mechanisms of GRN evolution. Based on the initial hypotheses that the development of the larval skeleton in ophiuroids and echinoids is morphologically similar but is exectued by different GRNs, mostly due to a 480 million years of independent evolution, I designed an experimental approach divided in two major parts aimed at identifying differences and similarities in the GRN nodes underlying mesoderm development and more specifically the development of the larval skeleton.

First I describe a candidate gene approach based on isolation and high-resolution characterization of orthologs to sea urchin skeletogenic and mesodermal genes along with *A. filiformis* morphological observation, with the aim to answer the following questions:

- What is the developmental mode (stages of development and speed in natural conditions) of *A. filiformis*?
- Which cells are giving rise to the larval skeleton?
- What is the dynamic of regulatory states of these cells during development?
- What similarities and differences in GRNs between *S. purpuratus* and *A. filiformis* can be identified?

Second, I describe an unbiased approach that is based on a *de novo* developmental transcriptome in the brittle star and differential screening in embryos with impaired skeleton development, with the aim to build a global view of mesoderm development in *A. filiformis* and answer to the following questions:

- What genes are expressed in *A. filiformis* development?

- Which orthologs to *S. purpuratus* genes are present in the brittle star?
- What is the core set of genes involved in skeleton formation in echinoderms?
- What genes are unique for the brittle star development of the larval skeleton?

I finally, bring my findings in an evolutionary context with the aim to address the unsolved question of independent or common origin of larval skeleton in echinoderms.

Part I

Evolution of gene regulatory network for specification of skeletogenic lineage in Echinoderms

Chapter 3

METHODS

3.1 Embryological techniques

3.1.1 Animal collection and embryo culture for the brittle star *Amphiura filiformis*

Animal collection and embryo culture were set up similar to the protocol described in (Dupont et al., 2009). Adult animals of *Amphiura filiformis* were collected during their reproductive season (July-August) in the Gullmarsfjörd, Sweden. Sediment from the bottom of the fjörd was collected at various locations in the vicinity of the Kristineberg marine station (Sven Loven Centre for Marine Science, Sweden) using a boat equipped with an Ekman Sediment Sampler. The animals buried in the softer upper part of the sediment were moved with a spade into buckets on the boat and residual mud was discarded back into the fjörd. At the marine station all animals were kept in buckets with sediment under constant sea water (SW, salinity between 30-35ppt salt) flow for long term storage. For usage the animals were sieved from the mud and kept in buckets under constant SW flow at 14°C in a thermostatic chamber. Food for the animals was provided by the highly rich organic matter present in the mud.

To induce spawning in *A. filiformis* 5 male and 15 females were put together into a beaker. The animals were heat-shocked at 28°C for 15min while exposed to sunlight and then transferred back to 14°C SW and kept in the dark at a constant temperature of 14°C. The animals were observed approximately every 10min for any sign of spawning. Once spawning occurred the eggs were checked for the presence of a fertilisation membrane under a dissecting-scope and fertilisation efficiency was estimated. Fertilised embryos (E) were washed several times with filtered sea water

(FSW) to remove debris and excess of sperm. If only males spawned, the animals were left in the beaker for longer to induce female spawning. Sperm were also collected dry by dissecting the male bursae and kept on ice for several hours. To activate the sperm a single bursa was squeezed in FSW to release the sperm. The active sperm were then added to the unfertilised eggs when only females had spawned. For each culture fertilisation efficiency and number of embryos were estimated and the culture was diluted to 10 embryos per ml for optimal development at 14°C.

In the following steps the desired number of embryos (1,000 E to 10,000 E) was concentrated using a 70µm nitex mesh and then transferred into 1.5-2ml Eppendorf tubes for further treatments. In cases where embryos developed in plates, the concentration step with the Nitex mesh, was skipped. Depending on the purpose of a culture small adjustments had to be made. To soften the fertilisation membrane, when pre-hatching embryos were needed, Trypsin (Sigma) (c_f = 1mg/ml in FSW) was added to the fertilised eggs for two hours, followed by several washes. For post-hatching embryos no such procedure was necessary.

3.1.2 Animal collection and embryo culture for the sea urchin *Strongylocentrotus purpuratus*

Adult sea urchins of the species *Strongylocentrotus purpuratus* were obtained from Pat Leahy (Kerchoff Marine Laboratory, California Institute of Technology, USA). On arrival, the animals were kept in large tanks of artificial seawater ($\sim$36ppt salt, Instant Ocean Acquarium Sea Salt Mixture) at 12-13°C, and fed regularly with seaweed (*Ulva lactuca*) from the Mediterranean sea.

When sea urchin embryos or larvae were required, mature adults were initially induced to spawn by vigorous shaking and, if necessary, intracoelomic injection of 0.55M KCl into the soft tissue around the mouth. Because sea urchins show no sexual dimorphism, it is only possible to identify male and female individuals after spawning. Eggs were collected by placing a female upside-down in a glass beaker filled with filtered artificial seawater (FASW). FASW was made up by 28.3g NaCl, 0.77g KCl, 5.41g $MgCl_2.6H_2O$, 3.42g $MgSO_4$, 0.2g $NaHCO_3$, 1.56g $CaCl_2$

dehydrate in 1 litre of deionized H_20 and pH adjusted to 8.2 and a salinity of 34 ppt. This was then filtered through a 0.45µm filter unit (Nalgene) and allowed to settle by gravity. All glassware and plastic used for animals and embryos cultures were kept free from any detergent and washed only with deionized H_2O as detergent can disturb normal development of the embryos. Concentrated sperm (dry sperm) was collected using a pipette and kept on ice until it was used for fertilisation or alternatively, stored at 4°C for up to two weeks. Collected eggs were passed through a 70µm nitrex mesh to remove debris and washed twice with FASW. Sperm was activated by dilution of 5-10µl of concentrated sperm in 10ml of FASW and used to fertilise the eggs.

Embryos that were required for microinjection or were fixed before hatching, were fertilised in 2mM Para Amino Benzoic Acid (PABA) in FASW, to avoid the hardening of the fertilisation membrane. Successful fertilisation was checked by elevation of the fertilisation membrane and then two washes were carried out to remove remaining sperm. Developing embryos were cultured in FASW at 15°C and a mixture of Streptomycin (50 µg/ml) and Penicillin (20U/ml) were used as antibiotics to stop bacterial growth.

3.1.3 Staining of skeletal elements using calcein

Calcein was added at a final concentration of 100µg/ml to embryo culture and incubated for several hours, following several washes with FSW. Embryos were imaged at various time-points.

3.2 Bioinformatic Techniques

3.2.1 Primer design

3.2.1.1 General design

Cloning and QPCR primers were designed using primer3[1], described in (Rozen and Skaletsky, 2000) with the following changes from default parameters:

Max 3 Stability: 8 (instead of 9),

[1] http://bioinfo.ut.ee/primer3/

Max Poly-X: 3 (instead of 4),

Product size range QPCR: 120-180nt,

Product size range cloning: >500nt.

All primers were mapped back onto sequence and checked for similarity against other genes using blastn against a database for the species of interest. All primers sequences used in this study are listed in Appendix A.

3.2.1.2 Degenerate primers

Before the availability of sequencing data, primers were designed by multi-alignment using ClustalW[2] (Thompson et al., 2002) of orthologous sequences that were obtained from GenBank[3]. Degenerate primers were chosen from regions that were highly conserved with a length bigger than 20bp.

3.2.1.3 RACE primers

Primers for rapid amplification of cDNA ends (RACE) were designed using primer3, as described above. For each sequence two primer-pairs were obtained (outer and inner). Outer primers were designed as above. Inner primers, also called nested primers, were designed by either moving the outer primer by at least 5bp in 5' to 3' direction or by taking the sequence within the outer primer as input to primer3 (Rozen and Skaletsky, 2000).

3.2.2 Phylogenetic analysis

3.2.2.1 Identification of orthologs

Orthologs to a list of sea urchin skeletogenic genes were identified using a blast search against a *Amphiura filiformis* database of a development transcriptome (see Part II). Obtained candidates were reciprocally confirmed as potential orthologs against a *S. purpuratus* peptide database using

[2] http://www.ebi.ac.uk/Tools/msa/clustalw2/
[3] http://www.ncbi.nlm.nih.gov/genbank/

blast. Blast e-value was set to 1e-6 in both cases. For details see main text.

3.2.2.2 Phylogenetic gene tree re-construction

To specifically determine orthology of genes, a number of genes was selected using a BLAST search on various echinoderms, deuterostomes and the non-redundant (nr) database. Sequence alignments on their amino-acid sequences were performed using MAFFT[4] v7 (Pfaffl et al., 2004) with default parameters. Most conserved alignments were selected using GBlocks[5] (Talavera and Castresana, 2007) with all options activated for less stringent selection (Selected options: "Allow smaller final blocks", "Allow gap positions within the final blocks" and "Allow less strict flanking positions"). Phylogenetic tree was estimated with MEGA[6] (Tamura et al., 2011) using a JTT model with gamma distribution, invariant sites with 500 bootstraps and with PhyloBayes[7] (Lartillot and Philippe, 2004, 2006; Lartillot et al., 2007) using a CAT-GTR model. PhyloBayes was run until the largest discrepency observed across all bipartitions was below 0.1.

3.3 Molecular techniques

3.3.1 RNA Extraction

Total RNA samples were extracted from embryos of different developmental stages. After a brief spin of 30sec at max speed the remaining FSW was removed, leaving a compact pellet of embryos at the bottom of the tube, which was resuspended in at least 10 volumes of RLT (Qiagen). This was followed by extensive vortexing (1min at least), in order to completely lyse the embryos. Initially, the samples were stored at -80°C for later RNA extraction. For each sample it was noted how many embryos were used. For each RNA extraction we used at least 100 E applying the Ambion RNAqueous Micro kit (Life Technologies). For the extraction to 1 volume of RLT, 1 volume of lysis buffer was added, then the mix was vortexed and finally incubated at 65°C for 10min,

[4] http://mafft.cbrc.jp/alignment/software/
[5] http://molevol.cmima.csic.es/castresana/Gblocks_server.html
[6] http://www.megasoftware.net
[7] http://www.atgc-montpellier.fr/phylobayes/

then on ice for 5min. After this step the rest of the RNA extraction followed the manufacturers protocol. For every sample DNAse treatment was carried out as described in the protocol. After each extraction the concentration of RNA was measured using the spectrophotometer Nanodrop 2000c. For 1000 E we usually extracted 0.7µg to 1.5µg.

3.3.2 cDNA Synthesis

3.3.2.1 cDNA synthesis for QPCR

For quantitative polymerase chain reaction (QPCR) the extracted total RNA from 1,000 E was reverse transcribed into cDNA using the iScript cDNA Synthesis Kit (BioRad) according to manufacturer instructions. The cDNA was synthesised in a 20 l reaction from up to 1 g of total RNA, which uses a mixture of both oligo(dT) and random primers in order to guarantee an unbiased copy of different target sequences. The reagents were kept on ice but the reaction was set up at room temperature according to manufacturers instructions. The reaction was incubated in a BioRad thermal cycler using the following conditions: 25°C for 5min, 42°C for 30min, 85°C for 5min, and finally 4°C forever. All samples were diluted to a final concentration of 2 embryos/µl. To estimate absolute abundance levels of transcripts per embryo the Ambion TaqMan Cells-to-C_T Control Kit (Life Technologies) was used as a spike-in control. In a solution of 1,000 E in 100µl of RLT 1,000,000 XenoRNA transcripts were added, for an equivalent of 1,000 transcripts per embryo, followed by the extraction procedure described in chapter 3.3.1. QPCR was performed on an ABI 7900HT machine.

3.3.2.2 cDNA synthesis for regular cloning

For regular cloning cDNA was synthesised as for QPCR, but was diluted to 10 ng/µg using DEPC H_2O and stored at 20°C.

3.3.2.3 cDNA synthesis for RACE

For RACE (see below), a cDNA library was prepared using the FirstChoice RLM-RACE Kit (Life Technologies). 5' and 3' libraries for RACE were produced using total RNA from 5hpf, 25hpf and 72hpf. For the 5' library, for each time point 10µg of total RNA were used . Briefly, the 5' library is made by first removal of 5' PO_4 from degraded RNA and DNA, followed by cap removal from full-length mRNA, then adapter ligation on the 5' end of the mRNA and reverse transcription with random decamers. All reactions were set up according to manufacturers instructions. The 3' library was set up using 1µg of total RNA. For this reaction the RNA was directly reverse transcribed, in which the random decamers were replaced with the 3'RACE adapaters. This reaction was set up according to manufacturer instructions.

3.3.3 Quantitative polymerase chain reaction (QPCR)

All QPCR experiments followed the guideline presented in (Materna et al., 2013; Rast et al., 2000). All combinations of primers and cDNA were set up on at least 3 technical replicates on a 384 well plate using 9µl of reaction containing a cDNA amount corresponding to 1 E and Ambion Power SYBR Green reaction mix (Life Technologies). H_2O was used instead of cDNA for negative control. For time-course the internal standard *Afi-16S* was used, whereas for differential expression *Afi-UCE* (ortholog to sea urchin ubiquitin SPU_023613) was used. For the spike-in control the primer set part of the Ambion TaqMan Cells-to-C_T Control Kit (Life Technologies) was used. Other internal standards were tested using the bestkeeper analysis (Pfaffl and Pfaffl, 2001) including the spike-in control (*Afi-16S* and *Afi-UCE* vs bestkeeper showed high correlation $>$0.82) and both genes showed the highest correlation against the spike-in (*Afi-16S*: 0.94; *Afi-UCE*: 0.78). The final primer concentration for all experiments was 0.3µM for each primer. The PCR was done as two steps PCR: after an initial denaturation step at 95°C for 10 min, 40 cycles of 1 min at 60°C and 15 sec at 95°C, a final dissociation step was added to ensure a single fragment was amplified. Quality of QPCR results was evaluated using dissociation curves.

QPCR counts the cycle number at the threshold (C_t) for successful amplification by means of fluorescence detection. Normally, successfully amplified fragments have a C_t between 12 to 31. The water negative control was usually expected to be undetected or to have a C_t value at least 4 times bigger than the sample. After 32 cycles, the technological error makes it difficult to assess reliable amplification. The relative transcript abundance was estimated using the following set of equations.

$$\Delta C_t = C_t(\text{Gene}) - C_t(\text{Internal Standard}) \tag{3.3.1}$$

$$FC = 1.9^{(-\Delta C_t)} \tag{3.3.2}$$

$$Expression = 1,000,000 \cdot FC \tag{3.3.3}$$

The fold change (FC) is calculated by assuming an amplification efficiency of 1.9, however, in theory PCR should double the transcripts under optimal conditions. Expression was calculated by multiplication with 1,000,000 to shift all values towards whole numbers.

3.3.4 Embryo fixation

All embryos of different developmental stages were fixed in a solution containing 4% PFA, 32.5% FSW, 32.5mM MOPS pH7, 162.5mM NaCl final concentrations (c_f) overnight at 4°C. The fixation step was followed by 3 washes in MOPS buffer (c_f: 0.1M MOPS pH7, 0.5M NaCl and 0.1% Tween-20) on ice or at 4°C. The embryos were stored indefinitely in 80% EtOH at -20°C.

3.3.5 Molecular cloning

The general strategy for cloning can be summarised as follows: before sequencing data was available degenerate cloning was used as means to ”fish out” genes. If the obtained fragment was longer than 500bp, then it was immediately used for further procedures. If it was shorter than 500bp, RACE was applied to obtain longer fragments. Once sequencing data was available regular cloning was used to obtain fragments of interest. For the genes *Afi-ets1/2*, *Afi-tbr*, *Afi-*

alx1, *Afi-foxB* and *Afi-dri* cloning was performed using degenerate primers, listed in Appendix A and subsequent RACE when needed. All other genes were cloned using primers designed on fragments which were determined using the reciprocal blast search with sea urchin candidate genes in an *A. filiformis* transcriptome database, described in part II.

3.3.5.1 Polymerase chain reaction (PCR)

Independent of cloning method, all PCR reactions were set up using the High Fidelity kit (Kapa or Roche) and performed on a BIO RAD C1000 Thermal Cycler. The cycling conditions were used as described by the individual PCR-kits. Annealing temperature was set as a gradient between 50-65°C. In general 30sec per 500bp were used for extension times. If known, a stage of cDNA was used as template in which the gene of interest showed peak of expression. For fragments with unresolved temporal expression pattern a cDNA mix was used containing the stages 2hpf, 12hpf, 24hpf, 36hpf, 48hpf and 72hpf. Each PCR reaction ran for 30-40 cycles. Cycling conditions for cloning with Roche and KAPA were set as described by the manufacturer. All PCR reaction set-ups are described in Table 3.1.

3.3.5.2 PCR for RACE

For RACE, PCR was performed twice. The first reaction was performed using as forward primer the outer primers, one designed on the fragment of interest and one provide by the RLM RACE kit. Outer RACE used either the 5' or the 3' cDNA library as template. The resulting reaction was cleaned using the Nucleospin Gel and PCR Clean up kit (Machinery and Nagel) and subsequently used as template for the second reaction using the inner primers, one designed and the other part of the RLM RACE kit. Extension times for RACE were predicted based on alignment of *A. filiformis* transcript to *S. purpuratus* exon sequence. Each PCR reaction was performed as shown in Table 3.1. With cycling conditions as described above. RACE primers can be found in the manual of the FirstChoice RLM-RACE Kit (Life Technologies).

Table 3.1: PCR reactions

Ingredients	Cloning Roche	Colony In-vitrogen	Probe Roche	**Ingredients**	Cloning Kapa
10X Buffer	5µl†	2µl	5µl	5X Buffer	10µl
$MgCl_2$	-	0.75mM	1.5mM	$MgCl_2$	-
dNTP	200µM	200µM	200µM	dNTP	300µM
Forward Primer	0.4µM	0.4µM	0.3µM	Forward Primer	0.3µM
Reverse Primer	0.4µM	0.4µM	0.3µM	Reverse Primer	0.3µM
cDNA	10ng	2µl††	2ng	cDNA	4E
Taq	1.4U	1U	1.75U	Taq	1U
H_2O	up to 50µl	up to 20µl	up to 50µl	H_2O	up to 50µl

†10X Buffer with 15mM $MgCl_2$

††2 µl of a single colony inoculated for one hour at 37°C in 20µl LB-Broth

Table 3.2: PCR cycling

Procedure Steps	Colony PCR	Probe Template
1 Initial Denaturation	95°C 5min	95°C 5min
2 Denaturation	94°C 5min	94°C 5min
3 Annealing	55°C 30sec	55°C 30sec
5 Elongation	72°C Xsec	72°C
GO TO 2	25times	30times
6 Final Elongation	72°C 5min	72°C 5min
7 Cooling	0°C ∞	0°C ∞

3.3.5.3 Ligation, transformation and plasmid extraction

Finished PCR runs were checked on an agarose gel (0.8-1.2%) and visualised with ethidium bromide for successful amplification. Fragment length was estimated on the same gel using a Invitrogen 1kb DNA Plus Ladder (Life Technologies). The successfully amplified fragments were either PCR purified or gel extracted using the Nucleospin Gel and PCR Clean up kit (Machinery and Nagel). The purified fragments were then ligated into either pGEMt-easy (Promega), Topo pcr II (Life Technologies) when amplified with High Fidelity (Roche) or Topo pcr II Blunt (Life Technologies) or pcr Blunt (Life Technologies) vector when amplified with High Fidelity kit (Kapa). All the ligations were transformed using either Subcloning Efficiency Invitrogen DH5α Competent Cells (Life Technologies) or One Shot Top10 Chemically Competent E. Coli (Life Technologies) following manufacturers instructions. After each transformation selected colonies were individually picked and inoculated in 20µl LB Broth plus the selective antibiotic (Ampicillin c_f 100µ/ml, Kanamycin: c_f 50µ/ml), corresponding to the used vector, for roughly one hour at 37°C. To check for incorporation of gene fragment colony PCR on the selected colonies with T7 and Sp6 primers and the Invitrogen Taq polymerase (Life Technologies) was used. The Invitrogen polymerase amplifies with a speed of 1000bp per 30sec and was adjusted based on observed cloning fragment length to each individual sample. Reaction set up can be found in Table 3.1 and cycling conditions in Table 3.2. Colonies with plasmid and fragment were selected for growing overnight in 4ml LB Broth plus the according antibiotic (Ampicillin c_f 100µ/ml, Kanamycin: c_f 50µ/ml). 500ml of successfully grown colonies were stored with 500ml 50% Glycerol at -80°C as stock and the rest was applied for plasmid DNA purification using the Nucleospin Plasmid Kit (Machinery and Nagel). All plasmids were checked using EcoRI digestion (Promega) for incorporation and correct size of the fragment following manufacturers instructions. For sequencing 10µl of successfully cloned fragments incorporated in a plasmid were diluted to 100ng/µl and send for sequencing at the UCL Cancer Institute and Wolfson Institute for Biomedical Research. A summary of all the primers can be found in Appendix A.

3.3.6 Synthesis of antisense RNA probes

Templates for RNA transcription were prepared using PCR on plasmids diluted to 2ng/µl with primers outside of the T7 or SP6 promoter sites such as M13-forward and M13-reverse (for sequences see appendix). This PCR reaction was performed using the Invitrogen Taq DNA Polymerase (Life Technologies). Reaction set up can be found in Table 3.1 and cycling conditions in Table 3.2. Most of the genes were labeled with DIG using the 10X DIG RNA labelling mix (Roche) and were transcribed in antisense direction using either T7 RNA polymerase or SP6 RNA polymerase (Roche), according to the orientation of the cloned fragment as determined by sequencing result. Depending on the probe orientation, a 20µl reaction included 500ng of DNA template, 1.6µl of enzyme (2U/µl), 0.4µl of RNAsin (1U/µl) and 2µl of 10X DIG RAN labelling mix and was incubated for longer than 3hr at 37°C. Afterwards the DNA template was removed by incubating for 15min at 37°C with 1µl DNAse I (Roche; 1U/µl). Transcription reaction was diluted to 50µl and precipitated with 0.5 volume of 7.5M LiCl overnight. For co-expression analysis some probes were labeled with DNP using the Label IT Nucleic Acid Labelling Reagents (Mirus). Initially a cold antisense transcript was produced as described above, without 10X DIG and with ribo-nucleotides (Promega; c_f 4mM). The DNP labelling was performed on 2.5 μg of cold transcript accordingly to manufacturers instructions. All DNP labeled probes were purified using the G50 Quick Spin columns (Roche) as instructed by the manufacturer. The quality and quantity of each probe was checked on an agarose gel and through spectrophotometry. Each probe was diluted to a final concentration of 50ng/µl and stored at -80°C.

3.3.7 Whole mount *in situ* hybridization (WMISH)

3.3.7.1 Enzymatic WMISH

The whole mount *in situ* hybridisation protocol presented here is an adaptation of the protocol presented in (Croce, 2010). It shows similarities to protocols used in star fish and sea urchins but has differences in hybridisation temperature, number of washes and concentration of antibodies

(Ransick, 2004). Depending on whether the protocol was performed in 1.5ml tubes or 96 well plates all washes were done either in 1ml or 200 µl respectively. Embryos stored in 80% EtOH were first rehydrated using 70%, 50% and 25% EtOH washes, subsequently 4-5 washes with TBST (c_f: 0.2M Tris pH7.5, 0.15M NaCl, 0.1% Tween-20) were applied. This was followed with a 1:1 wash in TBST and fresh hybridisation buffer (HB; c_f: 50% De-ionized formamide, 10% PEG, 0.6M NaCl, 0.02M Tris pH7.5, 0.5mg/ml yeast RNA, 0.1% Tween-20, 5mM EDTA, 1X Denhardt's). The embryos were then pre-hybridised in HB for 1 hour at 55°C without probe. To a fresh HB each probe was added at a final concentration of 0.05 ng/µl and then denatured as follow: first 10min at 95°C, then 10min on ice and finally at 55°C until the HB probe mix reached the temperature of the embryos that were in the pre-hybridisation step. Finally, HB was replaced with HB including the probe and embryos were left to hybridise overnight at 55°C. After completion of hybridisation a series of washes was performed. First embryos were washed with a gradient of 75%, 50% and 25% of HB in TBST, then twice in TBST and finally twice in 1X SSC and once in 0.1X SSC. All these washes were done at 55°C. After the final 0.1X SSC wash, the embryos were washed twice in TBST at room temperature. For antibody detection the embryos were initially incubated in blocking buffer (BB; TBST with 5% Goat Serum) for at least half an hour. Then the alkaline phosphates (AP) conjugated antibodies, either Anti-Dig AP (Roche) or TSA Anti-DNP AP (PerkinElmer) at a dilution 1:1000 in BB, were applied. The Anti-Dig AP was incubated for 1 hour at room temperature and the Anti-DNP AP overnight at room temperature. Excess of antibody was removed with 5 TBST washes at room temperature. Embryos were washed twice with alkaline phosphate buffer (AP; c_f: 0.1M Tris pH9.5, 0.1M NaCl, 0.05M MgCl2, 0.1% Tween-20, 1mM Levamisole) and the chromogenic probes detected using 10µl NBT/BCIP mix (Roche) with 10% dimethylformamide in a final volume of 1ml AP . The staining was stopped with 2 washes TBSTE (1mM EDTA in TBST) and 3 washes with TBST. The embryos were stored in 30% or 50% Glycerol. Embryos were imaged using the Zeiss AxioZoom M1 light microscope.

3.3.7.2 Multi-colour fluorescent WMISH

The multi-colour fluorescent WMISH protocol (FISH) follows an adapted version of the protocol presented in (Andrikou et al., 2013). WMISH was performed in 1.5ml tubes (Eppendorf) with 1ml washes. Embryos stored in 80% EtOH were first rehydrated using 70%, 50% and 25% EtOH washes, and subsequently washed 3 times with MABT (c_f: 0.1M Maleic Acid pH7.5, 0.15M NaCl, 0.1% Tween-20). This was followed by a single wash in 1:1 MABT with HB (the same as for the enzymatic WMISH). Pre-hybridisation was performed for 3 hours in HB without probe. To a fresh HB two probes were added at a final concentration of 0.05 ng/µl each and then denatured as follow: first 10min at 95°C, then 10min on ice and finally at 55°C until the HB probe mix reached the temperature of the embryos that were in the pre-hybridisation step. Finally, HB was replaced with HB including the probe and the hybridisation was done for at least 2 days to a maximum of 1 week at 55°C. Once hybridisation completed, the HB with probe was replaced with new HB without and post-hybridisation for 3hr was performed. This was followed by 3 washes of MABT and blocking with the Perking Elmer blocking reagent dissolved in MABT (0.5%) 30min at room temperature. The first antibody, either TSA Anti-DNP-HRP and TSA Anti-DIG-POD (PerkinElmer), was applied overnight at room temperature at a concentration of 1:1000 in the blocking buffer provided by the TSA kit. The first antibody was removed by 3 washes with MABT, followed by a 100µl wash with the amplification buffer (PerkinElmer). The weaker expressed gene was stained first for 15min with TSA-Cy3 in amplification buffer 1/400 (total volume 100µl). Subsequently, 5 washes of MABT were applied to remove the staining solution, followed by a single wash of 1%H_2O_2 in MABT for 30min and another 5 washes in MABT. Afterwards, the embryos were blocked for 30min as before and the second antibody was applied overnight at room temperature. Subsequently, the embryos were washed 5 times with MABT and incubated in amplification buffer (100µl) without fluorophore for 15min. Then, the embryos were incubated with 100µl amplification buffer with TSA-Cy5 (PerkinElmer) for 15min, followed by another 5 washes in MABT. A nuclear counter staining with DAPI (Roche, c_f: 1µg/ml) was done at the moment of observation. This 3

colour version allowed the counting of expression in individual cells and the estimation of cells showing co-expression of multiple genes. Embryos were imaged using the Leica SP2 or SP8.

3.4 Microinjection of sea urchin zygotes

3.4.1 Preparation

For microinjection of sea urchin embryos, unfertilised eggs had to be immobilised on protamine-coated plates (60 mm plastic Petri-dish lids (Flacon) were filled for one minute with 1% W/V protamine sulphate (Sigma) solution in distilled H_2O). Following protamine coating, the lids were washed thoroughly with distilled water to remove excess solution, and air-dried overnight at room temperature.

Needles for microinjection were prepared from 1.0 mm outside diameter, 0.75 mm inside diameter, borosilicate glass supplied by Sutter Instrument Co. Novato, CA. Fine-tipped microinjection needles were pulled on a Sutter PO97 micropipette puller (P=300; H=560; Pu=140; V=80; T=200). To avoid clogging of needles, all solutions to be microinjected were centrifuged for 5-15min at maximum speed.

Glass Pasteur pipettes were pulled in a Bunsen flame and broken off at the end to obtain the desired size for the collection of eggs and embryos. The internal diameter of a rowing pipette should be roughly the same as the egg diameter (70µm) to warrant optimal rowing of eggs.

3.4.2 Constructs used for injections

3.4.2.1 Afi-pplx in expression vector for mRNA injection

For injection of *Afi-pplx* in sea urchin embryos, a fragment with a synthetic stop-codon (Figure 3.1) was cloned into pBluescript RN3 expression vector (Lemaire et al., 1995), similar to its ortholog of *Spu-pmar1* described in (Oliveri et al., 2002). Primers can be found in Appendix A. The cloned product was linearised using template PCR with M13F and M13R primers, as described in Table 3.1. Capped mRNA for injection was prepared using the Ambion T3 mMessage mMachine

```
Afi-pplx-synthetic   743bp...CCCCATCTGCAGTGTACCCAAGTTTTGA---------
Afi-pplx-original    743bp...CCCCATCTGCAGTGTACCCAAGTTTTCATCTGTTTCG

Afi-pplx-synthetic   ----------------------------------------
Afi-pplx-original    AGAGTGGAACCCGTCACCAATGTAGTGGACGTTTGCCAGTAA
```

Figure 3.1: **Construct to test conserved function of the *Spu-pmar1* ortholog *Afi-pplx* in sea urchin embryos.**

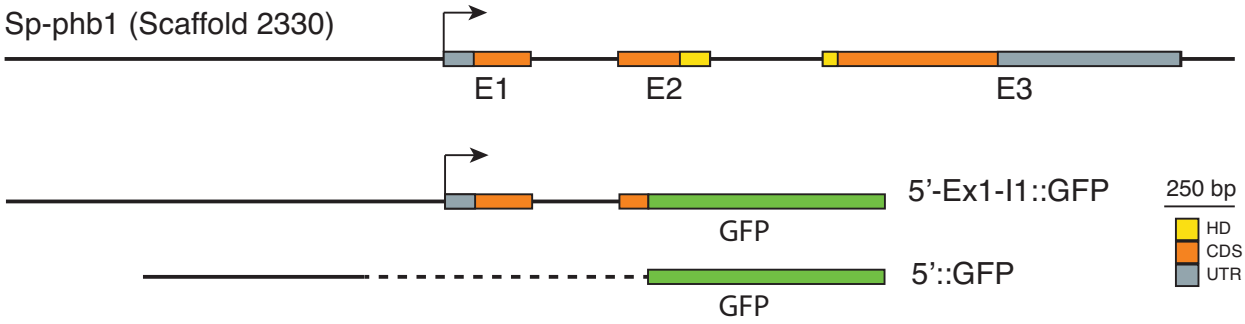

Figure 3.2: **Constructs to test regulatory regions of *Spu-phb1*.** Squares show exonic regions and green square shows fused GFP region.

Kit (Life Technologies) in 20µl final volume (c_f: 1µg Template, 1X T3 NTP/CAP, 1X Buffer, 1X T3 enzyme) and incubated for around 2hr at 37°C. For the final 15min of this incubation and to remove residual DNA 1µl of DNAse I (Roche) was added. This was followed by addition of 60µl of DEPC H_2O and Phenol/Chloroform extraction. The extracted product was purified using G50 Quick Spin columns (Roche) as instructed by the manufacturer and precipitated overnight using 0.5 volume of 7.5M NH_4AC and 2.5 volumes of 100%EtOH at -20°C. The precipitated mRNA was washed twice with 80%EtOH, then air-dried and re-suspended in 50µl DEPC H_2O. Concentration was checked using spectrophotometry. For long term storage aliquots containing 2.5µg were made, re-precipitated as described above and stored at -20°C.

3.4.2.2 Spu-phb1 fragments in GFP vector for DNA injection

In order to identify the *cis*-regulatory region of *Spu-phb1* that is responsible of driving expression in skeletogenic cells, we cloned two genomic fragments of *Spu-phb1*. The first contained roughly 2kb upstream of its transcription start site, Exon1 and Intron1 and the second just the upstream region (Figure 3.2). These fragments were fused to the GFP reporter in frame using

Table 3.3: Fusion-PCR cycling

Procedure Steps	Fusion PCR	
1 Initial Denaturation	95°C 5min	
2 Annealing	55°C 30sec	
3 Elongation	72°C 15min	add primers in the end
4 Denaturation	95°C 30sec	
5 Annealing	55°C 30sec	
6 Elongation	72°C Xsec	depending on length
GO TO 4	35times	
7 Final Elongation	72°C 5min	
8 Cooling	4°C ∞	

a 2-fragment fusion PCR. The GFP and the *Spu-phb1* fragments were first individually amplified and purified as previously described. For the fusion, both fragments were added in a 1:1 ratio of molecules for which the shorter one contained at least 20ng. First, a reaction was set up as in Table 3.1 using HiFi (Roche) without the primers in order to fuse both fragments using the cycling conditions as described in Table 3.3. Then the nested primers (see Appendix A) were added and the normal cycling continued. Successfully fused fragments were PCR purified using PCR Clean up kit (Machinery and Nagel) and concentration was measured using the Nanodrop 2000c. For further use, fused fragments were sub-cloned into pGEMT-easy vector (Promega) as described in chapter 3.3.5. The quality of the fusion constructs was controlled by sequencing.

3.4.3 Microinjection procedure

Eggs and sperm were collected from adult urchins, and a small fertilisation test was carried out to make sure the gametes were healthy. For microinjection, eggs were de-jellied by passing through a 60µm nitrex mesh several times and stored at 15°C in ASW. The eggs were then rowed using a pulled glass pasteur pipette onto protamine-coated plates and kept covered at 15°C in 2 mM PABA-ASW until injection. The microinjection needles were loaded with injection solution. The rowed embryos were then fertilised and injected with the appropriate DNA construct or synthetic mRNA using a picospitzer III. Following injection, embryos were incubated in protamine plates in SW containing a mixture of Streptomycin (50µg/ml) and Penicillin (20U/ml) at 15C, until

15 hours (just before hatching). Directly after hatching embryos were transferred into plates filled with a fresh mixture of Streptomycin (50µg/ml) and Penicillin (20U/ml) in FASW. Once the desired stage was reached, a desired number of embryos was used for further procedures.

3.4.3.1 Afi-pplx mRNA injection experiment

Injection solutions (c_f: 11ng/µl, 120mM KCl) were prepared in a final volume of 5µl DEPC H_2O. Next to *Afi-pplx* mRNA we injected newly transcribed *Spu-pmar1* mRNA (Oliveri et al., 2002, 2003) as positive and *Spu-foxA-GFP* mRNA (Oliveri et al., 2006) or *Spu-pmar1-GFP* mRNA as negative controls. For each mRNA roughly 200 Embryos were injected and phenotypic changes were observed and counted at 24hpf and 48hpf. Additionally, at 24hpf some of the embryos were fixed for WMISH. Two-sample t-test was used to assess equality of means.

3.4.3.2 Spu-phb1 mRNA injection experiment

Injection solutions (c_f: 1000mol/2pl DNA, 100ng/µl Carrier DNA, 120mM KCL) were prepared in a final volume of 5µl DEPC H_2O. In addition to the two DNA constructs, a hatching enzyme (HE-GFP) DNA was injected as positive control (Bogarad et al., 1998) and the EpGFP construct without promoter as negative control. To test for localization in skeletogenic cells, additionally to each DNA construct the regulatory region γ(2) module of *Spu-tbr* fused with RFP was injected (Wahl et al., 2009). In two independent replicas more than 100 embryos per construct were injected and at least 25 embryos for each construct pair were imaged for three channels (DIC, 488 and Cy3 filters) using 20-40X on a Zeiss AxioZoom M1 light microscope. Images were taken at 24hpf and 48hpf. All images were analysed for presence of GFP and RFP. Two-sample t-test was used to assess equality of means.

3.5 Microscopy and image analysis

3.5.1 Differential interference contrast (DIC) & epi-fluorescent microscopy

5-10 embryos, stored in glycerol, were collected using a glass pasteur pipette and deposited to 37µl of glycerol on a microscope slide under a dissecting scope (Zeiss). Small balls of plasticine were placed on the four corners of a cover slip (22x22mm), in order to lift it from the slide, which was carefully placed over the solution containing the embryos. In some cases, the slide was sealed using transparent nail varnish. Bright-field and DIC images were taken with a Zeiss AxioImager M1 coupled to a Zeiss AxioCam HRc using 20X and 40X magnification. Images were usually taken at different focal planes and often the same embryo was rolled to enable images to be taken from different perspectives. Photoshop CS4 (Adobe) was used to make basic adjustments to brightness and contrast, and for cropping. For fluorescent stained embryos, each embryo was imaged multiple times using different channels and DIC. Photoshop was then used for basic image processing and adjustments in order to merge the multiple channels into the same image using liner dodge tool.

3.5.2 Confocal microscopy

Up to 10 E were collected using a glass pasteur pipette and deposited to 37µl of glycerol or MOPS buffer on a microscope slide. Cover slips (22x22mm) were carefully placed on top of the embryos and sealed with nail varnish. Images were collected using an Leica SP2 or SP8 confocal microscope, with more than 30 Z-stacks for all channels required for each embryo. Optical sections were stacked and analysed using Fiji/ImageJ[8] software package (Schindelin et al., 2012) and cell counts were obtained using the Cell-Counter plugin. The final merged images were produced using Photoshop CS4 (Adobe).

[8] http://fiji.sc/Fiji

Chapter 4

RESULTS

In Part I of this thesis I will introduce the brittle star *Amphiura filiformis* as a developmental system to study GRN evolution. Firstly, I will start of by describing our pioneering observations on the development of the brittle star *Amphiura filiformis* in detail and its comparison with the sea urchin *Strongyloncentrotus purpuratus* development as a reference species. Using marker genes, I will explain how I identified cells that exhibit a skeletogenic molecular signature from early blastula stage onwards. Then I will shift to a high-resolution spatio-temporal expression analysis, in which I will show an analysis of 24 sea urchin skeletogenic specification orthologs in the brittle star and a comparison of those to their sea urchin counterpart in terms of spatial expression and dynamics of spatial expression over time, highlighting commonalities and differences. This part will lay the foundation for the transcriptome analysis conducted in Part II.

4.1 The development of *Amphiura filiformis*

Before starting with a molecular dissection of the *A. filiformis* skeletogenesis process it is important to clearly understand the timing and mode of development of this evolutionary relevant echinoderm. Because no data were available in literature for this species, we studied this process for the first time. Every gravid induced female that was collected around the Kristineberg marine station (Sweden), spawns a few thousand mature eggs ready to be fertilised. If the culture is set up using a single male and a single female, the zygotes develop synchronously (for culturing details see chapter 3.1.1). After fertilisation (Figure 4.1 A), the embryo divides equally into a two cell stage roughly 2 hours post fertilisation (hpf) (Figure 4.1 B). The second division gives rise to a tetrahedral positioning of cells where the two cleavage planes are perpendicular to each other (Figure 4.1 C) and occurs at 3hpf, similarly observed in another species of brittle star *Ophiopholis aculeata* (Primus, 2005). This is followed by another equal division creating 8 cells that are similar in orientation and in size (Figure 4.1 D). The embryo continues to divide equally for another six divisions (no obvious morphological differences are distinguishable during the cleavages) and reaches blastula stage at $\sim$12hpf (as shown in Figure 4.1 K). In this moment the blastocoel expands and is surrounded by a single cell layer of tightly connected cells, the embryo is still spherical and its anatomical orientation is not yet definable. In the early stages of development the embryo shows proportionally large cell nuclei, suggesting an early and extensive start of transcription, consistent with the observation that some transcription factors show a significant rise in mRNA levels early in development (see below). At $\sim$15hpf a break out of the fertilisation envelope is observed at which moment the cilia start to beat (Figure 4.1 M and N) and the embryo begins to swim slowly. As the embryo continues to develop, the first morphological differences become clear, it elongates along the animal-vegetal axis and flattens in the vegetal plate, resulting in a bullet-shaped form. Around $\sim$20hpf a group of cells detach from the vegetal plate of the embryo and ingress into the blastocoel, where they remain in a basal position adjacent to the

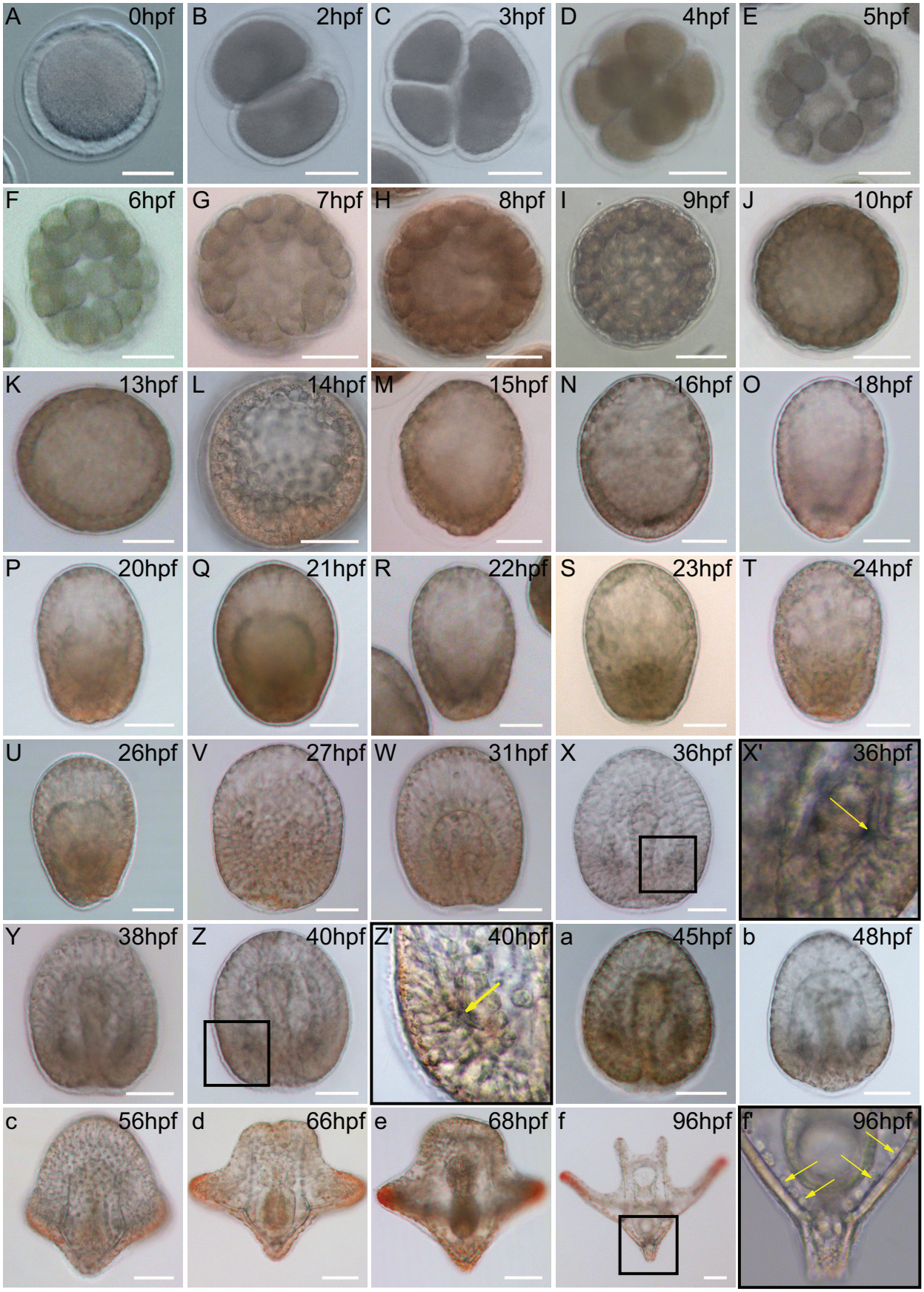
A 0hpf
B 2hpf
C 3hpf
D 4hpf
E 5hpf
F 6hpf
G 7hpf
H 8hpf
I 9hpf
J 10hpf
K 13hpf
L 14hpf
M 15hpf
N 16hpf
O 18hpf
P 20hpf
Q 21hpf
R 22hpf
S 23hpf
T 24hpf
U 26hpf
V 27hpf
W 31hpf
X 36hpf
X' 36hpf
Y 38hpf
Z 40hpf
Z' 40hpf
a 45hpf
b 48hpf
c 56hpf
d 66hpf
e 68hpf
f 96hpf
f' 96hpf

vegetal plate (Figure 4.1 P). I call this stage mesenchyme blastula (MBl). During the mesenchyme blastula stage the cells at the animal side of the embryo (opposite to the vegetal plate) start to thicken, reducing the blastocoelar space (Figure 4.1 Q). Few hours after the first cells ingress into the blastocoel a second set of cells begins ingression from the vegetal plate. Shortly after, the invagination of the gut (archenteron) starts at 30hpf (Figure 4.2 W), and gastrulation begins. During the next hours of development two spicules of a tri- to tetraradiate shape will form at the base of the archenteron and their extension will ultimately give rise to the characteristic pluteus larvae (Figure 4.1 X-f). The extension of the spicules is guided by the skeletogenic mesodermal cells (SM) which secrete all necessary biomineralization components in the extracellular space (Figure 4.1 f' yellow arrows). The secreted bio-mineralization proteins drive the assembly of the calcite skeleton structure. Once the archenteron reaches its target in the oral ectoderm the mouth opens and the larva is now able to feed by 65hpf forming the complete pluteus larvae (Figure 4.1 f). A detailed description of early brittle star development can be found only for another species of brittle star *Ophiopholis aculeata* in (Primus, 2005) and shows remarkable similarity with what we have observed in *A. filiformis*.

Figure 4.1 *(preceding page)*: **High-resolution developmental time-line of *A. filiformis* reveals distinct stages of morphological change.** (A-I) Cleavage stages with equal cell divisions. At late cleavages, a hollow blastocoel becomes visible at the center. (J-O) Blastula stage embryos. Between 14hpf to 16hpf hatching occurs as visualized by the disappearance of the outer most fertilisation membrane. Embryos acquire a characteristic bullet shape. Animal to vegetal orientation is visible through thickening of cells at vegetal side of embryo. (P-V) Mesenchyme blastula stage is characterized by ingression into the blastocoel of first and second round of mesenchymal cells from the vegetal plate. At the end of this stage and before gastrulation becomes clear (27hpf) the blastocoel is engulfed with mesenchymal cells, due also to a contraction of the blastocoelar space. (W-Z) Gastrula stages are characterized by the invagination of the archenteron. Mesenchymal cells in the blastocoel form two lateral clusters that give rise to primordia of spicules (yellow arrows in X' and Z'). (a-e) Extension of skeleton and bending of gut in order to create a second opening characterize stages here called prism for analogy with sea urchin development. (f) Pluteus larva with extended skeleton. Mesenchymal cells are juxtaposed and periodically distributed along the length of the skeleton rods (yellow arrows in f'). They are likely the cells responsible for the deposition of the bio-mineralised skeleton. Developmental time, in standard laboratory conditions (see Methods), is indicated in hours post fertilisation (hpf). Embryos were imaged *in vivo*. All scale bars are 50μm.

4.1.1 Comparison of developmental timing between *Amphiura filiformis* and *Strongylocentrotus purpuratus*

In order to better understand the evolution of the GRN encoding for larval skeletogenesis, we first have to compare the development between two classes of echinoderms taken into consideration, which develop extended skeleton producing a pluteus larva. For this reason, here we compare side by side the ophiuroid *A. filiformis* and the echinoid *S. purpuratus*, to pinpoint their developmental similarities and differences. Based on our *in vivo* observations (Figure 4.1), and on the extensive knowledge available for sea urchin development, we constructed a timeline highlighting the developmental speed and stages between these two species (Figure 4.2 B). This timeline shows that brittle star and sea urchin development shares the same sequence of events and that both species undergo similar morphological stages (compare Figure 4.2 A with Figure 4.2 C). In particular, the development of the larval skeleton is remarkably similar; both animals have a mesenchyme blastula stage, where the ingressing mesenchymal cells accumulate at gastrula stage in lateral clusters, next to archenteron where the spicules are formed (Figure 4.2 A and C). While this process is overall strikingly similar, some differences can be observed when looking in depth: 1) brittle stars do not form micromeres and have exclusively equal cell division; 2) after hatching, the brittle star obtains a bullet shape form whereas the sea urchin stays spherical; 3) ingression of different mesenchymal cells into blastocoel happens almost simultaneously in brittle star whereas in sea urchin this process is clearly time-separated; 4) gastrulation in this brittle star is faster than in sea urchin; and 5) under comparable conditions brittle stars reach a feeding pluteus larval stage earlier (Figure 4.2 B). Due to the absence of micromeres in brittle stars the skeletogenic lineage is morphologically not evident, thus, raising several questions: which part of the embryo gives rise to the precursor cells of the skeletogenic lineage and at what stage of development is this lineage clearly separated from others.

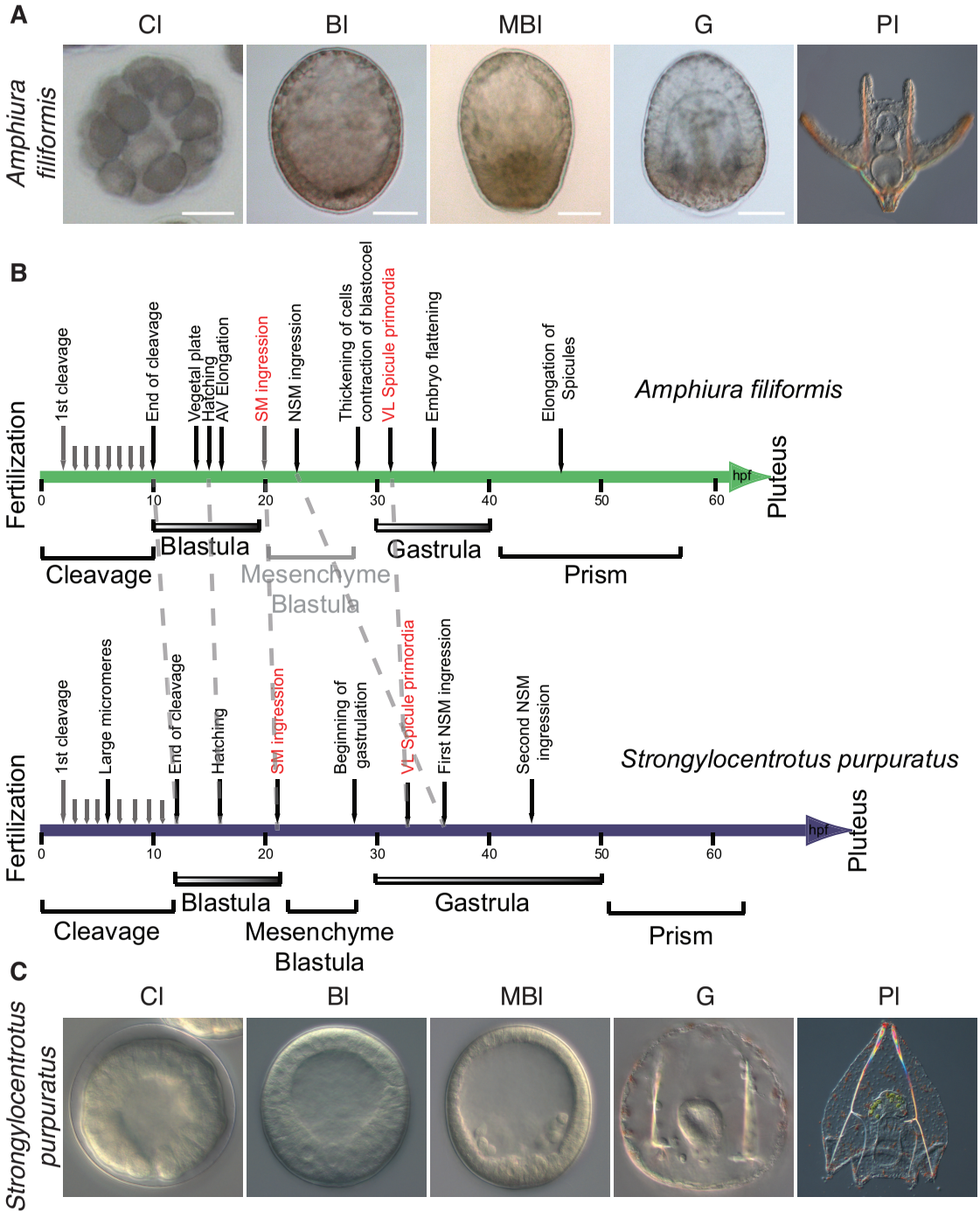
A
Cl
Bl
MBl
G
Pl
Amphiura filiformis
B
Fertilization
1st cleavage
End of cleavage
Vegetal plate
Hatching
AV Elongation
SM ingression
NSM ingression
Thickening of cells
contraction of blastocoel
VL Spicule primordia
Embryo flattening
Elongation of Spicules
Amphiura filiformis
hpf
0
10
20
30
40
50
60
Pluteus
Blastula
Gastrula
Cleavage
Mesenchyme Blastula
Prism
Fertilization
1st cleavage
Large micromeres
End of cleavage
Hatching
SM ingression
Beginning of gastrulation
VL Spicule primordia
First NSM ingression
Second NSM ingression
Strongylocentrotus purpuratus
hpf
0
10
20
30
40
50
60
Pluteus
Blastula
Gastrula
Cleavage
Mesenchyme Blastula
Prism
C
Cl
Bl
MBl
G
Pl
Strongylocentrotus purpuratus

4.2 Identification of skeletogenic mesodermal cells in brittle star

To identify the cells belonging to the skeletogenic lineage and their earliest appearance I analysed the expression of genes known to be involved in both adult and larval skeletogenesis in other echinoderms. Based on the expectation that skeletogenic genes should be expressed in the lateral clusters of the *A. filiformis* gastrula stage, where the spicules are formed (Figure 4.3 A and Figure 4.1 X' yellow arrow), I first studied the expression of orthologous genes exclusively expressed in sea urchin skeletogenic cells throughout development (Ettensohn et al., 2003; Costa et al., 2012; Rafiq et al., 2012; Gao and Davidson, 2008). These genes are *Afi-alx1*, *Afi-jun* and *Afi-p19* (Figure 4.3 B), which indeed are expressed in the same location as where *A. filiformis* skeleton primordia appear (Figure 4.3 B gastrula stage). In order to establish the onset of expression of these skeletogenic lineage specific genes, I performed QPCR on mRNA samples collected every three hours (Table A.6). I observed zygotic expression of *Afi-alx1* and *Afi-p19* at 12hpf, while the maternally abundant *Afi-jun* showed a decrease in the first 9hrs of development until its zygotic expression was raised back at 12hpf (Figure 4.3 D and Table A.6). The fact that all the three genes start their zygotic expression at early blastula stage suggests that the specification of this cell lineage might occur at this moment in development. Whole mount in situ hybridization (WMISH) of *Afi-alx1* at early blastula stage showed expression in roughly 8 ± 1 (n=3) cells grouped together on one side of the embryo (Figure 4.3 B). *Afi-alx1* positive cells are located in the vegetal plate of the late blastula and possibly divide once more (Figure 4.3 B). As expected, I found consistent expression of all three genes at blastula stage in 18 ± 3 (n=17) cells at the vegetal pole of the hatched blastula stage embryo (Figure 4.3 B), suggesting co-expression in the same cells, confirmed by double FISH of *Afi-alx1* and *Afi-p19* at this stage (Figure 4.3 C). At

Figure 4.2 *(preceding page)*: **Comparison between *A. filiformis* and *S. purpuratus* development.** (A) Representative stages of brittle star development. (B) Timeline comparison between brittle star and sea urchin, showing similarities and differences in the development of these two organisms. (C) Representative stages of sea urchin development (kindly provided by Libero Petrone). Cl - cleavage; Bl - blastula; MBl - mesenchyme blastula; G - gastrula; Pl - pluteus.

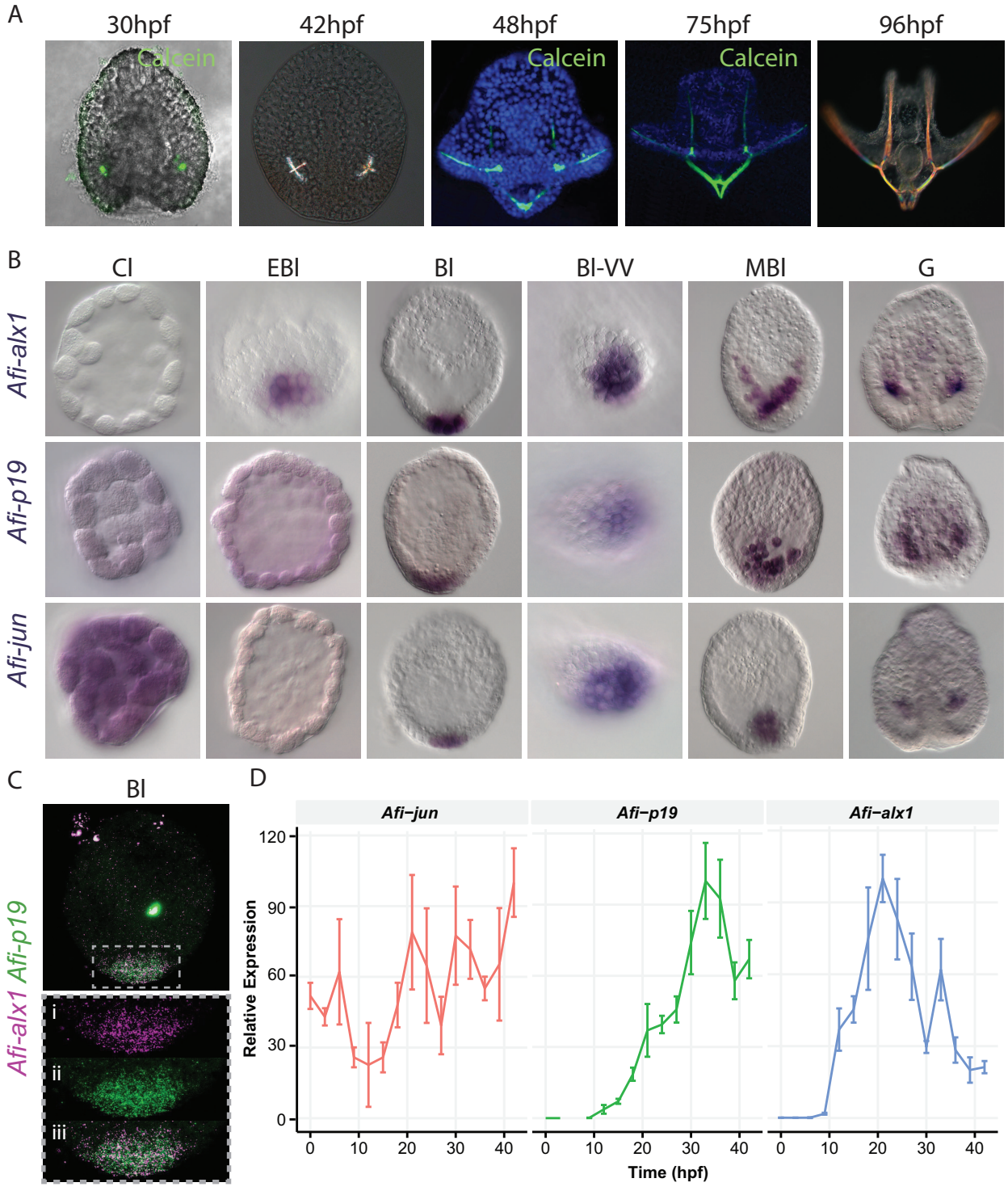
A
30hpf
42hpf
48hpf
75hpf
96hpf
Calcein
Calcein
Calcein
B
Cl
EBl
Bl
Bl-VV
MBl
G
Afi-alx1
Afi-p19
Afi-jun
C
Bl
Afi-alx1 Afi-p19
i
ii
iii
D
Afi−jun
Afi−p19
Afi−alx1
Relative Expression
120
90
60
30
0
0
10
20
30
40
Time (hpf)

mesenchyme blastula stage all these genes continue to mark the first ingressed cells (Figure 4.3 B). This strongly suggests that as in sea urchin, the primary mesenchyme cells are likely to be the precursors of the skeletal cells and, thus, are named skeletogenic mesodermal cells (SM). Our expression data indicate that the regulatory program for skeletogenesis in *A. filiformis* is already defined at early blastula stage. It is characterized by the presence of a specific regulatory state, which includes *Afi-alx1* and *Afi-jun*, and it is segregated from other cell lineage programs.

Figure 4.3 *(preceding page)*: **Skeletogenic cells in the brittle star *A. filiformis***. (A) Different stages of skeleton development in the brittle star. The first spicules appear at 30hpf and form a tri- or tetraradiate structure as seen in 42hpf that is getting extended until the characteristic pluteus larva is formed, as displayed at 48hpf, 75hpf and 96hpf. In green the newly formed skeleton is stained with calcein and in blue the cell nuclei are marked with DAPI. Larva at 96hpf was imaged with on a dark field. (B) WMISH in different stages of brittle star development showing expression of orthologs to genes exclusively expressed in skeletogenic cells in the sea urchin. The first gene showing restricted expression in skeletogenic cells is *Afi-alx1* at early blastula. At this stage *Afi-p19* and *Afi-jun* are still ubiquitosly expressed. From blastula stage onwards all three genes are co-expressed in a subset of cells at the vegetal side of the embryo and importantly, at gastrula stage in the same location where the spicules appear. (C) Double FISH showing co-expression of *Afi-alx1* and *Afi-p19* in cells at the vegetal pole of the embryo. (D) Time-courses obtained by QPCR showing each gene normalized by its peak of expression. Error bars show standard deviation of three technical replicas. Cl - cleavage; EBl - early blastula; Bl - blastula; Bl-VV - blastula vegetal view; MBl - mesenchyme blastula; G - gastrula.

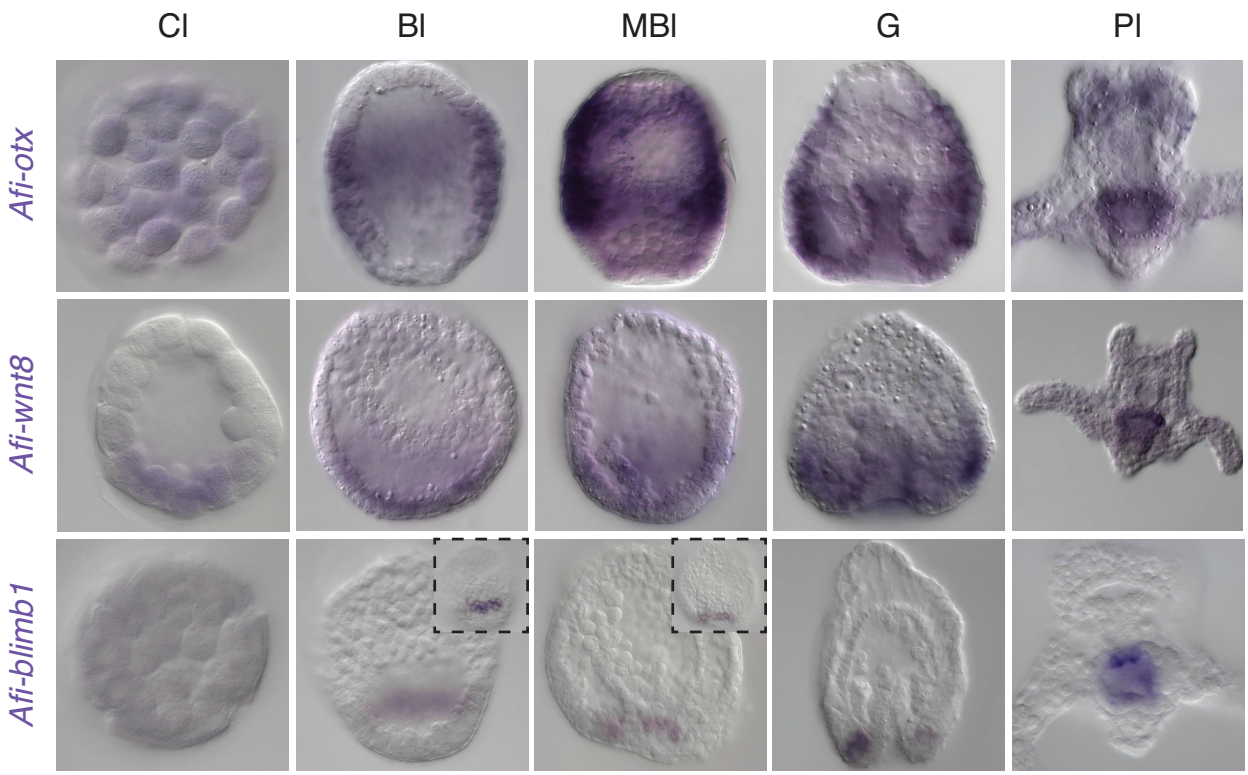

Figure 4.4: **Expression of *Afi-otx*, *Afi-wnt8* and *Afi-blimp1* shows major differences in translation of maternal cues for SM specification**. All expression patterns shown were obtained using WMISH. *Afi-otx* is ubiquitously expressed during cleavage stage and gets then cleared from vegetal and apical areas forming a band of expression at the ectoderm through blastula to gastrula stage. During pluteus stage expression is restricted to the mid-gut and some single cells close to the mouth area, possibly neurons. *Afi-wnt8* shows specific expression during cleavage stage in a group of cells. From blastula to mesenchyme blastula stages it is expressed as circle at the vegetal half of the embryo and is also expressed in the gut during gastrulation. At pluteus stage *Afi-wnt8* is expressed in the mid-gut. *Afi-blimp1* is expressed as a ring above the vegetal plate from blastula stage onwards and get restricted to the blastopore area at mid-gastrula stage. At pluteus *Afi-blimp1* expression is similar to the other two genes. Top right corners of *Afi-blimp1* blastula and mesenchyme blastula stage embryos show image focused on ectodermal cell layer with visible staining in these cells.

4.3 Comparison of sea urchin and brittle star skeletogenesis

Based on the fact that I identified the lineage with skeletogenic mesodermal signature in brittle stars, I can now start to compare activity and expression of sea urchin orthologs of the larval skeleton GRN in brittle star.

4.3.1 Early regulatory inputs initiating the GRN for larval skeletogenesis

In sea urchin the specification of micromeres, the cell-type destined to form the larval skeleton, is performed by a set of three genes, *Spu-otx*, *Spu-wnt8* and *Spu-blimp1*, and initiated through a gradual enrichment of nuclearized β-catenin at the vegetal side of the embryo throughout the first cleavages (Logan et al., 1999). There, by fifth cleavage nuclearized β-catenin is bound to TCF where it activates, with maternal *Spu-blimp1*, the expression of *Spu-wnt8* using an AND promoter logic (Smith et al., 2007). By sixth cleavage zygotic expression of *Spu-blimp1* is observed, which is activated by an enhanced level of β-catenin/TCF through *Spu-wnt8* and maternally abundant *Spu-otx* (Li et al., 1997). In this moment maternal *Spu-otx* and nuclearized β-catenin/TCF are activating the expression of *Spu-pmar1* only in the mircromeres, whereas expression of *Spu-hesC* is inhibited in these cells by repression of *Spu-blimp1* and *Spu-pmar1*. By blastula stage *Spu-blimp1* and *Spu-wnt8* are no longer expressed in the SM lineage and form a torus surrounding the micromeres in a pre-endoderm territory (Livi and Davidson, 2007; Wikramanayake et al., 2004). The recursive wiring of *Spu-blimp1* and *Spu-wnt8* enforces their co-expression for the rest of development. In sea urchin and starfish multiple alternative transcripts have been identified for *otx*, each of which has a different domain of expression (Li et al., 1997; Hinman et al., 2003). To avoid confusion, I will describe only one of the isoforms (for starfish *Pmi-otx*-$\beta - \alpha$ and for sea urchin *Spu-otx*$\beta 1/2$). Importantly, in sea urchin and in starfish expression of the *otx* is initially ubiquitous. Throughout blastula and mesenchyme blastula stages it gets restricted to a band of ectodermal cells, clearing from the vegetal plate in both and from the apical plate only in sea urchin. Subsequently, *otx* becomes restricted to gut later in development (Li et al., 1997; Hinman et al., 2003). But how are these genes expressed in the brittle star?

The first important and obvious difference from the sea urchin is morphological. That is the absence of micromeres in the brittle star, suggesting differences in the mechanisms for early segregation of skeletogenic cells. Despite this morphological difference, I investigated whether the cells at the vegetal side of the *A. filiformis* embryo undergo similar initiation mechanisms. For

this purpose I cloned orthologous genes to *Spu-blimp1*, *Spu-wnt8* and *Spu-otx* and resolved their expression throughout various stages of development using WMISH (Figure 4.4). The only gene showing restricted specific expression to a subset of all cells throughout cleavage is *Afi-wnt8*, while *Afi-otx* shows ubiquitous expression and *Afi-blimp1* no expression at all (Figure 4.4). The absence of expression throughout cleavage stages of *Afi-blimp1* is supported by the low expression values observed in the mRNA seq dataset (see Part II). Interestingly, *Afi-blimp1* shows no expression in skeletogenic cells throughout any stage of development tested, however, conserved expression with sea urchin is visible from blastula stage onward in pre-endoderm territory, suggesting the absence in SM specification in brittle star. Unlike *Afi-blimp1*, the genes *Afi-otx* and *Afi-wnt8* can both participate in the early specification of SM during cleavage stage. However, only *Afi-wnt8* stays enriched throughout blastula stage in SM cells at the vegetal plate and remains then active in the vegetal half of the embryo until it is restricted to the mid-gut of the pluteus larvae. Expression of *Afi-otx* seems to be highly conserved with sea urchin, indicating a similar role in development. Taken together, especially the absence of *Afi-blimp1* in skeletogenic cells makes a similar wiring of SM initiation by this maternal factor as in sea urchin unlikely and is consistent with the absence of micromeres in brittle star.

4.3.2 Identification of a brittle star ortholog of the sea urchin *Spu-pmar1*

In sea urchin the skeletogenic program is initiated by the zygotic expression of the paired-like homeodomain transcriptional repressor *Spu-pmar1*, which starts to be expressed as early as 4th cleavage only in micromeres (Oliveri et al., 2003) where it is engaged with HesC in a double negative gate (DNG). *Spu-hesC* additionally receives a repressive input by *Spu-blimp1* in these cells. A brittle star *pmar1* was reported to be present in the developmental transcriptome of *Ophiocoma wenditii*, however a closer look into this sequence revealed that no orthology statements could be made (Vaughn et al., 2012). Using a reciprocal blast approach I identified a sequence with closest similarity to *Spu-pmar1c* in an *A. filiformis* developmental transcriptome (see Part II). In

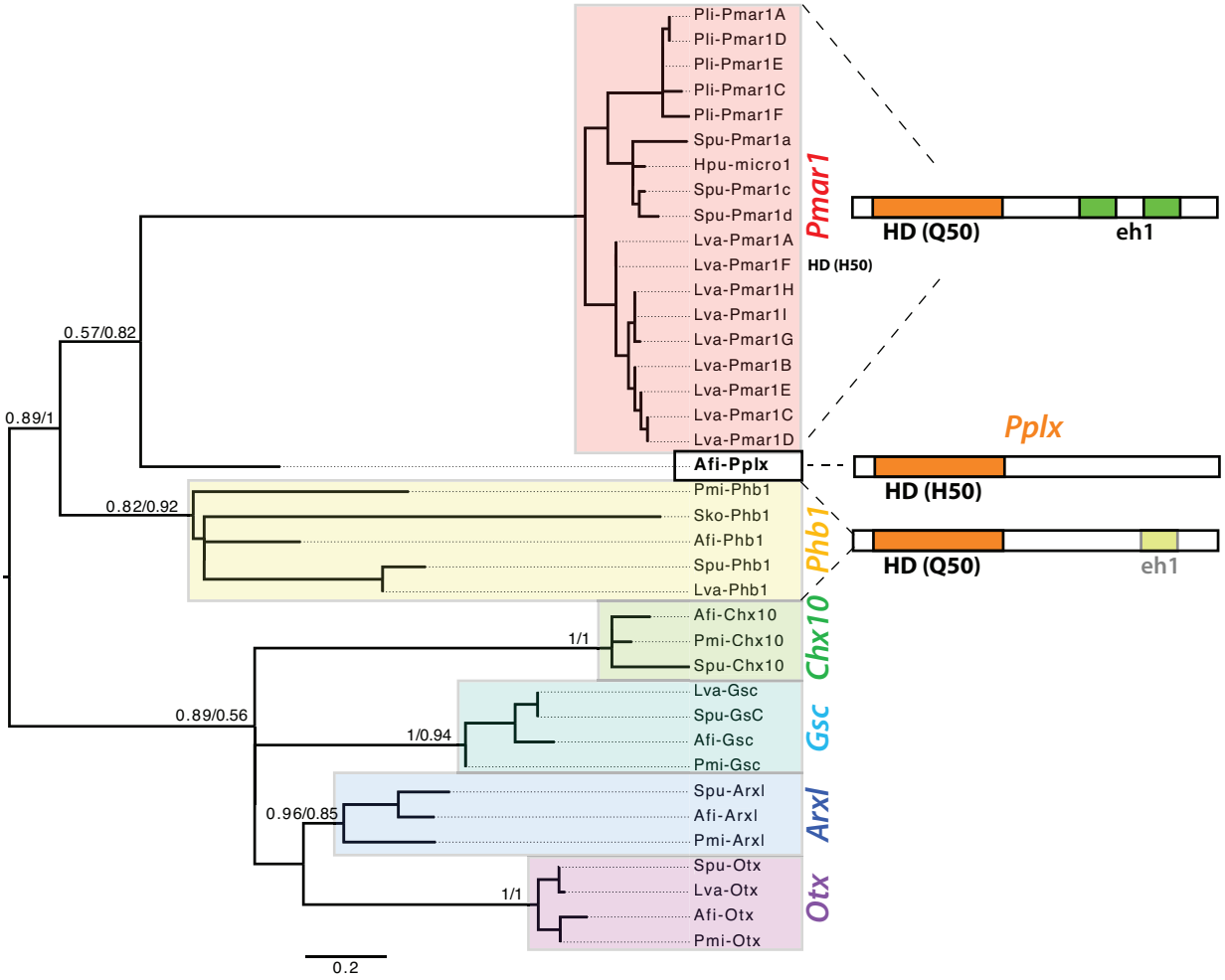
Pli-Pmar1A
Pli-Pmar1D
Pli-Pmar1E
Pli-Pmar1C
Pli-Pmar1F
Spu-Pmar1a
Hpu-micro1
Spu-Pmar1c
Spu-Pmar1d
Lva-Pmar1A
Lva-Pmar1F
Lva-Pmar1H
Lva-Pmar1I
Lva-Pmar1G
Lva-Pmar1B
Lva-Pmar1E
Lva-Pmar1C
Lva-Pmar1D
Pmar1
HD (Q50)
eh1
HD (H50)
Pplx
Afi-Pplx
HD (H50)
Pmi-Phb1
Sko-Phb1
Afi-Phb1
Spu-Phb1
Lva-Phb1
Phb1
HD (Q50)
eh1
Afi-Chx10
Pmi-Chx10
Spu-Chx10
Chx10
Lva-Gsc
Spu-GsC
Afi-Gsc
Pmi-Gsc
Gsc
Spu-Arxl
Afi-Arxl
Pmi-Arxl
Arxl
Spu-Otx
Lva-Otx
Afi-Otx
Pmi-Otx
Otx
0.57/0.82
0.89/1
0.82/0.92
1/1
0.89/0.56
1/0.94
0.96/0.85
1/1
0.2

order to better understand its true evolutionary relationship with the Pmar1 genes I used a phylogenetic approach. First, I used a blastx search against the non-redundant database and selected genes, part of several classes of paired-like homeodomain, from various echinoderms and a hemichordate as outgroup. Second, I obtained a multiple alignment of the protein coding sequences using MAFFT (Pfaffl et al., 2004) and removed un-alignable sequences with GBLOCKS (Talavera and Castresana, 2007). Finally, I computed trees using a maximum likelihood and a Bayesian approach. Depending on the sequences used and the method, the *A. filiformis* sequence was consistently placed as sistergroup to the sea urchin Pmar1 (Figure 4.5) or within the Phb1 genes. For this reason we decided to name the gene pmar1-phb1-like-homeobox (pplx). Interestingly, I was unable to find any *pmar1* close hit in the available starfish (*Patiria miniata*) and hemichordate (*Saccoglossus kowalewskii*) genomic sequences, although a *phb1* sequence was present. Our phylogeny clearly reveals that: 1) the phb1 and the pmar1 + pplx1 genes form a distinct class of paired-like homeodomain, supported by high bootstrap values in all analysis; 2) in sea urchins the pmar1 genes have been extensively duplicated (The Lvpmar1 and Plhbox12 partial locus; Sea Urchin Genome Project BAC Clone #170H13 and #020N20 respectively).

Figure 4.5 *(preceding page)*: **Phylogenetic tree of paired-like homeodomains in echinoderms supports orthology of *Afi-pplx* to sea urchin pmar1 genes.** First value on branch was computed using a maximum likelihood approach and second value using a Bayesian approach. Sequences were identified using a blast search (e-value: 1e-6) of Spu-Pmar1 peptide sequence against various echinoderm databases and a database of the hemichordate *Saccoglosus kowalevskii*. Amino acid sequences were aligned with MAFFT and trimmed using GBlocks, maintaining just the homeodomain regions for tree reconstruction. Phylogenetic tree was estimated with MEGA using a JTT model with gamma distribution and invariant sites using 500 bootstraps (first value on branch) and with PhyloBayes using a CAT-GTR model (diff=0.013) (second value on branch). Otx, Arlx, Gsc and Chx10 paired-like homeodomain proteins are used as outgroup. All Pmar1 sequences were obtained from (The Lvpmar1 and Plhbox12 partial locus; Sea Urchin Genome Project BAC Clone #170H13 and #020N20 respectively). On the right column are schematically represented the predicted Pmar1, Pplx and Phb1 proteins with identified functional domains. Orange, homeodomain (HD); green, engrailed homology domain (eh1). In parenthesis is specified the recognition amino acid (amino acid number 50 of the homeodomain), which is a Histidine (H) in Pplx and likely confers a different specificity of binding to the DNA compared to the the Q50 Pmar1 proteins. Lva: *Lytechinus variegatus*; Pli: *Paracentrotus lividus*; Hpu: *Hemicentrotus pulcherrimus*; Spu: *Strongyloncentrotus purpuratus*; Afi: *Amphiura filiformis*; Pmi: *Patiria miniata*; Sko: *Saccoglossus kowalevskii*.

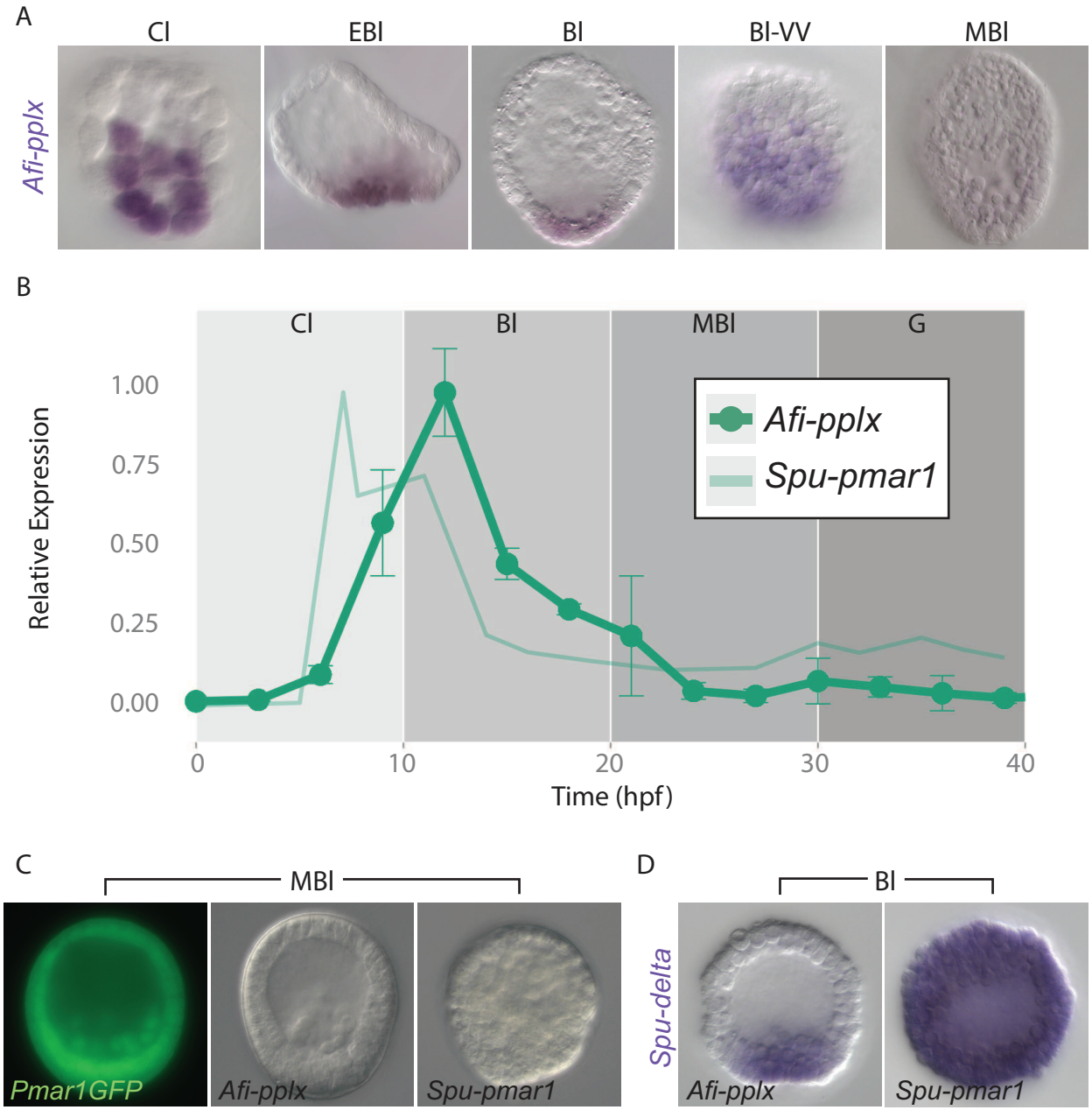
A
Cl
EBl
Bl
Bl-VV
MBl
Afi-pplx
B
Cl
Bl
MBl
G
Relative Expression
1.00
0.75
0.50
0.25
0.00
Afi-pplx
Spu-pmar1
0
10
20
30
40
Time (hpf)
C
MBl
Pmar1GFP
Afi-pplx
Spu-pmar1
D
Bl
Spu-delta
Afi-pplx
Spu-pmar1

Importantly, the temporal and spatial expression of *Afi-pplx* shows a remarkable degree of similarity to the sea urchin *Spu-pmar1* (Figure 4.6 A and B). *Afi-pplx* is transiently expressed only in the zygote, starting its expression at late cleavage stage in a group of 10±3 (n=7) blastomeres (Figure 4.6). It has a maximum level of expression at early blastula stage, when it is clearly expressed in 20±5 cells (n=4) at the vegetal plate, then in 35±6 cells (n=7) at blastula stage (Fig 2. D), dropping down to undetectable levels by mesenchyme blastula (Figure 4.6). However, protein domain and sequence comparison analyses revealed an important difference between the *Spu-pmar1* and the *Afi-pplx*: the absence in the brittle star protein of two engrailed homology motif 1 (eh1), which are necessary for the *Spu-pmar1* repressive function (Oliveri et al., 2002). It has been shown that this protein motif can be easily acquired and lost throughout evolution (Copley, 2005). In *Afi-pplx*, moreover, the amino-acid (aa) 50 of the homeodomain, known as the recognition aa, is an Histidine instead of a Glutamine (Figure 4.5). Thus, I hypothesized that *Afi-pplx* is functionally not similar with *Spu-pmar1* and unlikely acts as transcriptional repressor. To test the functional divergence of *Afi-pplx*, we injected in two independent experiments an *Afi-pplx* synthetic mRNA into sea urchin fertilized eggs (see methods for details). Previously, it was shown that ectopic expression of *Spu-pmar1* lead to re-specification of every cell of the embryo into

Figure 4.6 *(preceding page)*: ***Afi-pplx* is expressed similarly to *Spu-pmar1*, but does not function as repressor in sea urchin embryos.** (A) WMISH showing the expression of *Afi-pplx* during development. Expression of *Afi-pplx* is consistently restricted to 10±3 cells (n=7) at late cleavage stage, 20±5 cells (n=4) at early blastula and 35±6 cells (n=7) at the vegetal pole of the blastula stage embryo. Consistently to the quantitative time course data (Table A.6), from mesenchyme blastula stage onwards *Afi-pplx* is no longer detectable. (B) Time-line comparison of *Spu-pmar1* and *Afi-pplx* transcript abundance normalized to stages of development (see Appendix A) and to their individual peaks of expression shows high correlation of expression dynamic (cross-correlation: 0.801). For brittle time-courses error bars represent standard deviation of two experimental replicas. (C-D) Injection in sea urchin embryos of synthetic mRNA for *Spu-pmar1*, *Afi-pplx* and GFP control. (C) Phenotypic observation at mesenchyme blastula stage shows no observable phenotype in embryos injected with Afi-pplx-mRNA, while injection of Spu-pmar1-mRNA induces skeletogenic fate in all cells. (D) WMISH of *Spu-delta* shows restricted expression in skeletogenic cells in embryo injected with Afi-pplx-mRNA shows expression. WMISH of *Spu-delta* on Spu-pmar1-mRNA injected embryos shows expansion of *Spu-delta* expression to the whole embryo. VV - vegetal view, CI cleavage, EBl early blastula, Bl blastula, MBl mesenchyme blastula.

skeletogenic fate (Oliveri et al., 2002), due to the repressive action of Spu-Pmar1 on *Spu-hesC* gene in every cell of the embryo. This is also visible at molecular level by the activation of ectopic expression of genes immediately regulated by the double negative gate (DNG), such as *Spu-delta*. As predicted, mRNA ectopic expression of *Afi-pplx* in sea urchin embryos, in similar amount to *Spu-pmar1*, does not show re-specification of cells consistent with no observable expansion of *Spu-delta* expression in injected embryos (Figure 4.6 D). This indicates that *Afi-pplx*, once introduced in the sea urchin, is not capable of repressing the target gene *Spu-hesC* and, thus, operates differently from *Spu-pmar1* (Figure 4.6).

Interestingly, Afi-pplx-mRNA injected sea urchin embryos show a reduced skeleton at later stage (Figure 4.7), possibly due to a partial competition with endogenous *Spu-pmar1* but lack of repressive function. To control for possible phenotype due to injection procedure, we injected synthetic RNA encoding for GFP at levels higher than the *Spu-pmar1* and *Afi-pplx* mRNAs. These data point to a different regulatory mechanism of initiation of the skeletogenic program in sea urchin and brittle star and suggest a lack of pmar1/hesc double negative gate in the early regulatory network of *A. filiformis* skeletogenic lineage.

4.3.3 Evolutionary origin of the pplx/pmar1 genes

Our phylogenetic analysis revealed that the sister groups of Phb1 and Pmar1+Pplx genes likely derived from a common ancestor (Figure 4.5). When looking in depth into the sea urchin gene structure it is evident that *Spu-phb1* consists of three exons, whereas *Spu-pmar1* has only two. Interestingly, the two exons of *Spu-pmar1* have similar lengths to the last two exons of *Spu-phb1* (*Spu-pmar1-exon1* with 342bp and *Spu-phb1-exon2* with 314bp and *Spu-pmar1-exon2* with 658bp and *Spu-phb1-exon3* with 1253bp) (Figure 4.8 A), which encode for the homeodomain, and in both cases the last exon starts with the VWFQNRR aa sequence, which is part of the homeodomain. This is conserved for all paired-class homeobox genes (Galliot et al., 1999). Interestingly, the sea urchin *Spu-phb1* is initially expressed in the SM lineage (micromeres) from

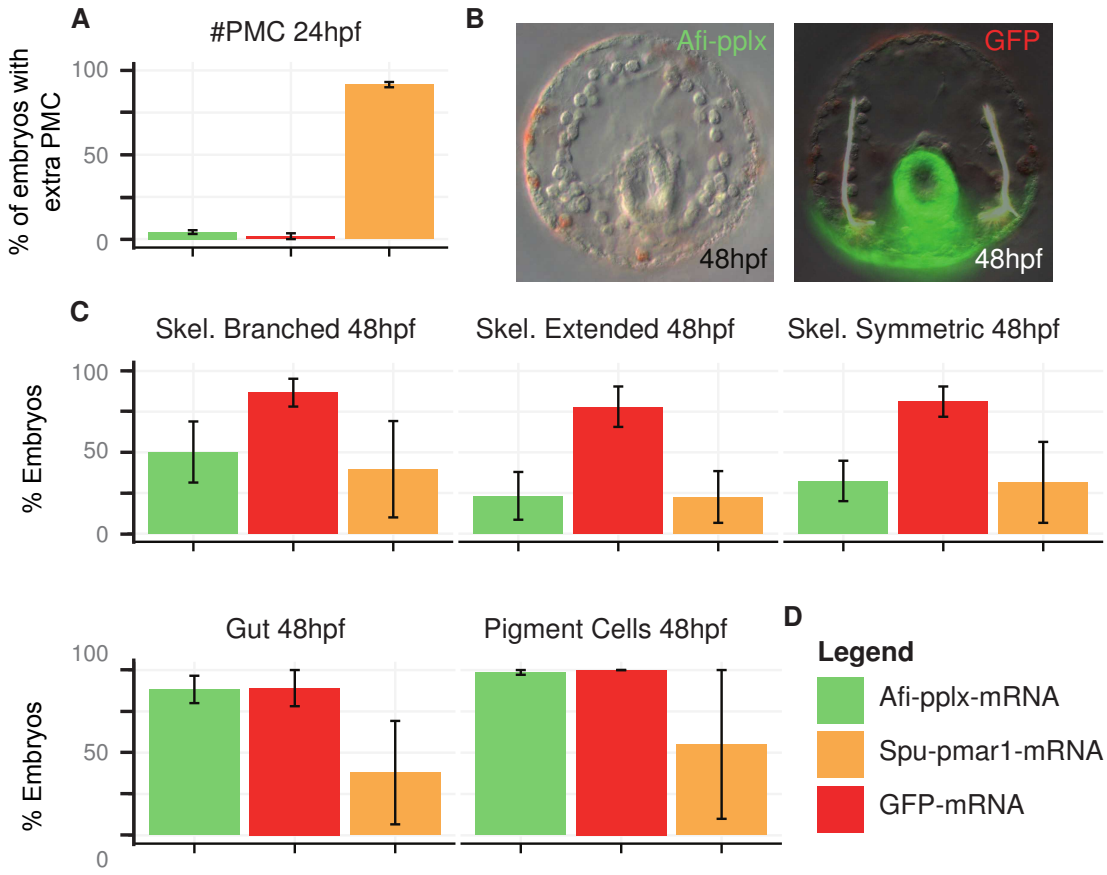

Figure 4.7: ***Afi-pplx* is functionally different from the sea urchin pmar1 repressor.** All bar-graphs are percentage of embryos displaying a particular phenotype. (A-D) Synthetic mRNA for *Afi-pplx* or *Spu-pmar1* is injected into fertilised egg and embryos are observed for specific phenotype at mesenchyme blastula (24 hpf) and late gastrula (48 hpf). (A) Injection statistics at mesenchyme blastula stage of two biological replicas showing normal number of mesenchymal ingressing cells in Afi-pplx-mRNA injected embryos (n_1=38, n_2=33) and GFP-mRNA injected controls (n_1=16, n_2=30), on the contrary in Spu-pmar1-mRNA injected embryos (n_1=50, n_2=29) the blastocoel fill up with primary mesenchymal cells. #PMC indicates the percentage of embryos that showed a number of more than normal PMCs. (B) Representative Afi-pplx-mRNA injected embryo at late gastrula stage (48 hpf) shows reduced skeleton, consistently with a translation of the Afi-Pplx protein and a partial displacement of the endogenous Spu-Pmar1. Representative of GFP-mRNA injected embryo shows normal development and expression of GFP. (D) Injection statistic of specific phenotypic characters of two biological replicas at gastrula stage confirms the skeleton of Afi-pplx-mRNA injected embryos (n_1=35, n_2=29) as the only territory affected similar to Spu-pmar1-mRNA (n_1=39, n_2=30). GFP-mRNA control embryos show normal development (n_1=21, n_2=32). The graphs indicate the percentage of embryos at 48 hpf scored for fully Skel. Branched (showing triradiate structure); Skel. Extended (extension of skeleton compared to control); Skel. Symmetric (showing a similar skeleton of both sides of the two ventro-lateral clusters); Gut (normal developing archenteron compared to control); and Pigment Cells (normal number of pigment cells compared to control). Error bar represents standard deviation of two independent biological replicas. GFP-mRNA is the average between Spu-foxA::GFP and Spu-pmar1::GFP mRNA constructs.

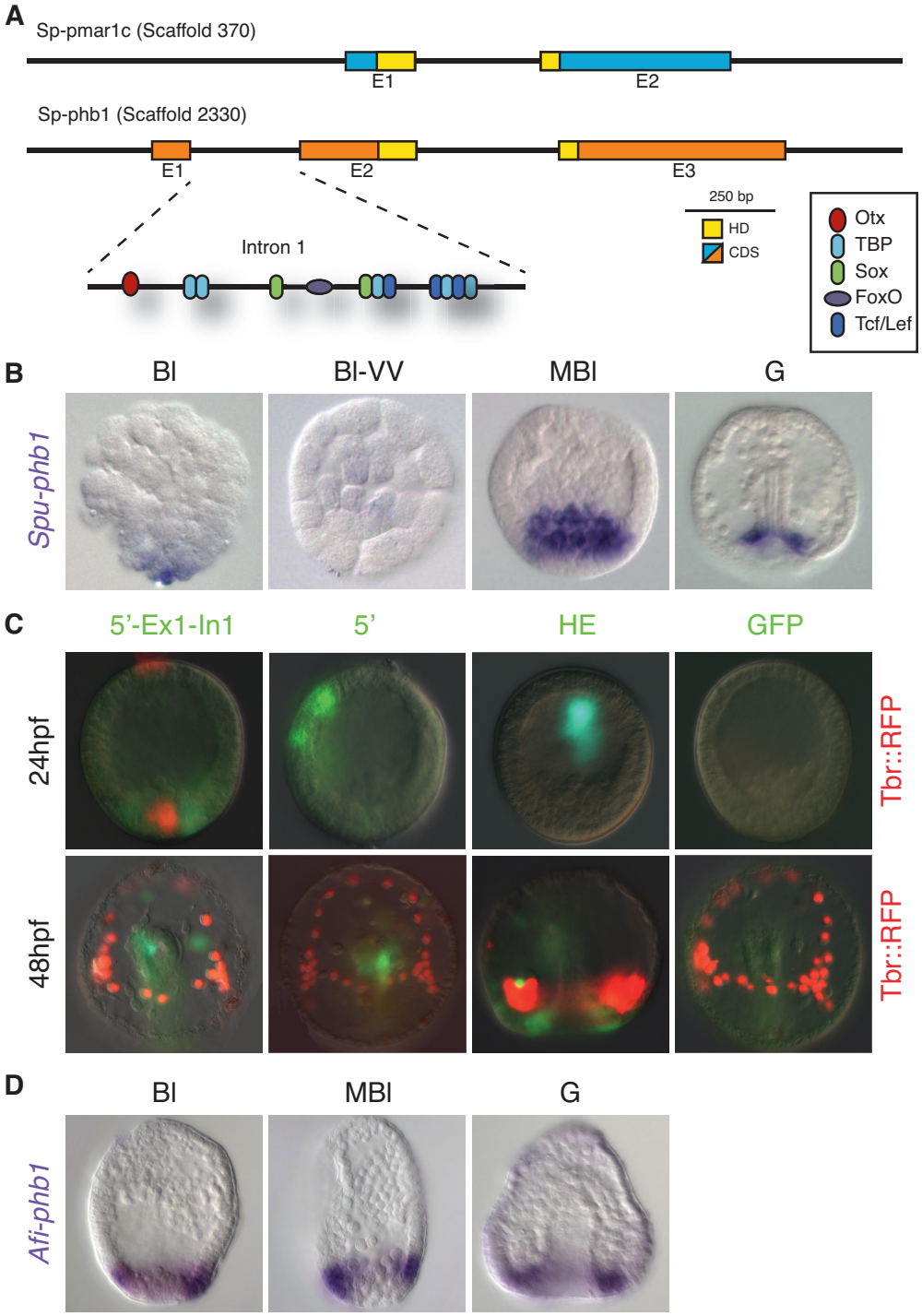

Figure 4.8: ***Spu-pmar1* as possible gene duplication of *Spu-phb1*.** (A) Comparison of gene structures of *Spu-pmar1* and *Spu-phb1*, with potential binding sites on intron 1 of *Spu-phb1*. (B) WMISH of *Spu-phb1* shows localised expression in SM cells from blastula to mesenchyme blastula stage and gets then restricted to cells part of the archenteron. (C) Microinjection experiment to determine regulatory control region of *Spu-phb1* that drives expression in SM cells. Positive control is hatching enzyme (HE), 5'-Ex1-In1 is the 5' region infront of and with exon 1 and intron 1 of *Spu-phb1* and 5' is just the 5' region of *Spu-phb1*. Constructs are described in detail in chapter 3.4.2.2. Images are representatives of most commonly observed phenotypes at 24hpf and 48hpf. (D) WMISH of *Afi-phb1* in brittle star embryos, shows expression as torus at the vegetal half of the embryo similar to sea urchin, but without expression in SM lineage througout development.

cleavage to mesenchyme blastula stage and is then expressed only at the blastopore-side of the invaginating archenteron (Figure 4.8). In contrast, *Spu-pmar1*is only transiently expressed in SM lineage and turned off during mesenchyme blastula stage (Oliveri et al., 2002). Thus, both genes are expressed in the same SM territory during early development and might be regulated in the same way. Therefore, it is conceivable that if the sea urchin *Spu-pmar1* derived as gene-duplication of exons two and three of *Spu-phb1* the *cis*-regulatory control region for expression in the SM lineage could be found in intron one of the *Spu-phb1*, which became the upstream region of *Spu-pmar1*. We first, used two online resources, TransFac (Biobase) and ConSite that uses the Jasper database, to predict potential binding sites present in the first intron of *Spu-phb1*. Interestingly, both analysis identified potential binding sites for Otx, TCF/Lef and Sox genes, next to several TATA-box elements (Figure 4.8 A). This is particularly interesting since it has been shown that the Spu-pmar1 gene is regulated by Otx and Tcf/Lef elements (Oliveri et al., 2008; Smith et al., 2007).

In order to evaluate whether intron 1 contains the regulatory region for expression in the SM lineage, I prepared two Spu-phb1::GFP fusion constructs (Figure 3.2) and checked their expression in injected sea urchin embryos at two stages of development. The first construct contained a fragment just upstream of the *Spu-phb1* gene in front of the GFP reporter and the other the same fragment plus the start of the transcription up to mid of exon 2. Both constructs consistently drive the expression of the GFP reporter above the background level (two tailed t-test $p<0.01$), determined by the EpGFPII construct that contains only the basal promoter of Spu-endo16 (Cameron et al., 2004) at mesenchyme blastula stage (24 hpf). However, both are expressed way below the HE reporter construct (Bogarad et al., 1998) that is expressed ubiquitously, thus suggesting the presence of regulatory sequence that drive localised expression of the GFP. My analysis revealed that both constructs showed no differences in expression pattern observed in different territories of the embryo (Figure 4.8 A and Table 4.2). Additionally, I never observed co-expression with the PMC marker tbr (Wahl et al., 2009). Both constructs were expressed in more embryos in

Table 4.1: Injection statistics for embryos imaged after 24hpf

Name	**GFP 1 Patch** (% ± sd)†	**GFP>1 Patch** (% ± sd)	**RFP** (% ± sd)	**Replicates** (n1/n2/n3)
HE	38.57±6.57	54.52±7.56	5.80±5.02	(26/23/23)
5'Phb1	55.34±3.13	7.06±0.14	0	(29/14/14)
5'-Ex1-I1-Phb1	43.21±4.48	9.48±0.17	20.83±18.04	(31/32/32)
epGFP	13.32±4.85	0.9±1.56	0.9±1.56	(37/19/19)

†Percentage of embryos displaying phenotype and standard deviation of three biological replicas (n1/n2/n3)

Table 4.2: Injection statistics for embryos imaged after 48hpf

Name	**GFP**			**RFP**		**Replicates**
	PMC (% ± sd)†	GUT (% ± sd)	Else (% ± sd)	PMC (% ± sd)	Else (% ± sd)	(n1/n2)
HE	67.11±24.19	51.32±1.86	5.26±7.44	3.12±4.42	21.38±22.79	(16/19)
5'Phb1	67.41±12.15	79.18±4.49	2±2.83	0	29.76±8.82	(17/25)
5'-Ex1-I1-Phb1	42.98±13.65	82.11±2.98	0	16.67±23.57	31.05±15.63	(15/19)
EpGFPii	51.39±13.75	49.31±40.27	0	5.56±7.86	54.86±0.98	(24/18)

†Percentage of embryos displaying phenotype and standard deviation of two biological replicas (n1/n2)

the gut (Figure 4.8 A and Table 4.2), indicating that the *cis*-regulatory element for gut expression is probably located in the 5' region of the *Spu-phb1* gene. A two-tailed t-test however could not support the higher levels of expression in the gut compared to the background ($p>0.05$). In order, to fully understand whether the intron 1 of the *Spu-phb1* gene can drive expression in SM lineage, another experiment has still to be conducted, using this intron1 solely upstream of a GFP reporter construct. This will be performed in future.

Based on the fact that *Spu-phb1* is expressed in SM in sea urchin I investigated whether this expression pattern is conserved in brittle star. I did not observe *Afi-phb1* expression in SM throughout the developmental stages tested. Interestingly, similar to sea urchin *Afi-phb1* was expressed in a ring of cells from blastula to mesenchyme blastula stage and later on in the gut (Figure 4.8). The absence of *Afi-phb1* in SM comprises another difference between the GRNs for larval skeletogenesis of the two species.

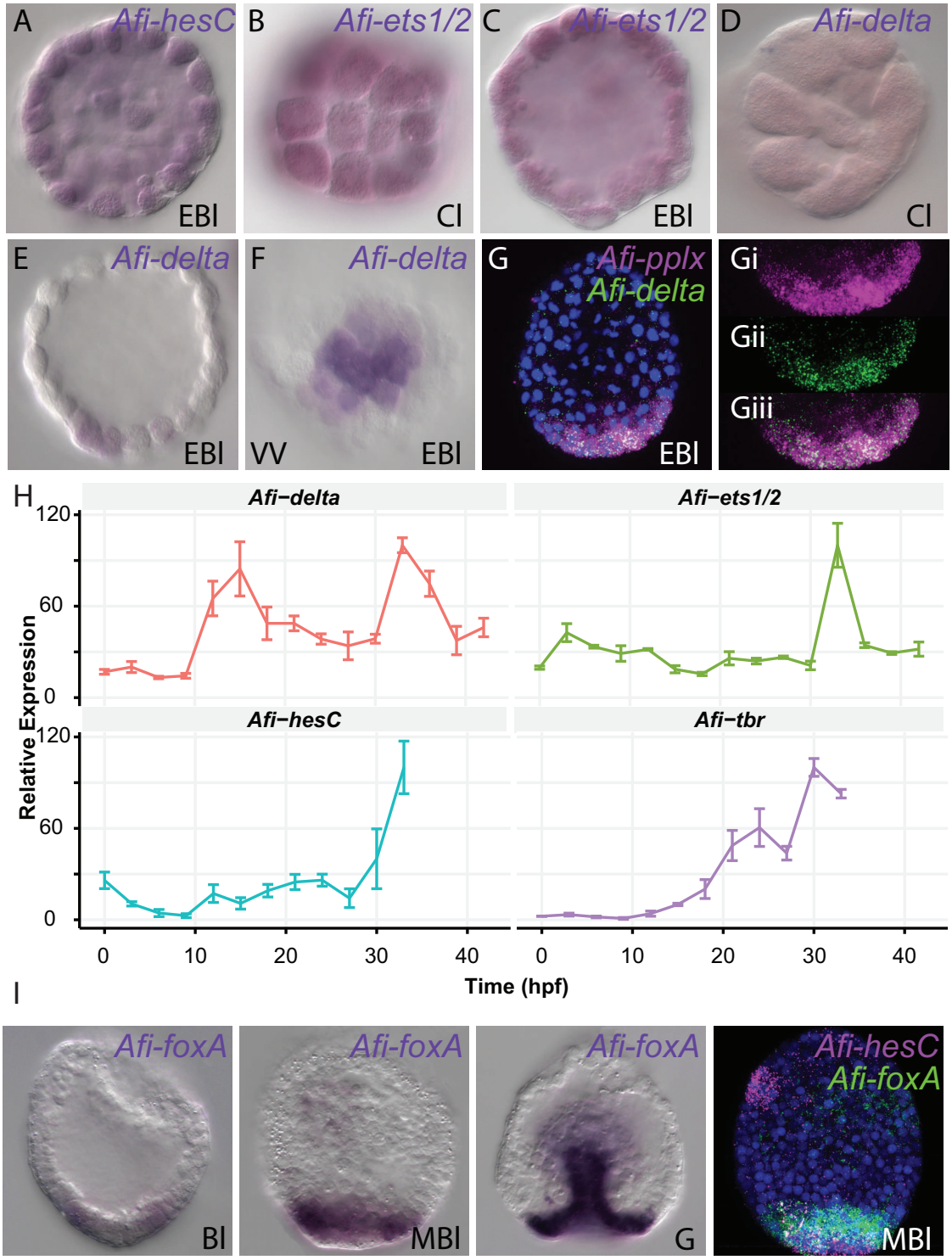
A
Afi-hesC
EBl
B
Afi-ets1/2
Cl
C
Afi-ets1/2
EBl
D
Afi-delta
Cl
E
Afi-delta
EBl
F
Afi-delta
VV
EBl
G
Afi-pplx
Afi-delta
EBl
Gi
Gii
Giii
H
Afi−delta
Afi−ets1/2
Afi−hesC
Afi−tbr
Relative Expression
120
60
0
0
10
20
30
40
Time (hpf)
I
Afi-foxA
Bl
Afi-foxA
MBl
Afi-foxA
G
Afi-hesC
Afi-foxA
MBl

4.3.4 The initial specification of *A. filiformis* skeletogenic mesoderm lineage

As already mentioned in *S. purpuratus* and other euechinoids the micromere restricted *Spu-pmar1* represses the expression of the globally expressed repressor *Spu-hesC* forming a NOT logical gate (Oliveri et al., 2008, 2003; Revilla-i Domingo et al., 2007). Directly downstream of this NOT gate, *Spu-hesC* represses a cohort of genes encoding for TF (*Spu-ets1/2*, *Spu-alx1*, *Spu-tbr* and *Spu-soxC*) and signalling molecules (*Spu-delta*), which run on ubiquitous activators, thus restricting their spatial activity into the skeletogenic lineage. The sequential connection of two NOT logical inputs results in a double negative gate (DNG). The genes downstream of *Spu-hesC* drive forward the skeletogenic program up to the activation of differentiation gene batteries (Oliveri et al., 2008). Although, I showed that *Afi-pplx*, the closest gene to sea urchin *Spu-pmar1*, is likely to function not as a transcriptional repressor and, thus, is not part of a DNG, I cannot exclude that *Afi-hesC* might still be responsible for spatially restricting the expression of the same downstream genes via its repressive action.

To investigate this possibility I isolated and analyzed the spatio-temporal expression of *Afi-hesC* and its immediate downstream genes *Afi-ets1/2*, *Afi-alx1*, *Afi-tbr* and *Afi-delta*. At the sequence level *Afi-hesC* shows conservation of all its distinctive domains, including the VRPW repressor domain making it likely to retain a transcriptional repressor function. Even though it

Figure 4.9 *(preceding page)*: **Expression of mesodermal genes in early stages of *A. filiformis* development identifies only *Afi-delta* localised at early blastula stage in the same cells as *Afi-pplx*.** (A-G) Single and double fluorescent WMISH. *Afi-hesC* (A) is not visible at cleavage stage, while *Afi-ets1/2* (B-C) is ubiquitously expressed at cleavage and early blastula stage. (D-F) *Afi-delta* spatial expression in early embryo stages. Although, quantitative data (Table A.6) show low levels of expression of *Afi-delta*, WMISH (D) fail to detect a localised expression before early blastula stage when it gets restricted to 19 ± 6 cells (n=5). (G) Double WMISH showing *Afi-delta* and *Afi-pplx* co-expressed at early blastula stage. Developmental stages are indicated at the bottom right corner of each image and probes at the top tight. (H) Time-courses for expression of mesodermal genes throughout development. *Afi-tbr* is the only gene with no maternal contribution. Error bars represent standard deviation of three technical replicas. (I) Expression pattern of *Afi-foxA* for different stages of development and double FISH showing that whereas *Afi-hesC* gets expressed in the center of the vegetal plate *Afi-foxA* remains in a torus surrounding *Afi-hesC* expression. Cl - cleavage; EBl - early blastula; Bl - blastula; MBl - mesenchyme blastula; G - gastrula; VV - vegetal view.

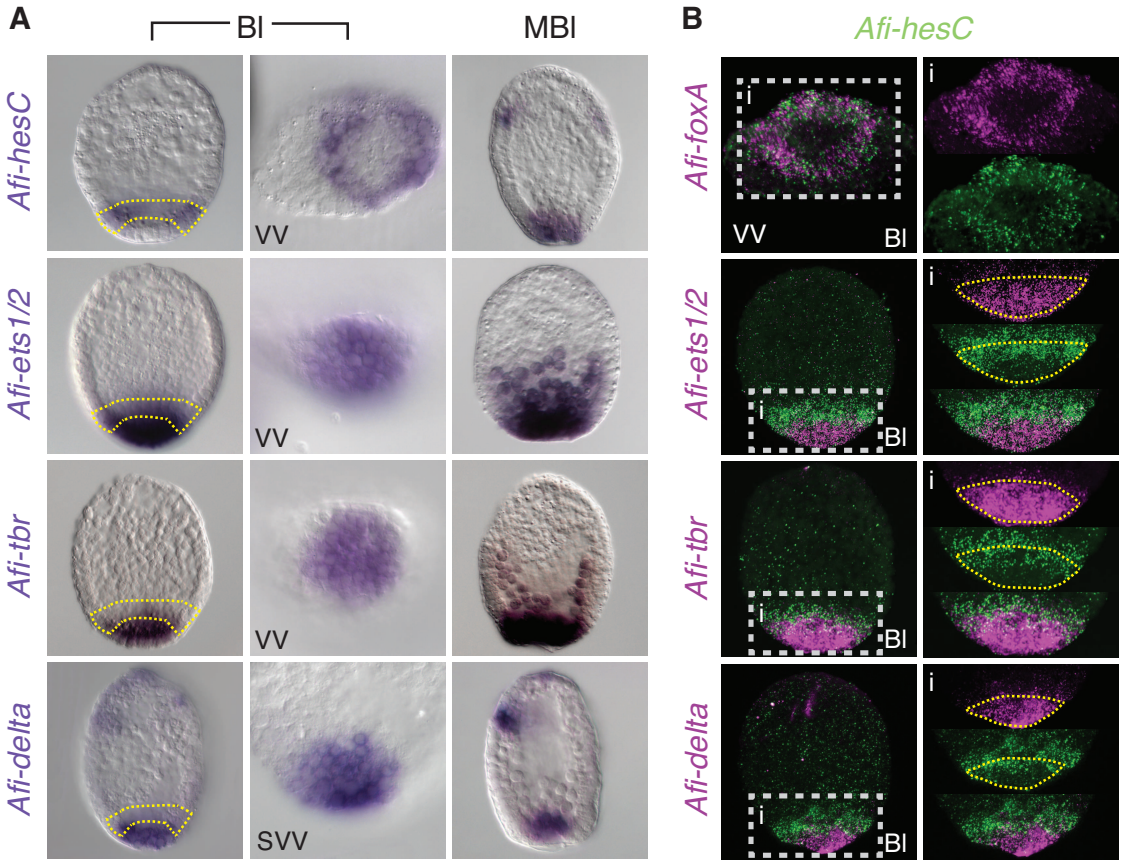

Figure 4.10: ***A. filiformis hesC* is not the global repressor that restricts the skeletogenic fate to SM cells only at the vegetal pole.** (A) Single WMISH for blastula and mesenchyme blastula stage embryos. (B) Double fluorescent WMISH on blastula stage embryos. *Afi-hesC* expression is restricted to a ring of cells in the vegetal half and co-expressed with the endomesodermal marker *Afi-foxA*. *Afi-ets1/2*, *Afi-tbr* and *Afi-delta* are co-expressed with *Afi-hesC* in one cell layer (yellow area) at the vegetal plate of the embryo at blastula stage and completely co-expressed at mesenchyme blastula stage. VV - vegetal view, SVV - semi vegetal view, Bl - blastula, MBl - mesenchyme blastula.

is ubiquitously expressed at cleavage stages (Figure 4.9), *Afi-hesC* expression at blastula stage becomes restricted to a ring (Figure 4.10), allowing a role as local rather than a global repressor. Furthermore, double-FISH shows complete co-expression of *Afi-hesC* with the *Afi-foxA* at this stage (Figure 4.10), whereas at the later mesenchyme blastula stage, it will occupy the center of the vegetal plate delimited by a ring of *Afi-foxA* expressing cells (Figure 4.9 I). In sea urchin, the *Spu-foxA* gene is initially expressed in the entire endomesoderm territory except for the SM lineage, while later in development it becomes restricted to the endoderm lineage only (Peter and Davidson, 2011). A similar expression is likely to occur in brittle star. The *A. filiformis* orthologs of the DNG downstream genes, *Spu-tbr*, *Spu-ets1/2* and *Spu-delta*, are all expressed in a large domain at the vegetal plate and importantly are all partially co-expressed with *Afi-hesC* (Figure 4.10 B). This co-expression at blastula stage makes a direct repressive action of *Afi-hesC* on them unlikely. Furthermore, Double-FISH shows that *Afi-pplx*, *Afi-ets1/2*, *Afi-tbr* and *Afi-delta* are all expressed in a larger domain than *Afi-alx1*, identified as skeletogenic precursor cells (compare Figure 4.1 with Figure 4.10 and Figure 4.14). Since *Afi-ets1/2* is expressed in 32$\pm$2 cells (n=6), *Afi-tbr* in 40$\pm$3 cells (n=5) and *Afi-delta* in 32$\pm$3 cells (n=5), their expression likely correspond to all the mesoderm (skeletogenic and non-skeletogenic) and possibly part of the endoderm territory and are not restricted only to the skeletogenic precursor cells as in sea urchin. This is consistent with the fact that at early blastula stage *Afi-delta* and *Afi-pplx* are expressed in a wider domain (20$\pm$5 cells; n=5) compared to *Afi-alx1* (8$\pm$1 cells; n=2) (compare Figure 4.3 C with Figure 4.9). *Afi-hesC* could still, as repressor, restrict *Afi-alx1* into a small domain in the center of the vegetal plate at blastula stage. Assuming that *Afi-hesC* was the main direct repressor of *Afi-alx1* in the vegetal plate, as it is in sea urchin (Damle and Davidson, 2011), the expression pattern of the genes should be mutually exclusive. The double FISH identifies some cells that do not express *Afi-alx1*, within the domain delimited by *Afi-hesC*, suggesting either a non-direct relationship between *Afi-alx1* and *Afi-hesC* or the presence of another repressor of *Afi-alx1* in these cells (Figure 4.14). Taken together, this evidence supports the absence of a pplx/hesC DNG in the

brittle star as a mechanism of SM specification.

4.3.5 High-resolution gene expression of regulatory genes reveals major differences between sea urchin and brittle star skeletogenic GRNs

Downstream of the initial tier of regulatory genes activated by the DNG, the SM network in sea urchin is stabilised by an interlocking loop (IL) engaging the three genes *Spu-tgif*, *Spu-erg* and *Spu-hex* in a recursively wired positive feed-back loop (Oliveri et al., 2008). Interestingly, it has been shown that the skeletogenic IL is conserved in mesodermal cells of starfish, a species that does not form a larval skeleton (McCauley et al., 2010), suggesting an ancestral function not directly linked to larval skeletogenesis. I isolated the orthologs of these three genes and studied their expression using QPCR and WMISH during *A. filiformis* development. In brittle star *Afi-tgif*, *Afi-erg* and *Afi-hex* are expressed only or enriched in a group of cells at the vegetal plate at blastula stage, similar to sea urchin and starfish, but with some differences in the pattern of co-expression (Figure 4.11 A). In brittle star *Afi-erg* is expressed in a smaller domain nested within *Afi-hex*- and *Afi-tgif*-expressing cells (Figure 4.11 A). *Afi-tgif* is ubiquitously expressed at low levels and enriched only at blastula stage in the cells at the vegetal pole (Figure 4.11 A). This suggests a transient function of the IL in *Afi-erg* positive cells of the vegetal plate only at blastula stage. Whereas, *Afi-erg* stays active in SM until gastrula (Figure 4.11 A), *Afi-hex* even though active in SM throughout blastula is turned off from SM as soon as they enter the blastocoel at mesenchyme blastula (Figure 4.11 A) and cannot, thus, act as a driver of skeletogenic genes at later stages. It is important to notice that at mesenchyme blastula stage these same three genes are now co-expressed in the non-skeletogenic mesoderm (NSM) and thus possibly re-establish an IL in this cell type (Figure 4.11 A). The comparison of high-resolution temporal expression patterns in the two species considered here can pinpoint the differences and similarities of initial inputs responsible for the onset of these genes. In sea urchin the three genes are activated in the following order: *Spu-hex* then *Spu-erg* and finally *Spu-tgif*, in all cases needing the prior for

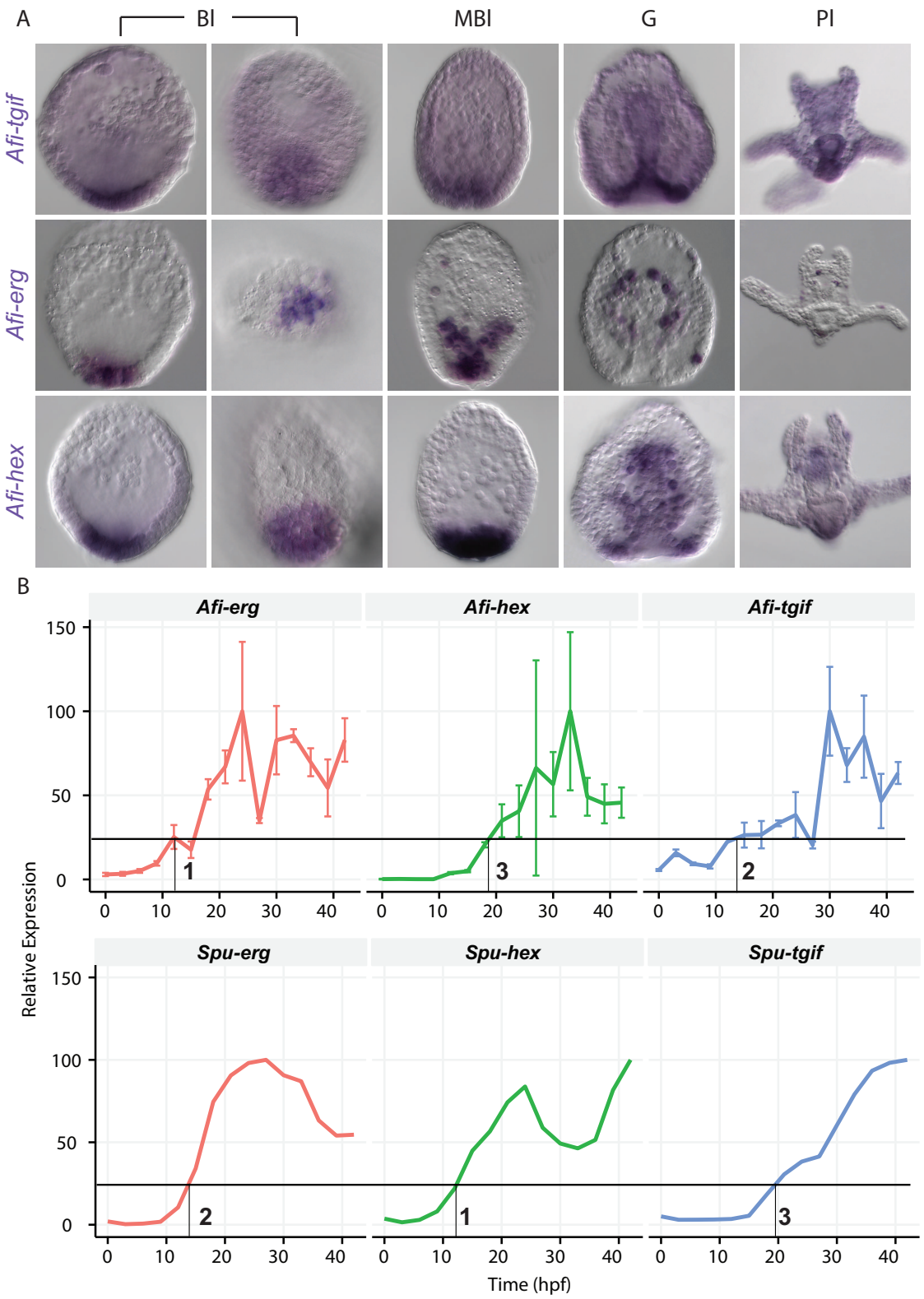

Figure 4.11: **Expression pattern of genes part of the interlocking loop.** (A) Expression pattern of *Afi-tgif*, *Afi-erg*, *Afi-hex* at different stages of development obtained by WMISH. All genes part of the interlocking loop show expression in skeletogenic mesodermal cells during blastula stage. However only, *Afi-erg* prevails expression in SM cells until mesenchyme blastula. (B) Time-line comparison of the three genes shows re-shuffling of activation order in *A. filiformis* (top) compared to *S. purpuratus* (bottom). Error bars for the brittle star time courses show standard deviation of three technical replicas. Data from the bottom was obtained from Materna et al. (2010). *VV- vegetal view, Bl blastula, MBl mesenchyme blastula, G gastrula.*

the activation of the successor (Figure 4.11 B dashed lines). Interestingly, in brittle star the order of activation is re-shuffled (Figure 4.11 B), where *Afi-tgif* and *Afi-erg* are activated first and *Afi-hex* last. Giving the fact that the precise gene expression is the direct outcome of the regulatory inputs, the differing order of onset of expression suggests potentially different initial inputs as well as different wiring of the IL in brittle star compared to sea urchin. It is important to notice that orthologs of main drivers of the sea urchin IL *Spu-tbr* and *Spu-ets1/2* in brittle star are expressed not only in SM lineage, but also in a wider mesodermal area consistent with the expression of *Afi-hex* and *Afi-tgif*, but not *Afi-erg*. This implies that *Afi-erg* requires extra input(s) to be restricted in a subset of cells at blastula stage. These data are in agreements with an ancient pan-mesodermal role of the hex-erg-tgif IL as seen in starfish rather than a dedicated SM function as evolved in euechinoids (McCauley et al., 2010).

During sea urchin skeletogenesis two extra TF, *Spu-foxB* and *Spu-dri* regulated by the gene directly downstream of the DNG (ets1/2, alx1 and tbr), are necessary for the expression of some of the differentiation genes (Amore et al., 2003; Minokawa et al., 2004). In some cases their direct inputs have been verified by promoter analysis (Amore and Davidson, 2006). Whereas *Spu-foxB* is only employed in larval skeletogenesis in sea urchin, *Spu-dri* is also expressed in the adult skeletogenic domain (Gao and Davidson, 2008). These, however, are neither involved in larval nor adult skeletogenesis in the brittle star (Czarkwiani et al., 2013), confirmed by WMISH and QPCR (Figure 4.12 and Table A.6). Taken together our data show major differences in the architecture of the *A. filiformis* skeletogenesis GRN downstream of the DNG compared to sea urchin. Indeed, the IL, while possibly still active in brittle star, is likely to be initiated by different inputs. Additionally, the late skeletogenic regulators, *Afi-foxB* and *Afi-dri*, are not responsible for driving the expression of any skeletogenic differentiation genes.

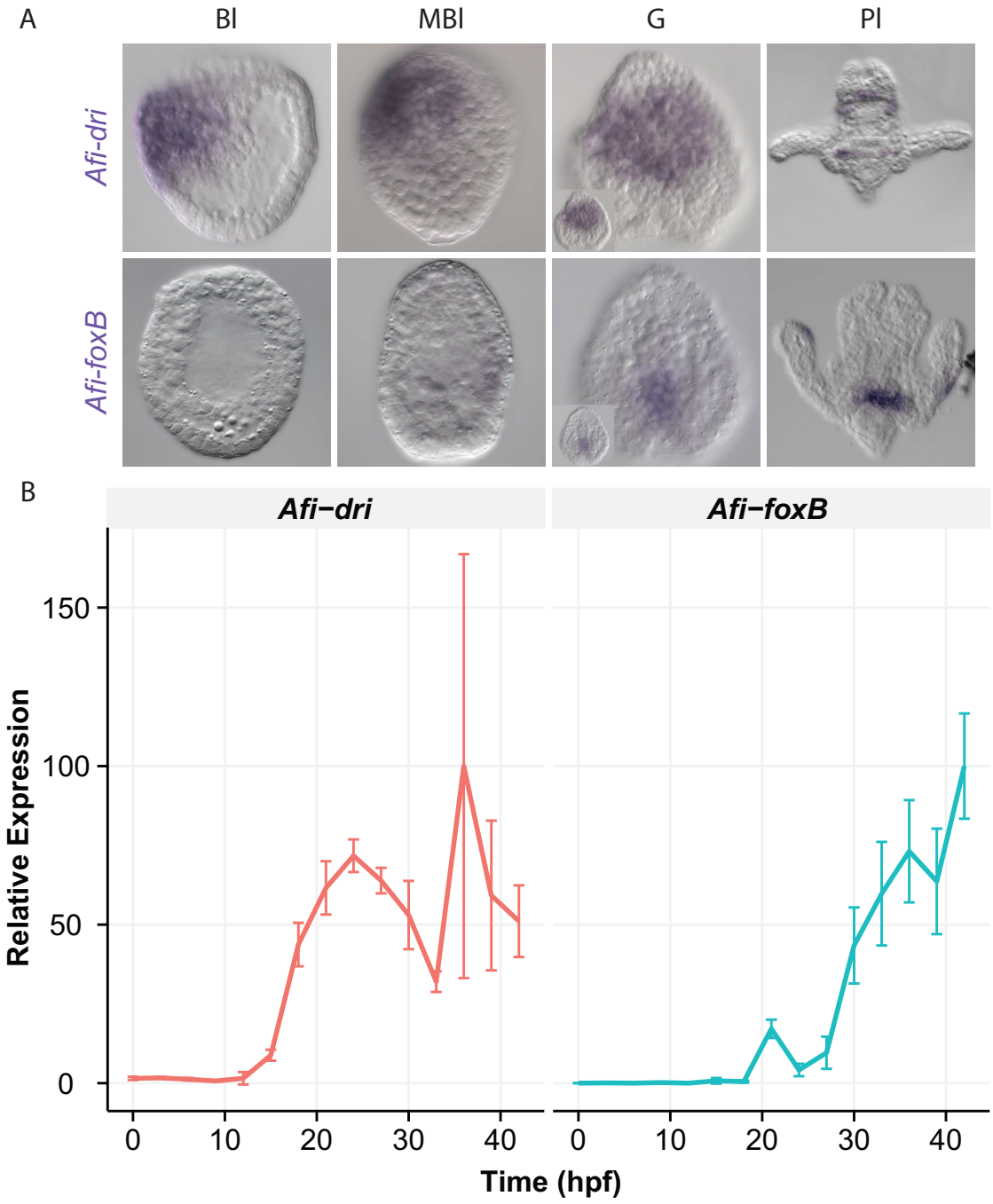

Figure 4.12: **Expression of other orthologs part of the skeletogenic GRN in *A. filiformis*.** (A) Expression pattern of *Afi-dri* and *Afi-foxB* in various stages of development, obtained by WMISH. Both genes show no expression in cells belonging to the skeletogenic lineage throughout development. (B) Time-series data shows temporal expression of both genes obtained by QPCR and normalised by the individual peak of expression. Time-series data shows consistent occurrence of expression with WMISH data. Error bars show standard deviation of three technical replicas. Cl - Cleavage; Bl - blastula; MBl - mesenchyme blastula; G - gastrula.

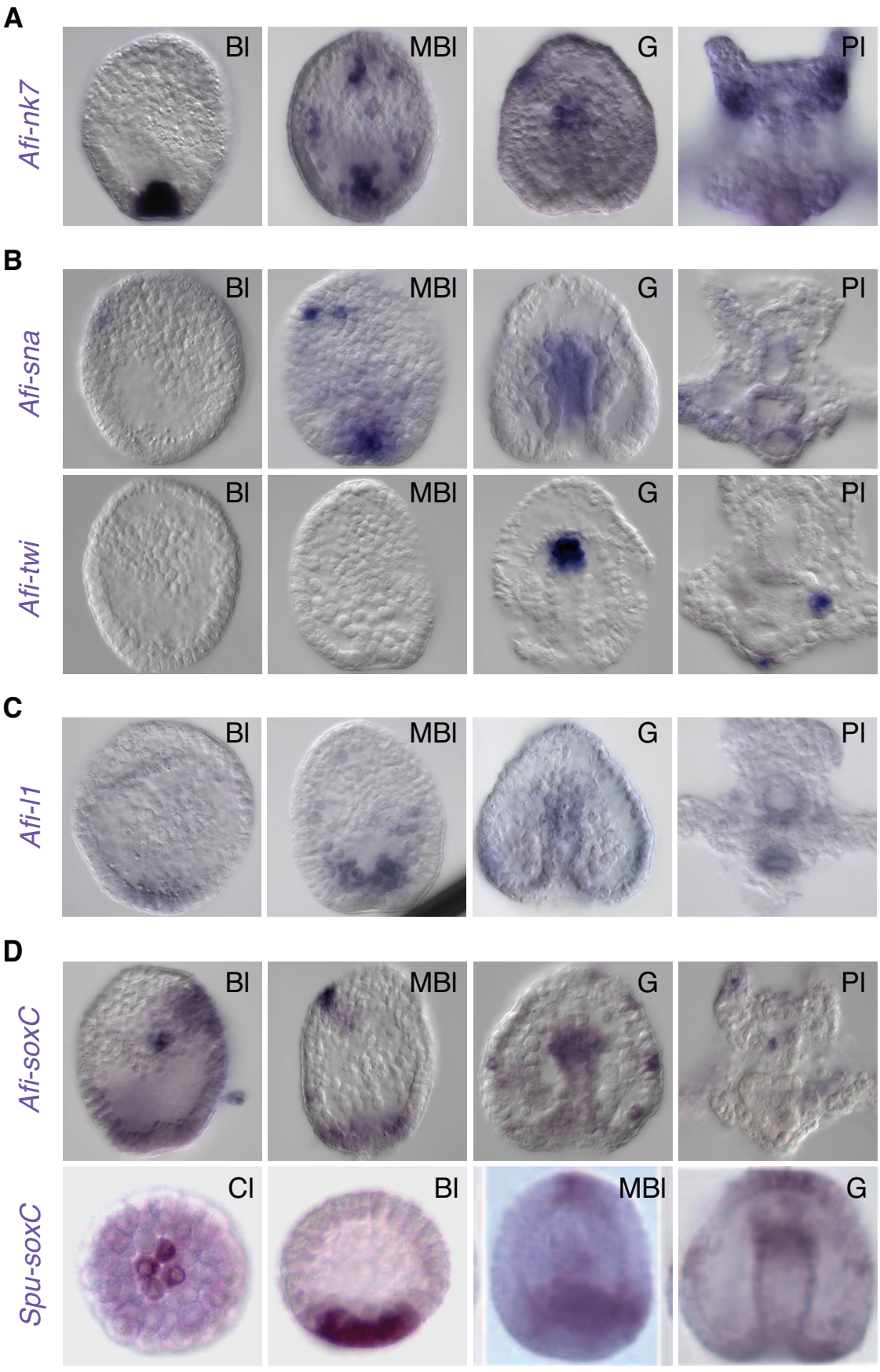
A
Afi-nk7
Bl
MBl
G
Pl
B
Afi-sna
Bl
MBl
G
Pl
Afi-twi
Bl
MBl
G
Pl
C
Afi-l1
Bl
MBl
G
Pl
D
Afi-soxC
Bl
MBl
G
Pl
Spu-soxC
Cl
Bl
MBl
G

4.3.6 Other transcription factors of skeletogenic GRN in brittle star and sea urchin

Recently, several new genes have been found to participate in the GRN for larval skeletogenesis of sea urchin. These genes are *Spu-nk7*, *Lva-sna*, *Lva-twi*, *Spu-soxC* and *Spu-l1*. In spite of their discovery, so far a detailed functional analysis of their connections within the skeletogenic GRN has not been performed. Whilst this makes a detailed comparative analysis of GRN rewiring between sea urchins and brittle stars challenging, I am still able to compare the regulatory states and analyze the evolutionary implications.

A recent study using an mRNA sequencing differential screen between embryos with and without PMCs identified the TF *Spu-nk7* as a novel candidate for the larval skeletogenesis GRN in sea urchin (Rafiq et al., 2014). WMISH of *Spu-nk7* in sea urchin confirmed its activity during SM specification showing restricted expression of this gene in SM lineage from mesenchyme blastula stage onwards (Rafiq et al., 2014). This indicates a role as late driver gene for the differentiation cascade in sea urchin. In order to see whether the ortholog of this TF exhibited similar expression in brittle star I performed WMISH of *Afi-nk7* on various developmental stages (Figure 4.13 A). In *A. filiformis* this gene shows strong expression by blastula stage, stays restricted to SM lin-

Figure 4.13 *(preceding page)*: **Expression of other skeletogenic specification orthologs.** Expression patterns obtained using WMISH. (A) *Afi-nk7* is expressed in SM during blastula and mesenchyme blastula stage. It gets restricted to the tip of the archenteron during gastrulation and ends up finally in two symmetric areas close to the mouth. (B) Expression of the EMT genes *Afi-sna* and *Afi-twi*. *Afi-sna* is first expressed in SM lineage from mesenchyme blastula stage onwards and gets restricted to some cells at the ectoderm around archenteron area until it ends up to be expressed in scattered cells in the pluteus. *Afi-twi* shows first expression in the tip of the archenteron during gastrulation and is gets restricted to the coelomic pouch during pluteus stage. (C) *Afi-l1* starts expression at blastula stage in SM cells and continues through mesenchyme blastula stage. During gastrulation expression is ubiquitous and enriched in the gut until it gets restricted to the mid and hind gut with additional scattered cells at pluteus stage. (D) Comparision of *soxC* expression in *A. filiformis* and *S. purpuratus*. In brittle star expression is restricted to one side of the embryo incorporating the cells in the SM lineage with additional enriched expression is scattered cells in the ectoderm, marking potential neuronal percursors. During mesenchyme blastula stage it gets restricted to a ring at the vegetal plate. Expression stays restricted to the tip of the archenteron and some scattered ectodermal cells during gastrulation until only scattered cells at pluteus stage show expression. In sea urchin expression is visible in micromeres during cleavage and then in the vegetal plate during blastula stage. Mesenchyme blastula and gastrula stages show similar expression to brittle star. Cl - Cleavage; Bl - blastula; MBl - mesenchyme blastula; G - gastrula; Pl - pluteus.

eage throughout mesenchyme blastula and changes activity to the tip of the archenteron during gastrulation. Finally, *Afi-nk7* ends up in a yet undefined territory at pluteus stage, on both sides symmetrically close to the mouth region (Figure 4.13 A). This suggests that compared to sea urchin *Afi-nk7* is only transiently involved in SM cells and is probably not essential to drive the differentiation cascade as in sea urchin in later stages of development.

In order for the skeleton to be formed in the lateral clusters the skeletogenic cells have to ingress from the vegetal plate into the blastocoel. This process is commonly referred to as epithelial to mesenchymal transition (EMT). A recent study in the sea urchin *L. varigatus* linked components of the GRN for larval skeletogenesis with the process of EMT (Saunders and McClay, 2014). The genes twist (*twi*) and snail (*sna*) have been identified in many taxa as participants in epithelial to mesenchymal transition (Yang et al., 2004; Peinado et al., 2004) and knockdown experiments in the sea urchin *L. varigatus* showed their involvement specifically in the process of de-adhesion (Saunders and McClay, 2014). WMISHs in sea urchin show that both *Lva-twi* and *Lva-sna* are expressed in SM from blastula to mesenchyme blastula stage. Later *Lva-sna* is expressed in NSM during gastrulation and then again SM in later stages (Wu and McClay, 2007), while *Lva-twist* always remain expressed in SM throughout development and is also activated in NSM and endoderm territories at gastrula stage (Wu et al., 2008). Consistent with the expression pattern observed, knockdown of both genes showed inhibition of EMT in sea urchin (Saunders and McClay, 2014). In brittle star, *Afi-sna* starts to be expressed at the vegetal plate during ingression of cells at mesenchyme blastula stage and is then restricted to the archenteron (Figure 4.13 B). On the other hand, *Afi-twi* first shows expression during gastrulation at the tip of the archenteron and gets then restricted to a subset of cells at one side of the gut, potentially marking the coelomic pouch. The expression of *Afi-sna* indicates a potential involvement in EMT, although, the inactivity of *Afi-twi* argues for a different mechanism compared to the sea urchin *L. varigatus*. Interestingly, in another species of sea urchin *S. purpuratus* quantification of a developmental transcriptome shows no expression of *Spu-twi* until gastrula stage (Tu et al., 2014) allowing the

hypothesis that EMT in sea urchins might have various mechanisms depending on the species. My data support closer similarity with *S. purpuratus* than *L. varigatus* in the context of EMT.

Another gene that is included in the sea urchin GRN for larval skeletogenesis is the neurofascin gene *Spu-l1*, which was proposed to act as binding partner to *Spu-vegfR* in order to facilitate the ectodermal *Spu-vegf* signalling for cell guidance during migration. Even though present in the GRN in sea urchin, I could not find any evidence for its involvement. Since it was included in my candidate list I cloned its ortholog in brittle star. WMISH showed enriched expression of *Afi-l1* during blastula stage in the vegetal pole and in SM cells during mesenchyme blastula. During gastrula stage, expression was restricted to the tip of the archenteron and remained visible in the gut region at pluteus stage (Figure 4.13 C). Assuming that the role proposed in sea urchin is correct, these results suggest conservation in the brittle star GRN for its early activity.

Finally, I looked into *Spu-soxC*. Previous work in our lab found this gene to be involved in SM specification throughout development (Figure 4.13 D), but despite being placed in the GRN for larval skeletogenesis no inputs and outputs have been identified (Oliveri et al., 2008). In order to complete my analysis of selected sea urchin skeletogenic candidates in brittle star, I analysed the expression pattern in different stages of development using WMISH. In brittle star *Afi-soxC* shows enriched expression in the vegetal half of the embryo during blastula stage and is expressed on one side of the ectoderm with strong expression in single cells (Figure 4.13 D). At mesenchyme blastula stage the expression becomes more specific in single cells of the ectoderm and in a ring of cells at the vegetal plate. At gastrula stage the expression of *Afi-soxC* is similar to *Spu-soxC*, with scattered cells in the ectodermal field and expression at the tip of the archenteron, and the subsequent restriction to scattered cells during pluteus stage.

Taken together, the genes *Afi-l1*, *Afi-sna*, *Afi-nk7* and *Afi-soxC* are all expressed during blastula stage in the vegetal plate and can thus be placed in the GRN for larval skeletogenesis in brittle star. However I observe differences in spatial activity over time, suggesting a stage-dependent re-wiring.

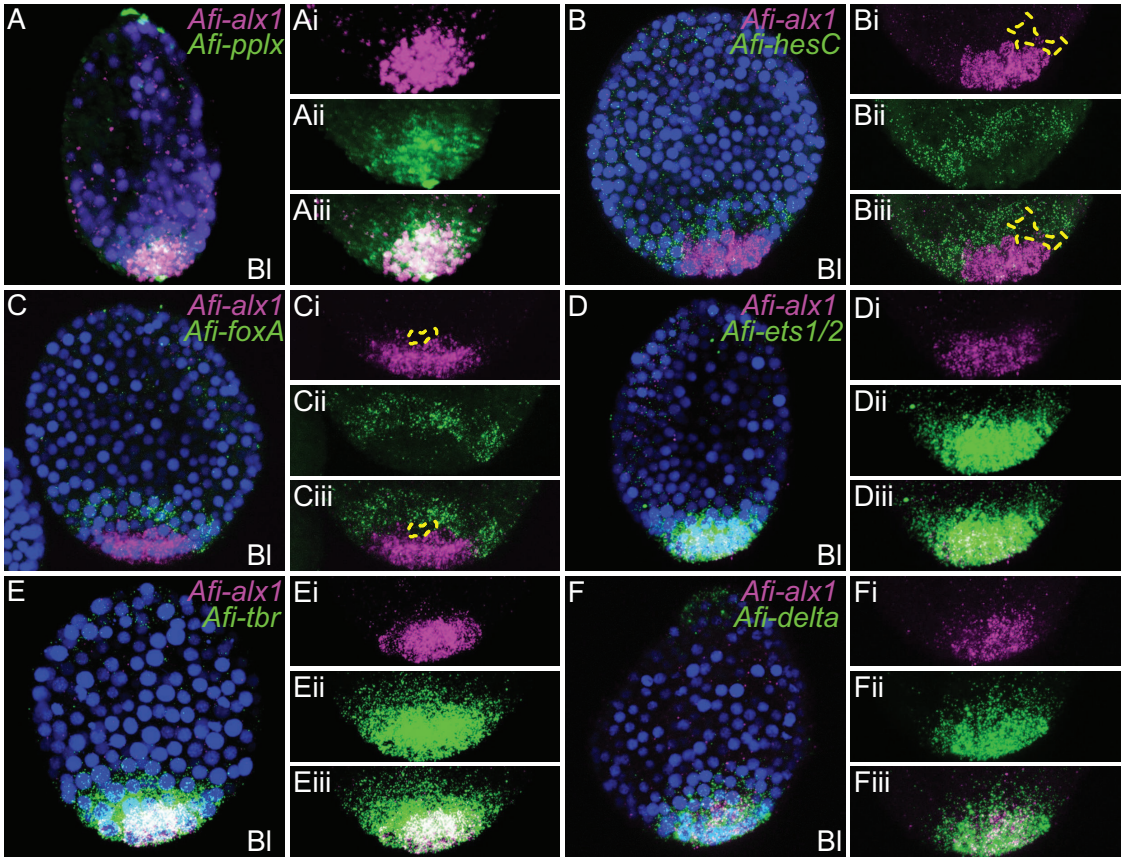

Figure 4.14: **The endomesodermal regulatory states of the brittle star *A. filiformis* at blastula stage.** (A-F) Double FISH using *Afi-alx1* expression as marker for SM cells. (A) *Afi-pplx* is expressed in a wider domain than *Afi-alx1*. (B) *Afi-hesC* is expressed as ring around the vegetal pole of the embryo and is surrounding *Afi-alx1*. The area in yellow shows cells in the vegetal plate that do not express neither *Afi-hesC* nor *Afi-alx1*.(C) Expression of *Afi-foxA* and *Afi-alx1* during blastula stage is similar to (B) and consistent to the complete co-expression of *Afi-hesC* and *Afi-foxA* at this stage (Figure 4.10 B). (D-F) *Afi-ets1/2*, *Afi-tbr* and *Afi-delta* are expressed in a large domain in the vegetal plate larger than *Afi-alx1*. Cell nuclei are stained with DAPI (blue). Bl blastula

4.3.7 Dynamic regulatory states during *A. filiformis* mesoderm development

In sea urchin and sea cucumber the skeletogenic mesoderm is formed within the mesoderm by a subpopulation of cells and it is therefore important to investigate not only the SM lineage but also the cells surrounding it. A recent study aimed to compare the development of mesoderm in different classes of echinoderms, excluding brittle stars, and showed a great degree of conservation of the blastula mesodermal regulatory state (McCauley et al., 2012), although the relative positioning of the different mesodermal cells within the vegetal plate shows certain variability.

To better understand the disposition of the SM within the mesodermal field I performed a series

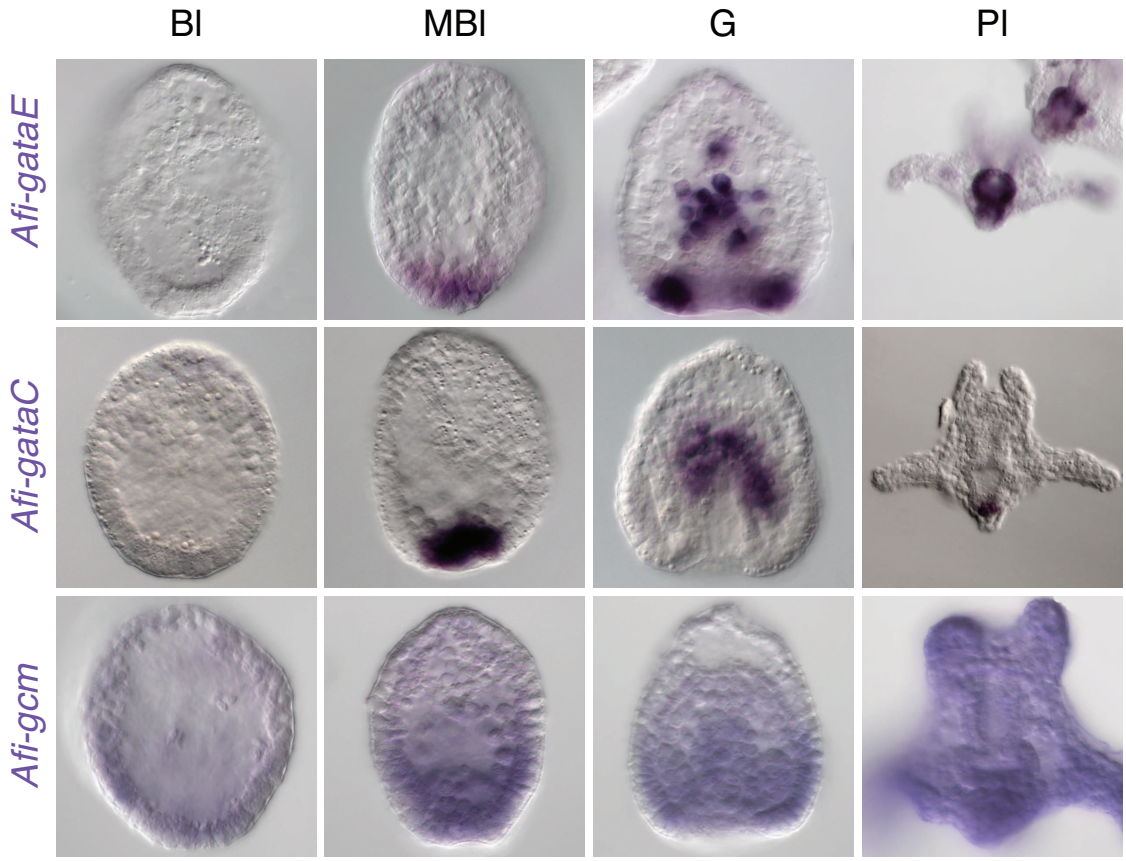

Figure 4.15: . **Expression during *A. filiformis* development of sea urchin orthologous genes involved in early specification of non skeletogenic mesoderm.** WMISH at different developmental stages. *Afi-gcm* is not detectable by WMISH at any of the stages analysed, consistent with QPCR expression levels (compare Table A.6). *Afi-gataC* expression becomes detectable at mesenchyme blastula stage in NSM cells and it stays active at the tip of the archenteron at gastrula stage. *Afi-gataE* expression becomes active in a similar fashion to Afi-gataC at mesenchyme blastula stage. At the beginning of gastrulation it marks the secondary mesenchyme cells and the cells at the tip of the archenteron. Different to *Afi-gataC*, *Afi-gataE* is additionally expressed in cells at the base of the archenteron. Both *Afi-gataC*, *Afi-gataE* are not expressed at blastula stage. Bl - blastula; MBl - mesenchyme blastula; G - gastrula; Pl - pluteus.

of WMISH on orthologs of non-skeletogenic mesoderm (NSM) specification in sea urchin, using *Afi-alx1* as a landmark for SM and *Afi-hesC* and *Afi-foxA* as the outer boundary (Figure 4.14). The TF orthologs to non-skeletogenic mesoderm specification genes (*gataE*, *gataC* and *gcm*) are not expressed during blastula stage in *A. filiformis*, confirmed by QPCR and WMISH (Figure 4.15 and Table A.6). Interestingly the SM is eccentric to the boundary delimited by *Afi-hesC*, creating yet a third mesodermal domain of unknown function (Figure 4.14). At mesenchyme blastula stage, once the SM cells ingress into the blastocoel and leave the vegetal plate, the NSM orthologs *Afi-gataE* and *Afi-gataC* are expressed in the entire vegetal plate (Figure 4.15) along with *Afi-hesC* (Figure 4.14) and other mesodermal genes (i.e. *tbr*, *ets1/2*, *tgif*, *erg*, *hex* and *delta*). Importantly, although I successfully isolated a *Afi-gcm* cDNA clone, from my quantitative and spatial analysis it is clear that *Afi-gcm* is not expressed throughout the stages analysed (up to late gastrula) and that it is not involved in early mesodermal cell specification (Figure 4.15, Table A.6 and transcriptomic data). Whereas in sea urchin the expression of *Spu-gcm* in NSM and the repression of *Spu-gcm* by *Spu-alx1* in the skeletogenic lineage plays a crucial role in the spatial separation of these two types of mesoderm, this mechanism might rely on different regulatory genes or might be completely absent in brittle stars. Indeed, brittle star larvae do not present any obvious pigment cells. The late expression of *Afi-gataE* and *Afi-gataC* also highlight major differences in the mesodermal regulatory states and suggests that NSM specification and patterning might occur at later stages compared to sea urchin.

Given that cell specification is not a single step process and that several genes contribute dynamically to different aspects of this biological process, it is essential to study the dynamics of regulatory states. To this purpose and to better understand the timing of mesodermal cell lineage separation in *A. filiformis*, the dynamics of their regulatory states and their spatial arrangement within the vegetal plate, I built a cellular resolution map of the different mesodermal regulatory states up to mesenchyme blastula stage based on the spatial data so far described integrated with quantitative data (Table A.6) and double FISH. My analysis (Figure 5.1) revealed that:

1. Only two genes (*Afi-pplx* and *Afi-delta*) have localized expression in a group of cells already visible by the end of cleavage stage (Figure 4.6 and Figure 4.9). These two genes are consistently co-expressed in $\sim$8 cells (n=2).

2. Most of the mesodermal genes, including the SM genes, start their zygotic expression around early blastula stage (12 hpf), suggesting that the initiation of mesoderm specification occurs at this stage (Table A.6).

3. At free-swimming blastula stage a cohort of regulatory genes are expressed in all mesodermal cells and likely specify a pan-mesodermal state. They are *Afi-tbr*, *Afi-ets1/2*, *Afi-tgif*, *Afi-hex*, *Afi-pplx* and *Afi-delta*.

4. At this stage (14-15 hpf) at least three distinct domains, characterised by a unique combination of transcription factors genes, are identified in the vegetal half of the embryo. A distinct SM domain in a population of roughly 16 cells is marked by the expression of *Afi-alx1*, *Afi-jun* and *Afi-erg*. A one cell-wide ring domain, expressing also *Afi-foxA* and *Afi-hesC*, surrounds the SM domain plus a small domain expressing only the pan-mesodermal genes.

5. By mesenchyme blastula the SM and the NSM are now completely segregated although both express pan mesodermal genes. The first is constituted by mesenchymal cells, which are ingressed into the blastocoel and express *Afi-alx1* and *Afi-jun* as distinctive markers. The second (NSM) remains in the vegetal plate of the blastula epithelium and is distinguished by the expression of *Afi-hesC*, *Afi-delta*, *Afi-hex*, *Afi-tgif*, *Afi-gataC* and *Afi-gataE*.

Chapter 5

DISCUSSION

In the pluteus larvae of sea urchins and brittle stars the extended mineralized skeleton is formed by a sub-population of mesodermal cells specifically expressing the transcription factors *alx1* and *jun*. These skeletogenic cells ingress as mesenchymal cells into the blastocoel before gastrulation. Despite the morphological similarities of the skeleton and its mode of development in both echinoderm classes, I reveal several differences in GRN architecture using a high-resolution multi-gene expression analysis (summarized in Figure 5.1 B). Foremost, side-by-side comparison of brittle star and sea urchin mesodermal regulatory states reveals that many differences in network architecture are apparent at the level of the initiation of the expression of skeletogenic genes, and at the level of the regulation of the differentiation gene batteries. This is consistent with the hourglass model of evolution (von Bear, 1828; Kalinka et al., 2010), in which evolutionary plasticity of network linkages differs depending on their position in the network hierarchy (early-, mid- or late-,). Our analysis also shows that gene duplication, protein function diversification, and cis-regulatory evolution took place over 480 million years of evolution to shape the larval skeletogenic networks as we see them now in the echinoderm classes which develop pluteus-like larvae.

5.1 Evolution of GRN by protein function diversification

Skeletogenesis in the regular sea urchin is unlocked at cleavage stage by the action of the pmar1/hesC DNG. In this study, I identified in a developmental transcriptome of *A. filiformis* (see

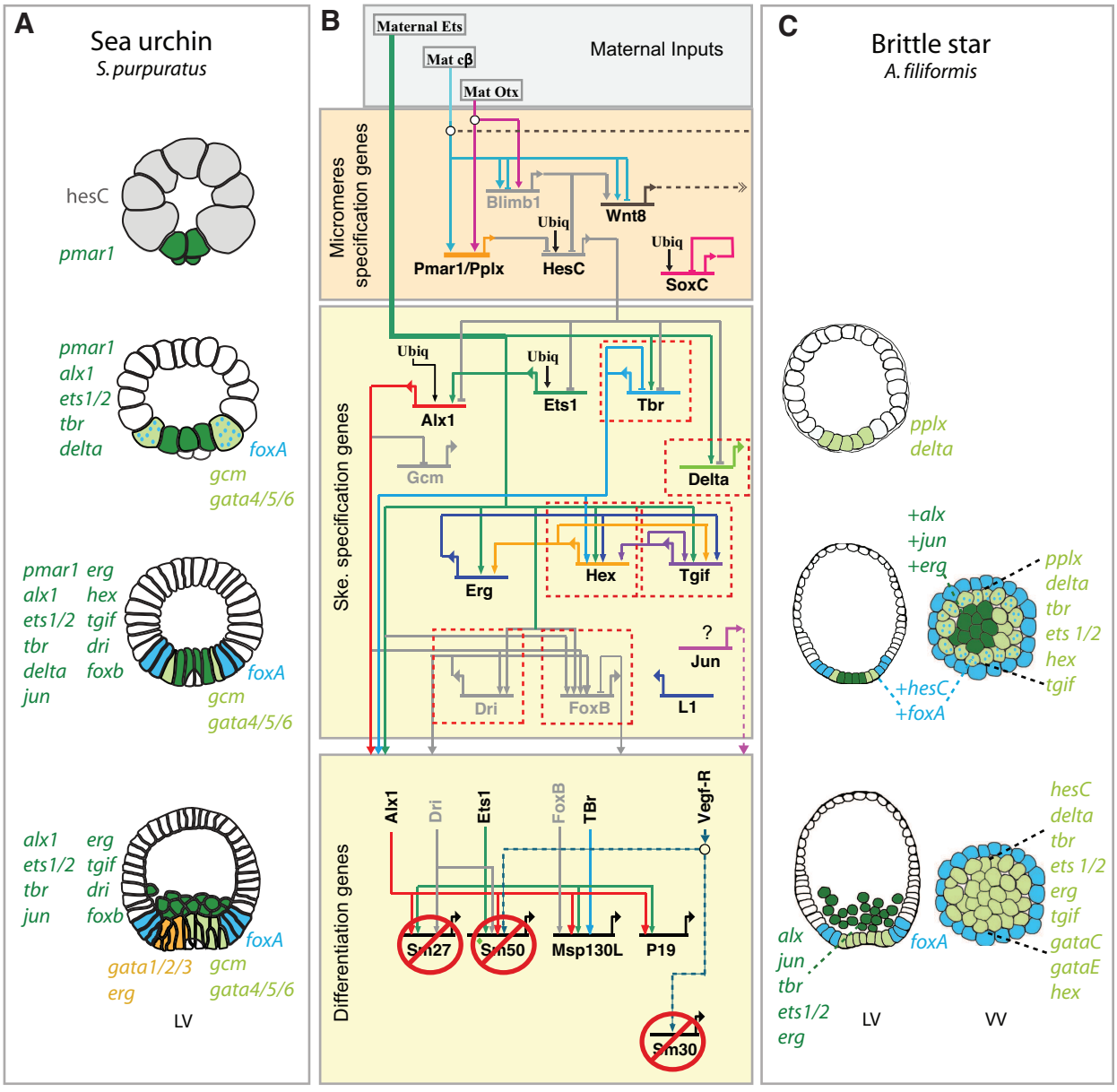
A
Sea urchin
S. purpuratus
hesC
pmar1
pmar1
alx1
ets1/2
tbr
delta
foxA
gcm
gata4/5/6
pmar1 erg
alx1 hex
ets1/2 tgif
tbr dri
delta foxb
jun
foxA
gcm
gata4/5/6
alx1 erg
ets1/2 tgif
tbr dri
jun foxb
foxA
gata1/2/3 gcm
erg gata4/5/6
LV
B
Maternal Ets
Mat cβ
Mat Otx
Maternal Inputs
Micromeres specification genes
Blimb1
Ubiq
Wnt8
Pmar1/Pplx
HesC
Ubiq
SoxC
Ske. specification genes
Ubiq
Ubiq
Alx1
Ets1
Tbr
Gcm
Delta
Erg
Hex
Tgif
?
Jun
Dri
FoxB
L1
Differentiation genes
Alx1
Dri
Ets1
FoxB
TBr
Vegf-R
Sm27
Sm50
Msp130L
P19
Sm30
C
Brittle star
A. filiformis
pplx
delta
+alx
+jun
+erg
pplx
delta
tbr
ets 1/2
hex
tgif
+hesC
+foxA
hesC
delta
tbr
ets 1/2
erg
tgif
gataC
gataE
hex
foxA
alx
jun
tbr
ets1/2
erg
LV
VV

Part II) and by phylogeny an ortholog of the sea urchin Pmar1, named here *Afi-pplx*. This ortholog was also identified in a transcriptomic study in the brittle star *Ophiocoma wendtii* (Vaughn et al., 2012). While being an ortholog I showed with a cross-species analysis that *Afi-pplx* is functionally not equivalent to its sea urchin counterpart *Spu-pmar1*. According to the gene phylogeny (Figure 4.5), gene duplication and protein function diversification events are likely to have occurred to shape the sea urchin Pmar1 into a potent repressor of the DNG. My protein phylogeny (Figure 4.5) and gene expression data (Figure 4.6) support a likely ancient duplication of the phb1 gene, which led to the emergence of the pplx/pmar1 gene expressed at the vegetal plate of the early embryo of the last common ancestor of sea urchins and brittle stars, 480 Mya. If duplicated from the phb1 gene, we hypothesised that the regulatory region driving expression in the SM lineage would be located in intron 1. Although our co-injection experiments with an SM marker could not sustain our hypothesis, we found a regulatory element that is driving expression in other territories. The functional non-equivalence of *Spu-pmar1* and *Afi-pplx* might have been caused by

Figure 5.1 *(preceding page)*: **Dynamic of mesodermal regulatory states in A. filiformis blastula and summary diagram highlighting inferred differences of skeletogenic lineage GRN architecture relative to sea urchin.** (A) Regulatory states for the mesodermal territories are shown on cellular maps of cleavage (Cl), pre hatching blastula (EBl), hatched blastula (Bl) and mesenchyme blastula (MBl). In grey all cells not part of the skeletogenic lineage marked by *hesC*. In dark green the micromeres and then the SM lineage marked by *pmar1* and then additionally at EBl by *alx1*, *ets1/2*, *tbr* and *delta*. At Bl stage, additionally *jun*, *erg*, *hex*, *tgif*, *dri* and *foxB* get activated. At MBl stage only the genes *pmar1*, *hex* and *delta* stop being part of the SM lineage. In blue the endomesodermal marker *foxA*. In light green the NSM marker genes *gcm* and *gata4/5/6*. At MBl stage the NSM is split in two territories orange marked by *gata1/2/3* and *erg* and light green. (B) *S. purpuratus* SM-GRN architecture (`http://sugp.caltech.edu/endomes/`) of the genes analysed in this study. In gray are nodes and regulatory linkages not taking place in A. filiformis SM specification, based on the observations in Figure 4.1 - Figure 4.15. In colour are the nodes and connections potentially conserved in A. filiformis. Regulatory genes in red dashed square are not expressed in skeletogenic cells during A. filiformis adult arm regeneration (Czarkwiani et al., 2013). (C) Regulatory states for the mesodermal territories are shown on cellular maps of pre hatching blastula (EBl), hatched blastula (Bl) and mesenchyme blastula (MBl). The light green cells represent the mesoderm initially identified by the expression of *pplx* and *delta*; and later expressing the pan-mesodermal genes *ets1/2*, *tbr*, *hex* and *tgif*. The dark green represent the SM cells expressing the skeletogenic marker genes *alx*, *jun* and *p19*; blue dots represent the expression of *hesC* and *foxa* within the mesoderm territory, while blue cells represents the endodermal territory that surrounds the mesoderm. At blastula stage the SM is clearly separated by the rest of NSM, while the segregation of NSM and endoderm occurs at MBl stage. Genes expressed in each territory are listed.

relaxed selective pressure on the duplicant, thus allowing the diversification of the protein function by the acquisition and loss of short linear protein motifs (i.e. eh1). These are reported as easily evolvable (Copley, 2005). The presence in all euechinoid species analyzed of several almost identical copies of pmar1 (Figure 4.5) arrayed in tandem in the same fragment of DNA (Sea Urchin Genome Project BAC Clones #170H13 and #020N20; GeneBank AC131562) suggests a further gene duplication event that possibly occurred concomitant with the emergence of the stereotypical quartet of micromeres at the vegetal pole of the euechinoid embryo. The pmar1/pplx gene type has so far been identified only in euechinoids and ophiuroids, probably due to limited sequence resources available for other echinoderm species. Most publicly available data consist of transcriptome data of specific developmental stage(s) and do not sample early embryonic stages, when the pmar1/pplx gene is likely to be expressed. An exception is given by the draft of the starfish *P. miniata* genome (Cameron et al., 2009), for which we can state confidently that no pmar1/pplx gene is present, although a clear phb1 gene is identified (Figure 4.6). Our evolutionary scenario in light of recent echinoderm phylogeny (Telford et al., 2014; O'Hara et al., 2014; Cannon et al., 2014) implies the loss of the pmar1/pplx gene at least in the Asteroidea lineage, although we cannot exclude the alternative hypothesis of independent duplication of pmar1 and pplx genes respectively in the Echinoidea and Ophiuroidea lineages. Both scenarios, however, point at the high plasticity of the pmar1/pplx node in the GRN underlying echinoderm mesoderm specification.

5.2 Evolution of GRN by changes in *cis*-regulation

High-resolution expression data of *Afi-hesC* and its immediate targets (*Afi-et1/2*, *Afi-tbr*, *Afi-delta*) integrated with the echinoderm phylogeny allows the reconstruction of the nature and timing of the molecular changes occurred to setup the DNG responsible for the precocious specification of skeletogenic fate in micromeres in the euechinoid lineage (Figure 5.1 A and C). As laid out in Figure 5.2, the predicted changes in cis-regulatory apparatus of *ets1/2*, *delta* and *tbr* to become

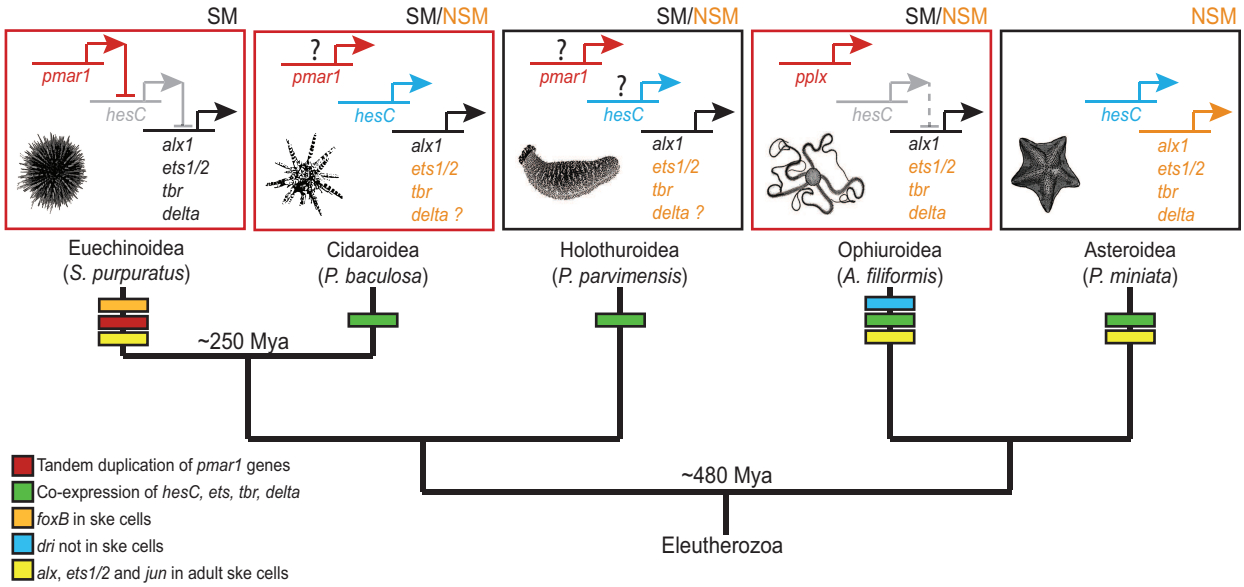

Figure 5.2: **Evolution of echinoderm larval skeletogenesis.** Simplified phylogeny of Eleutherozoa derived from recent phylogenomic studies (Telford et al., 2014; O'Hara et al., 2014; Cannon et al., 2014) summarizing in different classes our knowledge of key features relevant for larval skeleton development. Box on top indicate the skeletogenic mesoderm (SM, black) or the non-skeletogenic mesoderm (NSM, orange) and inside the boxes are depicted the key regulators of the euechinoid DNG. Red boxes indicate extended larval skeleton. HesC is in gray, instead of blue, when not expressed in skeletogenic cells. Question mark indicates no data is available on the presence and/or the expression of a specific node in a specific lineage. Dashed line, indicate possible indirect linkage. Regulatory linkages in A. filiformis are based on the observations in this study, in other species are described in (Oliveri et al., 2008; McCauley et al., 2012, 2010; Gao and Davidson, 2008; Czarkwiani et al., 2013; Yamazaki et al., 2014).

negatively regulated by HesC, and for the hesC gene to become repressed by Pmar1 (Gao and Davidson, 2008), likely occurred in the euechinoid lineage once split from the cidaroid sister group. Support for this is given by the pencil urchin (cidaroids) *hesC*, the expression of which is not consistent with a function in a DNG at the top of the skeletogenic regulatory cascade (Yamazaki et al., 2014). In cidaroids as well as in asteroids (McCauley et al., 2010) and ophiuroids (this study) *hesC* is coexpressed with its sea urchin immediate targets, *ets1/2*, *tbr* and *delta*, which are expressed in all mesodermal cells and not restricted only to the skeletogenic lineage as in sea urchin (Figure 5.1 B). This implies that *ets1/2*, *tbr* and *delta* in *A. filiformis*, as well as other classes, cannot be directly repressed by HesC and that a different mechanism must exist to drive their precise spatial expression pattern. A possible molecular mechanism emerged recently in starfish, where expression of these genes was shown to be regulated by sustained high levels of nuclear β-catenin (McCauley et al., 2014). It is interesting to notice that the expression pattern of *hesC* is dramatically different in the species studied so far (and belonging to different classes) ranging from a ubiquitous expression excluded only from a few mesodermal cells (euechinoids) to a restricted ring of cells in the vegetal half of the embryo (ophiuroids), or an ubiquitous expression excluded from the endodermal cells (asteroids), highlighting the high evolutionary plasticity of the *hesC* cis-regulatory apparatus.

Other substantial differences between the sea urchin and the brittle star are identified at the periphery of the skeletogenic network, at the level of the downstream differentiation genes, which in *A. filiformis* are not regulated by the TF Afi-FoxB and Afi-Dri either in the larva or in the adult (Amore and Davidson (2006); Czarkwiani et al. (2013) and our unpublished data). Whilst the expression of *foxB* exclusively in skeletogenic cells of euechinoid embryos supports a cooption of this gene in the larval skeletogenesis of sea urchins, the absence of *dri* function in the brittle star skeleton GRN is specific to ophiuroids, given the fact that in both sea urchin and starfish *dri* is expressed in association with skeletogenic cells (Gao and Davidson, 2008). Accordingly, extensive rewiring at the level of cis-regulatory apparatus of several differentiation genes as well

as foxb and dri themselves must have occurred to change the expression in the two classes of echinoderms.

5.3 Common regulatory state for skeletogenesis

The precise spatio-temporal expression of a developmental gene is controlled by its own cis-regulatory apparatus, which is capable of integrating multiple inputs (*i.e.* transcription factors) present in a given combination (regulatory state). Therefore, if no changes occur in the inputs or in the *cis*-regulatory apparatus of a developmental gene during evolution, the expression pattern of orthologous genes will be maintained in related species. Our experimental approach is designed to pinpoint regulatory differences in the skeletogenic GRN of sea urchin and brittle star, which result in different spatial or temporal expression of orthologous genes in the two species, given an identical regulatory state. Conversely, we assume in a conservative way that when similar expression patterns are observed, the regulatory functional connections are conserved (Figure 5.2), therefore we might actually underestimate the amount of architectural differences between the two networks in the two classes of echinoderms. Although functional studies are needed for validation, expression of *alx1* and jun at blastula stage, along with the pan-mesodermal regulatory genes *ets1/2*, *tbr*, *tgif*, *hex* and *erg*, is a common feature of the initial state of the skeletogenic program in both sea urchin and brittle star, as well as in sea cucumbers (McCauley et al., 2012), which produce small mineralized spicules. This set of regulatory genes is likely to constitute the core of a *cis*-regulatory module essential to set up the right combinatorial code responsible for echinoderm larval skeletogenesis. A direct consequence of this hypothesis is that many of the downstream genes should be directly regulated by Alx1 and other mesodermal TFs in a combinatorial fashion, and thus be expressed long before the mineralized skeleton is formed. Indeed, in sea urchin as well as in brittle star (data not shown) several mineralization genes are already expressed at blastula stage, and genome wide analyses identify *alx1* and *ets1/2* as major controllers of these differentiation genes (Rafiq et al., 2014, 2012). Furthermore, these two transcription fac-

tors along with *jun* are expressed in the plesiomorphic adult skeleton of brittle star (Czarkwiani et al., 2013), starfish and sea urchin (Gao and Davidson, 2008) (Figure 5.2).

5.4 Independent or common evolution of larval skeleton?

My data reveal substantial differences in the regulatory programs underlying the development of mineralized skeleton in the morphologically similar pluteus larvae of sea urchins and brittle stars. Adult calcitic endoskeleton is a plesiomorphic character of echinoderms, also apparent in ancient extinct species (Bottjer et al., 2006). It has been proposed that the sea urchin larval skeleton evolved by a simple co-option of an ancient adult skeletogenic GRN module (Gao and Davidson, 2008), consistent with the expression of many skeletogenic regulatory genes also in the adult skeleton, as already discussed. What about ophiuroid larval skeleton? Did it originate with the same co-option event of sea urchin or with an independent co-option event? To address this question two key aspects need to be considered: 1) the phylogenetic relationship of the five echinoderm classes; 2) the developmental-specific network nodes rather than the regulatory genes also expressed in adults and being part of an ancient skeletal GRN module. The recent availability of transcriptomic and genomic data from several echinoderm species gave rise to several phylogenomic analyses based on large data-set including representative of all echinoderm extant classes (Telford et al., 2014; O'Hara et al., 2014; Cannon et al., 2014). All these extensive molecular phylogenies converge on the consensus tree (Figure 5.2), in which echinoderms and holothurians form a distinct clade (Echinozoa) from the ophiuroids and asteroids clade (Asterozoa) and all the crinoids are sister taxa to these four classes (Eleutherozoa). In the light of this recent phylogeny (Telford et al., 2014; O'Hara et al., 2014; Cannon et al., 2014) my data, advocates for the the independent evolution of this distinctive larval character. If independently originated, a similar co-option would have occurred during brittle star larval evolution, although using different developmental genes. In fact, many sea urchin specific skeletogenic developmental genes, such as *pmar1*, *foxb*, *dri*, are not part of the *A. filiformis* larval skeletogenic GRN. On the

other hand, in the case of a single co-option event for common evolution the role of developmental genes should have been at least partially conserved (*e.g. pmar1*, *hesC* and *foxB*) between brittle star and sea urchin. Despite this, the ancient split (roughly 480 Mya) of all classes and their long branches of independent evolution make the exclusion of divergent evolution as an alternative scenario difficult. In this case the larval skeleton would have originated only once at the base of the Eleutherozoa and would have been lost in asteroids and reduced in holothurians. Importantly, independent of common or independent evolution, it is likely that the co-option happened through the same genes *alx1* and *jun* and thus at the same tier of the GRN in both echinoderm classes. This implies that the *cis*-regulatory control initiating the expression of *alx1*, and possibly *jun*, in a subset of mesodermal cells, should reveal the exact evolutionary nature of sea urchin and brittle star larval skeleton and this would be a prime focus for future investigations.

Part II

A global view on *Amphiura filiformis* skeletogenesis

Chapter 6

METHODS

6.1 Experimental

6.1.1 mRNA Samples and Extraction

6.1.1.1 Time-series

For the mRNA sequencing of different stages of development (time-series), samples were collected from the fertilisation of a single male and female at 09hpf, 18hpf, 27hpf, and 39hpf.

6.1.1.2 Skeleton inhibition experiment

To inhibit the formation of the larval skeleton the drug SU5402 (Sigma) was used. A working dilution of this drug in DMSO was added at 18hpf to a final concentration of c_f=20µM. At 27hpf three samples were collected one treated, one just with DMSO and one untreated sample in filtered sea water (FSW). The 27hr FSW sample was additionally used for the time-series.

6.1.1.3 mRNA extraction

Total RNA extraction for all samples was performed as described in Chapter 3.3.1 and the samples were eluted in 5mM Tris pH 8.5. The quality of extraction and concentrations were checked with NanoDrop 2000 and Bioanalyser 2100, all the samples had a RIN$>$8.

6.1.2 mRNA sequencing

The libraries were prepared using the TruSeq RNA library preparation protocol. The samples were sequenced with the Illumina v3 chemistry using the multiplex paired-end sequencing

protocol. The protocol uses oligo dT beads to enrich for poly-A tailed mRNA species during the process. Long non-coding and rRNA species are mostly eliminated during this process. The sequencing was performed on an Illumina HiSEQ 2500 with 100bp paired-end reads. To reach optimal coverage we sequenced 2 lanes multiplexing the 6 samples. The library preparation and the sequencing were all done at the Sickkids Hospital Toronto, Canada.

6.2 Computational Procedures

If not otherwise stated, all computational work was performed on an Apple Mac Os X 10.6 server with 24 cores and 64GB of memory.

6.2.1 Required Software

In order to assemble a transcriptome the following software packages were used:

FastQC: Quality measuring of reads (`http://www.bioinformatics.babraham.ac.uk/projects/fastqc/`).

Trimmomatic: Filtering of Adapter, Trimming of low quality basepairs (`http://www.usadellab.org/cms/?page=trimmomatic`).

Screed: Short read sequence utilities (`https://github.com/ged-lab/screed`).

Khmer: Library toolkit for k-mer based dataset analysis and transformation (`https://github.com/ged-lab/khmer`).

Trinity: Assembly for deNovo transcriptoms (`http://trinityrnaseq.sourceforge.net/`).

libgtextutils: Text_utils library (`http://hannonlab.cshl.edu/fastx_toolkit/`).

fastx: Collection of command line tools for short read FASTAFASTQ file processing (`http://hannonlab.cshl.edu/fastx_toolkit/`).

Transdecoder: Tool for open reading frame extraction (https://transdecoder.github.io).

mpiBlast: Blast programme for use on multicore cluster (http://www.mpiblast.org).

CEGMA: Tool used to identify core eukaryotic genes in our dataset (http://korflab.ucdavis.edu/datasets/cegma/).

R: Programming environment for statistical analysis (http://www.r-project.org).

R-shiny: Environment to integrate R analysis dynamically in web environment (http://shiny.rstudio.com).

Blast2GO: Environment to perform gene ontology classification (https://www.blast2go.com).

PFAM: Protein family databases used for unbiased detection of homologous protein domains of amino acid sequences (http://pfam.xfam.org).

HMMER: Tool to find protein domains using hidden markov models (http://hmmer.janelia.org).

Detailed descriptions can be found on the individual webpages about installation and application.

6.2.2 Quality evaluation of reads

Quality of reads was checked using the FastQC package. This package offers a user interface and produces html-pages as result output (see attached CD).

6.2.3 Assembly of combined samples

The assembly pipeline (Figure 7.2) and annotation of the combined dataset followed a set of unified protocols described in (Brown et al., 2013). All files containing reads were obtained in fastq

format and each sample was split into multiple files. In order not to handle too many files we concatenated the files for each sample and read direction. This resulted in 2 files for each sample. All procedures up to the actual assembly were performed on those 12 fastq files (2 files per sample). Each of the 12 files containing reads was trimmed for adapters and for low quality sequences using Trimmomatic v0.27 (ILLUMINACLIP:Adapters.fasta:2:30:10; HEADCROP:12) (Bolger et al., 2014) followed by quality filtering using the FASTX-Toolkit (v0.0.13.2; fastq_quality_filter Q33 q 30 p 50). The quality filtered and trimmed reads were then digitally normalised (Brown et al., 2012). Once all filtering and the digital normalisation was completed reads from all stages were pulled together and the transcriptome was assembled using the trinity package with standard parameters (v2013-02-25) (Grabherr et al., 2011). This assembly resulted in a 629,470 sequences constituting the initial transcriptome (IT).

6.2.4 Assembly of individual samples

In addition to the combined assembly we performed assemblies on each individual sample separately. Similarly to that described in Chapter 6.2.3, we used for each assembly the 2 concatenated fastq files containing all reads for each sample and read direction. All reads were preprocessed by trimming of adapters and discarding of low quality sequences using Trimmomatic v0.27 (ILLUMINACLIP:Adapters.fasta:2:30:10) (Bolger et al., 2014). The trimmed and quality filtered reads were then assembled using the Trinity package with standard parameters (v2013-02-25) (Grabherr et al., 2011)), without previous digital normalization.

6.2.5 Post Assembly procedures

We post processed the IT by extraction of partial and complete open reading frames (ORFs) with a minimum length of 100 amino acids that were predicted using the TransDecoder (version rel16JAN2014) script. Potential bacterial contaminants were obtained using mpiBlast (v.1.6) (Darling et al., 2003) with e-value 1e-20 and crosschecked with hits obtained against UniProtKB-

SwissProtDB with the same e-value using a custom R-script. Searches with mpiBlast were run on the Legion HPC cluster at UCL on at least 40 cores. Sequences with higher similarity to the bacterial database were removed from the dataset. The cleaned ORF dataset represents the reference transcriptome (RT).

6.2.6 Other Echinoderm Datasets

The assembled transcriptome of the crinoid *Antedon mediterranea* (Elphick et al., 2015) was kindly provided by the Elphick Laboratory (Queen Mary University, London). A genome and transcriptome data for the asteroid *Patiria miniata* was acquired from the Echinodermata website (`http://echinobase.org`). To obtain a complete picture of coding sequences we combined both genomic derived coding sequences and transcriptome sequences for the star fish.

6.2.7 Quality Assessment

Length distributions and N50 values were calculated using a custom R script[1]. Completeness of our transcriptome was estimated using CEGMA (v2.5) (Parra et al., 2007). Full-length distributions were estimated by considering all unique hits determined by blastx (1e-20) against the UniProtKB-SwissProt database and application of the analyze_blastPlus_topHit_coverage.pl perl script that is part of Trinity.

6.2.8 Annotation

All BLAST searches were performed using a local ncbi-blast (v2.2.25) with e-value of 1e-6. The RT was annotated against the sea urchin *Strongyloncentrotus purpuratus* transcriptome sequences and against the non-redundant (nr) database. One directional blast identified presumed homologs and reciprocal blast identified presumed orthologs. Gene ontology classification was performed based on a previously sea urchin specific classification (Tu et al., 2012). For consistency, sequences obtained for the starfish *Patiria miniata* (echinobase.org) and the crinoid

[1] `http://faculty.ucr.edu/~tgirke/Documents/R_BioCond/My_R_Scripts/contigStats.R`

Antedon mediterranea (Elphick et al., 2015) were annotated using the same combination of one-directional and reciprocal blast (e-value 1e-6) against the sea urchin transcriptome database.

6.2.9 Gene Ontology (GO)

6.2.9.1 Echinoderm gene ontology

Echinoderm gene ontology searches were performed using the gene ontology established for the sea urchin (Tu et al., 2012). GOs were transformed into the WHL22 annotation as part of the sea urchin transcriptome + genome (Tu et al., 2014).

6.2.9.2 General GO

A general GO analysis was performed for the differentially expressed samples using Blast2GO. The initial blastx (e-value 1e-3) step against the nr database was run locally on the legion cluster HPC with mpiblast. All other steps were performed using the Blast2GO tool.

6.2.10 Abundance Estimation

The quality filtered trimmed reads were re-aligned on the reference transcriptome using Bowtie (v0.12.9) (Langmead, 2010) with parameters set as in RSEM (v1.2.11). The bowtie output was loaded into CORSET in order to obtain counts for expression clusters (ECs) of contigs that shared reads, rather than individual contigs (Davidson and Oshlack, 2014). This is equivalent to a potential gene count adding up all isoform counts. Normalisation by internal standard was performed as follows: First, individual ECs were normalised by their peak of expression in the time-course data (9hpf, 18hpf, 27hpf and 39hpf); then, for each EC the standard deviation between the individual time-points was calculated and ECs with standard deviation below 0.01 were chosen as internal standard. Finally, an average of these 331 ECs was used as a normalisation factor, each EC was divided by this normalisation factor and multiplied by 1,000,000. All downstream analysis was performed using customised R and bash scripts. In order to make statements about annotation content in the individual EC, the most frequent annotations for each expression cluster were

considered, giving orthologous annotation priority over homologous.

6.2.11 Differential Analysis

Differential analysis was conducted on all three 27hr samples. To obtain high probability true positives of significantly affected ECs, we used a combination of GFOLD (Feng et al., 2012), a procedure specifically designed for data without a second replica and the assumptions that we only considered clusters with an expression value bigger than 2 and a log fold change bigger than 1.6 or smaller than -1.6. Due to lack of a biological replica, our approach was used to find potential candidates and their statistical validity was controlled on at least one other biological replica with QPCR (described in chapter 3.3.3).

6.2.12 Expression clustering of time-series data

To sort expression clusters by their individual trajectories we applied the fuzzy clustering algorithm (Futschik and Carlisle, 2005). We used 27 fuzzy clusters, based on the assumption that between 4 time points we have at 3 times either an increase, decrease or constant changes in expression. (Note here the difference between a fuzzy cluster and an expression cluster: A fuzzy clusters describes a group of expression clusters that share similar trajectories over time.) Since fuzzy clustering does not allocate each transcript always to the same cluster, we repeated this algorithm 100 times to find, for each EC, the most probable fuzzy cluster membership.

6.2.13 Orthology analysis

To infer orthology of a subset of genes, where the reciprocal blast approach was inconclusive, we applied the following strategy. First we obtained sequences for various species of echinoderms (Table B.6). If no protein data was available we used TransDecoder to extract the longest open reading frames. Then we applied hmmer on the Pfam-A database for each species to detect protein domains, and extracted sequences that belong to a specifc PFAM ID using a custom R-script. The extracted sequences were then used as input for phylogenetic analysis or the

orthology matrix algorithm (Altenhoff et al., 2014).

6.2.13.1 Orthology through Orthologous Matrix (OMA)

Pre-computed all vs all for the species *Mus musculus*, *Branchiostoma floridae*, *Cavia porcellus*, *Ciona intestinalis*, *Ciona savignyi*, *Dipodomys ordii*, *Latimeria chalumnae*, *Ochotona princeps*, *Oryctolagus cuniculus*, *Rattus norvegicus*, *Spermophilus tridecemlineatus* and *Strongyloncentrotus purpuratus* datasets were obtained from `http://omabrowser.org/oma/home/`. Sequences were prepared for inclusion into OMA using a custom R-script. The OMA algorithm was run on the Legion HPC cluster and sequences of interest were queried for inclusion into orthologous groups.

Chapter 7

RESULTS

In part I, I have shown that the development of the larval skeleton in sea urchin and brittle stars involves two GRNs with considerable differences, through a study using sea urchin skeletogenic candidates. This approach, however, was limited to a pre-defined list of candidates and did not allow finding genes that are specific for brittle star or sea urchin skeletogenesis. Here, I am addressing the evolution of this feature in an unbiased way using a transcriptomic approach. In this part of my thesis, I will describe how we obtained, assembled and analysed a developmental transcriptome in order to obtain a global view of *A. filiformis* development and to detect novel, currently undescribed, candidates for brittle star skeletogenesis.

7.1 mRNA sequencing: Samples and Reads

To obtain a good idea of the dynamics of gene expression throughout development we decided to sequence mRNA from a cleavage stage (09hr), a blastula stage (18hr), a mesenchyme blastula stage (27hr), and a late gastrula stage (39hr). Additionally, we collected samples at mesenchyme blastula stage (27hr) where skeleton formation was inhibited (see below for details). After mRNA extraction we analysed the quality of our samples using the BioAnalyzer 2100 (Agilent Technologies) (Figure 7.1 A). The BioAnalyzer measures degradation of RNA, using the whole electrophoresis trace of all the RNA in a sample and returns an RNA integrity number (RIN) (Lightfoot, 2002). The RIN can be between 1 (lowest quality) and 10 (highest quality). We obtained RINs between 9.4 to 10.0 (Figure 7.1 A), showing that our samples are of high quality.

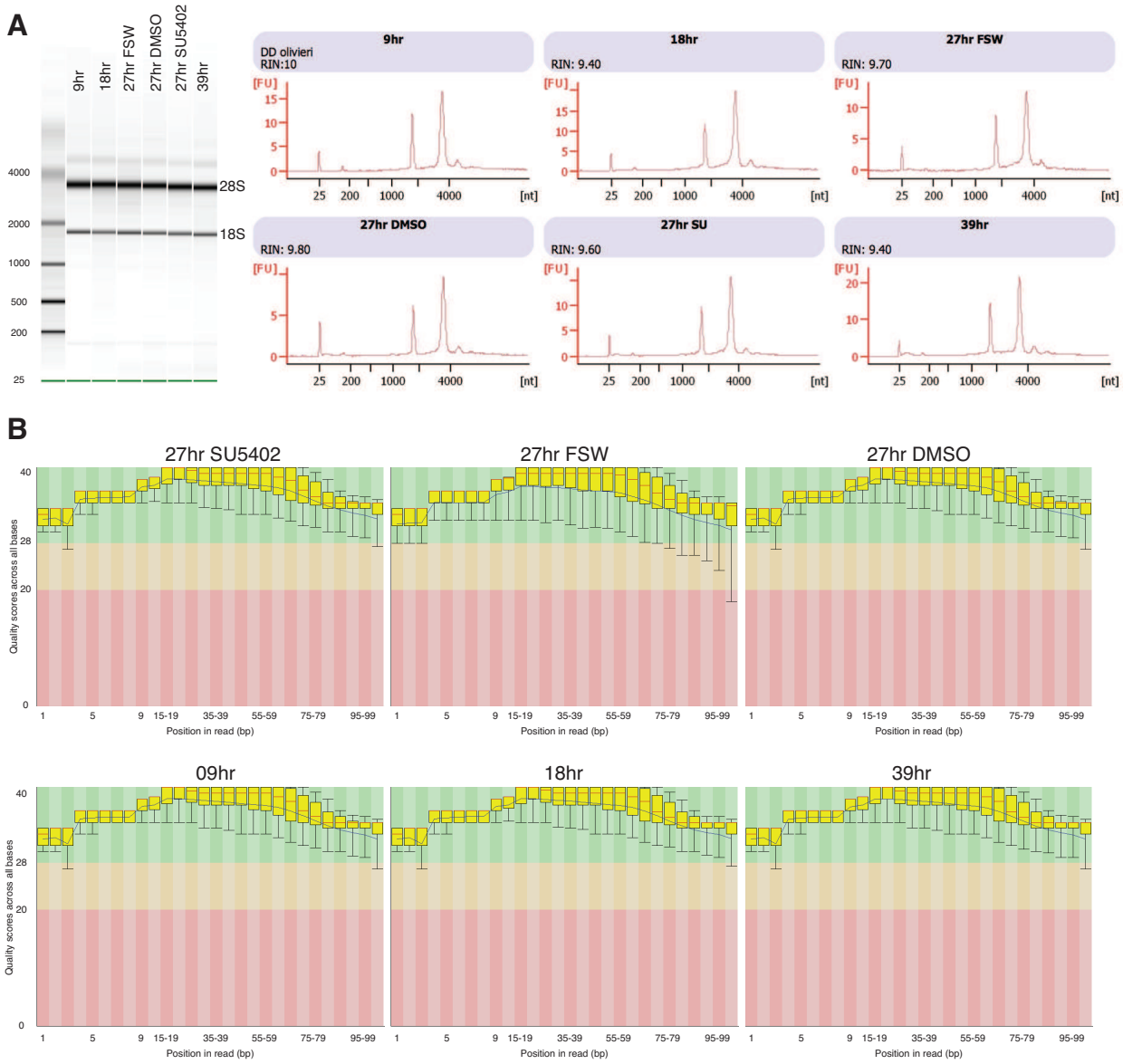

Figure 7.1: **High quality RNA samples resulted in high quality reads.** (A) Bioanalyser image and electropherogram of six samples sent for sequencing. The ribosomal RNAs 18S and 28S show little to no degradation. The Y-axis indicates the fluorescence (FU) and the x-axis indicates the molecular weight of the RNA in nucleotides (nt). (B) All samples have high quality reads (average of basepair quality within green area), as determined by FastQC.

Table 7.1: Samples and reads for assembly

Sample	Reads	Duplication Level	DigiNorm	Post-DigiNorm Duplication Level	Assembly Percentage†
09hpf	110,346,804	53.78%	38,316,233	29.45%	34.72%
18hpf	117,679,784	55.39%	39,997,943	28.81%	33.99%
27hpf	126,343,356	55.38%	41,364,607	31.78%	32.74%
27hpf-DMSO	124,834,432	57.62%	40,916,321	32.07%	32.78%
27hpf-SU	107,636,502	53.76%	39,610,310	29.97%	36.80%
39hpf	128,647,022	54.61%	44,834,020	29.8%	34.85%
Total	715,487,900		245,039,434		34.25%

†Equals Post-DigiNrom Duplication Level/Reads*100

For the sequencing we decided to use 100bp paired-end reads and to multiplex our 6 samples on 2 lanes of the Illumina HiSeq 2500 machine. The sequencing resulted in $\sim$100Million reads per sample (Table 7.1). Once I obtained the reads, I assessed the read quality using FastQC, a software package that establishes multiple measures of quality for a subset of all reads. Several of these measures are produced and all of them can be found in the attached CD. Here, I will limit description of one measure, which is the quality scores across all bases. This measure assesses the probability of a base being correct in a 100bp long read. The quality score for each base ranges from -5 to 40 and is defined as Qphred=-10log10(p), where p is the estimated probability of a base call being wrong. Thus, for example a Qphred of 20 corresponds to a 99% probability of a correctly identified base. The reads for each sample were of highest quality in the centre of their 100bp length (20-80bp) (Figure 7.1 B) and quality dropped at the edges. Despite the quality drop at the edges, the quality of our reads remained within a region that can be considered as of high quality (a score above 30 corresponding to a 99.9% probability of a correctly identified base). Generally, we obtained satisfying statistics for quality and length distribution, however FastQC estimated a duplication level of more than 50% per sample (Table 7.1). Such a high duplication level is an indicator that during the library preparation long non-coding and rRNAs have not been removed very efficiently. The processing of reads prior to assembly intends to remove overrepresented sequences, thus decreasing the duplication level (explained below).

Taken together, we sent high quality samples for sequencing and received in return high quality reads; a good basis to assemble sequences for further analysis.

7.2 Assembly of the *A. filiformis* transcriptome

To obtain all the genes expressed throughout the 4 developmental stages I assembled a reference transcriptome by joining the reads from each sample and following the khmer-protocols v0.84 (Brown et al., 2013) (Figure 7.2). These protocols offer clear guidelines for *de novo* assembly, annotation and quantification of mRNA sequencing data. Following the assembly part, I first trimmed all reads for Illumina adapters (Table B.1) and low quality basepairs, and then applied digital normalisation to remove overrepresented reads and erroneous k-mers (Brown et al., 2012). Digital normalisation distributes the reads uniformly and thus lowers the duplication levels. In our case I observed a reduction from $\sim$50% to $\sim$30% of duplication levels (Table 7.1). Once all the reads were pre-processed, I ended up with $\sim$245 million reads, which are around 34% of the original read number (Table 7.1). For the assembly I decided to apply Trinity; shown to perform better than other options in terms of gene recovery (Grabherr et al., 2011). After the computation completed I obtained 629,470 (N50: 1,094) sequences, which are here referred to as the initial transcriptome (IT). In order to assess whether digital normalisation removed essential transcripts, I attempted to assemble the combined reads without it. My attempt, however, remained unsuccessful due to the high memory requirements of trinity when working with $\sim$700 Mio reads. Thus, I assembled a transcriptome for each stage of development individually, omitting digital normalisation, to test for potential loss of data. An estimation of the basic statistics for the individual samples showed N50 values between 935bp to 1,352bp, comparable to the IT (Table B.2). However, whereas the transcriptomes of the individual samples contained 180.000-370.000 contigs the IT has nearly two times as many (Table B.2). I estimated the number of transcripts that were contained from each individual transcriptome in our IT using a blastn (evalue: 1e-20) search. The initial transcriptome contained more than 94% of sequences of the individual transcriptomes

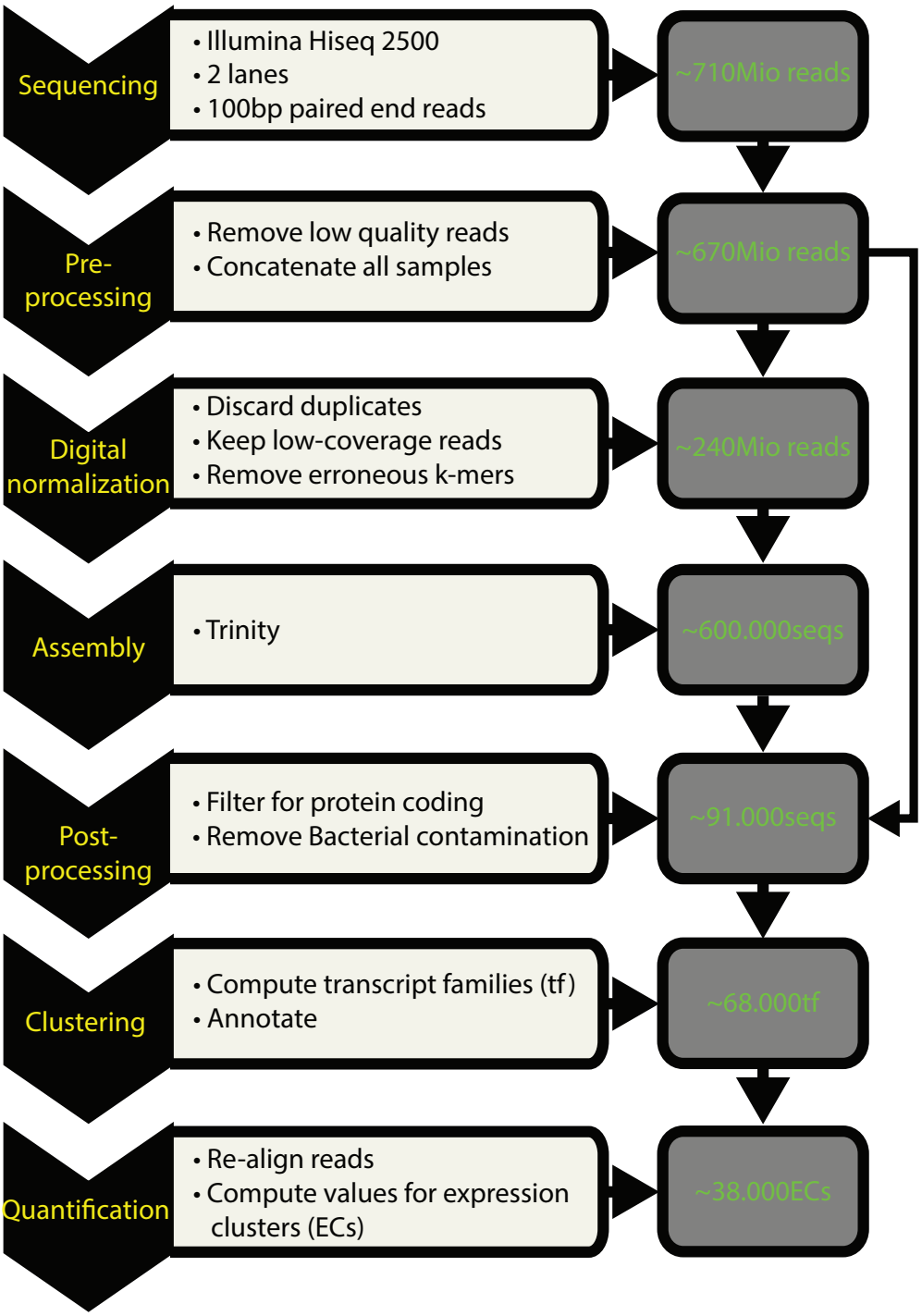

Figure 7.2: **Assembly pipeline and downstream procedures for combined dataset**

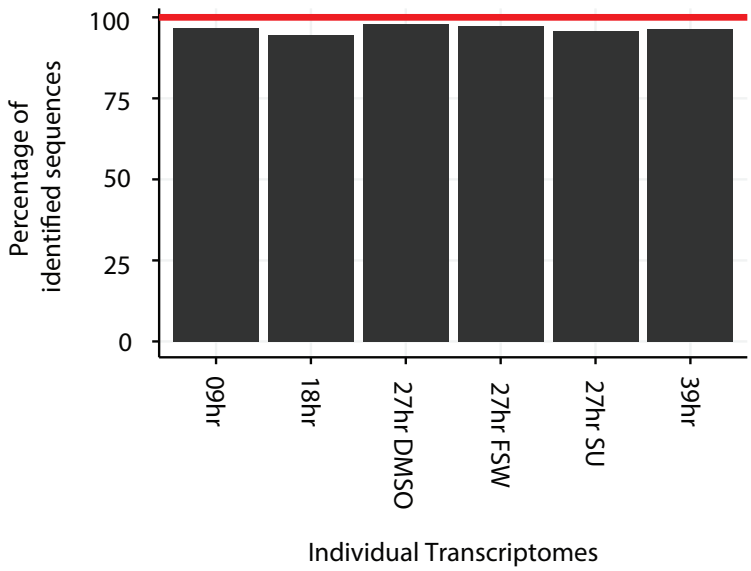

Figure 7.3: **Digital normalisation does not bias our samples.** Blastn search of individually assembled transcriptomes against the combined assembled transcriptome with digital normalisation step (IT), shows preservation of more than 94% of contigs of each individual transcriptome in the IT.

(Figure 7.3), leading us to conclude that our assembly correctly captured the majority of genes expressed throughout all stages used and that no computational artefacts were introduced with the inclusion of digital normalisation.

Using a set of assumptions previously presented for the sea urchin (Tu et al., 2012) and our main interest in protein coding sequence, I filtered the IT for all open reading frames that had an uninterrupted coding region larger than 300bp, reducing our dataset to 92.750 sequences. I removed contaminates through the application of a blastx search against 12,537,847 bacterial peptides and cross-examination with a blastx result against the Uniprot-SwissProt DB without bacterial sequences (both e-value: 1e-20). This resulted in isolating 91,311 (N50: 1,410) uncontaminated contigs, constituting our reference transcriptome (RT) (Table 7.2). Interestingly, in sea urchin, only around 29,000 transcripts are present, however, the brittle star RT has three times as many. The number of contigs produced by *de novo* transcriptome assemblers is typically large as assemblers cannot differentiate between isoforms of the same gene and thus report each separately. Moreover, artefacts such as repeats, sequencing errors, variation in coverage

or genetic variation within a diploid individual, create contigs that are not truly representative of different isoforms. As a result, transcriptome assemblers often report repeated contigs that differ only by a SNP, indel or fragmented versions of a transcript. Moreover, simulation studies using error-free reads showed that *de novo* assemblers inevitably produce multiple contigs for the same gene (Vijay et al., 2013). To account for this type of variation but not to lose sequences I clustered similar contigs that differ due to SNPs or indels into transcript families that share a protein identity of 97%. I identified 67,945 transcript families, which I used to assign unique identifiers to each contig, for example Afi.id120.tr61000 with an ID from 1 to 91,311 (number of contigs) and a TR from 1 to 67,945 (number of transcript families). On average this approach grouped 1.3 contigs to 1 transcript family. Unfortunately, splice variants and other artefacts are not incorporated into this type of clustering, resulting in a number still larger than the sea urchin assembly.

Table 7.2: Contig statistics

Species	N25	N50	N75	Longest	Mean	Median	Shortest	Contigs
Amphiura filiformis IT	2,194	1,094	538	32,304	746	452	201	629,470
Amphiura filiformis RT	2,601	1,410	639	18,993	925	525	297	91,311
Strongyloncentrotus purpuratus	6,297	4,108	2,438	22,850	2,821	2,139	400	29,072
Patiria miniata	1,131	474	351	23,898	524	369	63	263,867
Antedon mediterranea	1,508	443	186	36,836	302	156	100	607,455

Table 7.3: Length distributions

Species	#>1000bp	#>2000bp	#>3000bp
Amphiura filiformis IT	126,697	40,699	16,887
Amphiura filiformis RT	25,637	9,096	3,795
Patiria miniata	21,671	5,453	1,912
Antedon mediterranea	26,884	10,452	4,891
Strongyloncentrotus purpuratus	22,596	15,392	10,425

7.3 Transcriptome quality and datasets for comparison

Differences in samples, sequencing technology and assembly strategy make gene content comparisons from different species problematic. Therefore, quantity and quality measures are important in order to make meaningful statements in relation to the properties of the individual datasets. To assess the evolutionary conservation of gene content within echinoderms, I collected alongside the ophiuroid *Amphiura filiformois* (this study), datasets from the crinoid *Antedon mediterranea* (Ame), the asteroid *Patiria miniata* (Pmi) and the euechinoid *Strongyloncentrotus purpuratus* (Spu). Of these, only the sea urchin dataset has a well-curated genome and was recently improved by additional deep coverage transcriptome data (Sea Urchin Genome Consortium, 2006; Tu et al., 2012). Thus, it is used here as reference for comparative analysis (Table 7.2). The crinoid dataset is a transcriptomic dataset from adult arms that contain skeletal elements and the asteroid is a combined dataset of transcriptome and genome derived contigs. The first observable difference between the datasets is that all species have major differences in N50 values. N50 is a statistic that describes the length for which a collection of all contigs of that length or longer contains at least half of the sum of the lengths of all contigs. In other words a smaller number of sequences with a higher number of mean length will have a higher N50 value. The sea urchin has the highest N50 value (N50: 4208) followed by our assembly (N50: 1410) (Table 7.2). Ame (N50: 474) and Pmi (N50: 474), on the other hand, have lower but similar values for the N50 statistic (Table 7.2). Despite these differences, all datasets have similar numbers of sequences that are longer than 1000bp (Pmi: 21,671; Ame: 26,884; Spu: 22,596; and Afi: 25,637) (Table 7.3). This observation led me to conclude that the low N50 value of Ame and Pmi is masked by the high number of contigs (Pmi: 263,867 and Ame: 607,455) with many of small size.

The reference dataset of the sea urchin constitutes of 29,000 contigs, however, we have 3 times as many for Afi (91,311), 10 times as many for Pmi (263,867) and even more in Ame (607,455). Similar to Afi, I also clustered the contigs of Pmi, Ame and Spu using a protein identity

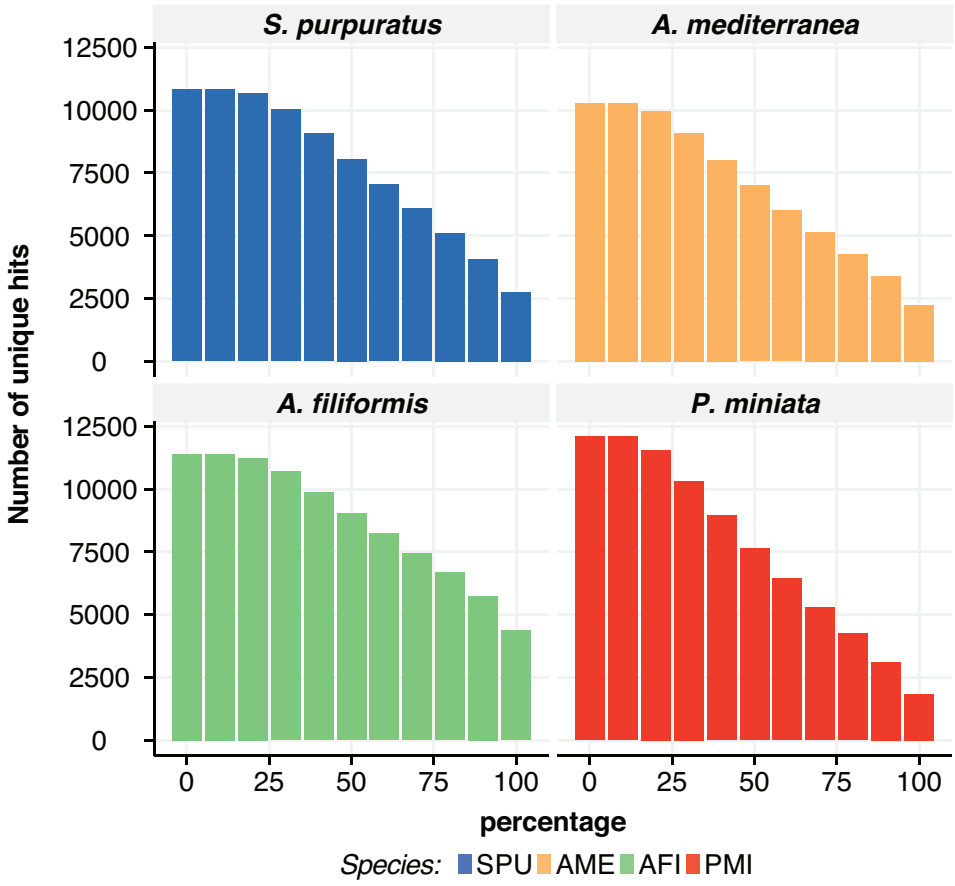

Figure 7.4: **Full length contig analysis for four representative species of the Echinodermata**. The brittle star AFI has the best >90% alignment coverage with 4,373 contigs, followed by sea urchin SPU with 2,748 contigs, then by sea lily AME with 2,234 contigs and by starfish PMI with 1,838 contigs. Values were obtained by blastx of each dataset against the SwissProt DB (evalue: 1e-20) and estimation of number of unique hits per percentage of alignment coverage.

of 97% and identified for Pmi 60,841, for Ame 598,777 and for Spu 22,112 transcript families. The estimated 22,112 transcript families in sea urchin are comparable to previously reported gene number estimates of 21,092 (Tu et al., 2012). Interestingly, while the star fish dataset is a combination of genome and transcriptome, I obtained a comparable number of transcript families to the brittle star (Afi: 67,945). The high number of clusters from the Ame contigs, on the other hand, is possibly due to the introduction of spacer nucleotides (NNNs) during the assembly in regions where a contig could not be fully assembled, and is thus an artefact of the clustering.

In order to determine how many contigs are nearly fully assembled (Figure 7.4) I performed

Table 7.4: CEGMA test for completeness of dataset

Species	# complete 248 CEGs	# partial 248 CEGs
Strongyloncentrotus purpuratus	209	246
Amphiura filiformis	205	238
Patiria miniata	193	240
Antedon mediterranea	221	246

a blastx (evalue 1e-20) search of each dataset against the Uniprot SwissProt DB and checked how many unique hits are covered by more than 90% of their sequence length with an uniprot sequence. Surprisingly, our RT showed an even higher number of more than 90% completely assembled transcripts than the well-established sea urchin dataset (compare Afi: 4,373 to Spu: 2,748) as well as both the crinoid and asteroid. The crinoid and asteroid have fewer than the other two, but are close to eachother (Pmi: 1,838 and Ame: 2,234). For transcripts that are covered by more than 40% of their length, the Pmi dataset (8,958) catches up to Spu contigs (9,063) and is even higher than Ame (8,010). The fact that the brittle star has the highest number of contigs with greater than 90% assembly is surprising, since one would expect less by sequencing of only developmental stages. A possible explanation is that our transcriptome might still contain residual human and/or other types of contamination. However, a detailed look into the first 100 Afi sequences that were covered by 100% by a human equivalent did not return a human sequence when using a blastn search. Another possibility might be that splice variants of one gene map to different closely related genes in the the Uniprot SwissProt DB, causing an artificial increase of this number.

One way to evaluate the completeness of genome or transcriptome assemblies is to scan all contigs for core eukaryotic genes, based on the assumption that the more genes are found, the more complete the dataset is. To perform such a test I applied the core eukaryotic gene mapping approach (CEGMA) and found for all datasets between 78% to 89% of 248 complete ultra-conserved core eukaryotic genes (CEG) and between 95% to 99% of 248 partial ultra-conserved core eukaryotic genes (Table 7.4). Interestingly, contrary to all other tests, the Ame

Table 7.5: Annotation

Species	evalue	reciprocal BLAST	single BLAST	other†	total	#Spu sequences	#Query sequences
Amphiura filiformis	1e-6	9,779	41,492	1,399	52,670	13,655	91,311
Patiria Miniata	1e-6	10,208	77,576	111,068	198,852	16,209	263,867
Antedon mediterranea	1e-6	9,164	26,997	1,140	37,301	12,980	607,454
Strongyloncentrotus purpuratus	1e-6	26,395	2,675	1	29,071	26,475	29,072

†Others are sequences that were automatically annotated because of the contigs belonging to a transcript family found an ortholog

dataset performed best followed by Spu, then Afi and finally Pmi.

Finally, for the brittle star I assessed the sequence quality of individual contigs by comparing our RT with 30 clones containing coding and UTR regions (cumulative length of 22,874bp), sequenced using Sanger dideeoxy sequencing technology. I used a blastn (evalue: 1e-20) search and obtained an average percentage of identity of 98.6%. On an average alignment length of 618bp the RT had 7.4 mismatches resulting in a polymorphism level of 1.2%; a value to be expected based on the fact that clones were obtained from various batches of cDNA. Taken together, I have established a high quality brittle star transcriptome and put it into context with data obtained for other echinoderms, allowing for a relative comparison of these species.

7.4 Echinomics: Annotation and Comparison

Since the closest species with a high quality genome (with more than 10,000 genes manually curated) is the sea urchin *S. purpuratus* that was recently updated with transcriptomic data (Tu et al., 2012), I used it for annotation of all the other echinoderm species used here. For the annotation I followed the khmer-protocols v0.84 (Brown et al., 2013). In this way with tblastx (evalue: 1e-6) reciprocally identified sequences were classified as orthologs and unidirectional identified sequences as homologs. Additionally, contigs that were grouped together to the same transcript family received the same annotation if no blast results were obtained. With this strategy I was able to annotate $\sim$58% of Afi sequences and $\sim$75% Pmi, however only $\sim$6% of Ame sequences. The low value for Ame might be caused due to many small sequences being part of the UTR regions and thus, are not identifiable. Detailed annotation statistics are presented in

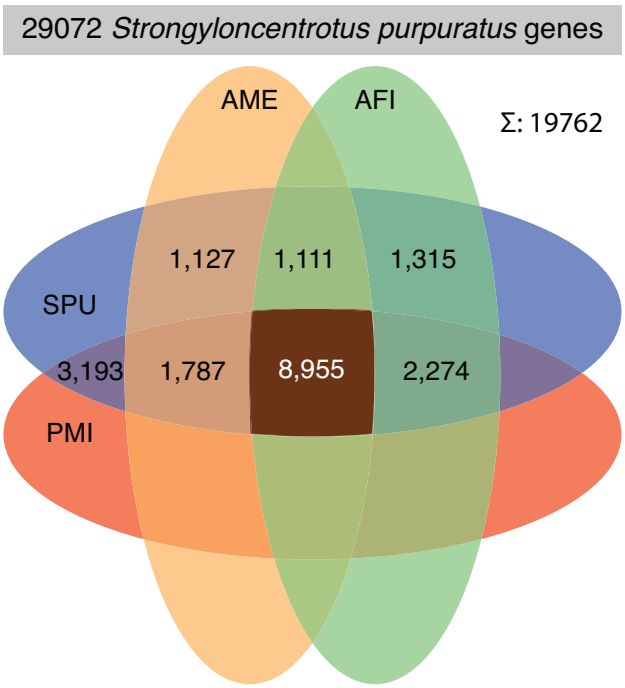

Figure 7.5: **Echinoderm gene set.** Venn diagram showing overlap of sea urchin found genes in the individual species. Afi - *Amphiura filiformis*, Pmi - *Patiria miniata*, Ame - *Antedon mediterranea*, Spu - *Strongyloncentrotus purpuratus*, Brown - Echinoderm Core (overlap of all four species).

Table 7.5. Importantly, the combined dataset of genome and transcriptome for Pmi contained the most unique sea urchin sequences (16,209), followed by brittle star (13,655) and sea lily (12,980). As positive control I annotated the Spu dataset against itself and found 91% true positives. The residual 9% were annotated by already found transcripts and are potentially wrongly identified due to recent gene duplications or splice variants Table 7.5. In order to find core echinoderm genes I computed the overlap of these four species and found 8,955 genes that were shared between all (Figure 7.5). Interestingly, each species contained subset of genes that was not present in the other (Figure 7.5). In total I find 19,762 out of 29,072 genes of the sea urchin in at least one of the other three datasets.

7.4.1 Comparison of echinoderm gene sets based on sea urchin gene ontology

A recent study explored in detail a developmental transcriptome of *S. purpuratus* in terms of gene content and established echinoderm specific ontology classifications (Tu et al., 2012). Since

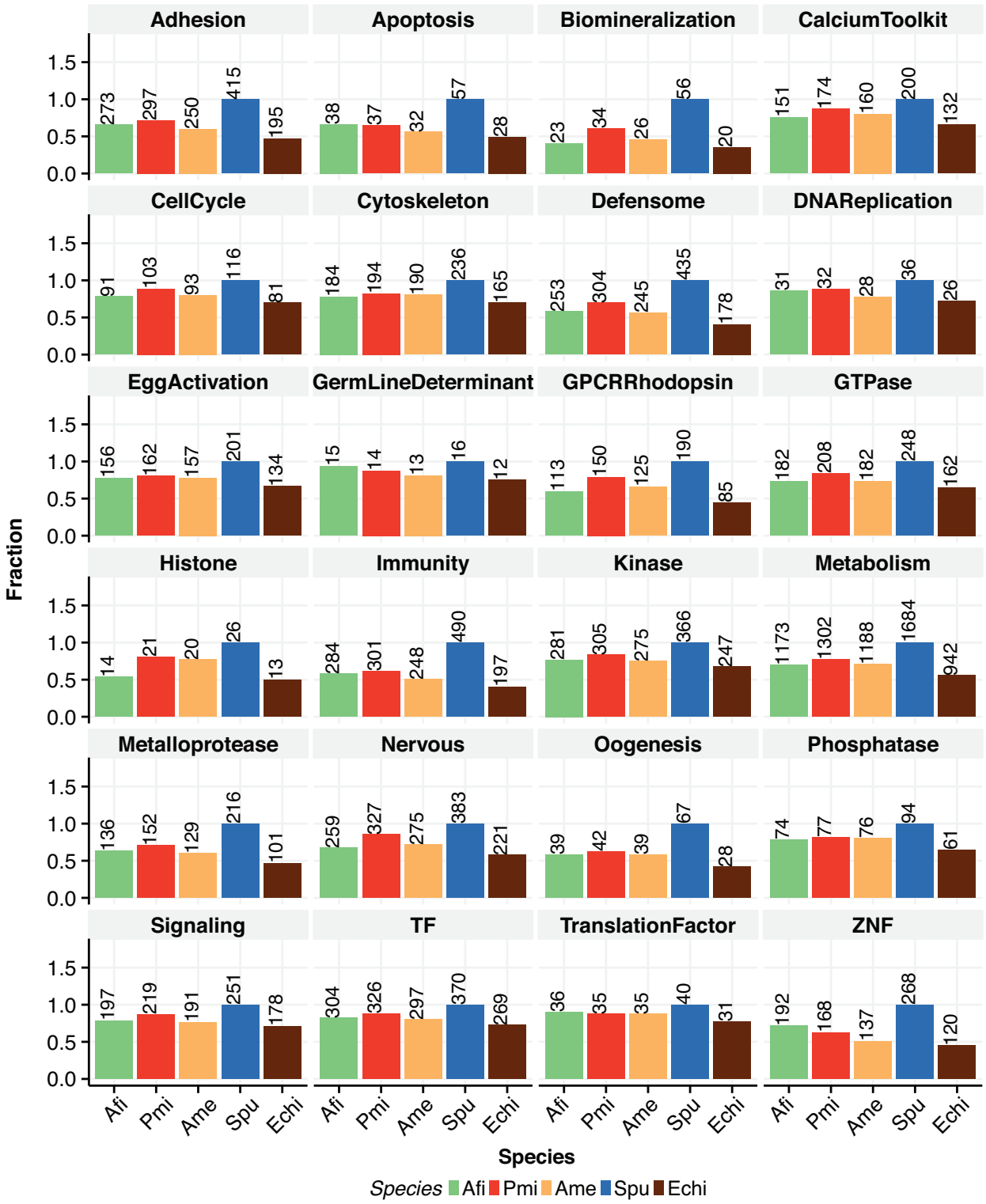

Figure 7.6: **Gene Ontology classification of echinoderms.** Annotated sequences were queried for sequences with assigned gene ontology classes established for sea urchin and numbers represent the sum of sequences belonging to one of the 24 GO classes. Afi - *Amphiura filiformis*, Pmi - *Patiria miniata*, Ame - *Antedon mediterranea*, Spu - *Strongyloncentrotus purpuratus*, Echi - Echinoderm Core (overlap of all four species).

these classes were established using the old sea urchin genome derived peptides (Sea Urchin Genome Consortium, 2006) I transformed these to the new transcriptome derived sequences (Tu et al., 2012)(see attached CD). The high quality RT and consistent post assembly data treatment of all species allowed me to apply these ontology classes and thereby compare abundance of specific functional classes with other echinoderms. I queried the annotations of the three species for sea urchin transcripts that belonged to a gene ontology class (Figure 7.6). From the total number of sea urchin transcripts with functional groups (6,461) I find 4,499 in brittle star, 4,411 in the sea lily, and 4,984 in the starfish. I observe a similar trend to the annotations with Pmi having most, Afi second and Ame least. Independently of this minor skew in annotations I am still able to find highly conserved classes in all 3 species ($>$75% each against sea urchin, sd$<$0.5). These classes are: Cytoskeleton, Transcription Factors (TF), EggActivation, Kinases, Phosphotases and TranslationFactor. On the other hand, less conserved classes are (at least one $<$65% and sd$>$0.05) include genes encoding GPCRRhodopsin, Defensome, Immunity, Adhesion, Biomineralisation, Metalloprotease, Apoptosis, zinc finger genes (ZNF) and Histones. Interestingly, the classes of Biomineralisation, Histones and ZNF showed the highest level of variation between the three groups (sd$>$0.1) and although Afi had fewer annotated genes than Pmi, I found higher conservation of ZNFs in the brittle star. Consistent with the annotation in all classes I observe some variation of genes found in one versus the other. This is shown by calculating the number of genes belonging to each class that are shared among all four species (Figure 7.6 brown bars). I refer to this subset as core echinoderm genes, due to the fact that the samples for all species were collected from different tissues, but are still shared between each other. Thus, especially these genes should have multiple roles throughout the lifetime of these echinoderms and are likely involved in basic cellular mechanisms. In total I find 3,226 genes with GO annotation in this core. One example of such a gene is MyoD (SPU_021119). While being present in Ame, Pmi and Spu it was not found in my analysis in brittle star, even though it was previously identified in a trancriptome from brittle star regenerating arms. This also consistent with the fact that in sea

urchin this gene starts its activity during gastrulation, at the onset of muscle formation (Andrikou et al., 2013; Tu et al., 2014). This additionally indicates that muscle formation might start after 39hpf in brittle star.

Since we are centrally interested in skeleton formation in these classes I examined in detail; TFs, signalling molecules and also genes involved in bio-mineralisation. I identified 304/370 transcription factors in the brittle star dataset with similar numbers in the crinoid 297/370 and the starfish 326/370. Assuming that the absolute number of TFs should be similar in echinoderms, I found 82% of TFs were employed in *A. filiformis* development; a number comparable to estimates for sea urchin development ($\sim$80% of 283 transcription factors by late gastrula (Howard-Ashby et al., 2006)). I obtained most TFs in the starfish class, consistent with the fact that this dataset is a combination of a genome and transcriptome and thus, is not limited to genes only expressed during a particular time or tissue. The fact that all datasets were collected from different samples is seen in the number of TFs 269/370 that are overlapping in the four species, which is lower than what is present in the individuals. Generally, a similar degree of conservation is observed in signalling molecules $\sim$76-87%. However, whilst showing a higher degree of variation between each other (sd$>$0.05), I observed the same trend as for the annotation. The high level of TF and signalling molecule conservation indicates, as expected that echinoderms share a similar regulome. In contrast, I generally found fewer conserved genes in the bio-mineralisation class $\sim$41-60%. Interestingly, when looking more thoroughly in this class, I found that most genes unique to the echinoids, belonged to the 14 spicule matrix genes (Afi: 1, Pmi: 5, Ame: 1), a specific type of C-lectin proteins containing a distinctive proline-rich domain (Livingston et al., 2006), and the 9 msp130 genes (Afi: 2, Pmi: 3, Ame: 4), which are glycosylated extracellular proteins (Anstrom et al., 1987). More than 50% genes encoding collagens, cyclophilins and carbonic anhydrases are, in contrast, present in all of the clades (Table B.5). Whereas the latter might comprise a core set for bio-mineralisation, the former might have evolved via echinoid-specific gene duplications. This is further supported by the fact that several spicule matrix genes, as well as msp130

genes, are in close vicinity to each other in the Spu genome (Figures B.2 and B.1), suggesting tandem duplication, and that for all three species I find the same two transcripts in our annotation (for spicule matrix genes: Spu-C-lectin and for msp130 genes: Spu-Msp130r6). Interestingly, 5 spicule matrix genes are found in star fish; a clade without larval skeleton. A detailed analysis of these sequences, using blastx, showed conservation of the proline rich repeat regions (Livingston et al., 2006) and equal similarity to many other sea urchin candidates. Thus, these 5 candidates might be an artefact of the annotation procedure. In summary, consistent with prior findings, echinoderms share a similar regulome and exhibit differences in the differentiation battery of genes. Furthermore, my search indicates that the sea urchin class of bio-mineralisation genes contains few genes and many of them sea urchin specific which raises the possibility that this class of genes is incomplete.

7.4.2 Comprehensive comparison of gene set involved in skeletogenesis

To obtain a more comprehensive picture of the genes involved in skeleton formation I gathered 1006 sea urchin skeletogenic candidates based on a literature search. This extended candidate list was compiled from proteomic studies based on skeletal elements obtained from adults and larvae (Mann et al., 2010a), a differential analysis of sea urchin mesenchyme blastula embryos where SM cells were removed (Rafiq et al., 2014), and a large-scale morpholino analysis (Oliveri et al., 2008). Similar to the GO classes, I transformed the old identifiers to the new list of sea urchin transcripts and obtained 901 candidates (see attached CD). In these 901 candidates, 37 are TFs and 32 are signalling molecules (Figure 7.8). Moreover, this dataset includes 41/56 genes previously classified as bio-minelization genes in the sea urchin GO classes, in which 14 sequences were lost when translating from the old to the new identifiers. The 901 candidates are here referred to as the skeletogenic gene set. I searched our annotated species for these candidates in order to find a core set of skeletogenic genes and possibly identify a subset specifically used in the development of the larval skeleton in echinoids and ophiuroids. Similar

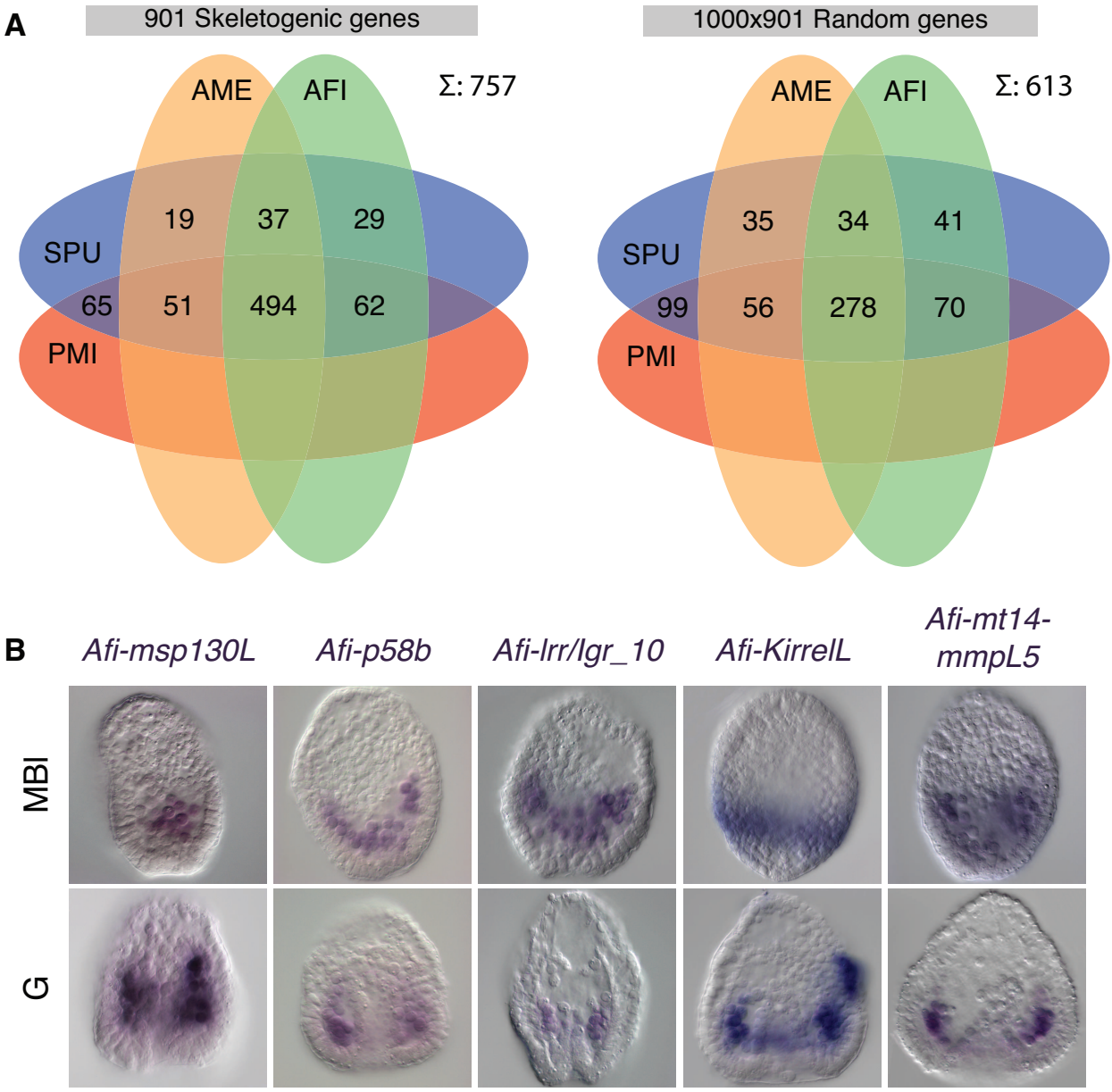

Figure 7.7: **Conservation of skeletogenic genes in echinoderms.** (A) Annotated species datasets were queried for a sea urchin list of skeletogenic genes or 1000 times random genes and overlaps were estimated. All species share 494 skeletogenic genes which represents a set of genes higher conserved than a randomly picked set of genes that share 278 in average (χ^2 proportion test: $p<0.001$). (B) Several orthologs to the downstream genes of the sea urchin skeletogenic list are also expressed in SM lineage in brittle star. Expression pattern were obtained using WMISH. MBL - mesenchyme blastula stage, G - gastrula stage.

to the trend observed in the annotation, I found the fewest skeletogenic genes in Ame (601/901), more in Afi (622/901) and most in Pmi (672/901) (Figure 7.7 A). In order to determine whether I could detect groups of genes that share more genes between two or three species, I computed species overlaps and compared these with 901 genes selected 1,000 times randomly (Figure 7.7 A). Interestingly, no clear interspecies bias was observable, suggesting no particular commonalities present in the species that develop extended larval skeleton (echinoids and ophiuroids). However, the skeletogenic list of candidates shared between all four groups seemed to be more highly conserved than a set of random genes (compare 494/757 to 278/613, χ^2 proportion test $p<0.001$).

To investigate what type of genes are part of this list, I applied the GO classification to the 901 skeletogenic candidates and the 494 core genes (Figure 7.8). I found 519/901 skeletogenic genes with GO classification and 348/494 core skeletogenic genes that are shared by all four organisms. The class of bio-mineralisation showed the biggest loss and only includes 10/41 that are shared by all four species, in line with our previous finding that this GO class contains many sea urchin specific genes. All other classes did not loose more than half of the genes that have a GO classification in the core set. The core of skeletogenic TFs consists of 32/37 genes. Of these 5 missing are TF like pmar1/pplx that so far has only been identified in brittle stars (see part I for details) and sea urchins or MyoD that is not present in Afi (explained above in detail).

From our list of skeletogenic candidates I selected several in order to confirm expression in SM lineage in brittle star. These genes are *Afi-msp130L*, *Afi-p58b*, *Afi-kirrelL*, *Afi-lrr/lgr_10*, *Afi-mt14-mmpL5* (Figure 7.7 B) and others (Figure 7.9 A). All of them, except *Afi-msp130L* and *Afi-mt14-mmpL5* that were only present in brittle star next to sea urchin, were found in all four species. Furthermore, from these genes *Afi-msp130L* (AfiCDS.id75849.tr3754) showed the lowest conservation and was only grouped as orthologous to *Spu-msp130L* before the genome was updated with transcriptomic data (Tu et al., 2012). The only shared characteristic are several repeats of the QG amino acids. A more detailed analysis using blastx against the non-redundant

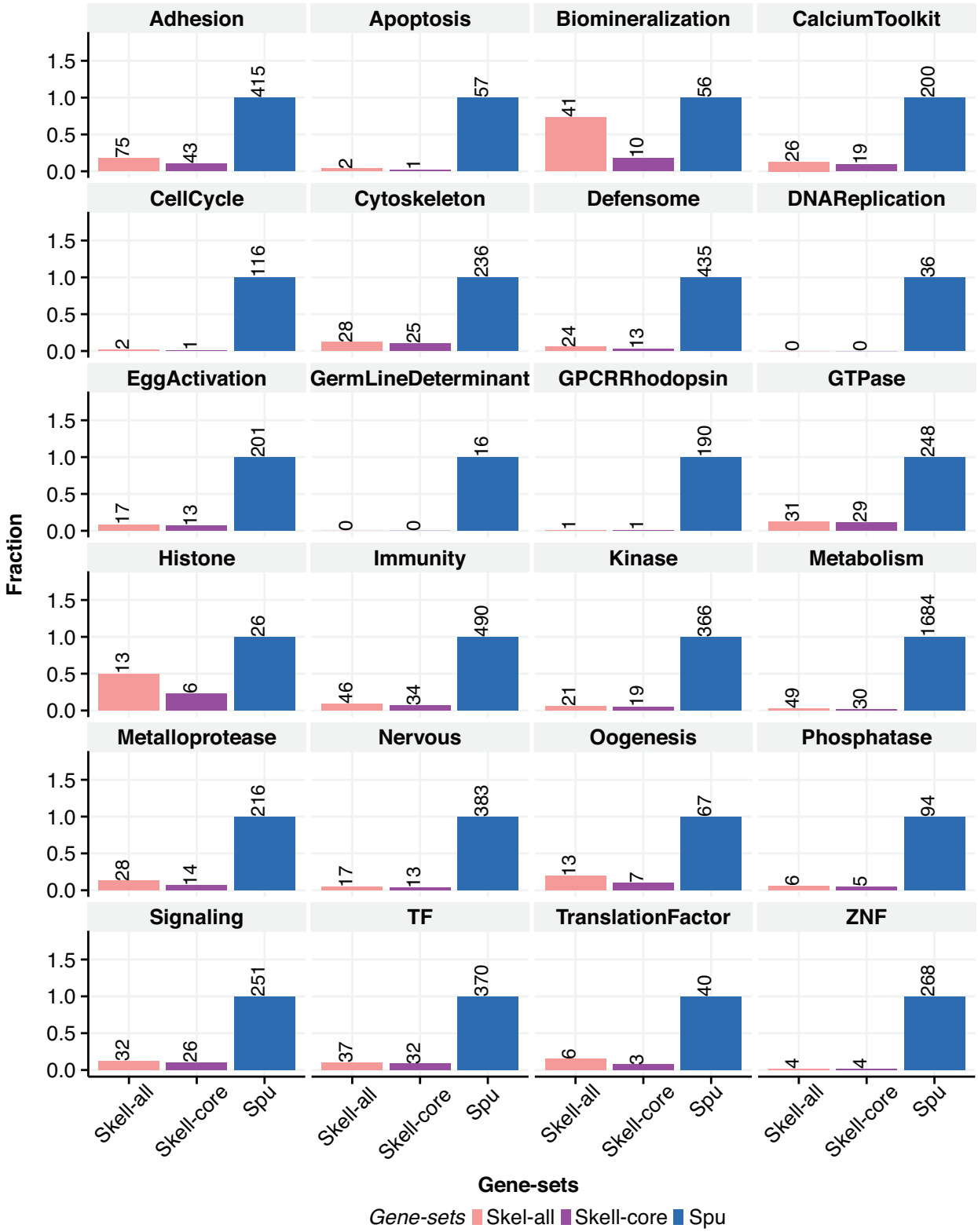

Figure 7.8: **Gene Ontology for sea urchin skeletogenic genes.** Annotated sequences of the skeletogenic list were queried for sequences with assigned gene ontology classes and numbers represent the sum of found genes belonging to one of the 24 GO classes. Skell-all - All skeletogenic genes (901), Skell-core - Core skeletogenic genes (494), Spu - All *Strongyloncentrotus purpuratus* genes with GO classification.

database however did not result in any hits and interpro did not find any conserved protein domains. Since no other annotation was available, I decided to keep the naming as *Afi-msp130L*. Most of the selected genes (9/13) show expression in the SM lineage in brittle star (Figure 7.7 B and Figure 7.9 A), whereas others (5/13) are either ubiquitously expressed or show no expression at all in the SM lineage (Figure 7.9 B). Genes expressed in both species in the SM lineage are likely part of the ancient adult skeletogenic module originated at the base of Eleutherozoa or echinoderms (if conserved in all the species analysed) and are likely to be expressed also in adult skeletogenesis, whereas the others might have been co-opted into this cell type in the sea urchins.

7.5 Quantification of *A. filiformis* transcriptome

Another advantage of mRNA sequencing is that next to information about the sequence of a contig, additional quantitative data is preserved. However, due to the high level of contig redundancy, shrewd methods have to be used in order to obtain realistic values for gene expression. Here, I used the CORSET algorithm (Davidson and Oshlack, 2014). This algorithm removes sequences for which less than 10 reads could be aligned to, forming expression clusters (EC) of contigs that share the same reads and results in expression values for each EC. These ECs are equivalent to potential gene counts and represent clusters that compensate for many redundancy artefacts described above (see 7.2). In this way 81,457 of Afi contigs were grouped to 37,999 ECs (min: 1seq, max: 66seq, mean: $\sim$2.1seq per cluster). In order to normalise the dataset between the individual samples I obtained, all ECs of the time series data set with expression values above 5 and normalised those by their individual peaks of expression. Each normalized EC that had a standard deviation between the 4 time-points (9hr, 18hr, 27hr, and 39hr) smaller than 0.01, which can be considered as constantly expressed, was used for the list of internal standards (331 ECs). I used the average value of this list as a normalisation factor. Because some ECs contained more than one annotation, I annotated each EC by their most frequent one giving

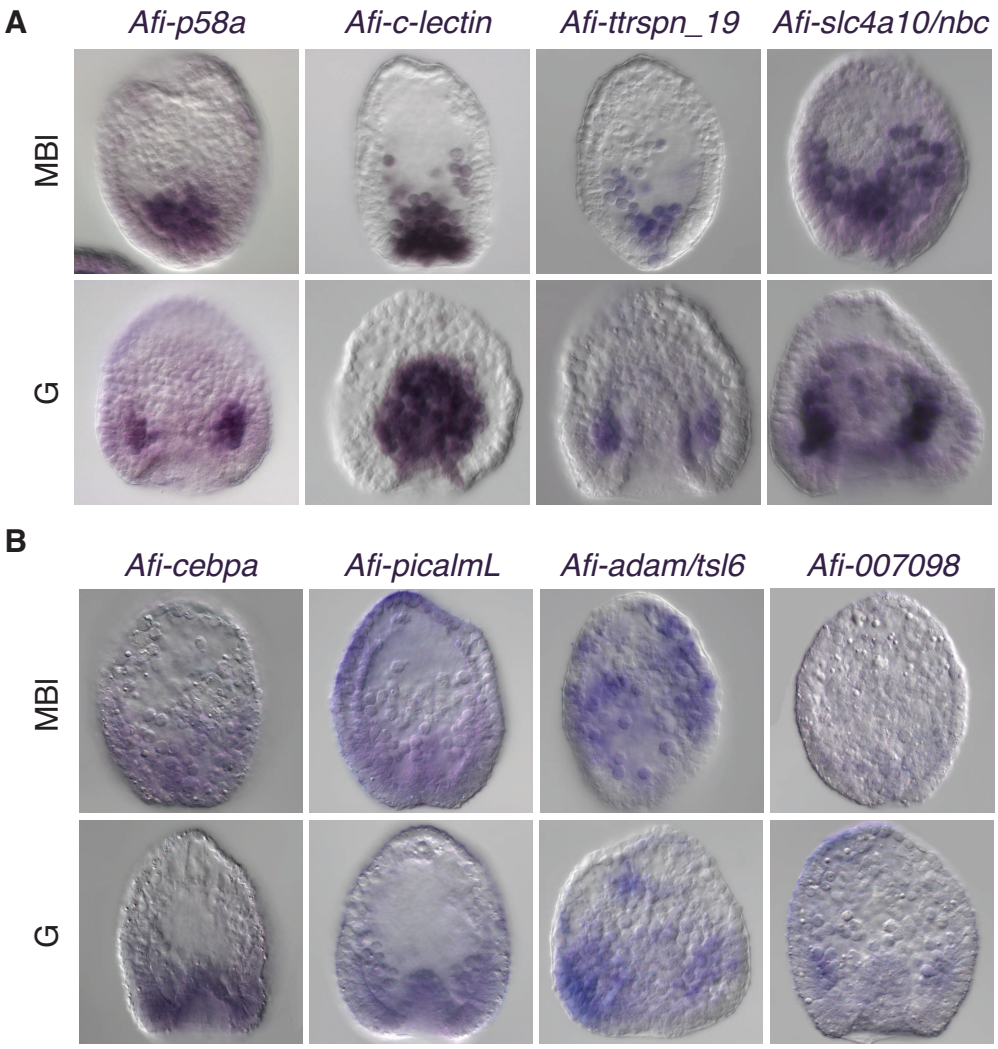

Figure 7.9: **Expression of orthologs of sea urchin skeletogenic genes in brittle star.** (A) Candidates that show restricted expression to SM lineage in brittle star. (B) Other orthologs to the downstream genes of the sea urchin skeletogenic show absent or enriched expression in SM lineage in brittle star. Expression pattern were obtained using WMISH. MBL - mesenchyme blastula stage, G - gastrula stage.

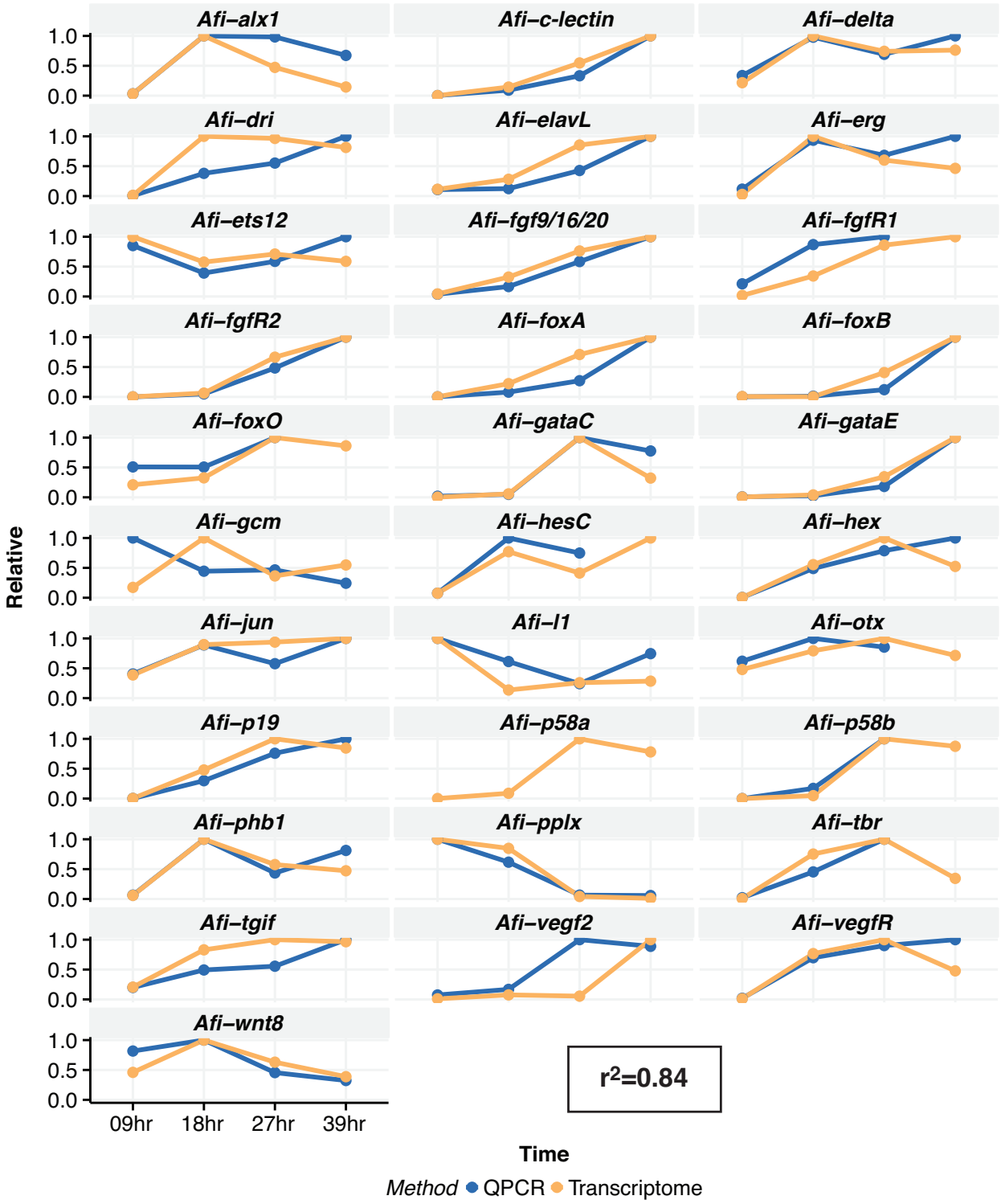

Figure 7.10: **Comparison of QPCR vs Transcriptome shows high correlation.** Comparison of normalised expression of QPCR and Transcriptome results in an average correlation r^2 =0.84. Low correlation is observed for *Afi-gcm*, however consistent with low absolute values for expression in both approaches.

orthologs priority over homologs. This caused a reduction of overall annotations from 13,656 to 11,695, however maintaining most reciprocally identified sequences 9,429/9,779. To understand in more detail the underlying causes for this reduction I looked into TF genes. I found ECs that consistent of several contigs with varying annotations. Due to the majority selection, where only the overrepresented annotation was kept or the one identified reciprocally, overall some annotations were lost. Moreover, some annotations belonged to contigs for which less than ten reads were aligned and thus removed. A summary for losses of GO classes is presented in Figure B.3 and the reasons for loss of TF annotations are presented in Table B.4. Despite this computational artefact, this method allowed me to compare normalised transcriptome expression values with normalised QPCR data. A comparison of 29 genes between QPCR and our RT showed a high level of correlation (r^2 =0.84), indicating the validity of our quantification method (Figure 7.10) for the retained genes. Interestingly, *Afi-gcm* was found not to be correlated (r^2 =-0.54), consistent, however, with the fact that accuracy decreases for low-expressed genes (Figure 7.10).

7.5.1 Clustering of expression profiles

In order to obtain a global view of time-series expression during development I used a fuzzy clustering approach that assigns each EC to one out of 27 fuzzy clusters. This algorithm assigned to 37900 ECs, 27 fuzzy clusters. 99 ECs were removed because whilst being expressed in the inhibited samples, interestingly, they were not active throughout our 4 developmental time points. I optimised the membership of each EC to a specific fuzzy cluster by re-iterating the algorithm 100 times. Each EC was then assigned to its most probable cluster. I then manually sorted the 27 clusters into 4 types of dynamical behaviour: EARLY with 10,593 f-clusters, LATE with 9,968 f-clusters, INTERMEDIATE with 8,531 f-clusters and BI-MODAL with 8,808 f-clusters (Figure 7.11). EARLY f-clusters contained ECs that showed decreasing expression across the first 3 time-points. In these f-clusters I expected to find genes that are responsible for early specification and are only transiently active and maternal genes, already present in the unfertilised egg. In to-

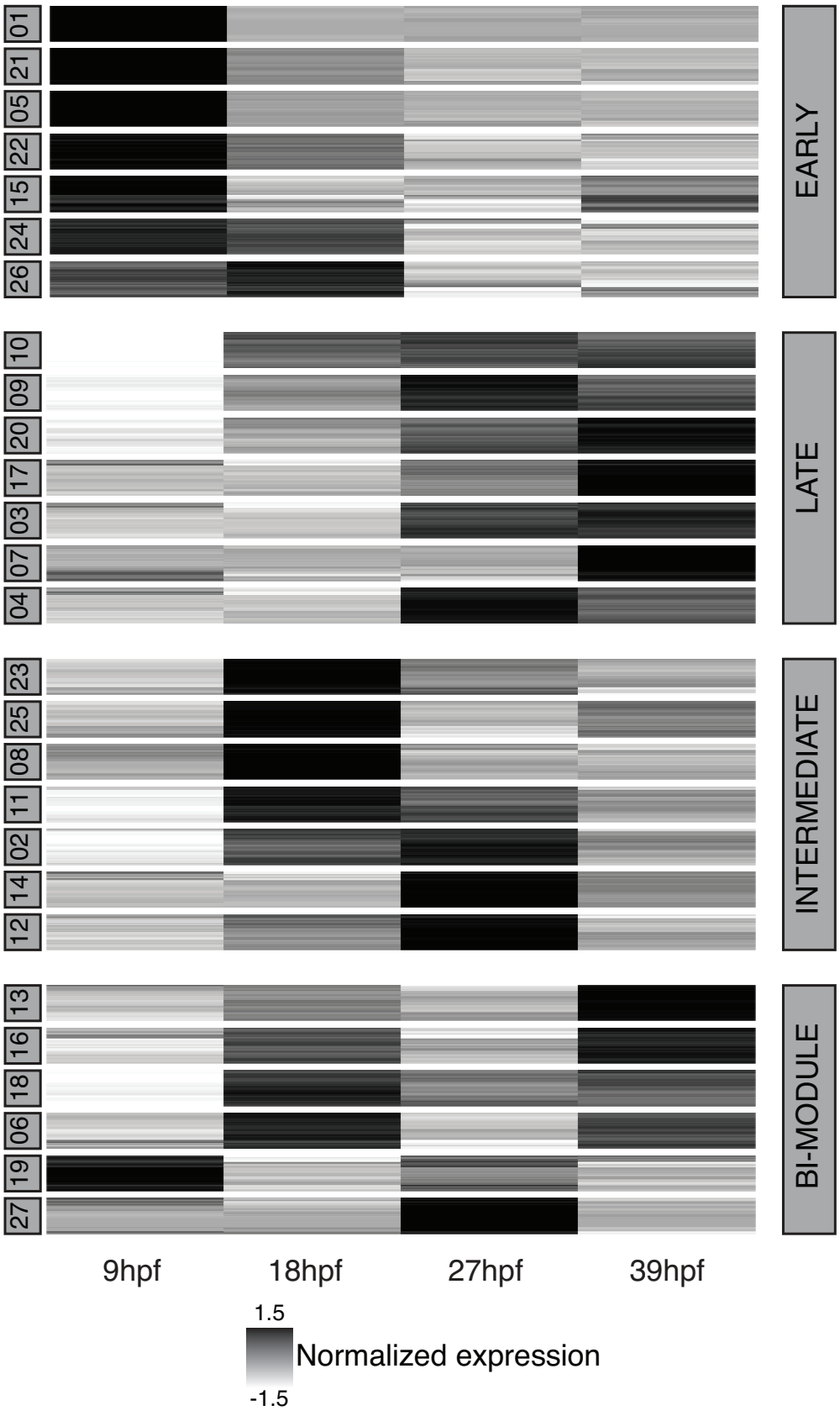

Figure 7.11: **Fuzzy Clustering of temporal gene expression pattern.** The 27 clusters were manually grouped in terms of activity. EARLY is active at 9hpf of development and then decreases. LATE exhibits an increasing trajectory. INTERMEDIATE has a peak of expression in either 18hpf or 27hpf and finally BI-MODULE shows two peaks of expression.

tal I found 60/289 TFs and 105/561 skeletogenic genes that showed a decreasing trajectory over the 4 time-points. However, none of them included a gene with a well studied skeletogenic function in either organism. In order to form the extended larval skeleton we expected skeletogenic genes to show an increasing pattern and indeed most skeletogenic genes are in fact part of the LATE group 287/561. Moreover, this group contains most of the active TFs, consistent with the increasing complexity of cell specification over time 133/289. In this group I, additionally, find the bio-mineralisation genes *Afi-p19(Cah10L)*, *Afi-p58a*, *Afi-p58b*, *Afi-ttrspn_19*, *Afi-slc4a10/nbc* and *Afi-c-lectin*. All are expressed in skeletogenic cells in brittle star throughout gastrulation and their orthologs have been shown to be essential in sea urchin larval skeletogenesis (Figure 7.7 B and Figure 7.9). In the INTERMEDIATE group were genes whose expression trajectories peak either at 18hpf or 27hpf and then decrease steadily. Indeed, we found *Afi-pplx* as part of f-cluster 8 (peak at 18hpf) a gene that was confirmed with WMISH and QPCR to have only transient activity in mesodermal cells throughout development (see part I). Additionally, I found *Afi-alx1*, *Afi-tbr*, *Afi-gataC* and *Afi-erg*; TFs involved in the separation of regulatory states in the mesoderm. In total this group comprises 66/289 TFs and 68/561 skeletogenic genes. The final group, called BI-MODULE consists of two expression peaks throughout the 4 time-points and contains 30/289 TF and 101/561 skeletogenic genes. This group contains genes that potentially that have two different roles throughout development. Examples of such a genes are *Afi-hesC* and *Afi-delta* which are first expressed in the mesodermal area at the vegetal side of the embryo and then in two different territories scattered in the ectoderm and at the tip of the archenteron throughout gastrulation. Based on the fact that our 4 time-points correspond to 4 different stages of development, our grouping shows consistent activity of TF involved in multiple stages of cell specification.

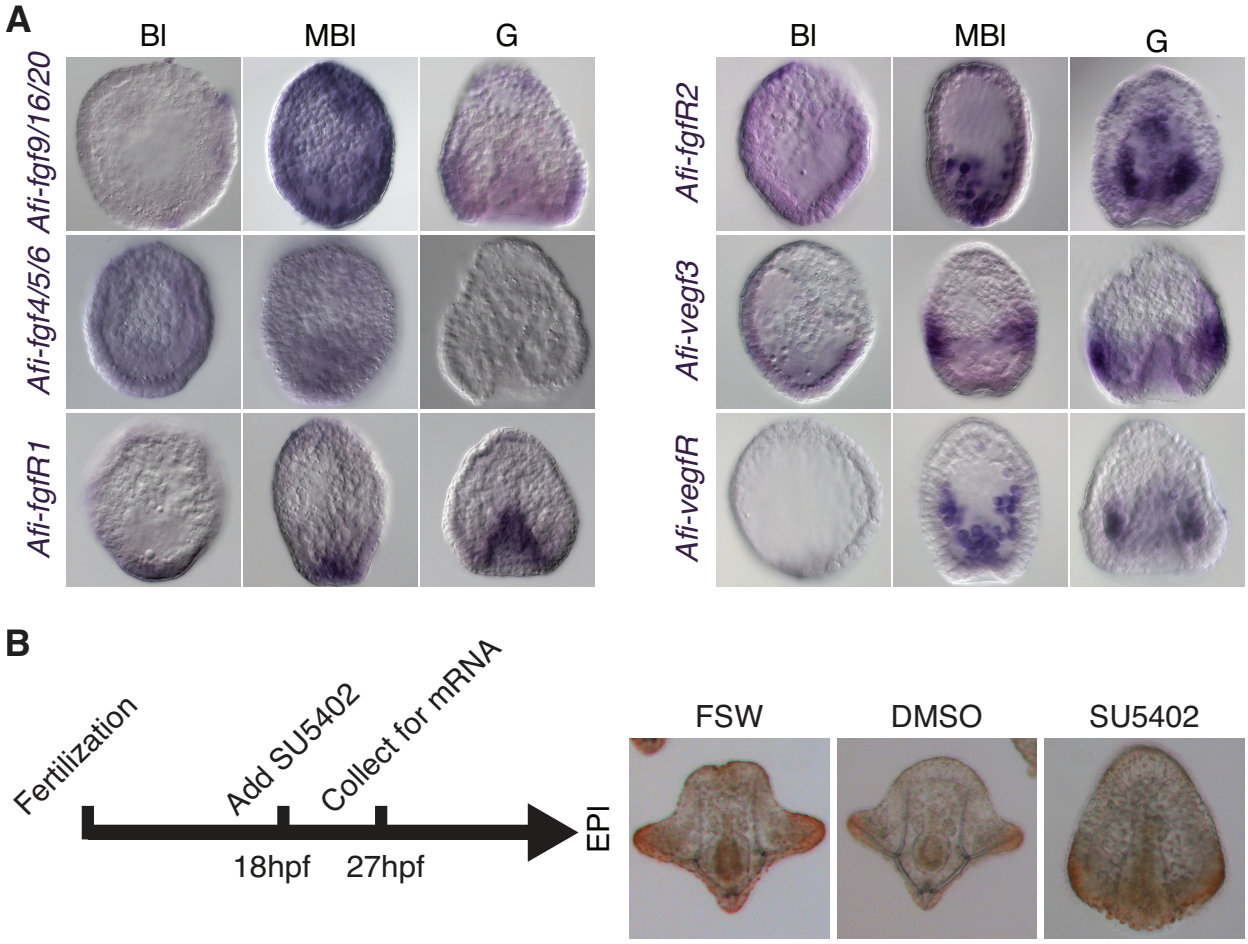

Figure 7.12: **Conservation of fgf and vegf signalling in brittle star.** (A) Expression analysis of key orthologous genes of the fgf and vegf signalling pathway in sea urchin. Along with to the orthologs of FGF signalling genes identified in sea urchin, a single ligand *Afi-fgf9/16/20* and two receptors *Afi-fgfR1* and *Afi-fgfR2*, we identified in brittle star another ligand *Afi-fgf4/5/6*. Expression of the three genes present also in the sea urchin genome is comparable to what described in euechinoids. The same applies for the vegf genes: *Afi-vegf3* and *Afi-vegfR*. (B) Set up of SU5402 inhibition experiment and in vivo imaging showing the absence of skeleton in treated samples. Bl - blastula stage, MBl - mesenchyme blastula stage, G - gastrula stage, EPl - early pluteus stage.

7.6 Unbiased approach to detect genes participating in larval skeletogenesis of *A. filiformis*

After thoroughly analysing our dataset based on the sea urchin annotation as a reference point I moved on to find genes that are specific for brittle star larval skeletogenesis. While looking in depth for similar spatial expression in the brittle star, of sea urchin skeletogenic orthologs, I found potential conservation of the FGF and VEGF signalling pathways. In both animals the *fgfR2* and *vegfR* are expressed in SM cells whereas their ligands show expression in the ectoderm close to the SM cells (Figure 7.12 A) (Röttinger et al., 2008). In sea urchin the VEGF-signalling pathway is essential for the correct localisation of the SM cells, once ingression into the blastocoel occurs (Duloquin et al., 2007; Adomako-Ankomah and Ettensohn, 2013). Moreover, knockdown experiments in sea urchin using either morpholinos or chemical drugs showed that *fgfR2* and *vegfR* are essential components for the expression of skeletogenic downstream genes (Duloquin et al., 2007; Adomako-Ankomah and Ettensohn, 2013; Röttinger et al., 2008). Based on the conservation of spatial expression we hypothesised that an inhibition of these pathways would also produce a similar effect on skeletogenesis in brittle star. We applied the drug SU5402, an fgfR and/or vegfR inhibitor, to Afi and indeed observed a drastically inhibition in the formation of spicules throughout development (Figure 7.12 B). In order to detect whether a similar effect is observed on skeletogenic differentiation genes, and to find novel brittle star specific skeletogenic genes, we collected samples for mRNA sequencing. To circumvent the early specification and to focus our attention on late differentiation genes we added the drug at 18hpf (late blastula stage), shortly before the SM cells start ingression, and collected mRNA at 27hpf (late mesenchyme blastula stage). As negative controls we used the solvent DMSO and filtered seawater (FSW). All samples were realigned to the RT and quantification was performed as described in chapter 6.2.10.

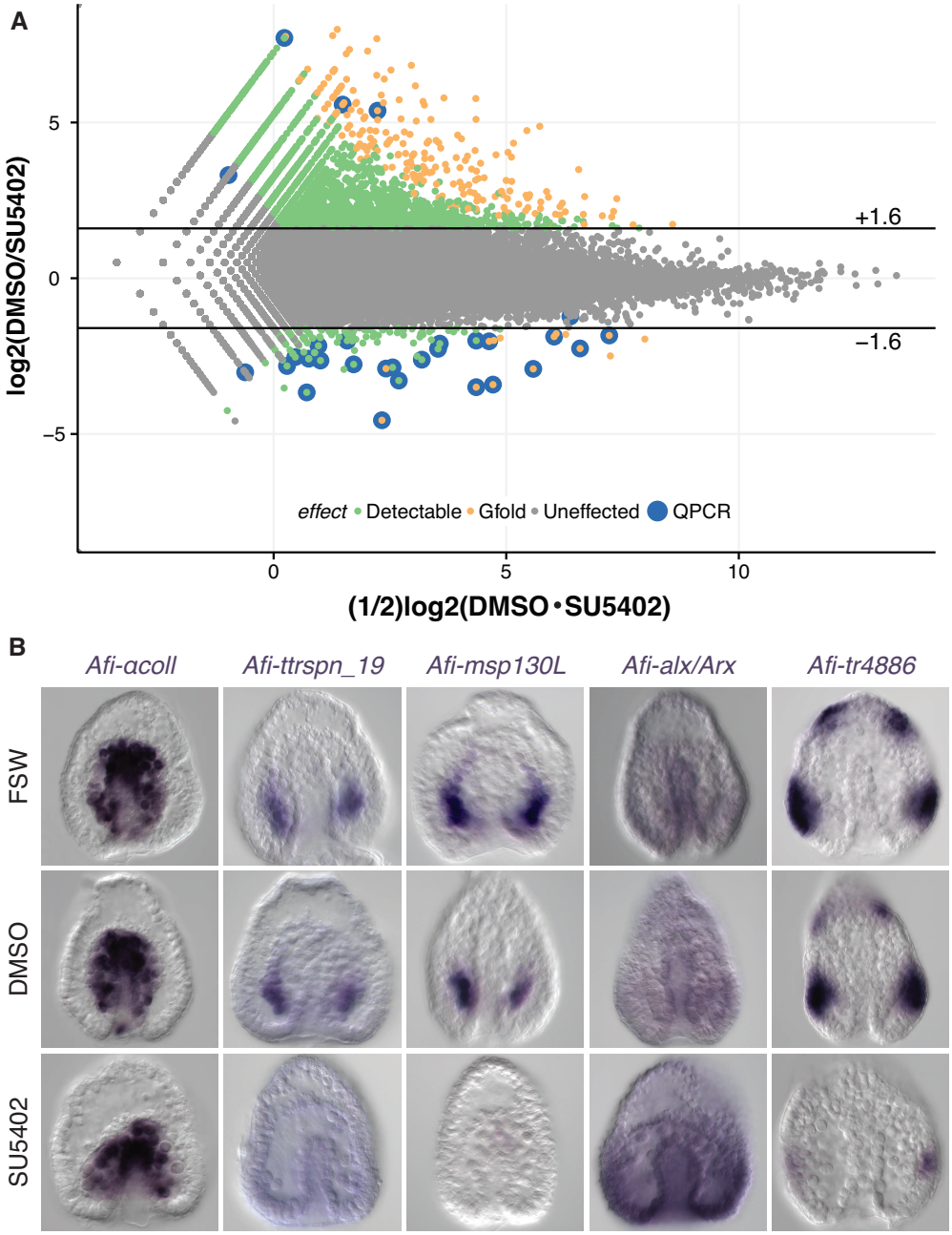

Figure 7.13: **Differential analysis for SU5402 treated samples and WMISH analysis on treated embryos.** (A) MA-plot showing upregulated samples on top and downregulated samples on the bottom. (B) WMISH on embryos treated with SU5402 that were fixed at gastrula stage. *Afi-αcoll* was used as negative control and no change in expression is observed. *Afi-ttrspn_19*, *Afi-msp130L* and *Afi-tr4886* are downregulated and *Afi-alx/arx* is upregulated in SU5402 treated samples. All embryos shown are at gastrula stage.

7.6.1 Differential gene expression analysis

Once the quantification was completed and normalisation was applied as previously described, I combined two approaches to detect differentially expressed ECs: 1) GFOLD, an algorithm that ranks ECs by posterior probibilities using a reliable statistics for expression changes (Feng et al., 2012), and 2) the criterion that significant up or down regulation in QPCR can only be detected above or below a log fold change of ± 1.6 (Figure 7.13) (Materna and Oliveri, 2008), which corresponds roughly to 3 folds of difference of level of expression. With these criteria, I found 140 downregulated and 2,366 upregulated ECs. In the upregulated ECs, 1,434 were annotated with sea urchin, of which 6 were TFs and 70 skeletogenic genes. Interestingly in these upregulated ECs, I observed a high degree of annotation redundancy (mulitple ECs annotated to the same gene). In the 1,434 ECs I found only 897 annotations. Of these, 210 annotations occured more than once. In order to investigate the 2,366 ECs more fully, I used the Blast2GO tool (Conesa and Götz, 2008). First, I applied a blastx search (evalue: 1e-3) against the non-redundant database, obtaining 1,784/2,366 hits (species distribution Figure B.5). Of these 1,784, 1,368 sequences were annotated with an according GO category. Gene ontology analysis showed that most of these sequences could be grouped for biological processes to cellular process, molecular function to catalytic activity and for cell compartment to cell (more details in Figure B.5). Interestingly, we identified the gene *Afi-vegf2*, a different *Afi-vegf* gene from the one shown in Figure 7.12, to be significantly upregulated. This gene is normally not expressed during development, as indicated by our transcriptome expression profile, but seems to be activated by treatment with SU5402 (Figure 7.14).

Based on the fact that inhibition of vegf-signalling in sea urchin led to significant downregulation of skeletogenic differentiation genes (Adomako-Ankomah and Ettensohn, 2013), we focused our attention on the downregulated ECs. There, 101 are annotated with a sea urchin gene of which 3 are TFs and 16 are skeletogenic genes. We selected 35 downregulated and 3 upregulated genes to to validate our result by QPCR on at least one other biological replica. 76%

(Figure 7.14 yellow and green) of the selected candidates were confirmed by QPCR and are thus significantly differentially expressed in SU5402 treated samples (false positive 24% Figure 7.14 white). To better understand if our cut-off value of log fold change of $\pm$1.6 was too stringent, we also selected several downregulated borderline ECs to be validated by QPCR, however, not one of them was significantly downregulated in any sample (Figure 7.14 grey). This supports our quantification strategy. We, additionally tested 5 genes with WMISH (Figure 7.13 B). Two out of the five genes, *Afi-msp130L* and *Afi-ttrspn_19* are expressed in SM in brittle star and their orthologs are essential for skeleton formation in sea urchin. *Afi-tr4886*, explained below in detail, is expressed in the ectoderm close to where the spicules are formed, a position similar to the vegf ligand (Figure 7.12). All three show a dramatic reduction of the chromogenic signal of the WMISH in the inhibited samples, consistent with the transcriptome and QPCR data. One homeo-domain aristaless TF *Afi-alx/arx* (AfiCDS.id68571.tr6658) similar to sea urchin sequence (WHL22.490216), the role of which is yet to be determined in the development in both organisms, showed significant upregulation in brittle star SU5402 treated samples. As a negative control we used *Afi-*α*coll*, a gene enriched in SM in brittle star, which was not shown to be affected using QPCR, WMISH and our transcriptomic analysis. Our differential screen, thus, allows the detection of genes that participate in the process of larval skeletogenesis in the brittle star and downregulation of several genes expressed in the skeleton is consistent with the observed phenotype.

7.7 Novel Genes in *A. filiformis* larval skeletogenesis

The inhibition of vegf signalling by Axitinib in sea urchin leads to a phenotype without skeleton and the downregulation of several skeletogenic genes (Adomako-Ankomah and Ettensohn, 2013). We observed a similar phenotype using another fgf/vegf inhibitor in brittle stars (Figure 7.12 B). Based on the observation that a reduction of skeleton is caused by downregulation of skeletogenic differentiation genes in sea urchin (Adomako-Ankomah and Ettensohn, 2013), our analysis should allow detection of species-specific genes for skeleton development in brittle

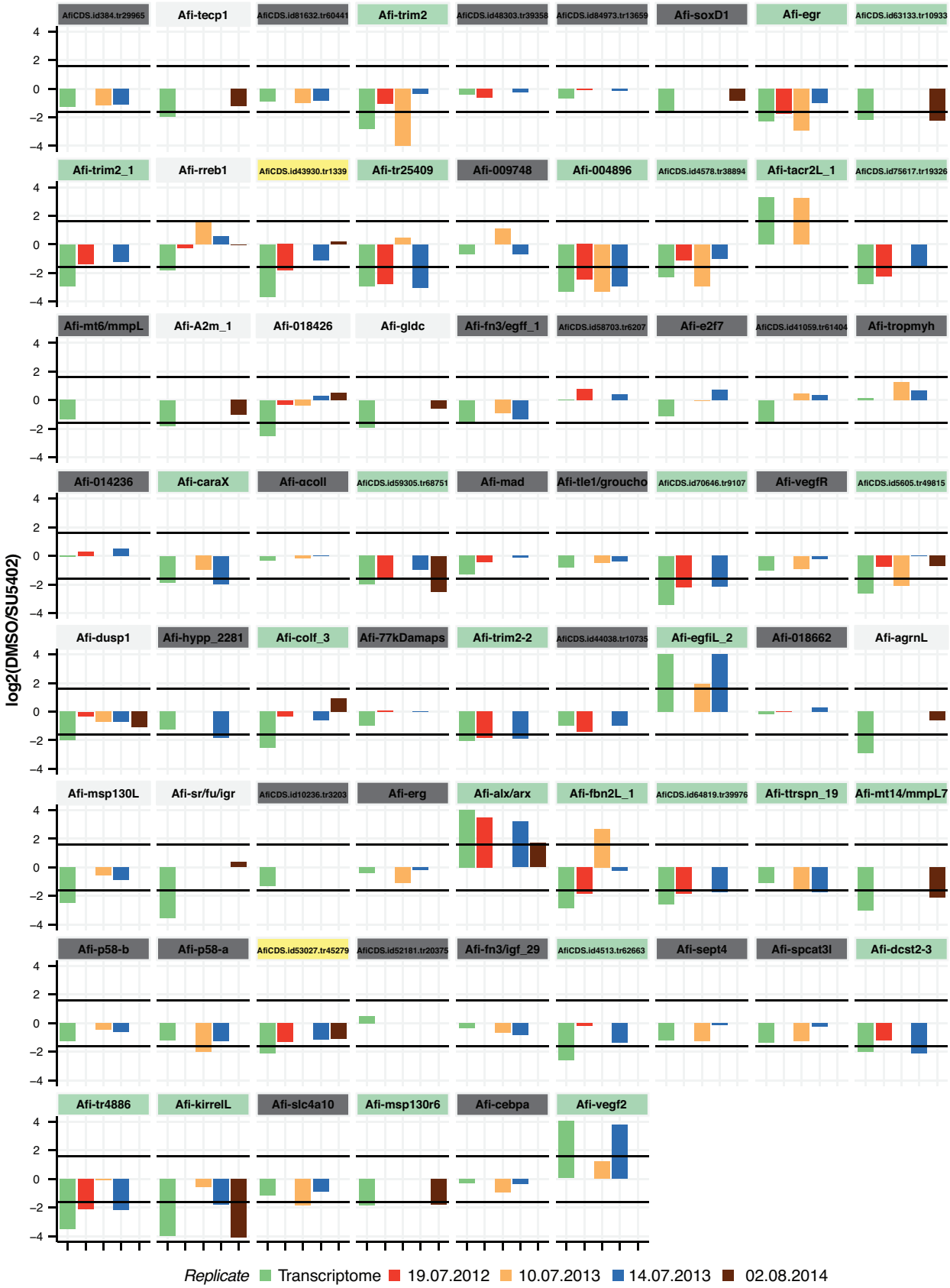
AfiCDS.id384.tr29965
Afi-tecp1
AfiCDS.id81632.tr60441
Afi-trim2
AfiCDS.id48303.tr39358
AfiCDS.id84973.tr13659
Afi-soxD1
Afi-egr
AfiCDS.id63133.tr10933
Afi-trim2_1
Afi-rreb1
AfiCDS.id43930.tr1339
Afi-tr25409
Afi-009748
Afi-004896
AfiCDS.id4578.tr38894
Afi-tacr2L_1
AfiCDS.id75617.tr19326
Afi-mt6/mmpL
Afi-A2m_1
Afi-018426
Afi-gldc
Afi-fn3/egff_1
AfiCDS.id58703.tr6207
Afi-e2f7
AfiCDS.id41059.tr61404
Afi-tropmyh
Afi-014236
Afi-caraX
Afi-acoll
AfiCDS.id59305.tr68751
Afi-mad
Afi-tle1/groucho
AfiCDS.id70646.tr9107
Afi-vegfR
AfiCDS.id5605.tr49815
Afi-dusp1
Afi-hypp_2281
Afi-colf_3
Afi-77kDamaps
Afi-trim2-2
AfiCDS.id44038.tr10735
Afi-egfiL_2
Afi-018662
Afi-agrnL
Afi-msp130L
Afi-sr/fu/igr
AfiCDS.id10236.tr3203
Afi-erg
Afi-alx/arx
Afi-fbn2L_1
AfiCDS.id64819.tr39976
Afi-ttrspn_19
Afi-mt14/mmpL7
Afi-p58-b
Afi-p58-a
AfiCDS.id53027.tr45279
AfiCDS.id52181.tr20375
Afi-fn3/igf_29
AfiCDS.id4513.tr62663
Afi-sept4
Afi-spcat3l
Afi-dcst2-3
Afi-tr4886
Afi-kirrelL
Afi-slc4a10
Afi-msp130r6
Afi-cebpa
Afi-vegf2
log2(DMSO/SU5402)
4
2
0
−2
−4
Replicate
Transcriptome
19.07.2012
10.07.2013
14.07.2013
02.08.2014

star. Due to the unbiased nature of a transcriptomic approach, we obtain 123/140 downregulated ECs, not defined as skeletogenic. Interestingly, of these 123 ECs, 39 do not have a sea urchin homolog. To obtain a more detailed idea of these ECs, we used Blast2GO with a blastx search (e-value: 1e-3) against the non-redundant database. The top hit distribution showed that most of the ECs are homologs to *S. purpuratus* (64/140) followed by *Saccoglossus kowalevskii* (16/144) and *Branchiostoma floridae* (5/144) (SFig. 5). At this e-value 25 ECs did not find any homolog in the database. Additionally, I performed an interproscan for all sequences to search for protein domains. Out of 25 ECs, I found 17 with recognisable protein domains. In order to check whether some candidates are involved in SM lineage throughout development we selected four candidates for cloning and WMISH analysis. Three of these four are expressed in SM cells, whereas one shows expression comparable to *Afi-vegf3* (Figure 7.15 A). Two of these sequences could not be annotated with our approach. The first one, *Afi-tr4886* is highly conserved to *Nematostella vectencis* (e-value: 1e-104) and *P. miniata* (e-value: 1e-178) sequences but is not found in *S. purpuratus* and is, moreover, not present in any vertebrate. This sequence belongs to the metallo-dependent hydrolase superfamily and can be characterised as amidohydrolase, as predicted by interproscan (Figure 7.15). Interestingly, many prokaryotes possess genes with an amidohydrolase domains and a blastx of *Afi-tr4886* finds, after *N. vecetencis*, many bacterial species. Expression pattern analysis shows similarities to *Afi-vegf3* and *Afi-fgf9/16/20* indicating a possible involvement in signalling between the ectoderm and the SM cells (Figure 7.14 B). The second not annotated sequence *Afi-tr25409* is not found in any public blast database, but is also present in a database established for the regenerating arm of *A. filiformis* (Purushothaman et al., 2014) and in the crinoid *A. mediterranea*. Using interproscan we found sequence characteristics

Figure 7.14 *(preceding page)*: **QPCR experiment on inhibited samples.** Barplots of the different replicates obtained by QPCR. In grey are samples that have not been found to be affected in the transcriptome and QPCR. In white are the samples affected in the transcriptome but not in QPCR. In yellow are the genes that were repeated with QPCR on the same samples that were used for the transcriptome. And in green are the samples that were repeated on at least one other biological replica.

of being a membrane bound protein and containing regions with signal peptide signature (Figure 7.14 B). Moreover, its clear expression in the cells of the SM lineage suggests an involvement in skeleton development in the brittle star. In conclusion, we were able to detect two novel brittle star specific genes that are potentially involved in the skeleton formation of the *A. filiformis* pluteus larvae.

The other two sequences tested showed close similarity to *Spu-rreb1* (AfiCDS.id62604.tr47807) and *Spu-caraX* (AfiCDS.id10597.tr30892) and are both expressed in the SM lineage in brittle stars (Figure 7.15 A). Rreb1 (ras-responsive element-binding protein 1) is a C2H2 zinc finger transcription factor (Figure 7.15 B). While its sea urchin ortholog is not part in our list of skeletogenic genes it is reported to be transiently expressed in sea urchin SM (Materna et al., 2006). Since the reported expression pattern contained a lot of noise, I repeated this WMISH in sea urchin. Importantly, I did not see expression in SM lineage during mesenchyme blastula or early gastrula stage, a striking difference compared to *A. filiformis* expression (Figure 7.15).

The other gene *caraX* belongs to the class of carbonic anhydrases that is a class involved in bio-mineralisation in many species (Voigt et al., 2014). Our annotation using tblastx was not able to clearly resolve the orthology relationship of the *A. filiformis* sequence to one of the six potential sea urchin cara genes. Hence, we collected cara sequences from 31 echinoderm species and performed a phylogenetic analysis. Unfortunately, no single tree converged to a satisfying optimum. Therefore, I applied the Orthology MAtrix algorithm (Altenhoff et al., 2014) with these species and several pre-computed all vs all species retrieved from the online database Table B.6. The OMA analysis did not group *Afi-caraX* to any orthologous group and even the skeleton specific sea urchin *Spu-cara7LA* was not grouped with its mouse counterpart. Only three out of six cara genes are reported to participate in skeletogenesis in sea urchin. This might indicate a high dynamicity of this class of genes during evolution. Since, orthology reconstruction will need further attention I left it open and denoted this cara gene as *Afi-caraX*. Importantly, WMISH of this brittle star *Afi-caraX* gene shows expression in SM lineage, indicating a role as potential skele-

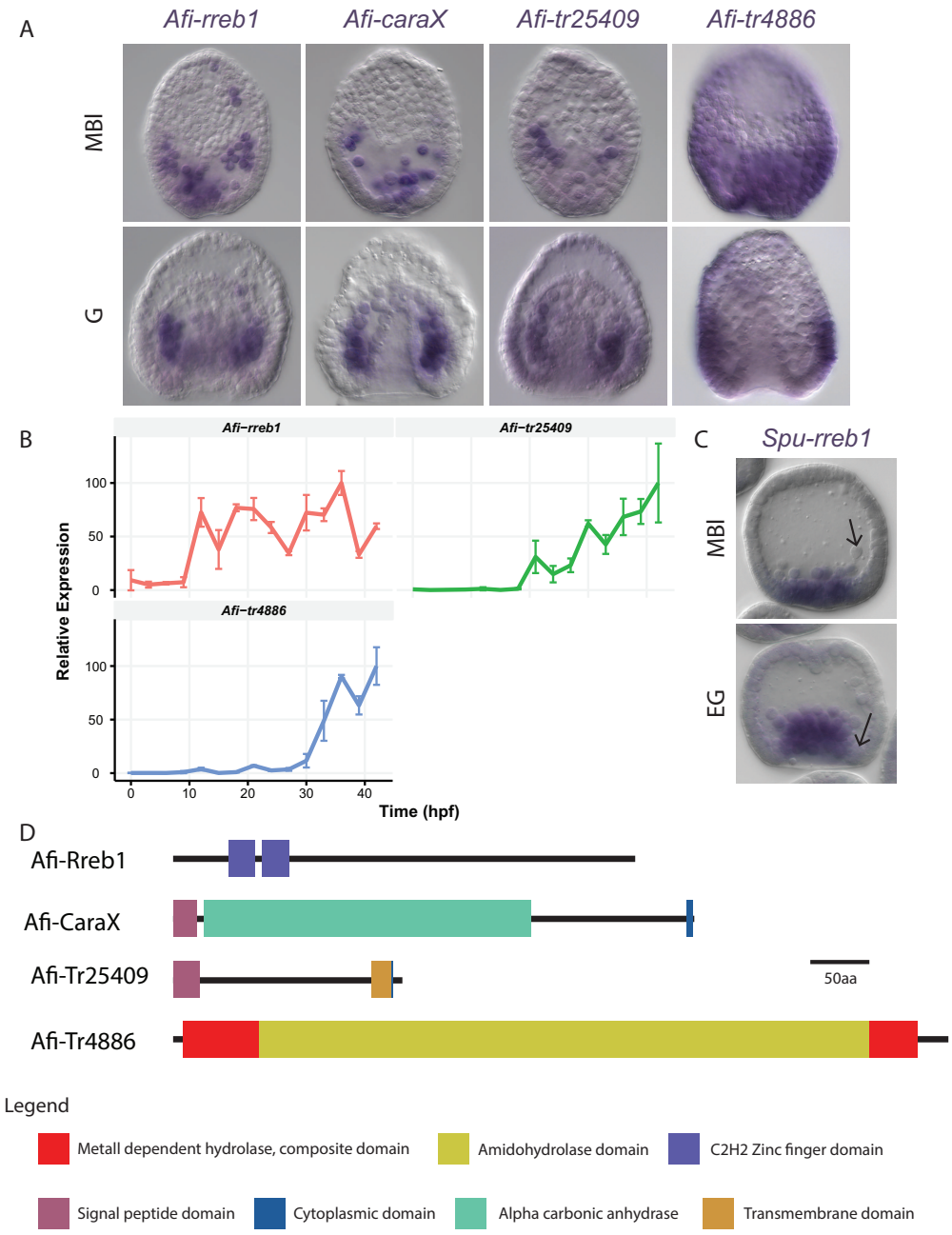

Figure 7.15: **Novel genes in skeletogenesis.** (A) Expression pattern of genes not yet implicated in skeletogenesis in echinoderms, obtained using WMISH. (B) QPCR time-courses showing temporal activity of genes. Time-courses are in relative expression, normalised to the individual peak of expression. Error bars represent standard deviation of three technical replicas. The two undescribed genes *Afi-tr4886* and *Afi-tr25409* show consistent with WMISH a rise of expression in later stages, whereas *Afi-rreb1* seems to have two modes of activity. (C) WMISH of *Spu-rreb1* in sea urchin show no expression in SM lineage. (D) Gene maps showing the different protein domains of the individual genes, obtained by InterProScan. MBl - mesenchyme blastula stage, EG - early gastrula, G - gastrula stage.

togenic differentiation gene. Taken together, our differential analysis allowed us to detect novel genes involved in brittle star skeletogenesis.

Chapter 8

DISCUSSION

In this part II, I have presented how we characterised gene expression in the brittle star *Amphiura filiformis* using an unbiased *de novo* transcriptome strategy. I also showed how we incorporated samples from 4 key stages of development along with samples where skeleton formation was inhibited to generate a reference transcriptome. This is, and will be used as a reference for future work on this species. I have initially focused my analysis on sequence information of the contigs from Chapter 7.3 to Chapter 7.4. To put my RT into an evolutionary context with other echinoderms, I collected data from the crinoid *Antedon mediterranea*, the asteroid *Patiria miniata*, and the euechnioid *Strongyloncentrotus purpuratus*. For all 4 species, I computed quality metrics and performed an annotation with the same strategy and parameters. I, moreover, evaluated the conservation of groups of genes with the sea urchin as reference using the euechinoid gene ontology and a manually curated set of euechinoid genes found to be involved in skeletogenesis. Secondly, I used the quantity information of the reads to characterise the brittle star transcriptome in terms of the dynamics of expression over time. Finally, I described how I used a differential analysis of samples with and without skeleton to find novel genes for the development of the skeleton that are specific to the brittle star.

8.1 *De novo* Transcriptomics

The constant improvement of high-throughput sequencing technology and associated decrease in sequencing price have accelerated exponentially the increase of genomes and tran-

scriptomes for individual species (van Nimwegen, 2003). mRNA sequencing especially is a cost-effective and experimentally feasible approach to obtain a systems perspective of any novel species in a short amount of time. In 2013, for our study, 2 lanes of Illumina HiSeq 2500 with library preparation for 6 samples were priced at around £2,000 and experimentally, it was possible to obtain reads in less than 2 months. The fast experimental procedure stands in contrast to the long and complicated bio-informatics analysis that is, thus creating a major bottleneck. First, high-throughput sequencing is a big data problem (our run on 2 lanes of this platform produced 250GB of data). State of the art assemblers (*i.e.* Trinity, SoapDENOVO) demand a lot of memory (mouse data: ∼53mio 76bp paired end reads needed 100GB of memory (Chang et al., 2015)) and need thus special hardware or high performance clusters. Second, constantly novel read-filtering, assembly, and quantification tools appear. However, only little comparative studies exist in order to choose the right strategy for the right problem, and it has been shown that for different datasets assembler and input parameters influence transcriptome quality (Chang et al., 2015; Li et al., 2014).

8.1.1 *Amphiura filiformis* assembly and quality

For the assembly of the brittle star *A.filiformis* mRNA sequencing data, I used a strategy with digital normalisation followed by application of the Trinity assembler. At the moment of assembly (October 2013), Trinity outperformed all other available assembly programmes in terms of full-length gene recovery (Grabherr et al., 2011). Our approach with digital normalisation allowed us to obtain a reference transcriptome that incorporated all 6 samples within 4 weeks of computation on a server with only 64GB of memory. This is in concurrence with observations in two closely related ascidians, for which a systematic comparison of assembly with and without digital normalisation showed no inclusion of computational artefacts, but a reduction of time and resources needed for the assembly (Lowe et al., 2014). This type of digital normalisation is similar to the *in silico* fragment normalisation part of trinity (Haas et al., 2013), which showed a higher degree

of full length recovered transcripts for a smaller amount of reads. My test excluding digital normalisation and individual assembly confirmed the recovery of more than 94% of each individual transcriptome in our reference. The comparison with previously obtained clones confirmed the high quality of our reference, and suggested a single nucleotide polymorphism of 1.2% within coding region of *A. filiformis*. Additionally, our transcriptome exhibited the highest number of more than 90% completely assembled transcripts when compared to other genome and transcriptome datasets. The extraction of open reading frames reduced the total number of contigs 7 times from 600,000 to 90,000 and increased the N50 value without effecting gene recovery, as shown in the CEGMA test and annotation statistics. The question arises: What are the lost contigs? Efforts to establish a genome for *A. filiformis* are on the way and one possibility is that they are part of non-coding sequence (i.e. introns and UTR regions) or partially or wrongly assembled transcripts. Indeed, a study of the sea urchin transcriptome (Tu et al., 2012) shows that the majority of the sequence of a mature transcript corresponds to UTRs. However, this remains to be addressed in future work, once a genome is available. Interestingly, whereas on the initial transcriptome around 65% of reads could be re-aligned, a re-alignment of only around 20% was observed when performed against the RT. This, however, poses a reduction only of 3 times compared to the 7 times reduction of number of contigs. Nevertheless, the high correlation between QPCR data and transcriptome shows correct recovery of gene quantity. Additionally, out of 69 genes tested in the differential screen only $\sim$15% are false positives. Collectively, these suggest that our transcriptome and our quantification strategy correctly characterises gene expression of the *A. filiformis* developing embryo. The constant development of new *de novo* assemblers (Peng et al., 2013; Chang et al., 2015) and a novel metric for quality assessment (Li et al., 2014) pave the way for an even better assembly of our high quality reads leading to a new and updated version. Several novel *de novo* assemblers (*e.g.* Bridger (Chang et al., 2015)) shows a reduction in computation time and allows, hence to establish several versions of different assemblies with different parameters for comparative analysis. This approach can be coupled with digital normalisation. A novel

statistical tool for quality assessment, RSEM-eval, can then be used to test different versions of assemblies for transcriptome quality in terms of complete gene recovery (Li et al., 2014). In conclusion, with the development of novel tools for *de novo* transcriptomics better assemblies will be made available.

8.2 Evolutionary implications for larval skeletogenesis

In order to obtain an evolutionary overview of gene content in echinoderms, I obtained sequence dataset for 3 key species: the crinoid *Antedon mediterranea*, the asteroid *Patiria miniata* and the euechinoid *Strongyloncentrotus purpuratus*. Excluding holothuriods, I am therefore covering most clades along the echinoderm phylogeny. With inclusion of the crinoid *Antedon mediterrane* I can draw conclusions about ancestrally derived genes. Importantly, ophiuroids and echinoids develop a skeleton in the larvae whereas the other two do not and thus, set up a unique opportunity to study the development of this feature using a comparative analysis.

8.2.1 Comparison to other echinoderms

All datasets have been generated using different approaches. Therefore, to draw conclusions about gene content, I systematically applied several quality measures using various methodologies. For the annotation, I chose *S. purpuratus* as reference. This sea urchin dataset is the closest species that due to constant improvements, increase of coverage and the recent addition of transcriptomic data (Tu et al., 2012), has the most refined dataset.

In general, in a multi-species genetic comparative analysis, statements about gene loss are difficult to sustain and it is thus easier to look at commonalities, especially when transcriptomic data are used. Nevertheless, gene-loss can only be addressed if a well curated quality genome is available and should otherwise be considered an artefact of low quality data. In this context, the assessment of transcriptome completeness using CEGMA alone can be misleading since the CEGMA families are enriched with metabolic and cellular function genes and consequently in-

troduce a slight bias in completeness (Parra et al., 2007). However, in my comparative analysis both transcriptomic datasets from ophiuroid and crinoid show similar levels of reciprocally identified sea urchin hits to the combined genome and transcriptome dataset for asteroid (AFI: 33% and AME: 32% compared to PMI: 35%). This suggests a similar level of gene recovery for all three species and is consistent with the CEGMA result. Many of the sea urchin GO classes show a high level of conservation in echinoderms. However, there is some variation in which genes are found individually (compare echinoderm core genes with the individual species Figure 7.6). This is probably caused by the difference in origin of the samples, *e.g.* stage of lifecycle, tissue. For highly conserved genes, *e.g.* TFs and signalling molecules, I expect to find an even higher number once for all species good quality genome data is available, while it is possible that for rapidly evolving functional classes, such as immunity genes, the recovery might remain low. My findings show for the first time that echinoderms have a conserved regulome, as proposed by Howard-Ashby et al. (2006); Erwin and Davidson (2002).

8.2.2 Evolution of skeletogenic differentiation genes

My analysis using 901 skeletogenic genes revealed a conserved toolkit of 494 genes, here referred to as the potential core of skeletogenic genes. Of these 901, only 37 account for TFs and 32 for signalling molecules, which is less than 10% of the total. Therefore, 90% of genes must belong to the differentiation tier of a GRN. Davidson and Erwin (2006) hypothesised that the final tier of a GRN, the one that drives the differentiation gene batteries, is under the least selection pressure and is therefore rapidly evolving and responsible for speciation. However, our analysis identified 436/494 core skeletogenic genes that are not TFs or signalling molecules and can, thus, be considered as part of the differentiation gene cassette. A closer look into these 436 genes using the sea urchin GO revealed that most categories are highly conserved, but metalloproteases and biomineralization genes are not. This observation indicates that solely looking into this two categories can produce a biased picture of evolution of the differentiation

genes within the GRN for larval skeleton development.

How can we explain the variation in the biomineralization class? The biomineralization genes are grouped in 6 categories of which collagens, cyclophillins, carbonic anhydrases and an unnamed category are highly conserved in our selected representatives of the 4 classes of echinoderms. Of these 6 categories, msp130 and spicule matrix show a high level of variation. First, of the 9 sea urchin *msp130* genes only 2 are found within the core. An in depth look into the brittle star transcriptome revealed that there are 6 *msp130* contigs that are different on the nucleotide level. Furthermore, all 6 map to the same sea urchin *msp130* gene (see appendix). The starfish and sea lily show a comparable situation. This observation indicates that a potential clade specific expansion took place. Be that as it may, only a thorough phylogenetic analysis can resolve the orthology of these 6 brittle star *msp130* genes and will be performed in future studies. Second, out of the 14 spicule matrix genes in sea urchin, I found only one that is conserved in all four species. Thus, spicule matrix genes, characterised by a C-lectin domain and a conserved proline-rich domain, are absent in all classes other than echinoids. These genes are considered an echinoid invention and support for this hypothesis is given by the following observations: First, a proteomic study of skeletal elements in another species of brittle star *Ophiocoma wendtii* did not find orthologs to these genes (Seaver and Livingston, 2015). However, other potential candidates of c-lectin type genes for brittle star skeletogenesis were obtained, which are also present in our transcriptome of *A. filiformis* and expressed during larval skeletogenesis (Figure 7.9). Second, the identified spicule matrix genes in star fish turned out to be artefacts of the annotation and seem not to be present (explained in detail in chapter 7.4.1). Third, they are present in the cidaroid *Eucidaris tribuloides* and fourth they appear in tandem in the *S. purpuratus* genome. Moreover, no such gene was found in the hemichordate *Saccoglossus kowalevskii* (Cameron and Bishop, 2012) and is confirmed by the absence of spicule matrix genes in our crinoid. Both spicule matrix genes and msp130 genes have been highly duplicated in sea urchin, as seen in the many tandem duplications, and the presence of both in the pencil urchin *Eucidaris tribuloidis* (Cameron et al.,

2009) suggests their evolution already in the common ancestor of cidaroids and euechinoids. My inability to find these genes in brittle star and star fish, indicates that they specifically evolved for echinoid larval skeletogenesis. However, only the inclusion of holothuroids will allow to pinpoint the exact moment of evolution of these two subcategories of biomineralization genes.

Taken together, this data suggests that the skeletogenic GRN potentially consists of 494 core skeletogenic genes that are highly conserved. Consistent with all echinoderms having an adult with a skeleton formed by similar ossicle units, the stereom (Bottjer et al., 2006), this indicates that the GRN for adult skeletogenesis is selected for. This is additionally supported by comparing expression patterns of several genes in juvenile or adult stages (Gao and Davidson, 2008; Morino et al., 2012; Czarkwiani et al., 2013), which show a high degree of conservation in cells that participate in adult skeletogenesis. Additionally, in brittle star development most differentiation genes show an increasing trajectory over time consistent with their role in the final differentiation of the biominerale structure. The conservation of many differentiation genes and their temporal expression patterns argues that the larval skeleton is a synapomorphy in echinoderms and was therefore lost in starfish and reduced in sea cucumber. Moreover, this data suggest that a top-down theory of evolution based solely on the GRN hierarchical properties might be too simplistic to account for the high level of highly conserved differentiation genes.

8.2.3 Conservation of fgf and vegf signalling

In the sea urchin, activity of the vegf3/vegfR pathway exhibits a crucial checkpoint to guide cell migration and initiate biomineralization (Duloquin et al., 2007). Crinoids, ophiuriods, asteroids and echinoids all have three Vegf ligands and one VegfR receptor. Additionally, all of them have at least two Fgf ligands and two FgfR receptors (Röttinger et al., 2008). Consistent with the sea urchin (Tu et al., 2014), in brittle star only vegf3 of the three vegf ligands is expressed at detectable levels throughout embryogenesis (Appendix B). Spatially, euechinoids and ophiuroids exhibit similar expression of *vegf3*, *vegfR*, *fgf9/16/20* and *fgfR2*. *vegfR* expression is also confirmed in

another species of brittle star *Amphipholis kochii* (Morino et al., 2012). In asteroids expression of vegf-signalling genes is not observed in the embryo, however vegfR is expressed in mesenchymal cells and vegf3 in the epidermis of the juvenile starfish (Morino et al., 2012). No data exists on fgf-signalling in this clade. In sea urchin juvenile *vegfR* is expressed in the SM lineage (Gao and Davidson, 2008) and no information exists for the vegf ligand or fgf-signalling components. In the regenerating arms of the brittle star adult *Afi-vegf* and *Afi-fgf9/16/20* are expressed in the epithelium and *Afi-vegfR* and *Afi-fgfR2* in cells of the sub-epithelial layer where the spicules (skeletal primordia) are formed (Anna Czarkwiani personal communication). These data show that vegf/vegfR signalling is also part of the adult skeletogenic program.

Morino et al. (2012) proposed two distinct heterochronic events during the co-option of this subcircuit into the larvae: the activation of *vegfR* in the SM lineage and the activation of the *vegf3* ligand in the ectoderm, within a band in the vegetal half of the embryo. Importantly, according to the best supported current phylogeny (asterozoa) (Telford et al., 2014; O'Hara et al., 2014; Cannon et al., 2014), two steps, each in a different territory, would make the independent evolution of brittle star and sea urchin larval skeletogenesis less parsimonious and instead support synapomorphy of the larval skeleton. This hypothesis would assume that starfish lost such signalling, although, such a loss would only need to remove either *vegfR* in the SM lineage or *vegf* in the ectoderm to abolish expression of the other by purifying selection (Morino et al., 2012). Contrastingly, Adomako-Ankomah and Ettensohn (2013) showed a co-dependence of vegf and fgf signalling and Röttinger et al. (2008) suggested that this is reciprocal between ectoderm and SM lineage. Furthermore, Duloquin et al. (2007) showed that knockdown of *vegf* in the ectoderm dramatically reduce the expression of *vegfR* in SM cells, supporting a co-dependence of ligand/receptor system. Such co-dependence allows for the possibility that this signalling pathway is set in place just by the activation of the general skeletogenic module in the mesoderm of the embryo. Unfortunately, an answer to this question would require many further experiments. First it would be important to know what is upstream of the ligands vegf3 and fgf9/19/20. Second,

the location of the node for fgfR2 should be identified in the sea urchin GRN for larval skeletogenesis. Third, investigation of fgf signalling in starfish would be critical to understand whether one part of this mechanism would already be in place. Fourth, experiments in the sea cucumber could give further support for one of the two evolutionary scenarios of larval skeleton in echinoderms.

Interestingly, our differential screen did not show any type of effect on the fgf/vegf genes, which contrasts to that observed in sea urchin using another tyrosine kinase inhibitor. One reason for the observed difference might be the experimental methodology. Whereas we added the SU5402 drug at 18hpf (late blastula stage) and collected 9hrs later at late mesenchyme blastula stage, Adomako-Ankomah and Ettensohn (2013) added the Axitinib drug at late cleavage stages and collected at mid gastrula stage (48hpf). Here, it would be important to perform a similar experiment in sea urchin as performed in brittle star and check for effects on the canonical fgf/vegf genes. Interestingly, my differential screen identified one gene of the vegf family: *Afi-vegf2*. This ligand is normally not expressed during development in sea urchin and brittle stars, but showed a significant upregulation at 27hpf in brittle star. A spatial analysis for this gene at this stage might help to elucidate whether the upregulation is observed in a specific territory, and should be performed in future.

In conclusion, resolving this signalling pathway will be crucial in establishing the evolutionary mode of this feature.

8.2.4 Novel skeletogenic genes in the brittle star larval skeleton development

Our differential screen was designed to find genes specifically involved in larval skeletogenesis in the brittle star. I identified 123 out of 140 downregulated genes that are not part of the 901 sea urchin skeletogenic genes, thus being candidates for brittle star skeletogenesis. Seven out of 8 tested genes are expressed in skeletogenic cells throughout brittle star development and only one is expressed in the ectoderm, close to the lateral clusters where the spicules are formed. From the 7 skeletogenic genes 4 are not found in the list of 901 skeletogenic sea urchin genes. Thus, they

are brittle star specific genes. Interestingly, in contrast to inhibition experiments in sea urchin of fgf/vegf signalling, where no *msp130* gene was found to be down-regulated, I identify two potential *msp130* genes in brittle star. While this might be caused by the different experimental setup (Adomako-Ankomah and Ettensohn, 2013) (as explained above), other perturbation experiments, *e.g.* knockdowns on fgf/fgfR genes, vegf/vegfR genes and inhibition of vegf-singalling, did not show any inhibition of *msp130* genes in sea urchin (Duloquin et al., 2007; Röttinger et al., 2008; Adomako-Ankomah and Ettensohn, 2013). This, combined with the absence of spicule matrix genes in brittle star, indicates that if a checkpoint in the GRN for larval skeletogenesis in brittle star exists similar to sea urchin, then this checkpoint might potentially involve the *msp130* genes instead of the spicule matrix genes.

The first of the four novel genes is *Afi-caraX*, which belongs to the carbonic anhydrases. In sea urchin, there are 6 different carbonic anhydrases (Killian and Wilt, 2008) of which 4 are expressed at significant levels during development (Tu et al., 2014). I identify in brittle star around 11 carbonic anhydrases that have different sequences, out of which 7 are expressed at significant levels in our developmental transcriptome. However, of these 11 there is a high degree of sequence redundancy. 4 are annotated with *Spu-cara7LB*, 3 with *Spu-cara7LA*, 2 with *Spu-cara14LA*, 1 with *Spu-cara8LA* and 1 with *Spu-cara12LB*. Thus, I conclude that our reciprocal blast approach was not able to resolve orthology and only a phylogenetic analysis will be able to address this conundrum. It would be important to look in both species for their expression pattern. Additionally, spatial and temporal expression analysis in the starfish embryo will help to answer such important evolutionary questions.

From the other three, only the ortholog to *Afi-rreb1* has been previously described in sea urchin. Rreb1 is a ras responive zinc finger transcription factor. In sea urchin this gene was reported to be expressed in the SM lineage briefly at blastula stage, however no evidence for this was provided (Materna et al., 2006). My repeat of this experiment did not support this claim. Expression of this gene is very different from brittle star: during brittle star development *Afi-rreb1*

is restricted to skeletogenic cells up to gastrula stage and its expression time-course suggests a very early role in brittle star specification. More WMISH data of earlier stages will help to elucidate its role in early development. Interestingly, an in depth look into the brittle star transcriptome revealed the presence of two sequences with similarity to *Spu-rreb1*, but no similarity between each other at the nucleotide level. Additionally, both show quantitative expression in the transcriptome time-courses. This indicates that this transcription factor specifically might have undergone duplication in brittle star and potentially acquired a novel role in skeletogenesis. Here, it will be important in future to resolve the expression of the other *Afi-rreb1* gene in brittle star. Additionally, a phylogenetic analysis will show the relationship between the two *rreb1* genes.

The last two genes that were selected from the screen are not found in sea urchin, but both are present in the Ambulaclaria. Since even in other species no clear annotation for these two candidates is available, I decided to call the genes according to their identifier from the initial transcriptome of brittle star. Whereas, spatial expression and temporal expression patterns suggest, for *Afi-tr25409*, a role in differentiation of the brittle star skeletogenic GRN, the same experiments suggest for *Afi-tr4886* to be potentially regulated similarly to vegf/fgf ligands in the ectoderm. Time-courses show that both genes are probably not involved in early processes of larval skeleton development. Spatial expression in starfish and ophiuroid adult could help to resolve the ancient role of *tr25409* this gene in larval skeletogenesis.

In conclusion, our unbiased approach through inhibition of the fgf/vegf signalling allowed the identification of genes expressed in SM lineage. Importantly, with *Afi-rreb1*, I potentially identified a novel regulatory gene for the specification of this lineage, adding another difference between sea urchin and brittle star GRNs for larval skeletogenesis.

8.3 Data Access through Website

The modelling of developmental GRNs requires knowledge of spatial and temporal expression patterns and how perturbation analysis effects those patterns. For a GRN analysis comprising

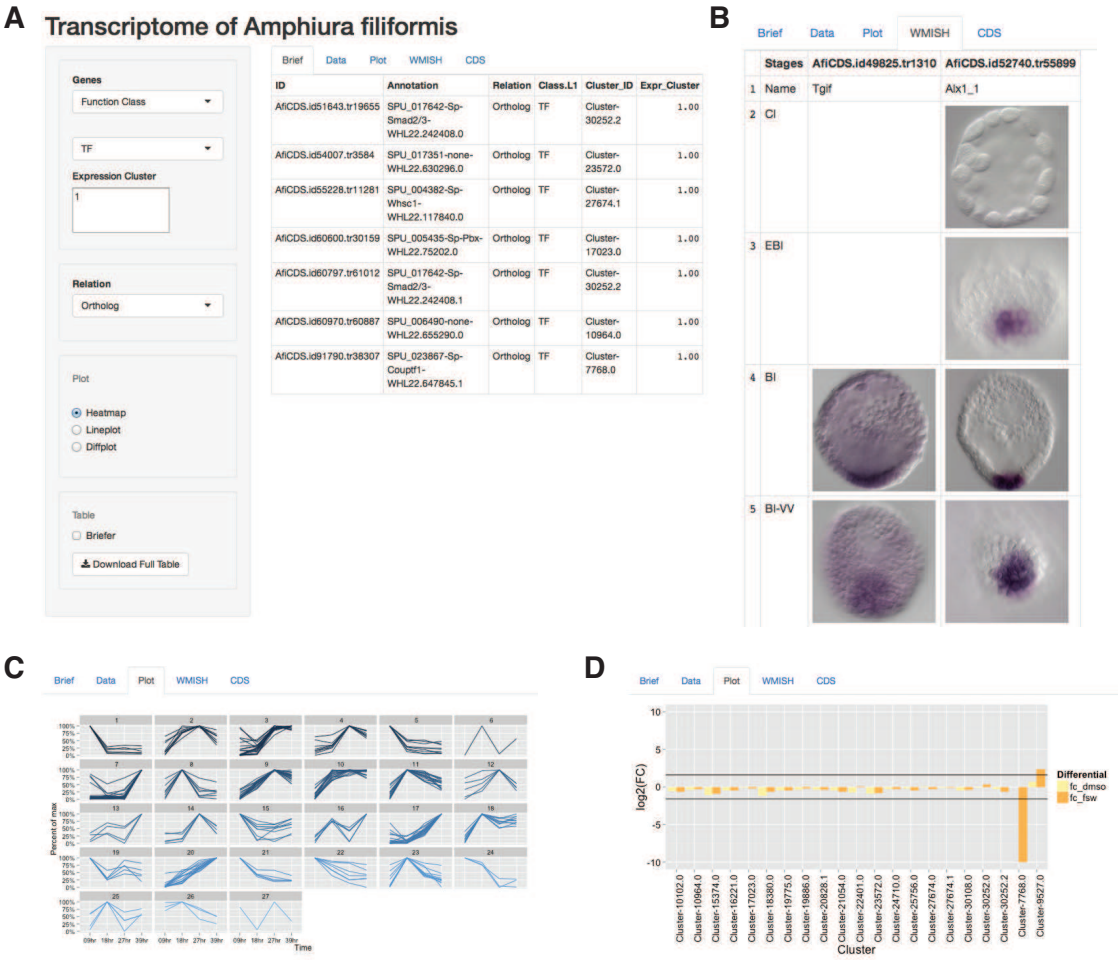

Figure 8.1: **R-shiny web application allows access to all transcriptomic and spatial data presented in this thesis.** (A) Layout of the webpage. (B) Example for access to WMISH data. (C) Example for access to time-course data. (D) Example for access to differential expression data.

a few genes, the integration of such is a relatively simple task. In a systems biology perspective, however, where hundreds or thousands of genes are considered simultaneously, it is easy to lose track of the important details of few or single genes. This is especially when working on novel systems with little to no access to the established data. Thus, I developed a website using R-shiny that allows to query different type of information (Figure 8.1), similar to (Tu et al., 2014). Using the statistical programming language R as the backbone, my website provides a platform to easily query and find genes of interest. It gives access to annotations, expression levels, sequence information, differential screening and spatial expression patterns. Contigs can be queried by annotation, expression cluster id, contig id and additionally by gene ontology class. Thus, for example one can easily access all transcription factors sequences and their expression temporarily and spatially (when available). Moreover, the website is programmed in a way that extension of spatial expression patterns is created by adding a folder with the contig id and the individual pictures as JPEG files. In future work, this website will be extended with the regeneration data produced in our laboratory and will thus create a unique resource to establish the brittle star *Amphiura filiformis* as developmental and regenerative model system.

Chapter 9

CONCLUSION

Although many studies have investigated the GRNs for mesoderm formation in echinoderms and especially larval skeletogenesis, so far no systematic study of brittle stars has been available. In this thesis I introduce the brittle star *Amphiura filiformis* as novel model system to study larval skeleton evolution in echinoderms and more specifically mechanisms of evolution of the animal body plan. I demonstrate, consistent with my initial hypothesis (see chapter 2) that two different GRNs underlie development of the larval skeleton. My genomic/transcriptomic comparison suggests that the gene content for skeleton formation in echinoderms is highly conserved, laying the foundation for the identification of an ancient module responsible for the synapomorphic character of echinoderms: the adult bio-mineralised skeleton. Furthermore, my in-depth characterisation of the SM regulatory state suggests that wiring between the genes involved in skeletogenic mesoderm (SM) specification shows several differences. Consistent with the hourglass theory (von Bear, 1828), the initiation tier of the larval skeleton GRN is not conserved between brittle star and sea urchin. Differences are found in: maternal initiation through *Afi-wnt8* and *Afi-blimp1*, the double negative gate and fate-exclusion by repression of *Afi-gcm* by *Afi-alx1*. On the other hand, the middle part of the GRN is largely similar: expression patterns of *tgif*, *hex*, and *erg* suggest a conserved sub-circuit across the Eleutherozoa. In addition expression pattern analysis indicate that *vegf/fgf* signalling is an essential and conserved part of the skeletogenic GRN. Finally, the tier directly before the differentiation cascade is quite different. The two drivers of skeletogenic differentiation genes *Afi-foxB* and *Afi-dri* are not expressed in the skeletogenic mesoderm lineage

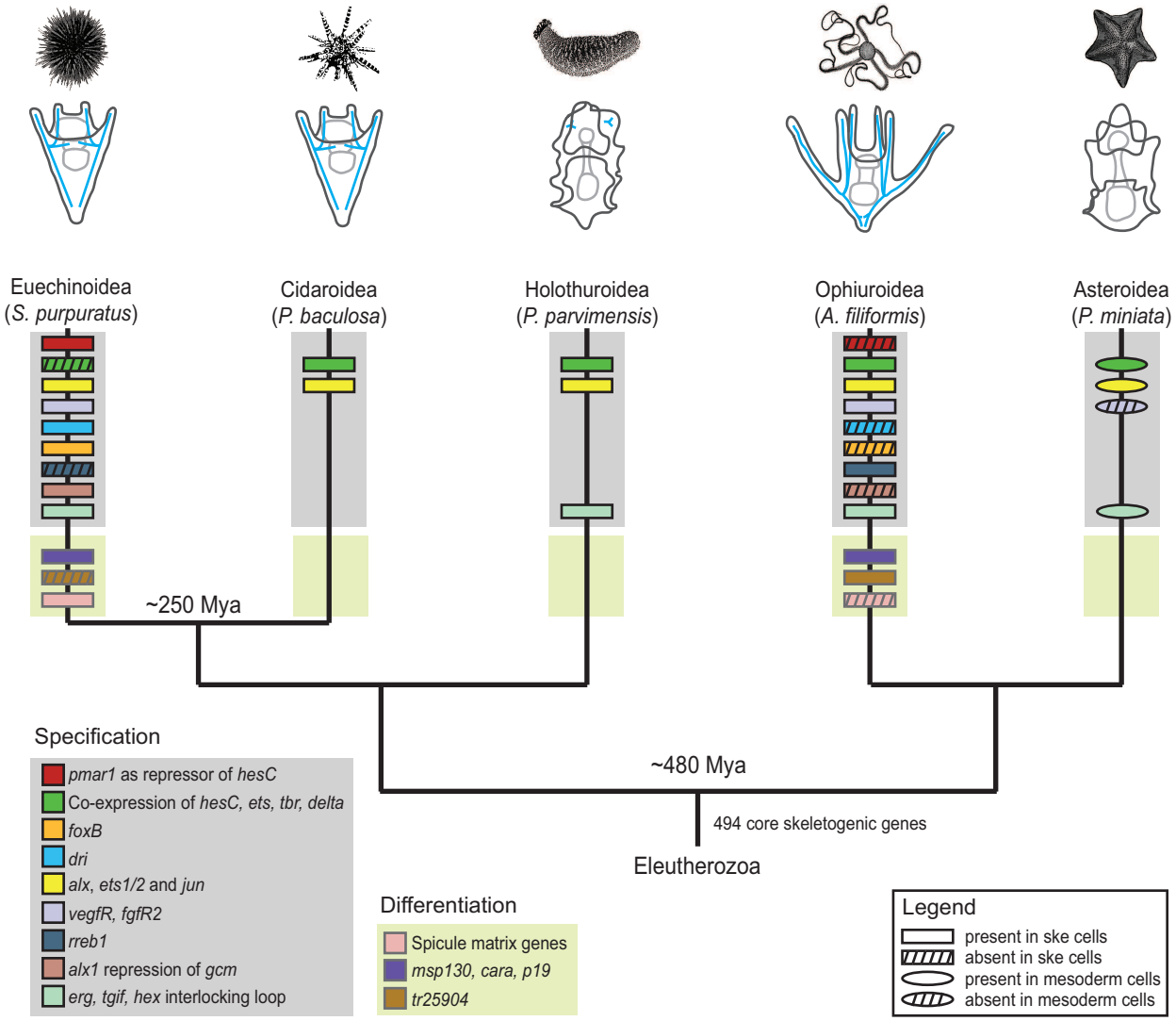

Figure 9.1: **Molecular characteristics of skeleton development mapped in Eleutherozoa.** On top are images of adults and below corresponding larvae. In light blue are the skeletogenic features of each larva. Boxes represent the molecular characters. Surrounded by a grey box are characters involved in the specification part of the GRNs (*i.e.* regulatory genes). Surrounded by a green box are genes in the differentiation part of the GRN. For branches lacking boxes no data was available. Branch for asteroids shows rounded boxes due to the lack of a SM lineage. The cladogram represents the currently best supported phylogeny (Telford et al., 2014; O'Hara et al., 2014; Cannon et al., 2014). Molecular data collected along the tree are based on the observations in this study and in other studies (Oliveri et al., 2008; McCauley et al., 2012, 2010; Gao and Davidson, 2008; Czarkwiani et al., 2013; Yamazaki et al., 2014; Röttinger et al., 2008; Duloquin et al., 2007; Adomako-Ankomah and Ettensohn, 2013; Seaver and Livingston, 2015; Livingston et al., 2006).

in the brittle star. Additionally, a novel skeletogenic gene *Afi-rreb1* has been identified and might be specific for brittle star SM lineage specification. From a GRN prospective, 480Mya of independent evolution were sufficient to accumulate various differences with different mechanisms. Gene duplication was used to expand the gene repertoire in sea urchin of *pmar1*, *sm*, and *msp130* genes. Additionally, protein function diversification was employed for the ortholog to sea urchin *Spu-pmar1*, *Afi-pplx*, in terms that it lacks two domains that are responsible for its repressive action. Finally, the presence and absence of genes in the SM lineage hints towards DNA binding motif evolution and is shown by the differences in expression pattern of the genes *foxB*, *dri*, *rreb*, and *nk7* between sea urchin and brittle star. In summary, in 480Mya of evolution all types of mechanisms are used for GRN diversification.

My second hypothesis (see chapter 2) relates to the question of how the larval skeleton evolved in echinoderms. As discussed in chapter 5 my observations strongly support the independent co-option of the larval skeleton in ophiuroids and echinoids, based on the differences of which and how specification genes are employed in the SM lineage throughout sea urchin and brittle star development, as described above. On the other the transcriptomic comparison in Part II showed many commonalities even with crinoids thus pointing towards an ancestral co-option event at the base of the Eleutherozoa. Nevertheless, while my project greatly increased the knowledge to address this question, more studies in holothuroids and asteroids are needed in order to undoubtedly resolve how the larval skeleton evolved in this phylum. For this several experiments have to be performed. Firstly, it would be important to reconstruct the ancestral regulatory state for the SM lineages of larvae and adult. A comparison between the adult and larval GRNs could help to pinpoint the true ancestral part of the GRN and the co-opted elements, and therefore clarify which genes are expressed only during larval development. Moreover, which genes are actually part of an early mesoderm specification mechanism versus pan-skeletogenic genes. One example of such, is the gene *alx1*, which is restricted to SM lineage in echinoids, holothuroids and ophiuroids but expressed in all mesoderm in asteroids during embryonic devel-

opment. Therefore, either *alx1* is a pan-mesodermal gene and got specifically restricted to the SM lineage during the co-option event, and its ancestral state would be represented by the asteroid as hypothesised by McCauley et al. (2012), or as being part an adult ancestral ske-GRN was part of the co-opted genes and represents a vestige in the asteroid. Indeed data show that in both, adult and embryo, it is one of the first markers of skeletogenic cells (Gao and Davidson, 2008; Czarkwiani et al., 2013). For this gene, a *cis*-regulatory analysis in sea urchin and star fish would reveal the necessary changes to be employed into the SM lineage. As seen in the phylogenetic tree in Figure 9.1, many other studies in the holothurian and asteroidian branches could give further support for independent or derived evolution. The presence and absence of *foxB* and *dri* in holothuroids, asteroids and cidaroids could resolve whether the inclusion of these genes into the skeletogenic GRN is a synapomorphy of euechinoids alone. Additionally, an investigation of FGF/VEGF signalling in holothuroids would show whether the positioning of the SM lineage in this branch is guided by the same mechanism. Especially, more transcriptomic and genomic data is needed in this branch of echinoderms.

In conclusion, my study establishes the brittle star *Amphiura filiformis* as a key developmental system for a detailed comparative analysis of the gene regulatory networks acting in skeletogenic lineages in distantly related echinoderms. My work not only brings new evidence to a long-debated issue on the evolutionary origin of echinoderm larval skeleton, but also clarifies specific mechanisms of GRN diversification, which sees not only the evolution of *cis*-regulatory elements, but also gene duplication, and protein function diversification as equally important mechanisms.

Appendix A

PART I

Table A.1: Degenerate primers for cloning

Gene Name	DEG Primer Seq
Afi-alx1	F: AAYCGNACNACNTTYACNTCNTAY
	R: RAANGCYTCNCGYTTNCGCCAYTT
Afi-ets1/2	F: GGNTCNGGNCCNATHCARCTNTGG
	R: RTCRCANACRAANCGRTANACRTA
Afi-foxB	F: AAYACNCARMGNTGGCARAAY
	R: GATGATRTTYTCGATRGTGAA
Afi-tbr	F: ATHACNAARCARGGNMGRMGRATG
	R: RTCRTARTTRTCYCKRAANCCYTT
Afi-dri	F: ACNTTYGARGARCARTTYAA
	R: RTCDATNGCNGCYTGNAGYTC

Table A.2: Primers for cloning

Gene	Or.	Sequene	Length	GenBank
Afi-alx1	F	Czarkwiani et al 2013	634bp	KC788414
	R			
Afi-jun	5O	ACCATGGACGGATCAAACAT	429bp	KM816839
	5I	GCCATTTAGCTCTGCGATTT		
Afi-p19	3O	TCGCATAGGTCTTGGGAAAC	697bp	KM816840
	3I	CCCTCCAACAGACCAAGAAA		
Afi-pplx	F	GCTTCGTGAGAAAGCGATGC	799bp	KM816841
	R	TAGCTTGGCAAGTTCACGGG		
Afi-pplx	F	GCTCCAACGAGAGCGAA	948bp	KM816841
	R	TCAAAACTTGGGTACACTGCAGATGG		
Afi-hesC	3O	TGTTTCCTGGAAGCTGTGTG	1414bp	KM816842
	3I	CATTGTCTTTGCCCTTGTT		
Afi-delta	F	TGCAACGGATCAGGCTCAAT	2156bp	KM816843
	R	GGCGATGAGTCCGGTGTATT		
Afi-ets1/2	F	Czarkwiani et al 2013	671bp	KC788415
	R			
Afi-tbr	F	Czarkwiani et al 2013	1127bp	KC788418
	R			
Afi-erg	F	GCGCATCGTGGTCAAATACC	2149bp	KM816844
	R	GCTTGACGCAACTTGGGAAG		
Afi-hex	F	TTGTCAAGTGGGCAGTTCGT	1243bp	KM816845
	R	CTTTGGCACAACAGCACTGG		
Afi-tgif	F	TCGCCAAAGCTAGCTGTCAA	1305bp	KM816846
	R	CCGAGTCTGACTTCAGCTTCAT		
Afi-dri	5O	GTCTTCCCTCACGACGATTG	1482bp	KM816847
	5I	CTCACGACGATTGCCATCTA		
Afi-foxB	F	Czarkwiani et al 2013	424bp	KC788416
	R			
Afi-gataC	F	Czarkwiani et al 2013	1021bp	KC788417
	R			
Afi-gataE	F	TCAATTCAACTGGAGATAGCGC	1736bp	KM816848
	R	GAGAGTTGCCGATGTGTGTC		
Afi-gcm	F	TCTCTGCGACAAATCCTGCC	1156bp	KM816849
	R	CTCATCGCGCTTGTATTGCT		
Afi-phb1	F	CAACCAACCAAAGCTGAGCC	910bp	KM816850
	R	TGGAGGAGCAGATGTCTTGG		
Afi-foxA	F	CCGGCTGAGTTCTCGAGTTT	1788bp	KM816851
	R	TTGTTTGCGCTGTGGCTAAC		
Afi-soxC	F	CGTGTCAATGGCAAGCTAGA		
	R	GGGACACGTTCTGGAGTCTG		

Table A.2: Primers for cloning

Gene	Or.	Sequene	Length	GenBank
Afi-twi	F	GGATCAGGAGCAGCAACCTA	755bp	
	R	GAAGTTACAATGGCGGCGAT		
Afi-sna	F	GGACAGCATTTGATCCGTCC	954bp	
	R	CTGTTACTCGGTGAAGCTGC		
Afi-otx	3O	GGGCCCTCCATACTCTGTTA	892bp	
	3I	CAGAGACGGGAGAGAACCACA		
Afi-wnt8	5O	CGATGCAAGTGTCATGGTGT	1208bp	
	5I	CCGCGTCATCGGATCTATAC		
Afi-blimp1	F	GATGGCTTTGACGCAGAGAG	1802bp	
	R	CACTTGCTGTTTGGTTCCGA		
Afi-phb1	F	CAACCAACCAAAGCTGAGCC	910bp	
	R	TGGAGGAGCAGATGTCTTGG		
Spu-phb1	F	TCCCAGATTGTGAAGCCGAT	1022bp	
	R	GTGAGTTGCTGGTAGTCCCT		
Afi-l1	F	AGCAGTCAGCTGCTTCATACC	584bp	
	R	TGGCAAGCTGTCCTCAGAC		
Afi-nk7	F	TTCAGCCCGACAATGTTTCC	1183bp	
	R	CTTCGTCCCGCTTCCTCTT		

Table A.3: Primers for injection constructs

Gene	Or.	Sequene
Spu-phb1	F1	TCAATTCAAAGGTGTGCTGAAC
	R1	AGCGGCGACGTCGTCGTCACACATTCGCGAGTTGATATCTGGGT
	F2	GTTATCAGCGATTCGTGGGA
	F3	TTCCCAGATTGTGAAGCCGAT
GFP	F1	ATGTGTGACGACGACGTC
	R1	TCCCCCGGGCTGCAGGAATT
	R2	GGGCTGCAGGAATTCATCGGT
Spu-pmar1	F	ATCAAAGGGACGTGCGCC
	R	GGGATAGAGGTGTGCTGTGT

Table A.4: Primers for QPCR

Gene	Or.	Sequene	Length
Afi-alx1	F	CCAAGTGGAGGAAACGAGAA	157bp
	R	GCTGGTGGTTGTGTGATGTC	
Afi-jun	F	CGGACGTACAAATGCTGAAA	171bp
	R	AGCTGCCTGTTCTTCGGTAA	
Afi-p19	F	CCCTCCAACAGACCAAGAAA	120bp
	R	CCTCTTGCTTCCTTCAGTGAG	
Afi-pplx	F	TCTGCCTTTGCTGACAACCA	168bp
	R	TGACGACGTCTCACTTGTGG	
Afi-hesC	F	AATCAGGTAGCGGCTCAAAC	146bp
	R	GGCCAGGTGGTTCAAGATT	
Afi-delta	F	GCGAAACACTCGATCACTGC	169bp
	R	TCTGAGATGCACGTTCCACC	
Afi-ets1/2	F	CGCGGCTAAGTTTCTCGTAG	133bp
	R	AACCTGCCAACACATCATCA	
Afi-tbr	F	TGATCCCAACCAGTGGAAGT	184bp
	R	CCATTGTCTTTGCCCTTGTT	
Afi-erg	F	CAACAGCAGCAAGGAAACGG	151bp
	R	GTTGCACACTTTCGTGTCCG	
Afi-hex	F	CAGGTCCGGTTCTCAAACGA	159bp
	R	CCTCCATTTCGCCCTTCTGT	
Afi-tgif	F	CGGTCCATCCATGTTTCCGTA	128bp
	R	TGTTTGGCGAGTAGCGATGA	
Afi-dri	F	ACCGCAGTAGTCAGCGGTAT	144bp
	R	TGCAGATAATGCATGGGTGT	
Afi-foxB	F	ACTTGAAACGCTTTCGTCGT	130bp
	R	GCAGAACTCTTTGCGTCACA	
Afi-gataC	F	GACCGCGTGGTTATAAGGAG	131bp
	R	ACTGAATGGCGGGTGTGT	
Afi-gataE	F	TCAAACCACAAAGACGGCTG	135bp
	R	TGAAGTAGAGACCGCAAGCA	
Afi-gcm	F	CAGCTAAACATGCACTGCTGG	133bp
	R	TCACGCAATTGTCTGGCAAC	
Afi-foxA	F	GGCTATGAAGCAATGGCAGC	145bp
	R	TTGTTTGCGCTGTGGCTAAC	
Afi-16S	F	CGGCTGCAGTACTCTGACTG	150bp
	R	GGGTCTTCTCGTCCCACTCT	
Afi-UCE	F	TTTCACAACTAAGATCTATCATCCAAACA	81bp
	R	TGGTGACCACTGTGACCTCAAG	

Table A.5: Sequence information

Name	tblastx evalue/score/pident	rec. blast	OMA	Phylogeny	Transcirptome ID	Spu ID	Note
Afi-wnt8	2e-90/208/50%	Yes	Yes	No	AfiCDS.id55172.tr11092	SPU_020371-Sp-Wnt8-WHL22.8923	
Afi-otx	8e-35/147/82%	Yes	No	No	AfiCDS.id6059.tr24500	SPU_010424-Sp-Otx-WHL22.532435	
Afi-blimp1	1e-137/281/76%	Yes	No	No	AfiCDS.id25396.tr42615	SPU_027235-Sp-Blimp1-WHL22.5073	
Afi-pplx	9e-13/73/58%	Yes	No	Yes	AfiCDS.id36883.tr33539	SPU_015828-Sp-Pmar1c-WHL22.462256	
Afi-alx1	2e-69/153/89%	Yes	Yes	No	AfiCDS.id52740.tr55899	SPU_022817-Sp-Alx1_1-WHL22.731056	
Afi-jun	2e-90/193/90%	Yes	Yes	No	AfiCDS.id55428.tr60572	SPU_003102-Sp-Jun-WHL22.318085	
Afi-p19	2e-12/72/42%	Yes	Yes	No	AfiCDS.id6273.tr13385	SPU_004135-Sp-Cah10L-WHL22.642603	
Afi-hesC	1e-44/112/72%	Yes	Yes	No	AfiCDS.id79437.tr59210	SPU_021608-Sp-HesC-WHL22.235339	
Afi-foxA	1e-109/303/84%	Yes	Yes	No	AfiCDS.id85717.tr16742	SPU_006676-Sp-FoxA-WHL22.439762	
Afi-gataC	1e-73/159/79%	Yes	Yes	No	AfiCDS.id61260.tr63157	SPU_027015-Sp-GataC-WHL22.660411	
Afi-gataE	8e-77/269/88%	Yes	No	No	AfiCDS.id38615.tr1992	SPU_010635-Sp-Gatae-WHL22.78013	
Afi-gcm	2e-48/170/69%	Yes	No	No	AfiCDS.id38146.tr47389	SPU_006462-Sp-Gcm-WHL22.54333	
Afi-erg	1e-171/342/87%	Yes	Yes	No	AfiCDS.id64071.tr2242	SPU_018483-Sp-Erg-WHL22.552472	
Afi-ets1/2	0/323/99%	Yes	Yes	No	AfiCDS.id20811.tr66263	SPU_002874-Sp-Ets1/2-WHL22.238821	
Afi-tbr	1e-109/394/73%	Yes	No	No	AfiCDS.id43541.tr66231	SPU_025584-Sp-Tbr-WHL22.503644	
Afi-hex	6e-53/188/97%	Yes	No	No	AfiCDS.id81692.tr22161	SPU_027214-none-WHL22.626418	SPU_027214 = SPU_027215
Afi-tgif	6e-44/171/85%	Yes	No	No	AfiCDS.id49825.tr1310	SPU_018126-Sp-Tgif-WHL22.614286	
Afi-foxB	1e-91/325/93%	Yes	Yes	No	AfiCDS.id1937.tr11127	SPU_004551-Sp-FoxB-WHL22.743430	
Afi-dri	6e-48/114/70%	Yes	No	No	AfiCDS.id16344.tr60844	SPU_005718-Sp-Dri_2-WHL22.544150	
Afi-soxC	1e-105/232/83%	Yes	Yes	No	AfiCDS.id33804.tr61034	SPU_002603-Sp-SoxC-WHL22.622787	
Afi-twi	8e-56/215/87%	Yes	No	No	AfiCDS.id89079.tr60007	SPU_030059-Sp-Twi-WHL22.118674	
Afi-sna	2e-90/321/82%	Yes	Yes	No	AfiCDS.id32534.tr38806	SPU_001113-Sp-Sna-WHL22.131363	
Afi-nk7	2e-58/191/76%	Yes	No	No	AfiCDS.id63655.tr58557	SPU_022573-Sp-Nk7-WHL22.567485	
Afi-l1	1e-147/99/34%	Yes	Yes	No	AfiCDS.id37274.tr11372	SPU_000125-none-WHL22.236839	SPU_000125 = SPU_021428

Table A.6: Time-courses

Gene	0hpf	3hpf	6hpf	9hpf	12hpf	15hpf	18hpf	21hpf	24hpf	27hpf	30hpf	33hpf	36hpf	39hpf	42hpf
Afi-alx1	0	0	0	3	63	67	101	165	141	100	79	122	88	68	60
Afi-p19	0	0	0	4	66	199	479	1084	907	1216	1578	2281	2078	1603	1597
Afi-jun	1143	830	1614	487	690	476	1072	1993	1370	695	1789	1385	992	1204	1866
Afi-pplx	9	11	50	233	482	206	143	127	22	15	43	27	19	13	17
Afi-hesC	44	15	4	3	21	12	36	42	41	27	76	168	NA	NA	NA
Afi-ets12	1686	3396	3215	2455	2250	979	1130	1972	1887	1694	2128	5158	3466	2882	3392
Afi-tbr	36	43	33	14	48	132	305	805	993	673	1447	1292	NA	NA	NA
Afi-delta	75	95	64	72	313	265	209	201	148	148	204	429	343	214	250
Afi-tgif	89	283	0	125	461	359	309	545	476	348	1358	1170	1145	627	1098
Afi-erg	14	20	31	53	138	120	428	592	625	312	625	737	614	458	573
Afi-hex	5	7	4	4	75	108	379	852	659	610	923	1531	930	775	894
Afi-dri	1	1	1	0	0	5	19	26	34	28	25	21	49	51	39
Afi-foxB	0	0	0	0	0	1	2	37	12	15	81	145	174	124	220
Afi-gcm	3	5	6	27	24	7	12	7	11	13	21	15	11	7	22
Afi-gataC	0	0	1	1	1	4	3	24	47	67	105	145	82	52	40
Afi-gataE	1	12	12	7	17	13	23	117	81	157	376	740	1130	861	1057
Afi-foxA	1	6	8	4	11	41	233	980	1152	790	2315	3888	3043	2914	4248
Afi-otx	528	1340	1049	728	926	477	984	1696	2143	1093	2989	2128	NA	NA	NA
Afi-phb1	0	0	7	57	537	649	842	698	595	355	797	1124	913	609	663
Afi-wnt8	0	2	28	137	281	147	178	144	97	62	109	61	51	80	55

Appendix B

PART II

Table B.1: Adapter sequences

Adapter	Sequence	Sample
TruSeq Universal	AATGATACGGCGACCACCGAGATCTACACTCTTTCCCTACACGACGCTCTTCCGATCT	9hr, 18hr, 27hr, 27hr-DMSO, 27hr-SU, 39hr
MultiplexingA	GATCGGAAGAGCACACGTCT	9hr, 18hr, 27hr, 27hr-DMSO, 27hr-SU, 39hr
MultiplexingR	GATCGGAAGAGCACACGTCTGAACTCCAGTCAC	9hr, 18hr, 27hr, 27hr-DMSO, 27hr-SU, 39hr
TruSeq Adapter 2	GATCGGAAGAGCACACGTCTGAACTCCAGTCACCGATGTATCTCGTATGCCGTCTTCTGCTTG	9hr
FastQC Identified	CTCCTATTTATTTCCTCAAAAAAAAGCTATCACAAAACTCGAAAAGCATA	9hr
TruSeq Adapter 4	GATCGGAAGAGCACACGTCTGAACTCCAGTCACTGACCAATCTCGTATGCCGTCTTCTGCTTG	18hr, 27hr
FastQC Identified	CTCCTATTTATTTCCTCAAAAAAAAGCTATCACAAAACTCGAAAAGCATA	18hr, 27hr-DMSO, 27hr-SU, 39hr
FastQC Identified	CCCTCTTTCAAAAGTCCTTTCGTACAAGAAGAAATTTTAAGGAAGTAGAT	18hr, 27hr-DMSO, 27hr-SU
FastQC Identified	CAAAAACAACGCCTTCGGATTTTGATCGTAAGGTTCTGCCTGCCCGGTGA	18hr
FastQC Identified	CTCCTATTTATTTCCTCAAAAAAAAGCTATCACAAAACTCGAAAAGCATA	27hr
TruSeq Adapter 5	GATCGGAAGAGCACACGTCTGAACTCCAGTCACACAGTGATCTCGTATGCCGTCTTCTGCTTG	27hr
TruSeq Adapter 6	GATCGGAAGAGCACACGTCTGAACTCCAGTCACGCCAATATCTCGTATGCCGTCTTCTGCTTG	27hr-DMSO
TruSeq Adapter 7	GATCGGAAGAGCACACGTCTGAACTCCAGTCACCAGATCATCTCGTATGCCGTCTTCTGCTTG	27hr-SU
TruSeq Adapter 12	GATCGGAAGAGCACACGTCTGAACTCCAGTCACCTTGTAATCTCGTATGCCGTCTTCTGCTTG	39hr

Table B.2: Contig statistics for individual assemblies

Sample	N25	N50	N75	Longest	Mean	Median	Shortest	Contigs
09hr	2,203	1,146	559	21,167	765	463	201	285,536
18hr	2,314	935	395	16,924	627	343	201	179,679
27hr FSW	2,530	1,345	626	20,576	835	482	201	314,188
27hr DMSO	2,594	1,352	632	22,055	842	486	201	292,331
27hr SU	2,408	1,258	585	20,474	796	461	201	334,802
36hr	2,234	1,120	536	20,535	747	445	201	359,728

Table B.3: Subclasses for bio-mineralisation gene ontology

Subclasses	Afi	Pmi	Ame	Spu
Carbonic Anhydrase	3	3	3	3
Collagen	10	15	9	15
Cyclophilin	7	7	9	11
MSP130	2	3	4	9
Spicule Matrix	1	5	1	14
Other	0	1	0	4
Total	23	34	26	56

Table B.4: Contig statistics

WHL ID	Reason for exclusion	Notes
WHL22.609261	408b only homolog	
WHL22.117376	321bp only homolog	
WHL22.714669	456bp ortholog	but deeper analysis shows that is artefact
WHL22.632079	not strong enough expressed to be part of EC	
WHL22.437349	not strong enough expressed to be part of EC	
WHL22.585512	recent gene duplication (see SPU scaffold:551)	
WHL22.568711	not strong enough expressed to be part of EC	
WHL22.486796	327bp only homolog	part of cluster with more individuals that belong to WHL22.82981
WHL22.485384	not strong enough expressed to be part of EC	
WHL22.15174	not strong enough expressed to be part of EC	
WHL22.40034	¡450bp	part of cluster with more individuals that belong to WHL22.622033
WHL22.636100	algorithm chose WHL22.674225 instead with same probility	mistake in sea urchin transcirptome are actually both the same transcript
WHL22.635901	algorithm chose WHL22.310280 instead with same probility	
WHL22.608861	algorithm chose WHL22.608876 instead with same probility	are actually the same gene one transcript however is not part of the GO table
WHL22.496011	not strong enough expressed to be part of EC	

Table B.5: Naming SU5402 QPCR experiment

Name	ID	Expression Cluster	Annotation
Afi-egfiL_2	AfiCDS.id85082.tr39719	Cluster-25982.2	SPU_003872-Sp-EgfiL_2-WHL22.289903.3
Afi-tropmyh	AfiCDS.id21782.tr976	Cluster-18373.0	SPU_015849-Sp-Tropmyh-WHL22.432759.1
Afi-alx/arx	AfiCDS.id68561.tr6658	Cluster-30632.0	SPU_030703-none-WHL22.490216.0
Afi-vegf2	AfiCDS.id11730.tr8523	Cluster-7997.0	SPU_005737-Sp-Vegf2-WHL22.194484.0
Afi-tacr2L	AfiCDS.id92119.tr44548	Cluster-15622.0	SPU_010179-Sp-Tacr2L_1-WHL22.581307.0
Afi-fn3/igf_29	AfiCDS.id62424.tr60943	Cluster-4641.0	SPU_004746-Sp-Fn3/Igf_29-WHL22.147868.1
AfiCDS.id81632.tr60441	AfiCDS.id81632.tr60441	Cluster-11727.4	
Afi-ttrspn_19	AfiCDS.id30755.tr5407	Cluster-31209.0	SPU_025068-Sp-Ttrspn_19-WHL22.748368.1
Afi-e2f7	AfiCDS.id13713.tr42693	Cluster-17970.0	SPU_023346-Sp-E2f7-WHL22.755786.0
Afi-slc4a10	AfiCDS.id61902.tr45342	Cluster-7256.0	SPU_025515-Sp-Slc4a10-WHL22.12691.2
Afi-p58-a	AfiCDS.id40036.tr13789	Cluster-3715.1	SPU_000439-Sp-p58-a-WHL22.23776.0
Afi-αcoll	AfiCDS.id28173.tr18060	Cluster-21780.0	SPU_026008-Sp-Fcoll/II/IIIf-WHL22.541149.0
Afi-p58-b	AfiCDS.id28024.tr11245	Cluster-3715.0	SPU_000438-Sp-p58-b-WHL22.23620.0
AfiCDS.id384.tr29965	AfiCDS.id384.tr29965	Cluster-10558.1	
Afi-sept4	AfiCDS.id4418.tr33430	Cluster-5808.0	SPU_003696-Sp-Sept4-WHL22.624760.0
Afi-mt6_mmpL	AfiCDS.id21881.tr9218	Cluster-16461.0	SPU_005576-Sp-Mt6_mmpL-WHL22.35130.0
AfiCDS.id10236.tr3203	AfiCDS.id10236.tr3203	Cluster-28643.1	SPU_005576-Sp-Mt6_mmpL-WHL22.35130.0
Afi-spcat3l	AfiCDS.id57192.tr60565	Cluster-5917.0	SPU_001545-Sp-Spcat3l-WHL22.670777.0
Afi_fn3/egff_1	AfiCDS.id3884.tr60838	Cluster-17570.0	SPU_011180-Sp-Fn3/Egff_1-WHL22.516341.0
Afi-soxD1	AfiCDS.id37686.tr6742	Cluster-13113.1	SPU_004217-Sp-SoxD1-WHL22.118185.2
Afi-vegfR	AfiCDS.id52869.tr20202	Cluster-23512.1	SPU_000310-Sp-Pdgfr/vegfrL-WHL22.240520.0
AfiCDS.id52181.tr20375	AfiCDS.id52181.tr20375	Cluster-4513.0	
AfiCDS.id41059.tr61404	AfiCDS.id41059.tr61404	Cluster-18217.0	SPU_009642-Sp-Rreb1-WHL22.421612.0
Afi-a2m_1	AfiCDS.id66422.tr18763	Cluster-16526.0	SPU_025922-Sp-A2m_1-WHL22.306546.0
Afi-hypp_2281	AfiCDS.id89402.tr3094	Cluster-2493.0	SPU_016833-Sp-Hypp_2281-WHL22.347032.0
Afi-cara7LA	AfiCDS.id10597.tr30892	Cluster-20452.0	SPU_012518-Sp-Cara7LA-WHL22.446073.1
Afi-erg	AfiCDS.id90393.tr2237	Cluster-29925.0	SPU_018483-Sp-Erg-WHL22.552472.1
AfiCDS.id84973.tr13659	AfiCDS.id84973.tr13659	Cluster-12844.62	
Afi-009748	AfiCDS.id65088.tr20037	Cluster-15262.0	SPU_009748-none-WHL22.397555.0
Afi-msp130L	AfiCDS.id75849.tr3754	Cluster-27881.0	BEFORE SEA URCHIN GENOME UPDATE
Afi-tr25409	AfiCDS.id88683.tr31926	Cluster-1517.1	
Afi-tr4886	AfiCDS.id5647.tr1291	Cluster-7020.0	
Afi-kirrelL	AfiCDS.id74191.tr58590	Cluster-720.0	SPU_024995-Sp-KirrelL-WHL22.699052.0
AfiCDS.id44038.tr10735	AfiCDS.id44038.tr10735	Cluster-25746.0	
Afi-tle1/groucho	AfiCDS.id4947.tr10732	Cluster-22948.0	SPU_017807-Sp-Tle1/Groucho-WHL22.510742.0
Afi-77kDamaps	AfiCDS.id4682.tr16558	Cluster-25122.0	SPU_005744-Sp-77kDamaps-WHL22.325883.0
Afi-0914236	AfiCDS.id31785.tr21	Cluster-20113.3	SPU_014236-none-WHL22.470491.3
AfiCDS.id58703.tr6207	AfiCDS.id58703.tr6207	Cluster-17600.0	
Afi-018662	AfiCDS.id61413.tr281	Cluster-26614.0	SPU_018662-none-WHL22.220192.0
AfiCDS.id48303.tr39358	AfiCDS.id48303.tr39358	Cluster-12844.127	NA-NA-WHL22.470012.13
Afi-cebpa	AfiCDS.id63703.tr20911	Cluster-7531.0	SPU_001657-Sp-Cebpa-WHL22.255599.0
Afi-tr4886	AfiCDS.id70646.tr9107	Cluster-23056.1	
Afi-004896	AfiCDS.id29222.tr34323	Cluster-1541.0	SPU_004896-none-WHL22.381788.2
Afi-trim2_1	AfiCDS.id8707.tr37166	Cluster-1364.0	SPU_007912-Sp-Trim2_1-WHL22.742590.0
Afi-fbn2L_1	AfiCDS.id12160.tr20206	Cluster-30786.1	SPU_008613-Sp-Fbn2L_1-WHL22.324858.1
AfiCDS.id64819.tr39976	AfiCDS.id64819.tr39976	Cluster-30937.0	NA-NA-WHL22.699079.0
AfiCDS.id4578.tr38894	AfiCDS.id4578.tr38894	Cluster-15464.0	SPU_009708-Sp-Trim2-WHL22.300164.0
Afi-egr	AfiCDS.id86638.tr27818	Cluster-13125.0	SPU_015358-Sp-Egr-WHL22.280477.0
AfiCDS.id53027.tr45279	AfiCDS.id53027.tr45279	Cluster-4270.0	
Afi-trim2-2	AfiCDS.id28262.tr65992	Cluster-2571.0	SPU_006071-Sp-Trim2-2-WHL22.674919.0
Afi-dcst2-3	AfiCDS.id51828.tr30296	Cluster-672.0	SPU_005390-Sp-Dcst2-3-WHL22.60281.0
Afi-dusp1	AfiCDS.id48508.tr53384	Cluster-24220.0	SPU_021143-Sp-Dusp1-WHL22.221547.1
Afi-rreb1	AfiCDS.id62604.tr47807	Cluster-13724.0	SPU_009642-Sp-Rreb1-WHL22.421612.0
Afi-mad	AfiCDS.id51560.tr55093	Cluster-22670.0	SPU_006583-Sp-Mad-WHL22.80541.0
AfiCDS.id43930.tr1339	AfiCDS.id43930.tr1339	Cluster-14335.0	NA-NA-WHL22.476817.0
Afi-trim2	AfiCDS.id537.tr30881	Cluster-1215.0	SPU_009708-Sp-Trim2-WHL22.300164.0
AfiCDS.id75617.tr19326	AfiCDS.id75617.tr19326	Cluster-15634.0	
AfiCDS.id5605.tr49815	AfiCDS.id5605.tr49815	Cluster-24029.0	NA-NA-WHL22.110836.1
AfiCDS.id4513.tr62663	AfiCDS.id4513.tr62663	Cluster-5507.0	
Afi-018426	AfiCDS.id76901.tr2369	Cluster-1724.0	SPU_018426-none-WHL22.372181.0
Afi-colf_3	AfiCDS.id53870.tr61382	Cluster-25105.0	SPU_011736-Sp-Colf_3-WHL22.97140.0
AfiCDS.id59305.tr68751	AfiCDS.id59305.tr68751	Cluster-21880.0	
Afi-gldc	AfiCDS.id77794.tr828	Cluster-17333.2	SPU_027673-Sp-Gldc-WHL22.765838.1
Afi-mt14/mmpl7	AfiCDS.id40247.tr45766	Cluster-3261.0	SPU_028748-Sp-Mt1-4/MmpL7-WHL22.312033.0
Afi-sr/fu/igr	AfiCDS.id35420.tr36288	Cluster-28510.0	SPU_006068-Sp-Sr/Fu/Igr-WHL22.362474.1
Afi-agrnL	AfiCDS.id36042.tr36266	Cluster-27739.0	SPU_017586-Sp-AgrnL-WHL22.218450.1
AfiCDS.id63133.tr10933	AfiCDS.id63133.tr10933	Cluster-13564.0	NA-NA-WHL22.555967.0
Afi-tcep1	AfiCDS.id1705.tr9893	Cluster-11257.0	SPU_006406-Sp-Tecp1-WHL22.573138.0
Afi-msp130r6	AfiCDS.id80760.tr10976	Cluster-7482.0	SPU_014492-Sp-Msp130r6-WHL22.405717.2

Table B.6: Sources of species sequences

Species	ID	Class	Source
Amphiura filiformis	AFI	Ophiuroidea	this study
Aplysia californica	ACAL	Mollusc	http://www.ncbi.nlm.nih.gov/Traces/wgs/?val=GBCZ01
Apostichopus japonicus	AJAP	Holothuroidea	http://datadryad.org/resource/doi:10.5061/dryad.kj4n8
Asterias amurensis	AAMU	Asterinidae	http://echinobase.org
Asterias forbesi	AFOR	Asterinidae	http://www.ncbi.nlm.nih.gov/Traces/wgs/?val=GAUS01
Asterias rubens	ARUB	Asterinidae	http://www.ncbi.nlm.nih.gov/Traces/wgs/?val=GAUU01
Astrotoma agssizi	AAGS	Ophiuroidea	http://www.ncbi.nlm.nih.gov/sra/SRX798213[accn]
Echinarachnius parma	EPAR	Echinoidea	http://www.ncbi.nlm.nih.gov/Traces/wgs/?val=GAVF01
Echinaster spinulosus	ESPI	Asterinidae	http://www.ncbi.nlm.nih.gov/Traces/wgs/?val=GAVE01
Eucidaris tribuloides	ETRI	Echinoidea	http://echinobase.org
Evechinus chloroticus	ECHL	Echinoidea	http://mrna.otago.ac.nz/Kina/
Heliocidaris erythrogramma	HERY	Echinoidea	http://www.ncbi.nlm.nih.gov/sra/SRX505743
Henricia species	HSPE	Asterinidae	http://www.ncbi.nlm.nih.gov/Traces/wgs/?val=GAVP01
Holothuria glaberrima	HGLA	Holothuroidea	http://www.researchgate.net/publication/264534267_H_glaberrima_RNC_transcriptome_Contigs.fasta
Leptasterias species	LSPE	Asterinidae	http://www.ncbi.nlm.nih.gov/Traces/wgs/?val=GAVC01
Luidia clathrata	LCLA	Asterinidae	http://www.ncbi.nlm.nih.gov/Traces/wgs/?val=GAVQ01
Lytechinus variegatus	LVAR	Echinoidea	http://echinobase.org
Marthasterias glacialis	MGLA	Asterinidae	http://www.ncbi.nlm.nih.gov/Traces/wgs/?val=GAVI01
Ophiocoma echinata	OECH	Ophiuroidea	http://www.ncbi.nlm.nih.gov/Traces/wgs/?val=GAUQ01
Ophionotus victoriae	OVIC	Ophiuroidea	http://www.ncbi.nlm.nih.gov/sra?LinkName=biosample_sra&from_uid=997899
Oxycomanthus japonicus	OJAP	Crinoidea	http://www.ncbi.nlm.nih.gov/Traces/wgs/?val=GAZO01
Parastichopus californicus	PCAL	Holothuroidea	http://www.ncbi.nlm.nih.gov/Traces/wgs/?val=GAVO01
Parastichopus parvimensis	PPAR	Holothuroidea	http://echinobase.org
Patiria miniata	PMIN	Asterinidae	http://echinobase.org
Patiria miniata	PMIN	Asterinidae	http://www.ncbi.nlm.nih.gov/Traces/wgs/?val=GAWB01
Patiria pectinifera	PPEC	Asterinidae	http://www.ncbi.nlm.nih.gov/Traces/wgs/?val=GAVK01
Pisaster ochraceus	POCH	Asterinidae	http://www.ncbi.nlm.nih.gov/Traces/wgs/?val=GAVN01
Sclerodactyla briareus	SBRI	Holothuroidea	http://www.ncbi.nlm.nih.gov/Traces/wgs/?val=GAUT01
Sphaerechinus granularis	AAMU	Echinoidea	http://www.ncbi.nlm.nih.gov/Traces/wgs/?val=GAVR01
Sterechinus neumayeriv	SNEU	Echinoidea	http://trace.ncbi.nlm.nih.gov/Traces/sra/?run=SRR1765201
Strongylocentrotus purpuratus	SPUR/TRSPU	Echinoidea	http://echinobase.org
Antedon mediterranea	AMED	Crinoidea	Elphick Laboratory

Table B.7: Primers for cloning

Gene	Or.	Sequene	Length	GenBank
Afi-msp130L	F	CGTCTTACTCGTACCAGCCT	878bp	
	R	CTACTCCTGCTGCTGTTCCT		
Afi-p58b	F	TGCTAAAGGAGGTGCTAAGGA	702bp	
	R	AATTCCTCCTCCAGCTCGTC		
Afi-lrr/lgr_10	F	TACGGCTTGGAGATCTGGAC	1316bp	
	R	CGCAGATTCGGTAGTGCAAA		
Afi-kirrelL	F	GGTGAAACCGCAACTCTGAA	1647bp	
	R	TGTTGAGTTCGTATCTGCGC		
Afi-mt14-mmpL5	F	ATCAAGAGTCCTAGGTGCGG	606bp	
	R	GTTGGTTGGTGTATTCGGTGT		
Afi-p58a	F	CCGTTCGAAACTAAGCATCGT	600bp	
	R	AGGTACCAGCTTTACTCTTGTT		
Afi-picalmL	F	AACACACAATTACCGGCTCC	1500bp	
	R	CCTGCCTCGTGATATCCAGA		
Afi-adam/tsl6	F	GATCCCGACGGTGGTAGTAG		
	R	GTCCTGGTACCACTTCCACA		
Afi-007098	F	ATGGGAATGTAGCCGATGTG	743bp	
	R	TGACAAACTCTCTGACAGTCTGA		
Afi-c-lectin	F	AGCAGCAATGAAGGTCTGGT	1317bp	
	R	AAGACTGGAAGAAAACAAGA		
Afi-ttrspn_19	F	GGCGCTCGATGGCTGTTC	716bp	
	R	GAGGCTGTTTCCGTAAATCTTGA		
Afi-scl4a10	F	CGATCCCTACTCGGTTCCTC	988bp	
	R	TCGCAGTCTTCCATAGCGAT		
Afi-fgf9/16/20	F	TGGTGTCAGTGCTAGCTTGA	1397bp	
	R	TTTGCTTTCGTCCTTGCTCC		
Afi-fgf4/5/6	3O	CGTCTCTGATGAACGCAATC	564bp	
	3I	TTTGCTATGCTCAAAGTGTCGT		
Afi-fgfR1	F	ATGGGAATGTAGCCGATGTG	743bp	
	R	TGACAAACTCTCTGACAGTCTGA		
Afi-fgfR2	3O	CCATTGAGTCTTGGGCTGAT	759bp	
	3I	CACTGGGTGCCAGACCTTAT		
Afi-vegf3	F	CCAATAGTCATGGCACGGTG	1152bp	
	R	GTTTAGGCATGGTGGTGTGG		
Afi-vegfR	F	TTGTTGCGTTCCAGACTGTG	1834bp	
	R	GGACATTACGAGCTGCCAAG		
Afi-$alpha$coll	F	(Burns et al. 2011)	3000bp	JG391435
	R			
Afi-alx/arx	F	GGGAAAGCGTCGACAAGATC	1008bp	
	R	CGGTGCAAATGATCGGTGAT		

Table B.7: Primers for cloning

Gene	Or.	Sequene	Length	GenBank
Afi-tr4886	F	ATCTTGCTGCACCAACCTTG	862bp	
	R	ACCACTAGATCGGCTTGCTT		
Afi-rreb1	F	TCAACTGCCAACGTCACATG	893bp	
	R	CTTAGCTGCCGTCTGAGAGT		
Afi-caraX	F	ACTTCTCTTTGGTCCGTCGA	1207bp	
	R	TATAGCGGTACCTGCGTTGT		
Afi-tr25409	F	ATCTCTAGCTTTCCCAGGCC	582bp	
	R	CACCAATAGCTGTGCCCAAA		

Table B.8: Primers for QPCR

Gene	FP	RP	Length
Afi-egfiL_2	GCCGCTGTCCAGAATCTTTC	TCAGGATCGTTGCAGACACA	139bp
Afi-tropmyh	GCAGGCAAGAGTGGAAGAAC	GCATCTCGCAGTTGTGTCTC	147bp
Afi-alx/arx	CAATGATGCGGGACCATGTT	CCATGACTTGTTGCCGCTAA	112bp
Afi-vegf2	GTCGTCCCAAACATGTCACA	TACAAGGCTTAACTCGGGCA	138bp
Afi-tacr2L	CCAGTCTACCCTCACCACAG	AGACACAGACCTCTCCAAGC	140bp
Afi-fn3/igf_29	CATCCCGACCACAATGATGG	ATTCCACCGATAAACAGCGC	146bp
AfiCDS.id81632.tr60441	CGCAACCAGTCCTGATCAAG	CGGTCTGGAAGGTAGTCGAA	122bp
Afi-ttrspn_19	CATCGCTGCTATGGGTTTCA	TGTCCCATGCCCTTGTAAGT	125bp
Afi-e2f7	CAGCTCCAAGTAGTCCTGCT	CTGTTGCATGCGTTCCTTCT	149bp
Afi-slc4a10	CCGCTCTCATTGCCTTCATC	CTGATGGTTCACAGACGCAG	141bp
Afi-p58-a	CTCGGCCAGTCTCAGTACAT	TGCCGCCATGTATTCCAAAC	101bp
Afi-αcoll	GGGAGGAACACAAGGACAAA	CTCCACGTTCTCCATCCTGT	152bp
Afi-p58-b	TTGAACAATATGTCGCCGGC	ACTTGTGGGAAATCAACGCC	147bp
AfiCDS.id384.tr29965	TGGACTCCAGCCCATCATTT	CCGTGTGTTGATCCTTGCAA	141bp
Afi-sept4	CGGATGACCTTCAAAGAACCG	ACTATGGCTAGCGTGACTCC	113bp
Afi-mt6_mmpL	ACTACCGTTACAACAGCCGT	AACGGTAGTAGTTGTCGCCA	150bp
AfiCDS.id10236.tr3203	TGCCGATGATGCCAGGATAT	AGGAAGAAATGGCAGCAACG	111bp
Afi-spcat3l	TGGACGTTAGCCTGTGTGAT	GTCCTGGTACCACTTCCACA	143bp
Afi-fn3/egff_1	AGCCCGAATCACAGTACACA	AGGGCCATGAATGTCAGTGA	149bp
Afi-soxD1	TGGTGTGGGCTAAGGAAGAG	GCTGAGACGTGCTTGTTCTT	150bp
Afi-vegfR	GATGAAACCACGGCAACAGT	CGCCAAGAACAACAGACACA	116bp
AfiCDS.id52181.tr20375	CCACTATGCGTTCAATGCCA	TGTCTCACTGGAAGCCTCTG	115bp
AfiCDS.id41059.tr61404	CACACCTGGAGACGATGAGA	CTTAGCTGCCGTCTGAGAGT	133bp
Afi-a2m_1	GCCGCGATCCATTTGAAATC	GGTAGCATCTCGAGGACCAA	113bp
Afi-hypp_2281	ACCACCAAGCAGACGTCATA	TTCGTTGAGCTGTTCCTTGC	128bp
Afi-caraX	GCGGTGACTACGCGAATTAC	GTGTATAGCGGTACCTGCGT	110bp
Afi-erg	CAACAGCAGCAAGGAAACG	GTTGCACACTTTCGTGTCCG	151bp
AfiCDS.id84973.tr13659	GCAAGTATGGATGTGTCGGC	ACGTCTTCCTCGACCAGATC	141bp
Afi-009748	ATTGCGTCAACCAGATTCCG	TAAGGACCTCAACAGCGTGT	146bp
AfiCDS.id75849.tr3754	ACCGAGTCAACATGGTCGAT	CACTGGATTGGGCATGATCG	132bp
Afi-tr25409	TGCCAATAACGAAGCTGGAC	CACCAATAGCTGTGCCCAAA	131bp
Afi-tr4886	TGCACCACTATTGACGAGGT	ACCACTAGATCGGCTTGCTT	113bp
Afi-kirrelL	GCGGTGAAACTTCCATTCCA	TCCCTGACCTGGCCAAATAG	128bp
AfiCDS.id44038.tr10735	GGTTTGTCTCCTTCTTCCGC	CGCCATTGGTTGCACGTATA	133bp
Afi-tle1/groucho	ACAACACCCTTTACCGCATG	GGTCCCGAGTTCATCATTGC	135bp
Afi-77kDamaps	TCTGGGATTGGGCCAAAGAA	CCATCAAACGCCCAGAAGAG	142bp
Afi-0914236	CGAAAGTGGCAGTCGAGTTT	CAAGCCCACCTCTGTTTCAC	131bp
AfiCDS.id58703.tr6207	CTGCATGTGGAGCCTAAACC	ATGCCCAACTTTGCCACAAT	114bp
Afi-018662	GGACCATTGGAGCAGAAACC	TCGGACTGTTCTTGCTCTGT	136bp
AfiCDS.id48303.tr39358	CATCAATGTCCGCACCACC	GACGTTGGAGGTGTAAAGCC	112bp
Afi-cebpa	GCTAAACGAGGAAGAGCACG	AGCTCATCTACCCGCTTCTG	146bp
Afi-tr4886	GCAACCTGCGTTCCTTCTTT	GTTCGCGAGCCTTTCATGAA	140bp
Afi-004896	CCTTCGGCACACTCAATGAA	GACCACATCCAACACGTGTC	121bp
Afi-trim2_1	CTAGCACTAAACCCAAGCCG	AACCCTAGAAGTGTCAGCCC	137bp
Afi-fbn2L_1	CCACGTGTTGTCAACCCATT	GAAAGTACCAGTTCCGCGAC	138bp
AfiCDS.id64819.tr39976	AACTACGCTTGTCTTGCACG	GCTGTATGCGTCGATGGTTT	113bp
AfiCDS.id4578.tr38894	GCGAGACCTGCAAGATAACC	GTAACGAGTCTGCCTGTTCG	114bp
Afi-egr	CCTCTCTCAAGTCGCACTGA	GTACCTGTCACGGCCATAGA	138bp
AfiCDS.id53027.tr45279	CTCGTAACGCTACTCTGCCT	AGAAACCACTGATGCGGAGA	113bp
Afi-trim2-2	ATGAAGCGGACCCTCTTGAA	CTGCGGTTTCTCTTGCGATT	118bp
Afi-dcst2-3	AATCATTTGGAGCGGCGATC	GTTTGTTGTGGCTCGGTCTT	118bp
Afi-dusp1	AGTCGATCGGCTACTGTCTG	CATGAAGGCGAGATTGGGTG	120bp
Afi-rreb1	GAGGATGAGCAGATACCGCT	GCTCTACACTGTTGCATCGG	124bp
Afi-mad	TCATCACGCCACACTACACT	TCTCTGTTCCCTTGCTAACTGT	117bp
AfiCDS.id43930.tr1339	CCCACACCACCCAAATGAAA	TCTGTGTTGTAACGGTGCTG	118bp
Afi-trim2	GACTGCGAGAAGAAAGAGCG	TCCCAACTCTTGCTCTCTGA	118bp
AfiCDS.id75617.tr19326	TCAGAGAGCGGAGGAGTAGT	TCTGTCGTATGTGGTTCCGT	146bp
AfiCDS.id5605.tr49815	AGCAACTCCGGCATAGGTAA	TGTCTGATCTCGTTGAGTGCT	116bp
AfiCDS.id4513.tr62663	TTGTTACGATGGAGAGCGGT	CATACCACCGCTAACATGGC	137bp
Afi-018426	GGGAAAGGAACAACAGCCAA	ATCTGGTCTCTCTGCCCAAA	121bp
Afi-colf_3	TGGCGAAGTATTCCTCCGAT	ATACCAACTCGATCCTCCGG	111bp
AfiCDS.id59305.tr68751	GTGACGCAGCTGAAAGTGAA	GGTGCAAGTGACAGAGTAGC	139bp
Afi-gldc	TCCAGATACAGAGGGCTCCA	CCTGGTGGTTGGATAAGGGT	120bp
Afi-mt14/mmpl7	CAAAGGGTTCAGCGTCGTC	CCATGGCGATCCCTATCCTT	119bp
Afi-sr/fu/igr	CTGGTGTACGATGTTCCGGA	CGGCAGTCTTCAGAGCAAAG	115bp
Afi-agrnL	CACCTGCAAACGTACCAACA	GCTCCTCCATCATCGCATTG	115bp
AfiCDS.id63133.tr10933	CTCGTGAAACAAGGAAGGGC	ACCCGGTGATGGATTGACTT	119bp
Afi-tcep1	TGTGCCACTATCCGTACCAG	TTGTTCTCCGCATCCAGTTG	136bp
Afi-msp130r6	GGACTGATGCGAAGAGAGGT	TCTAGCCGACCTAAACGAGC	112bp

Table B.9: Time-courses

Gene	0hpf	3hpf	6hpf	9hpf	12hpf	15hpf	18hpf	21hpf	24hpf	27hpf	30hpf	33hpf	36hpf	39hpf	42hpf
Afi-c-lectin	0	1	2	8	77	300	693	1853	2104	2459	4252	5586	5924	7192	8997
Afi-fgf4/5/6	5	6	14	6	21	6	3	19	10	7	7	14	1	0	0
Afi-fgf9/16/20	5	7	5	7	8	17	25	66	69	95	98	216	172	163	167
Afi-fgfR1	43	71	47	18	4	11	53	184	154	101	294	286	NA	NA	NA
Afi-fgfR2	0	0	1	0	1	2	10	45	78	76	79	187	227	157	175
Afi-p58a	2	2	2	0	0	2	0	10	1	5	9	1	NA	NA	NA
Afi-p58b	0	1	0	0	0	0	1	6	1	7	7	0	NA	NA	NA
Afi-rreb1	38	29	44	41	462	224	413	475	412	218	420	444	569	209	348
Afi-tr25409	25	0	4	5	4	1	11	323	172	255	595	474	811	847	951
Afi-tr4886	3	1	2	5	39	1	7	59	20	28	103	394	712	530	791
Afi-vegf3	41	57	49	43	27	36	89	236	418	484	617	915	704	521	578
Afi-vegfR	0	10	6	4	2	27	134	249	216	168	206	412	271	216	202

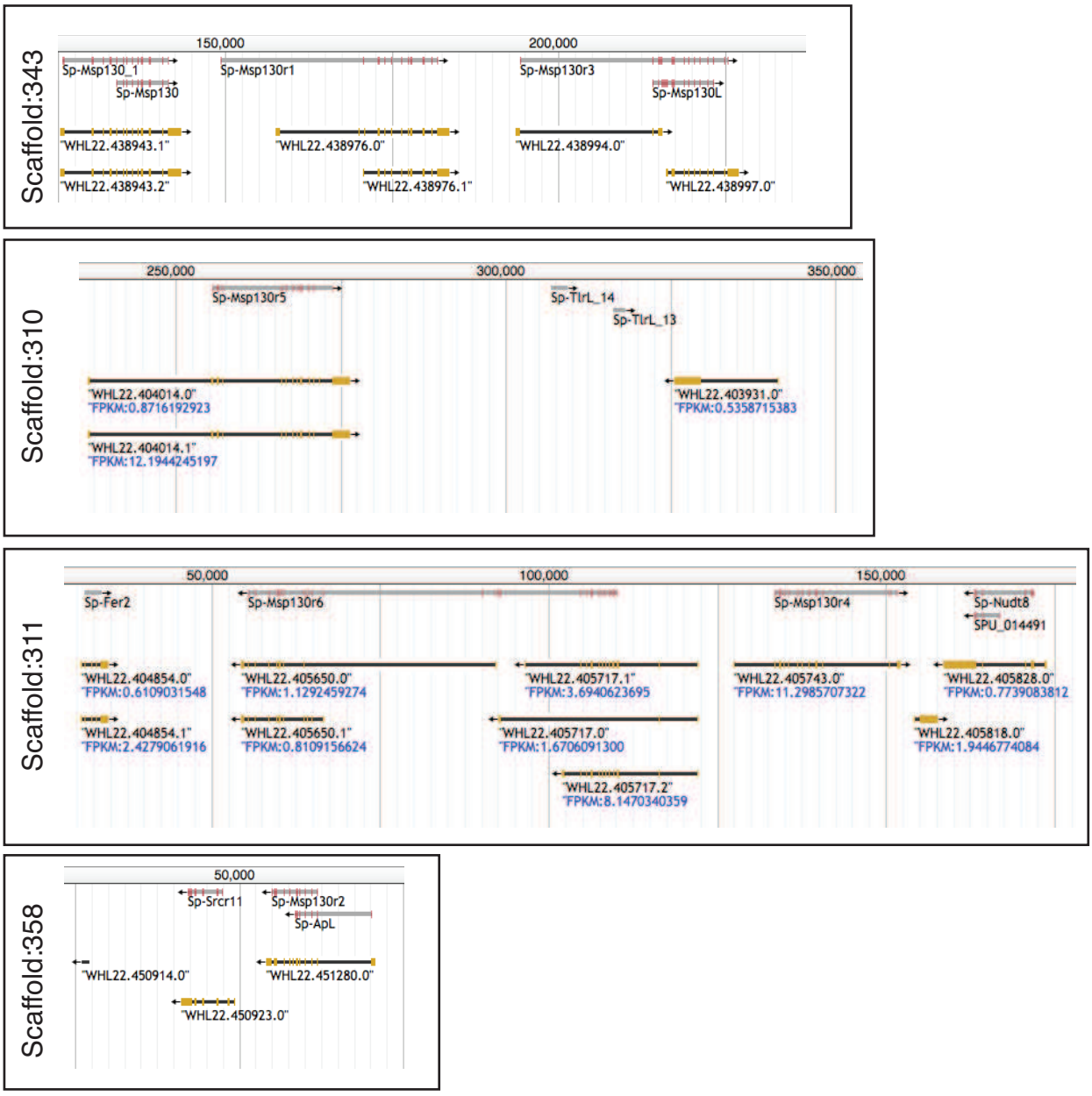

Figure B.1: **Sea urchin *msp130* genes on Scaffolds**.

Table B.10: Expression of genes used in part II

EC	Name	9hr	18hr	27hr	39hr	Fuzzy Cluster
Cluster-10558.1	*AfiCDS.id384.tr29965*	0	14	250	845	17
Cluster-11257.0	*Afi-tcep1*	772	356	481	604	15
Cluster-11727.4	*AfiCDS.id81632.tr60441*	6	7	544	1446	17
Cluster-1215.0	*Afi-trim2*	0	0	2	1	4
Cluster-12844.127	*AfiCDS.id48303.tr39358*	48	105	226	142	9
Cluster-12844.62	*AfiCDS.id84973.tr13659*	34	58	161	90	14
Cluster-13113.1	*Afi-soxD1*	48	3	58	20	27
Cluster-13125.0	*Afi-egr*	16	47	89	98	20
Cluster-13564.0	*AfiCDS.id63133.tr10933*	0	1	5	178	7
Cluster-1364.0	*Afi-trim2_1*	0	0	18	23	3
Cluster-13724.0	*Afi-rreb1*	3	167	128	44	11
Cluster-14335.0	*AfiCDS.id43930.tr1339*	5	7	5	9	16
Cluster-1517.1	*Afi-tr25409*	0	1	115	210	17
Cluster-15262.0	*Afi-009748*	23	5	24	27	3
Cluster-1541.0	*Afi-004896*	0	0	19	42	17
Cluster-15464.0	*AfiCDS.id4578.tr38894*	0	0	26	14	4
Cluster-15622.0	*Afi-tacr2L*	0	0	0	1	13
Cluster-15634.0	*AfiCDS.id75617.tr19326*	0	0	10	21	17
Cluster-16461.0	*Afi-mt6_mmpL*	94	2805	1712	3079	18
Cluster-16526.0	*Afi-a2m_1*	201	115	140	174	15
Cluster-1724.0	*Afi-018426*	0	35	18	11	23
Cluster-17333.2	*Afi-gldc*	471	44	58	53	1
Cluster-17570.0	*fn3/egff_1*	1	34	333	75	14
Cluster-17600.0	*AfiCDS.id58703.tr6207*	150	125	39	22	24
Cluster-17970.0	*Afi-e2f7*	758	1329	283	254	26
Cluster-18217.0	*AfiCDS.id41059.tr61404*	1	58	39	12	11
Cluster-18373.0	*Afi-tropmyh*	272	37	35	38	1
Cluster-20113.3	*Afi-0914236*	110	199	162	171	18
Cluster-20452.0	*Afi-caraX*	0	1	122	186	3
Cluster-21780.0	*Afi-αcoll*	29	26	2466	7638	17
Cluster-21880.0	*AfiCDS.id59305.tr68751*	0	0	7	27	17
Cluster-22670.0	*Afi-mad*	8	19	30	49	20
Cluster-22948.0	*Afi-tle1/groucho*	286	70	172	122	19
Cluster-23056.1	*Afi-tr4886*	0	3	108	230	17
Cluster-23512.1	*Afi-vegfR*	1	71	93	44	2
Cluster-24029.0	*AfiCDS.id5605.tr49815*	7	1	4	1	19
Cluster-24220.0	*Afi-dusp1*	82	37	55	50	19
Cluster-2493.0	*Afi-hypp_2281*	0	8	124	11	27
Cluster-25105.0	*Afi-colf_3*	0	1	3	8	17
Cluster-25122.0	*Afi-77kDamaps*	152	82	181	215	3
Cluster-2571.0	*Afi-trim2-2*	0	1	51	33	4
Cluster-25746.0	*AfiCDS.id44038.tr10735*	6	9	29	71	17
Cluster-25982.2	*Afi-egfiL_2*	1	1	0	2	6
Cluster-26614.0	*Afi-018662*	399	353	116	181	24
Cluster-27739.0	*Afi-agrnL*	0	0	9	1	27
Cluster-27881.0	*AfiCDS.id75849.tr3754*	0	0	375	1410	17
Cluster-28510.0	*Afi-sr/fu/igr*	0	3	4	7	20
Cluster-28643.1	*AfiCDS.id10236.tr3203*	105	2839	1710	3157	18
Cluster-29925.0	*Afi-erg*	10	363	218	168	11
Cluster-30632.0	*Afi-alx/arx*	0	2	0	2	6
Cluster-30786.1	*Afi-fbn2L_1*	1	0	18	189	7
Cluster-30937.0	*AfiCDS.id64819.tr39976*	0	1	26	100	17
Cluster-31209.0	*Afi-ttrspn_19*	0	75	179	106	9
Cluster-3261.0	*Afi-mt14/mmpl7*	0	0	2	6	17
Cluster-3715.0	*Afi-p58-b*	0	12	235	206	3
Cluster-3715.1	*Afi-p58-a*	0	10	157	120	4
Cluster-4270.0	*AfiCDS.id53027.tr45279*	0	2	23	20	3
Cluster-4513.0	*AfiCDS.id52181.tr20375*	0	0	1	0	14
Cluster-4641.0	*Afi-fn3/igf_29*	0	4	38	56	3
Cluster-5507.0	*AfiCDS.id4513.tr62663*	0	0	3	19	7
Cluster-5808.0	*Afi-sept4*	1	46	93	63	9
Cluster-5917.0	*Afi-spcat3l*	3	319	308	402	10
Cluster-672.0	*Afi-dcst2-3*	0	0	39	96	17
Cluster-7020.0	*Afi-tr4886*	0	3	84	188	17
Cluster-720.0	*Afi-kirrelL*	0	0	24	78	17
Cluster-7256.0	*Afi-slc4a10*	5	54	1272	2295	20
Cluster-7482.0	*Afi-msp130r6*	2	8	276	1031	17
Cluster-7531.0	*Afi-cebpa*	28	176	246	275	10
Cluster-7997.0	*Afi-vegf2*	0	1	1	10	7

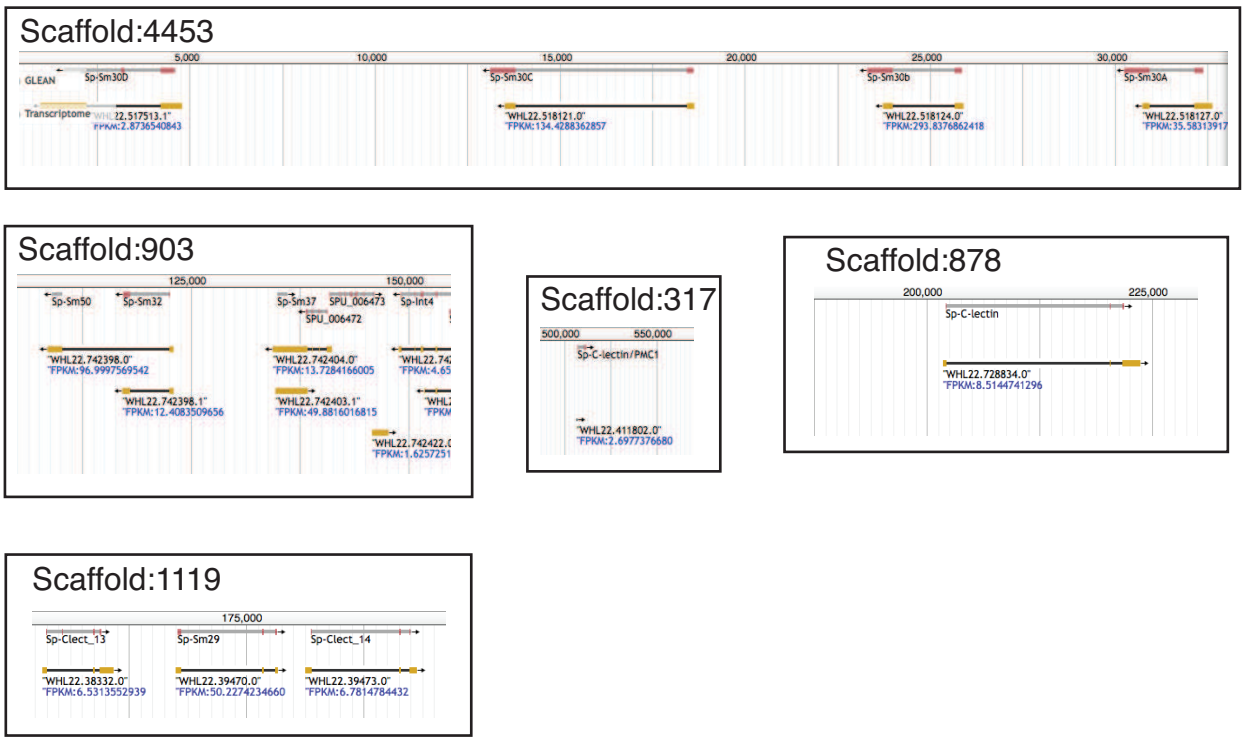

Figure B.2: **Sea urchin spicule matrix genes on scaffolds**.

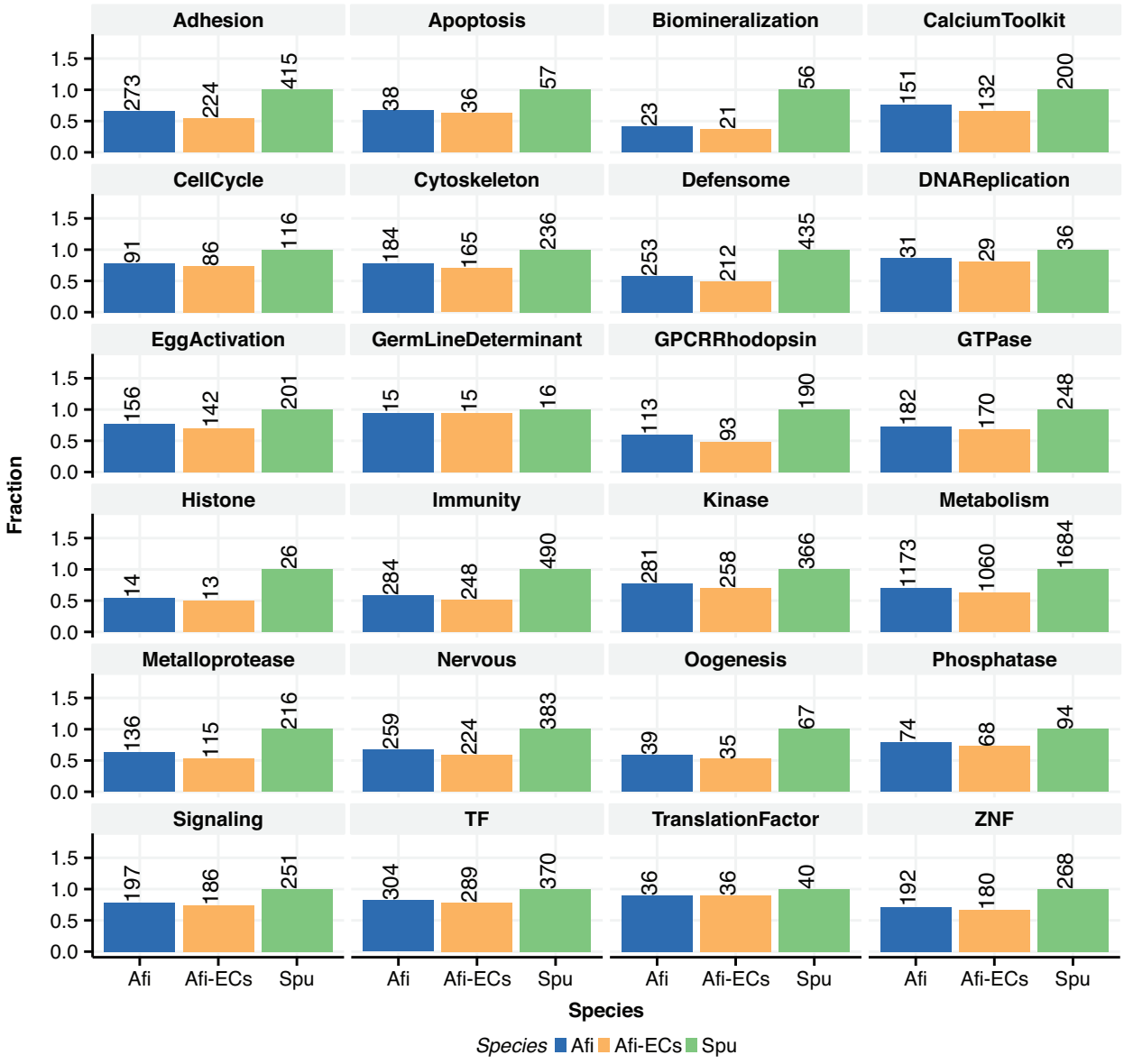

Figure B.3: **Gene ontology loss after grouping into ECs**.

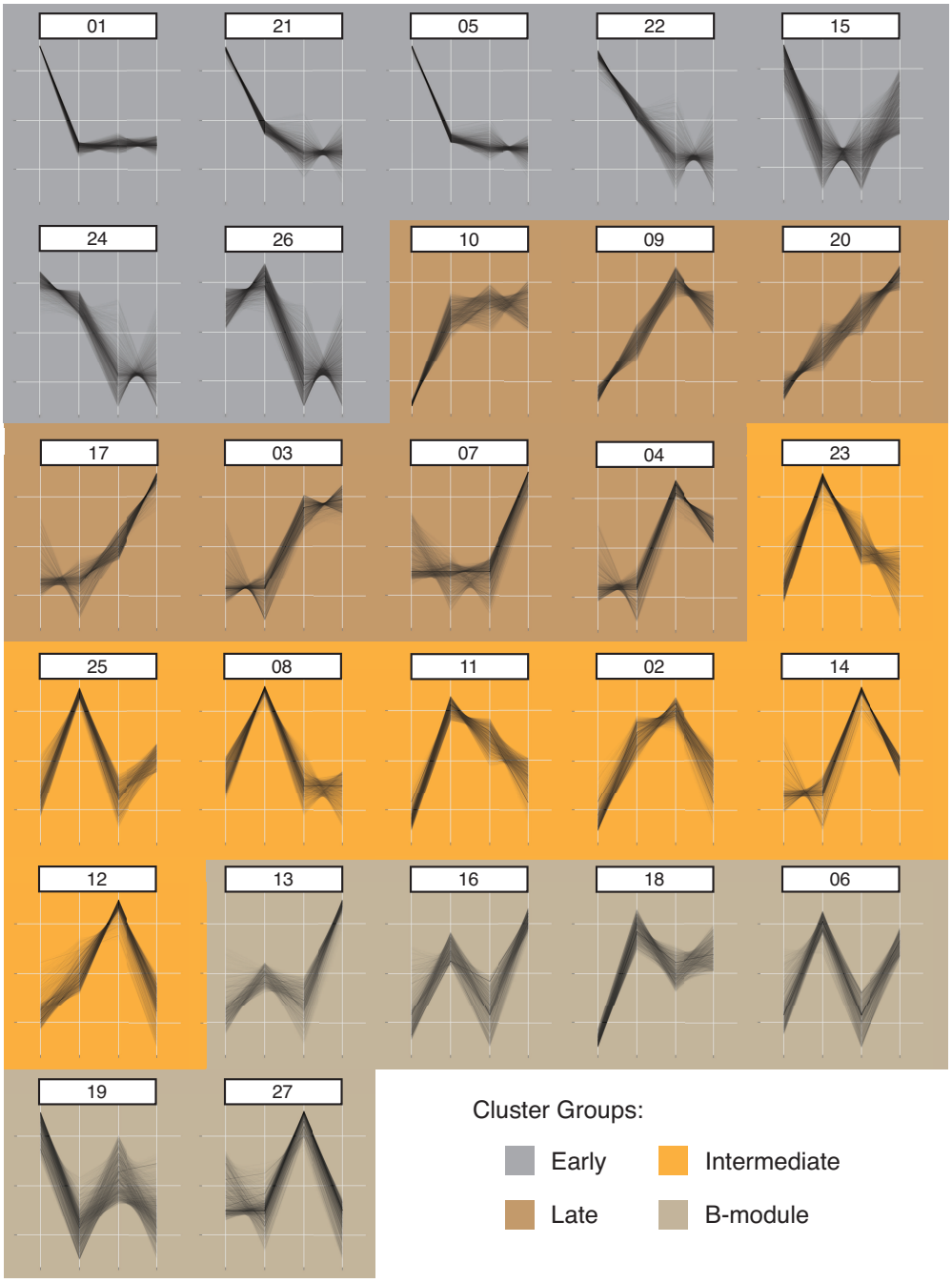

Figure B.4: **Line plots for fuzzy clusters**.

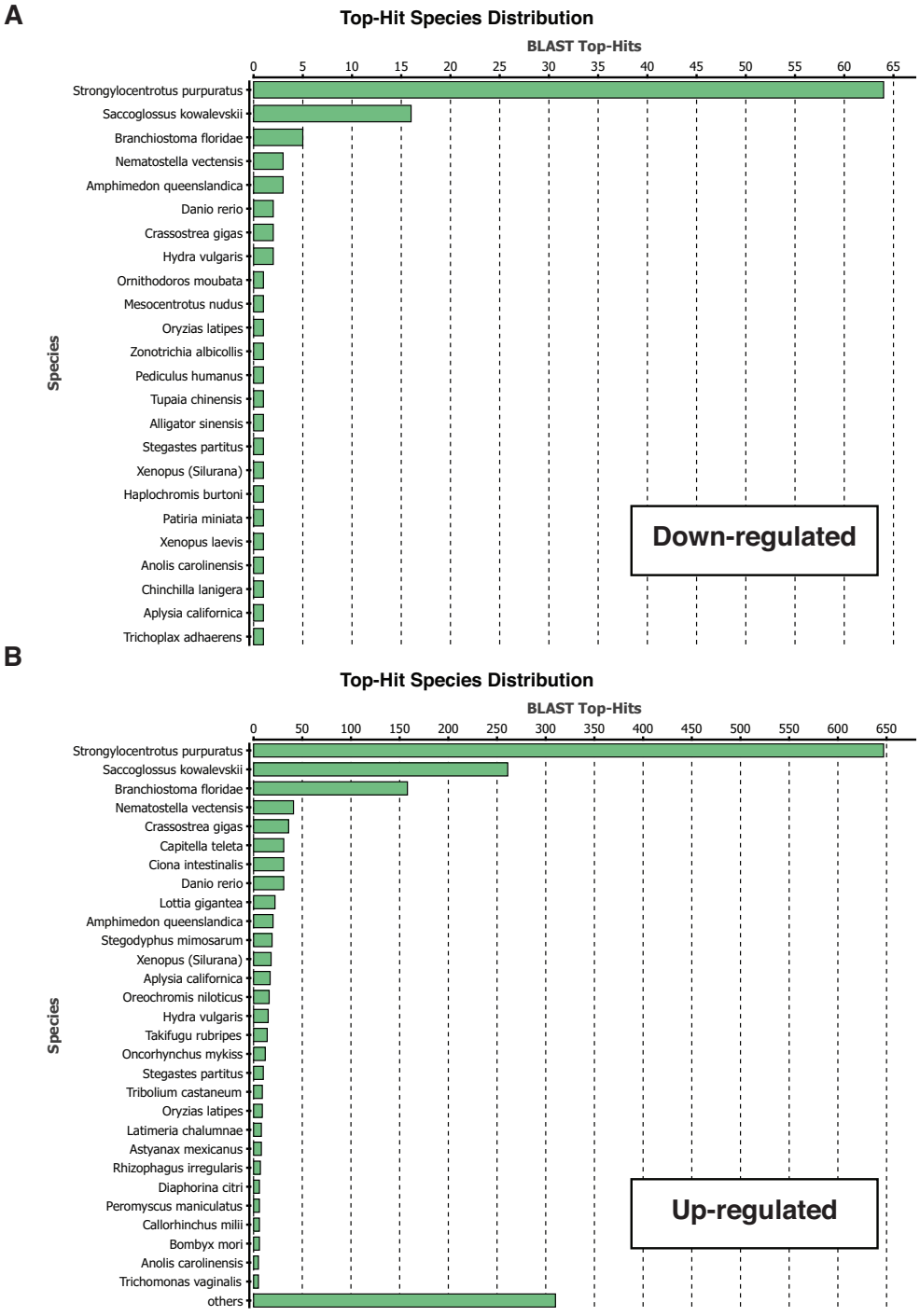

Figure B.5: **Blast2GO top hit distributions for differentially expressed samples**.

Msp130 alingment

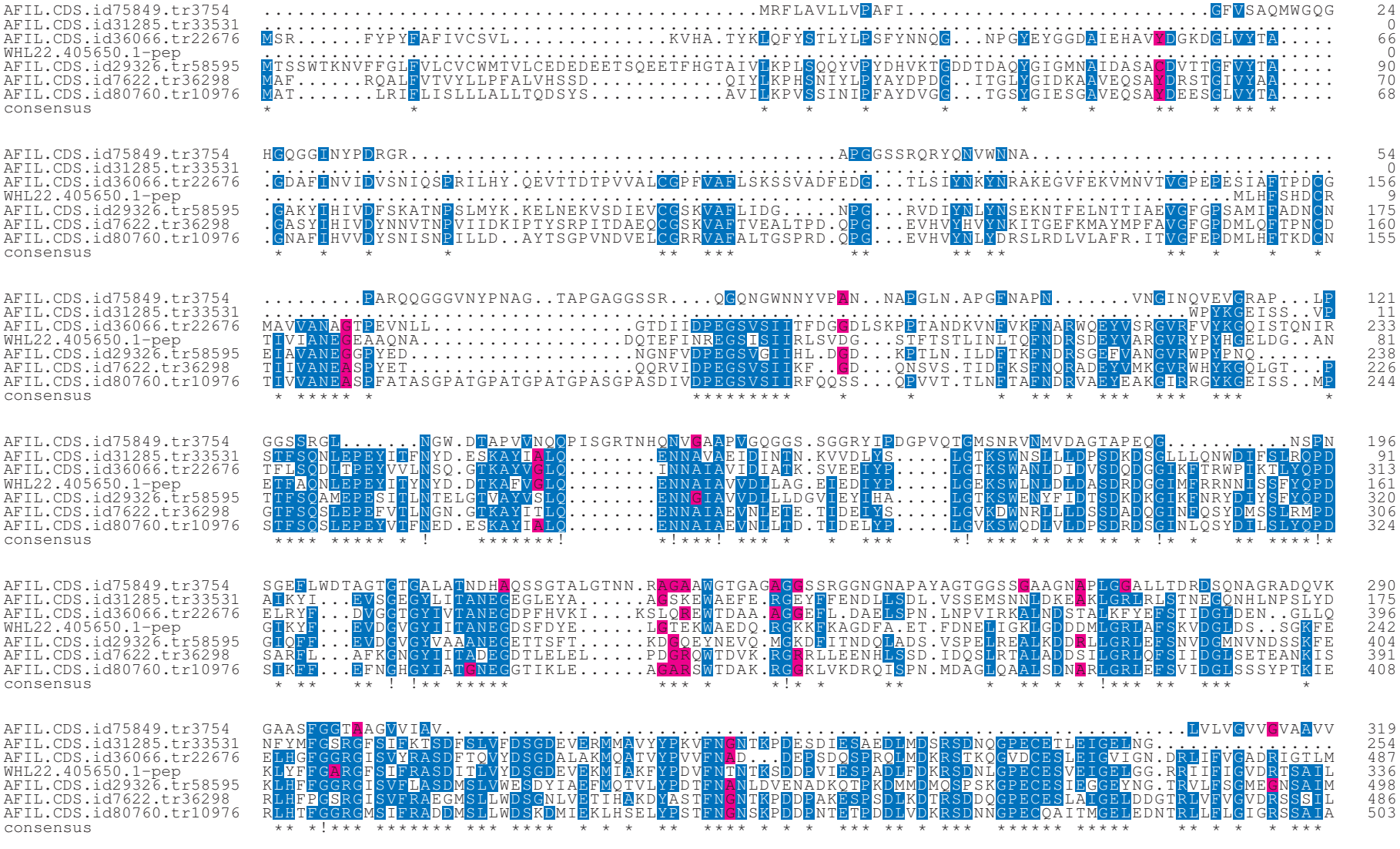

```
AFIL.CDS.id75849.tr3754   LVKQR.....................................................................................   324
AFIL.CDS.id31285.tr33531  .....................................................................................   254
AFIL.CDS.id36066.tr22676  IFRLD...KNSYTPK..LESIYRNGSTNRPISDLFKDQDLNDAAPEALTFIPCKTNSDQSFPILMVAGTESGTLSFYRIVNEG.....   565
WHL22.405650.1-pep        VYSLE...SGEIV..PTFETVYRAGGRNDTFQNLLDDRNLGDLDPEDLKFIPASV.SVTGVPMLMVTSAVSGTISLYEVYDD.....   412
AFIL.CDS.id29326.tr58595  VFSFA...QGSVEPK..FESIYRHGGIDKPFQKLLDEQNLGDLNPEELKFIPAEY.SSTGGPLLLVTGTFSGTLAMYEITEEYWEAPTDLPPHIF   587
AFIL.CDS.id7622.tr36298   IFSVD...EVGAEPRLEFQSILRDGGVDDTFNVLLENRNLGNLDPEDLRFIPAAF.SPTNKPLLLVTSAVSGTLAMYEVVKD.....   564
AFIL.CDS.id80760.tr10976  VFRIEATFESGHEPVLEFESLYRAGGTNQTFSTLLENENIGNLDPEDLRFIPAAK.SPTGKPLLLVTGTTSGNLVMYEVIDMS.....PQ..   587
consensus                  *           *   *** ** **    *  **   *** * ** * ****   * *  * * **   ****  **

AFIL.CDS.id75849.tr3754   .......ASRM.............MVQQV......   333
AFIL.CDS.id31285.tr33531  ..............................   254
AFIL.CDS.id36066.tr22676  .SGAGCRAPMIHISIVVALL..VLVKCIV....X   592
WHL22.405650.1-pep        ..............................   412
AFIL.CDS.id29326.tr58595  ELGKTPFEMYIHVX..................   601
AFIL.CDS.id7622.tr36298   .TGPGSGCESIHTWNVVILSMWL..MWLIIARQX   595
AFIL.CDS.id80760.tr10976  .TGDNGFCSRISSS..ILLTFFLLVGQMILSR.X   617
consensus                   *    *  *
```

LIST OF REFERENCES

Ashrifia Adomako-Ankomah and Charles a Ettensohn. Growth factor-mediated mesodermal cell guidance and skeletogenesis during sea urchin gastrulation. *Development (Cambridge, England)*, 140(September):4214–25, 2013.

Bruce Alberts, Alexander Johnson, Julian Lewis, Martin Raff, Keith Roberts, and Peter Walter. *Molecular Biology of the Cell*. 2002.

Uri Alon. *An Introduction to Systems Biology: Design Principles of Biological Circuits*, volume 10. 2007.

a. M. Altenhoff, N. Kunca, N. Glover, C.-M. Train, a. Sueki, I. Pili ota, K. Gori, B. Tomiczek, S. Muller, H. Redestig, G. H. Gonnet, and C. Dessimoz. The OMA orthology database in 2015: function predictions, better plant support, synteny view and other improvements. *Nucleic Acids Research*, 43(D1):D240–D249, 2014.

Gabriele Amore and Eric H. Davidson. cis-Regulatory control of cyclophilin, a member of the ETS-DRI skeletogenic gene battery in the sea urchin embryo. *Developmental Biology*, 293: 555–564, 2006.

Gabriele Amore, Robert G Yavrouian, Kevin J Peterson, Andrew Ransick, David R McClay, and Eric H Davidson. Spdeadringer, a sea urchin embryo gene required separately in skeletogenic and oral ectoderm gene regulatory networks. *Developmental Biology*, 261(1):55–81, 2003.

Carmen Andrikou, Edmondo Iovene, Francesca Rizzo, Paola Oliveri, and Maria Ina Arnone. Myogenesis in the sea urchin embryo: the molecular fingerprint of the myoblast precursors. *EvoDevo*, 4(1):33, 2013.

Lynne M Angerer and Robert C Angerer. Patterning the sea urchin embryo: gene regulatory networks, signaling pathways, and cellular interactions. *Current topics in developmental biology*, 53:159–198, 2003.

J a Anstrom, J E Chin, D S Leaf, a L Parks, and R a Raff. Localization and expression of msp130, a primary mesenchyme lineage-specific cell surface protein in the sea urchin embryo. *Development (Cambridge, England)*, 101(2):255–265, 1987.

M I Arnone, L D Bogarad, a Collazo, C V Kirchhamer, R a Cameron, J P Rast, a Gregorians, and E H Davidson. Green Fluorescent Protein in the sea urchin: new experimental approaches

to transcriptional regulatory analysis in embryos and larvae. *Development*, 124(22):4649–4659, 1997.

Laurent Arnoult, Kathy F Y Su, Diogo Manoel, Caroline Minervino, Justine Magriña, Nicolas Gompel, and Benjamin Prud'homme. Emergence and diversification of fly pigmentation through evolution of a gene regulatory module. *Science (New York, N.Y.)*, 339(6126):1423–6, 2013.

Albert-Laszlo Barabasi and Reka Albert. Emergence of scaling in random networks. *Science*, 286(October):11, 1999.

Albert-László Barabási and Zoltán N Oltvai. Network biology: understanding the cell's functional organization. *Nature reviews. Genetics*, 5(2):101–13, February 2004.

Julius C. Barsi, Qiang Tu, and Eric H. Davidson. General approach for in vivo recovery of cell type-specific effector gene sets. *Genome Research*, 24(5):860–868, 2014.

Inanç Birol, Shaun D. Jackman, Cydney B. Nielsen, Jenny Q. Qian, Richard Varhol, Greg Stazyk, Ryan D. Morin, Yongjun Zhao, Martin Hirst, Jacqueline E. Schein, Doug E. Horsman, Joseph M. Connors, Randy D. Gascoyne, Marco A. Marra, and Steven J M Jones. De novo transcriptome assembly with ABySS. *Bioinformatics*, 25(21):2872–2877, 2009.

L D Bogarad, M I Arnone, C Chang, and E H Davidson. Interference with gene regulation in living sea urchin embryos: transcription factor knock out (TKO), a genetically controlled vector for blockade of specific transcription factors. *Proceedings of the National Academy of Sciences of the United States of America*, 95(25):14827–14832, 1998.

Anthony M. Bolger, Marc Lohse, and Bjoern Usadel. Trimmomatic: A flexible trimmer for Illumina sequence data. *Bioinformatics*, 30:2114–2120, 2014.

Hamid Bolouri and Eric H Davidson. Modeling DNA sequence-based cis-regulatory gene networks. *Developmental biology*, 246(1):2–13, 2002.

Hamid Bolouri and Eric H Davidson. Transcriptional regulatory cascades in development: initial rates, not steady state, determine network kinetics. *Proceedings of the National Academy of Sciences of the United States of America*, 100(16):9371–9376, 2003.

David J Bottjer, Eric H Davidson, Kevin J Peterson, and R Andrew Cameron. Paleogenomics of echinoderms. *Science*, 314:956–960, 2006.

T Bowmer. Reproduction in Amphiura filiformis (Echinodermata: Ophiuroidea): Seasonality in Gonad Development. *Marine Biology*, 290:281–290, 1982.

Michael J Boyle, Emi Yamaguchi, and Elaine C Seaver. Molecular conservation of metazoan gut formation: evidence from expression of endomesoderm genes in Capitella teleta (Annelida). *EvoDevo*, 5(1):39, 2014.

R.J. J Rj Britten and E.H. H Eh Davidson. Gene regulation for higher cells: a theory. *Science*, 165(3891):349–357, 1969.

C. Titus Brown, Adina Howe, Qingpeng Zhang, Alexis B. Pyrkosz, and Timothy H. Brom. A Reference-Free Algorithm for Computational Normalization of Shotgun Sequencing Data. *arXiv*, 1203.4802:1–18, 2012.

C Titus Brown, Camille Scott, Michael R Crusoe, Leigh Sheneman, Josh Rosenthal, and Adina Howe. khmer-protocols 0.8.4 documentation., 2013.

John B. Buchanan. A Comparative Study of Some Features of the Biology of Amphiura Filiformis and Amphiura Chiajei [Ophiuroidea] Considered in Relation to their Distribution. *Journal of the Marine Biological Association of the United Kingdom*, 44(03):565–576, 1964.

M Burrows and DJ Wheeler. A block-sorting lossless data compression algorithm. *Algorithm, Data Compression*, (124):18, 1994.

Cristina Calestani, Jonathan P Rast, and Eric H Davidson. Isolation of pigment cell specific genes in the sea urchin embryo by differential macroarray screening. *Development (Cambridge, England)*, 130(19):4587–4596, 2003.

C. B. Cameron and C. D. Bishop. Biomineral ultrastructure, elemental constitution and genomic analysis of biomineralization-related proteins in hemichordates. *Proceedings of the Royal Society B: Biological Sciences*, 279(1740):3041–3048, 2012.

R. Andrew Cameron, Paola Oliveri, Jane Wyllie, and Eric H. Davidson. cis-Regulatory activity of randomly chosen genomic fragments from the sea urchin. *Gene Expression Patterns*, 4(2): 205–213, 2004.

R. Andrew Cameron, Manoj Samanta, Autumn Yuan, Dong He, and Eric Davidson. SpBase: The sea urchin genome database and web site. *Nucleic Acids Research*, 37(SUPPL. 1):750–754, 2009.

Johanna T Cannon, Kevin M Kocot, Damien S Waits, David a Weese, Billie J Swalla, Scott R Santos, and Kenneth M Halanych. Report Phylogenomic Resolution of the Hemichordate and Echinoderm Clade. *Current Biology*, 24(23):1–6, 2014.

Peter Carlsson and Margit Mahlapuu. Forkhead transcription factors: key players in development and metabolism. *Developmental biology*, 250(1):1–23, 2002.

Sean B. Carroll. Evo-Devo and an Expanding Evolutionary Synthesis: A Genetic Theory of Morphological Evolution. *Cell*, 134(1):25–36, 2008.

Zheng Chang, Guojun Li, Juntao Liu, Yu Zhang, Cody Ashby, Deli Liu, Carole L Cramer, and Xiuzhen Huang. Bridger: a new framework for de novo transcriptome assembly using RNA-seq data. *Genome Biology*, 16(1):1–10, 2015.

Xiao Chen, John R Bracht, Aaron David Goldman, Egor Dolzhenko, Derek M Clay, Estienne C Swart, David H Perlman, Thomas G Doak, Andrew Stuart, Chris T Amemiya, Robert P Sebra, and Laura F Landweber. The Architecture of a Scrambled Genome Reveals Massive Levels of Genomic Rearrangement during Development. *Cell*, 158(5):1187–1198, 2014.

Chin Kai Chuang, Athula H. Wikramanayake, Chai An Mao, Xiaotao Li, and William H. Klein. Transient appearance of Strongylocentrotus purpuratus Otx in micromere nuclei: Cytoplasmic retention of SpOtx possibly mediated through an α- actinin interaction. *Developmental Genetics*, 19(3):231–237, 1996.

Gavin Conant and Andreas Wagner. Convergent evolution of gene circuits. *Nature genetics*, 34 (3):263–264, 2003.

Ana Conesa and Stefan Götz. Blast2GO: A comprehensive suite for functional analysis in plant genomics. *International Journal of Plant Genomics*, 2008, 2008.

Richard R Copley. The EH1 motif in metazoan transcription factors. *BMC genomics*, 6:169, 2005.

Caterina Costa, Konstantinos Karakostis, Francesca Zito, and Valeria Matranga. Phylogenetic analysis and expression patterns of p16 and p19 in Paracentrotus lividus embryos. *Development Genes and Evolution*, 222:245–251, 2012.

J Croce. Dynamics of Delta/Notch signaling on endomesoderm segregation in the sea urchin embryo. *Development*, 137:83–91, 2010.

J Croce, G Lhomond, J C Lozano, and C Gache. ske-T, a T-box gene expressed in the skeletogenic mesenchyme lineage of the sea urchin embryo. *Mechanisms of development*, 107(1-2): 159–162, 2001.

Anton Crombach and Paulien Hogeweg. Evolution of evolvability in gene regulatory networks. *PLoS Computational Biology*, 4(7), 2008.

Anna Czarkwiani, David V Dylus, and Paola Oliveri. Expression of skeletogenic genes during arm regeneration in the brittle star Amphiura filiformis. *Gene Expression Patterns*, 13:464–472, 2013.

Sagar Damle and Eric H. Davidson. Precise cis-regulatory control of spatial and temporal expression of the alx-1 gene in the skeletogenic lineage of s. purpuratus. *Developmental Biology*, 357:505–517, 2011.

Aaron E Darling, Lucas Carey, and Wu-chun Feng. The Design, Implementation, and Evaluation of mpiBLAST. *Proceedings of ClusterWorld*, 2003:13–15, 2003.

Colin J. Davidson, Rabindra Tirouvanziam, Leonard a. Herzenberg, and Joseph S. Lipsick. Functional evolution of the vertebrate Myb gene family: B-Myb, but neither A-Myb nor c-Myb, complements Drosophila Myb in hemocytes. *Genetics*, 169(1):215–229, 2005.

Colin J Davidson, Erin E Guthrie, and Joseph S Lipsick. Duplication and maintenance of the Myb genes of vertebrate animals. *Biology open*, 2(2):101–10, 2013.

E H Davidson. *The regulatory genome: gene regulatory networks in development and evolution*, volume 310. 2006.

Eric H Davidson. Emerging properties of animal gene regulatory networks. *Nature*, 468:911–920, 2010.

Eric H. Davidson. Evolutionary bioscience as regulatory systems biology. *Developmental Biology*, 357(1):35–40, 2011.

Eric H. Davidson and Douglas H. Erwin. Gene regulatory networks and the evolution of animal body plans. *Science*, 311:796–800, 2006.

Nadia M Davidson and Alicia Oshlack. Corset: enabling differential gene expression analysis for de novo assembled transcriptomes. *Genome Biology*, 15:410, 2014.

Bernard M. Degnan, Michel Vervoort, Claire Larroux, and Gemma S. Richards. Early evolution of metazoan transcription factors. *Current Opinion in Genetics and Development*, 19(6):591–599, 2009.

Cristian Del Fabbro, Simone Scalabrin, Michele Morgante, and Federico M. Giorgi. An extensive evaluation of read trimming effects on illumina NGS data analysis. *PLoS ONE*, 8(12):1–13, 2013.

Jeffery P Demuth, Tijl De Bie, Jason E Stajich, Nello Cristianini, and Matthew W Hahn. The evolution of mammalian gene families. *PloS one*, 1(1):e85, 2006.

Patrik D'haeseleer. What are DNA sequence motifs? *Nature biotechnology*, 24(4):423–425, 2006.

Véronique Duboc and Thierry Lepage. A conserved role for the nodal signaling pathway in the establishment of dorso-ventral and left-right axes in deuterostomes. *Journal of Experimental Zoology Part B: Molecular and Developmental Evolution*, 310(1):41–53, 2008.

Louise Duloquin, Guy Lhomond, and Christian Gache. Localized VEGF signaling from ectoderm to mesenchyme cells controls morphogenesis of the sea urchin embryo skeleton. *Development*, 134:2293–2302, 2007.

S. Dupont, O. Ortega-Martínez, and M. Thorndyke. Impact of near-future ocean acidification on echinoderms. *Ecotoxicology*, 19:449–462, 2010.

Sam Dupont, William Thorndyke, Michael C. Thorndyke, and Robert D. Burke. Neural development of the brittlestar Amphiura filiformis. *Development Genes and Evolution*, 219(3):159–166, 2009.

Robert C. Edgar. Search and clustering orders of magnitude faster than BLAST. *Bioinformatics*, 26(19):2460–2461, 2010.

Eli Eisenberg and Erez Y Levanon. Preferential attachment in the protein network evolution. *Physical review letters*, 91(13):138701, 2003.

Maurice R. Elphick, Dean C. Semmens, Liisa M. Blowes, Judith Levine, Christopher J. Lowe, Maria I. Arnone, and Melody S. Clark. Reconstructing SALMFamide Neuropeptide Precursor Evolution in the Phylum Echinodermata: Ophiuroid and Crinoid Sequence Data Provide New Insights. *Frontiers in Endocrinology*, 6(February):1–10, 2015.

D. H. Erwin, M. Laflamme, S. M. Tweedt, E. a. Sperling, D. Pisani, and K. J. Peterson. The Cambrian Conundrum: Early Divergence and Later Ecological Success in the Early History of Animals. *Science*, 334(6059):1091–1097, 2011.

Douglas H Erwin and Eric H Davidson. The last common bilaterian ancestor. *Development (Cambridge, England)*, 129(13):3021–3032, 2002.

Douglas H Erwin and Eric H Davidson. The evolution of hierarchical gene regulatory networks. *Nature Reviews Genetics*, 10:141–148, 2009.

Charles a Ettensohn. Lessons from a gene regulatory network: echinoderm skeletogenesis provides insights into evolution, plasticity and morphogenesis. *Development (Cambridge, England)*, 136(1):11–21, 2009.

Charles A Ettensohn, Michele R Illies, Paola Oliveri, and Deborah L De Jong. Alx1, a member of the Cart1/Alx3/Alx4 subfamily of Paired-class homeodomain proteins, is an essential component of the gene network controlling skeletogenic fate specification in the sea urchin embryo. *Development*, 130(13):2917–2928, 2003.

Brent Ewing and Phil Green. Base-calling of automated sequencer traces using phred. II. Error probabilities. *Genome Research*, 8(3):186–194, 1998.

Emmanuel Faure, Isabelle S Peter, and Eric H Davidson. A new software package for predictive gene regulatory network modeling and redesign. *Journal of computational biology : a journal of computational molecular cell biology*, 20(6):419–23, 2013.

David E. Featherstone and Kendal Broadie. Wrestling with pleiotropy: Genomic and topological analysis of the yeast gene expression network. *BioEssays*, 24(3):267–274, 2002.

J. Felsenstein. Cases in which Parsimony or Compatibility Methods will be Positively Misleading. *Systematic Biology*, 27(4):401–410, 1978.

Jianxing Feng, Clifford A. Meyer, Qian Wang, Jun S. Liu, X. Shirley Liu, and Yong Zhang. GFOLD: A generalized fold change for ranking differentially expressed genes from RNA-seq data. *Bioinformatics*, 28(21):2782–2788, 2012.

Paolo Ferragina and Giovanni Manzini. An experimental study of a compressed index. *Information Sciences*, 135(1-2):13–28, 2001.

Limin Fu, Beifang Niu, Zhengwei Zhu, Sitao Wu, and Weizhong Li. CD-HIT: Accelerated for clustering the next-generation sequencing data. *Bioinformatics*, 28(23):3150–3152, 2012.

Takuya Fuchikami, Keiko Mitsunaga-Nakatsubo, Shonan Amemiya, Toshiya Hosomi, Takashi Watanabe, Daisuke Kurokawa, Miho Kataoka, Yoshito Harada, Nori Satoh, Shinichiro Kusunoki, Kazuko Takata, Taishin Shimotori, Takashi Yamamoto, Naoaki Sakamoto, Hiraku Shimada, and Koji Akasaka. T-brain homologue (HpTb) is involved in the archenteron induction signals of micromere descendant cells in the sea urchin embryo. *Development (Cambridge, England)*, 129 (22):5205–5216, 2002.

Matthias E Futschik and Bronwyn Carlisle. Noise-robust soft clustering of gene expression time-course data. *Journal of bioinformatics and computational biology*, 3:965–988, 2005.

Ron Galant and Sean B Carroll. Evolution of a transcriptional repression domain in an insect Hox protein. *Nature*, 415(6874):910–913, 2002.

Brigitte Galliot, Colomban De Vargas, and David Miller. Evolution of homeobox genes: Q 50 Paired-like genes founded the Paired class. *Development Genes and Evolution*, 209(3):186–197, 1999.

AustenR.D. Ganley, Takehiko Kobayashi, and Peter Little. Phylogenetic Footprinting to Find Functional DNA Elements. volume 395 of *Methods in Molecular Biology*, pages 367–379. Humana Press, 2008.

B Ganter and J S Lipsick. Myb and oncogenesis. *Advances in cancer research*, 76:21–60, 1999.

Feng Gao and Eric H Davidson. Transfer of a large gene regulatory apparatus to a new developmental address in echinoid evolution. *Proceedings of the National Academy of Sciences of the United States of America*, 105(16):6091–6096, 2008.

Manuel Garber, Manfred G Grabherr, Mitchell Guttman, and Cole Trapnell. Computational methods for transcriptome annotation and quantification using RNA-seq. *Nature methods*, 8(6):469–477, 2011.

David A. Garfield, Daniel E. Runcie, Courtney C. Babbitt, Ralph Haygood, William J. Nielsen, and Gregory A. Wray. The Impact of Gene Expression Variation on the Robustness and Evolvability of a Developmental Gene Regulatory Network. *PLoS Biology*, 11(10):e1001696, 2013.

Mark B. Gerstein, Can Bruce, Joel S. Rozowsky, Deyou Zheng, Jiang Du, Jan O. Korbel, Olof Emanuelsson, Zhengdong D. Zhang, Sherman Weissman, and Michael Snyder. What is a gene, post-ENCODE? History and updated definition. *Genome Research*, 17(6):669–681, 2007.

Manfred G Grabherr, Brian J Haas, Moran Yassour, Joshua Z Levin, Dawn a Thompson, Ido Amit, Xian Adiconis, Lin Fan, Raktima Raychowdhury, Qiandong Zeng, Zehua Chen, Evan Mauceli, Nir Hacohen, Andreas Gnirke, Nicholas Rhind, Federica di Palma, Bruce W Birren, Chad Nusbaum, Kerstin Lindblad-Toh, Nir Friedman, and Aviv Regev. Full-length transcriptome assembly from RNA-Seq data without a reference genome. *Nature biotechnology*, 29(7):644–652, 2011.

J K Grenier and S B Carroll. Functional evolution of the Ultrabithorax protein. *Proceedings of the National Academy of Sciences of the United States of America*, 97(2):704–709, 2000.

Brian J Haas, Alexie Papanicolaou, Moran Yassour, Manfred Grabherr, Philip D Blood, Joshua Bowden, Matthew Brian Couger, David Eccles, Bo Li, Matthias Lieber, Matthew D Macmanes, Michael Ott, Joshua Orvis, Nathalie Pochet, Francesco Strozzi, Nathan Weeks, Rick Westerman, Thomas William, Colin N Dewey, Robert Henschel, Richard D Leduc, Nir Friedman, and Aviv Regev. De novo transcript sequence reconstruction from RNA-seq using the Trinity platform for reference generation and analysis. *Nature protocols*, 8(8):1494–512, 2013.

Veronica F Hinman and Alys M Cheatle Jarvela. Developmental gene regulatory network evolution: insights from comparative studies in echinoderms. *Genesis (New York, N.Y. : 2000)*, 52(3): 193–207, March 2014.

Veronica F Hinman, Albert T Nguyen, R Andrew Cameron, and Eric H Davidson. Developmental gene regulatory network architecture across 500 million years of echinoderm evolution. *Proceedings of the National Academy of Sciences of the United States of America*, 100(23): 13356–13361, 2003.

Veronica F. Hinman, Albert Nguyen, and Eric H. Davidson. Caught in the evolutionary act: Precise cis-regulatory basis of difference in the organization of gene networks of sea stars and sea urchins. *Developmental Biology*, 312:584–595, 2007.

Veronica F. Hinman, Kristen a. Yankura, and Brenna S. McCauley. Evolution of gene regulatory network architectures: Examples of subcircuit conservation and plasticity between classes of echinoderms. *Biochimica et Biophysica Acta - Gene Regulatory Mechanisms*, 1789(4):326–332, 2009.

Taiji Hirokawa, Miéko Komatsu, and Yoko Nakajima. Development of the nervous system in the brittle star Amphipholis kochii. *Development Genes and Evolution*, 218(1):15–21, 2007.

P G Hodor and C a Ettensohn. The dynamics and regulation of mesenchymal cell fusion in the sea urchin embryo. *Developmental biology*, 199(1):111–124, 1998.

Nils Homer, Barry Merriman, and Stanley F. Nelson. BFAST: An alignment tool for large scale genome resequencing. *PLoS ONE*, 4(11), 2009.

S Hörstadius. *Experimental embryology of echinoderms*. Clarendon Press, 1973.

Meredith Howard-Ashby, Stefan C. Materna, C. Titus Brown, Qiang Tu, Paola Oliveri, R. Andrew Cameron, and Eric H. Davidson. High regulatory gene use in sea urchin embryogenesis: Implications for bilaterian development and evolution. *Developmental Biology*, 300:27–34, 2006.

L H Hyman. *The Invertebrates: Echinodermata*. 1955.

Michele R. Illies, Margaret T. Peeler, Anna M. Dechtiaruk, and Charles a. Ettensohn. Identification and developmental expression of new biomineralization proteins in the sea urchin Strongylocentrotus purpuratus. *Development Genes and Evolution*, 212(9):419–431, 2002.

Sorin Istrail and Eric H Davidson. Logic functions of the genomic cis-regulatory code. *Proceedings of the National Academy of Sciences of the United States of America*, 102(14):4954–4959, 2005.

Daniel Janies. Phylogenetic relationships of extant echinoderm classes. *Canadian Journal of Zoology*, 79(7):1232–1250, 2001.

Daniel a. Janies, Janet R. Voight, and Marymegan Daly. Echinoderm phylogeny including xyloplax, a progenetic asteroid. *Systematic Biology*, 60(4):420–438, 2011.

Alys M Cheatle Jarvela and Veronica F Hinman. Evolution of transcription factor function as a mechanism for changing metazoan developmental gene regulatory networks. *EvoDevo*, 6(1): 1–11, 2015.

H Jeong, B Tombor, R Albert, Z N Oltvai, and a L Barabási. The large-scale organization of metabolic networks. *Nature*, 407(6804):651–654, 2000.

Hui Jiang and Wing Hung Wong. SeqMap: Mapping massive amount of oligonucleotides to the genome. *Bioinformatics*, 24(20):2395–2396, 2008.

Alex T Kalinka, Karolina M Varga, Dave T Gerrard, Stephan Preibisch, David L Corcoran, Julia Jarrells, Uwe Ohler, Casey M Bergman, and Pavel Tomancak. Gene expression divergence recapitulates the developmental hourglass model. *Nature*, 468(7325):811–814, 2010.

Guy Karlebach and Ron Shamir. Modelling and analysis of gene regulatory networks. *Nature reviews. Molecular cell biology*, 9(10):770–780, 2008.

a P Kenny, D Kozlowski, D W Oleksyn, L M Angerer, and R C Angerer. SpSoxB1, a maternally encoded transcription factor asymmetrically distributed among early sea urchin blastomeres. *Development (Cambridge, England)*, 126(23):5473–5483, 1999.

Christopher E. Killian and Fred H. Wilt. Molecular aspects of biomineralization of the Echinoderm endoskeleton. *Chemical Reviews*, 108(11):4463–4474, 2008.

R D Knight and S M Shimeld. Identification of conserved C2H2 zinc-finger gene families in the Bilateria. *Genome biology*, 2(5), 2001.

Hiroyuki Koga, Mioko Matsubara, Haruka Fujitani, Norio Miyamoto, Miéko Komatsu, Masato Kiyomoto, Koji Akasaka, and Hiroshi Wada. Functional evolution of Ets in echinoderms with focus on the evolution of echinoderm larval skeletons. *Development Genes and Evolution*, 220 (3-4):107–115, 2010.

Gabriel Krouk, Jesse Lingeman, Amy Marshall Colon, Gloria Coruzzi, and Dennis Shasha. Gene regulatory networks in plants: learning causality from time and perturbation. *Genome biology*, 14(6):123, 2013.

Clemens Kühn, Christoph Wierling, Alexander Kühn, Edda Klipp, Georgia Panopoulou, Hans Lehrach, and Albert J Poustka. Monte Carlo analysis of an ODE Model of the Sea Urchin Endomesoderm Network. *BMC systems biology*, 3:83, 2009.

Daisuke Kurokawa, Takashi Kitajima, Keiko Mitsunaga-Nakatsubo, Shonan Amemiya, Hiraku Shimada, and Koji Akasaka. HpEts, an ets-related transcription factor implicated in primary mesenchyme cell differentiation in the sea urchin embryo. *Mechanisms of Development*, 80(1): 41–52, 1999.

B Langmead, C Trapnell, M Pop, and S L Salzberg. Ultrafast and memory-efficient alignment of short DNA sequences to the human genome. *Genome Biol*, pages 1–10, 2009.

Ben Langmead. Aligning short sequencing reads with Bowtie. *Current Protocols in Bioinformatics*, 2010.

François Lapraz, Lydia Besnardeau, and Thierry Lepage. Patterning of the dorsal-ventral axis in echinoderms: Insights into the evolution of the BMP-chordin signaling network. *PLoS Biology*, 7 (11), 2009.

Nicolas Lartillot and Hervé Philippe. A Bayesian mixture model for across-site heterogeneities in the amino-acid replacement process. *Molecular Biology and Evolution*, 21(6):1095–1109, 2004.

Nicolas Lartillot and Hervé Philippe. Computing Bayes factors using thermodynamic integration. *Systematic biology*, 55:195–207, 2006.

Nicolas Lartillot, Henner Brinkmann, and Hervé Philippe. Suppression of long-branch attraction artefacts in the animal phylogeny using a site-heterogeneous model. *BMC evolutionary biology*, 7 Suppl 1:S4, 2007.

P Lemaire, N Garrett, and J B Gurdon. Expression cloning of Siamois, a Xenopus homeobox gene expressed in dorsal-vegetal cells of blastulae and able to induce a complete secondary axis. *Cell*, 81(1):85–94, 1995.

Michael Levine and Eric H Davidson. Gene regulatory networks for development. *Proceedings of the National Academy of Sciences of the United States of America*, 102:4936–4942, 2005.

B. Li, N. Fillmore, Y. Bai, M. Collins, J. a. Thomson, R. Stewart, and C. Dewey. Evaluation of de novo transcriptome assemblies from RNA-Seq data. *Genome Biology*, pages 1–21, 2014.

Bo Li and Colin N Dewey. RSEM: accurate transcript quantification from RNA-Seq data with or without a reference genome. *BMC bioinformatics*, 12:323, 2011.

Bo Li, Victor Ruotti, Ron M. Stewart, James a. Thomson, and Colin N. Dewey. RNA-Seq gene expression estimation with read mapping uncertainty. *Bioinformatics*, 26(4):493–500, 2009a.

Heng Li and Richard Durbin. Fast and accurate short read alignment with Burrows-Wheeler transform. *Bioinformatics*, 25(14):1754–1760, 2009.

Heng Li, Jue Ruan, and Richard Durbin. Mapping short DNA sequencing reads and calling variants using mapping quality scores. *Genome Research*, 18(11):1851–1858, 2008a.

Ruiqiang Li, Yingrui Li, Karsten Kristiansen, and Jun Wang. SOAP: Short oligonucleotide alignment program. *Bioinformatics*, 24(5):713–714, 2008b.

Ruiqiang Li, Chang Yu, Yingrui Li, Tak Wah Lam, Siu Ming Yiu, Karsten Kristiansen, and Jun Wang. SOAP2: An improved ultrafast tool for short read alignment. *Bioinformatics*, 25(15): 1966–1967, 2009b.

Shenghua Li, Paul Brazhnik, Bruno Sobral, and John J. Tyson. A quantitative study of the division cycle of Caulobacter crescentus stalked cells. *PLoS Computational Biology*, 4(1):0111–0129, 2008c.

Siming Li, Christopher M Armstrong, Nicolas Bertin, Hui Ge, Stuart Milstein, Mike Boxem, Pierre-Olivier Vidalain, Jing-Dong J Han, Alban Chesneau, Tong Hao, Debra S Goldberg, Ning Li, Monica Martinez, Jean-François Rual, Philippe Lamesch, Lai Xu, Muneesh Tewari, Sharyl L Wong, Lan V Zhang, Gabriel F Berriz, Laurent Jacotot, Philippe Vaglio, Jérôme Reboul, Tomoko Hirozane-Kishikawa, Qianru Li, Harrison W Gabel, Ahmed Elewa, Bridget Baumgartner, Debra J Rose, Haiyuan Yu, Stephanie Bosak, Reynaldo Sequerra, Andrew Fraser, Susan E Mango, William M Saxton, Susan Strome, Sander Van Den Heuvel, Fabio Piano, Jean Vandenhaute, Claude Sardet, Mark Gerstein, Lynn Doucette-Stamm, Kristin C Gunsalus, J Wade Harper, Michael E Cusick, Frederick P Roth, David E Hill, and Marc Vidal. A map of the interactome network of the metazoan C. elegans. *Science (New York, N.Y.)*, 303(5657):540–543, 2004.

X Li, C K Chuang, C a Mao, L M Angerer, and W H Klein. Two Otx proteins generated from multiple transcripts of a single gene in Strongylocentrotus purpuratus. *Developmental biology*, 187(2):253–266, 1997.

Samar Lightfoot. Quantitation comparison of total RNA using the Agilent 2100 bioanalyzer , ribogreen analysis and UV spectrometry Application. *Agilent Technologies*, 2002.

D. T. J. Littlewood, a. B. Smith, K. a. Clough, and R. H. Emson. The interrelationships of the echinoderm classes: morphological and molecular evidence. *Biological Journal of the Linnean Society*, 61(3):409–438, 1997.

Carolina B. Livi and Eric H. Davidson. Regulation of spblimp1/krox1a, an alternatively transcribed isoform expressed in midgut and hindgut of the sea urchin gastrula. *Gene Expression Patterns*, 7(1-2):1–7, 2007.

B. T. Livingston, C. E. Killian, F. Wilt, a. Cameron, M. J. Landrum, O. Ermolaeva, V. Sapojnikov, D. R. Maglott, a. M. Buchanan, and C. a. Ettensohn. A genome-wide analysis of biomineralization-related proteins in the sea urchin Strongylocentrotus purpuratus. *Developmental Biology*, 300:335–348, 2006.

C Y Logan and D R McClay. The allocation of early blastomeres to the ectoderm and endoderm is variable in the sea urchin embryo. *Development (Cambridge, England)*, 124(11):2213–2223, 1997.

C Y Logan, J R Miller, M J Ferkowicz, and D R McClay. Nuclear beta-catenin is required to specify vegetal cell fates in the sea urchin embryo. *Development (Cambridge, England)*, 126(2): 345–357, 1999.

W. J R Longabaugh, Eric H. Davidson, and Hamid Bolouri. Computational representation of developmental genetic regulatory networks. *Developmental Biology*, 283(1):1–16, 2005.

WilliamJ.R. Longabaugh. BioTapestry: A Tool to Visualize the Dynamic Properties of Gene Regulatory Networks. volume 786 of *Methods in Molecular Biology*, pages 359–394. Humana Press, 2012.

Lars Ove Loo, Per R. Jonsson, Mattias Sköld, and Örjan Karlsson. Passive suspension feeding in Amphiura filiformis (Echinodermata: Ophiuroidea): Feeding behaviour in flume flow and potential feeding rate of field populations. *Marine Ecology Progress Series*, 139(1-3):143–155, 1996.

Elijah K Lowe, Billie J Swalla, and C Titus Brown. Evaluating a lightweight transcriptome assembly pipeline on two closely related ascidian species. *PeerJ PrePrints*, 2:e505v1, 2014.

Gerton Lunter and Martin Goodson. Stampy: A statistical algorithm for sensitive and fast mapping of Illumina sequence reads. *Genome Research*, 21(6):936–939, 2011.

Vincent J Lynch, Robert D Leclerc, Gemma May, and Günter P Wagner. Transposon-mediated rewiring of gene regulatory networks contributed to the evolution of pregnancy in mammals. *Nature Genetics*, 43(11):1154–1159, 2011.

Deirdre C. Lyons, Stacy L. Kaltenbach, and David R. Mcclay. Morphogenesis in sea urchin embryos: Linking cellular events to gene regulatory network states. *Developmental Biology*, 1: 231–252, 2012.

Lesley T Macneil and Albertha J M Walhout. Gene regulatory networks and the role of robustness and stochasticity in the control of gene expression. *Genome research*, 21(5):645–57, May 2011.

Piyush B Madhamshettiwar, Stefan R Maetschke, Melissa J Davis, Antonio Reverter, and Mark a Ragan. Gene regulatory network inference: evaluation and application to ovarian cancer allows the prioritization of drug targets. *Genome Medicine*, 4(5):41, 2012.

Karlheinz Mann, Albert J Poustka, and Matthias Mann. Phosphoproteomes of Strongylocentrotus purpuratus shell and tooth matrix: identification of a major acidic sea urchin tooth phosphoprotein, phosphodontin. *Proteome Science*, 8:6, 2010a.

Karlheinz Mann, Fred H Wilt, and Albert J Poustka. Proteomic analysis of sea urchin (Strongylocentrotus purpuratus) spicule matrix. *Proteome science*, 8:33, 2010b.

Samuel Marguerat and Jürg Bähler. RNA-seq: From technology to biology. *Cellular and Molecular Life Sciences*, 67(4):569–579, 2010.

John C. Marioni, Christopher E. Mason, Shrikant M. Mane, Matthew Stephens, and Yoav Gilad. RNA-seq: An assessment of technical reproducibility and comparison with gene expression arrays. *Genome Research*, 18(9):1509–1517, 2008.

Jeffrey a Martin and Zhong Wang. Next-generation transcriptome assembly. *Nature reviews. Genetics*, 12(10):671–682, 2011.

Stefan C Materna and Paola Oliveri. A protocol for unraveling gene regulatory networks. *Nature protocols*, 3(12):1876–1887, 2008.

Stefan C. Materna, Meredith Howard-Ashby, Rachel F. Gray, and Eric H. Davidson. The C2H2 zinc finger genes of Strongylocentrotus purpuratus and their expression in embryonic development. *Developmental Biology*, 300:108–120, 2006.

Stefan C. Materna, Jongmin Nam, and Eric H. Davidson. High accuracy, high-resolution prevalence measurement for the majority of locally expressed regulatory genes in early sea urchin development. *Gene Expression Patterns*, 10(4-5):177–184, 2010.

Stefan C Materna, S Zachary Swartz, and Joel Smith. Notch and Nodal control forkhead factor expression in the specification of multipotent progenitors in sea urchin. *Development*, 140(8): 1796–1806, April 2013.

Arianne J Matlin, Francis Clark, and Christopher W J Smith. Understanding alternative splicing: towards a cellular code. *Nature reviews. Molecular cell biology*, 6(5):386–398, 2005.

B. S. McCauley, E. Akyar, H. R. Saad, and V. F. Hinman. Dose-dependent nuclear beta-catenin response segregates endomesoderm along the sea star primary axis. *Development*, 142:207–217, 2014.

Brenna S McCauley, Erin P Weideman, and Veronica F Hinman. A conserved gene regulatory network subcircuit drives different developmental fates in the vegetal pole of highly divergent echinoderm embryos. *Developmental biology*, 340(2):200–208, 2010.

Brenna S McCauley, Erin P Wright, Cameron Exner, Chisato Kitazawa, and Veronica F Hinman. Development of an embryonic skeletogenic mesenchyme lineage in a sea cucumber reveals the trajectory of change for the evolution of novel structures in echinoderms. *EvoDevo*, 3:17–27, 2012.

Alistair P. McGregor. How to get ahead: the origin, evolution and function of bicoid. *BioEssays*, 27(9):904–913, 2005.

Cory Y McLean, Philip L Reno, Alex A Pollen, Abraham I Bassan, Terence D Capellini, Catherine Guenther, Vahan B Indjeian, Xinhong Lim, Douglas B Menke, Bruce T Schaar, Aaron M Wenger, Gill Bejerano, and David M Kingsley. Human-specific loss of regulatory DNA and the evolution of human-specific traits. *Nature*, 471(7337):216–219, 2011.

R Milo, S Itzkovitz, N Kashtan, and D Chklovskii. Network Motifs : Simple Building Blocks of Complex Networks. *Science*, 298(October):11–14, 2002.

Keiko Minemura, Masaaki Yamaguchi, and Takuya Minokawa. Evolutionary modification of T-brain (tbr) expression patterns in sand dollar. *Gene Expression Patterns*, 9(7):468–474, 2009.

Takuya Minokawa, Jonathan P. Rast, Cesar Arenas-Mena, Christopher B. Franco, and Eric H. Davidson. Expression patterns of four different regulatory genes that function during sea urchin development. *Gene Expression Patterns*, 4:449–456, 2004.

Ryan D. Morin, Matthew Bainbridge, Anthony Fejes, Martin Hirst, Martin Krzywinski, Trevor J. Pugh, Helen McDonald, Richard Varhol, Steven J M Jones, and Marco A. Marra. Profiling the HeLa S3 transcriptome using randomly primed cDNA and massively parallel short-read sequencing. *BioTechniques*, 45(1):81–94, 2008.

Yoshiaki Morino, Hiroyuki Koga, Kazunori Tachibana, Eiichi Shoguchi, Masato Kiyomoto, and Hiroshi Wada. Heterochronic activation of VEGF signaling and the evolution of the skeleton in echinoderm pluteus larvae. *Evolution and Development*, 14:428–436, 2012.

O. F. Müller. *Zoologica Danicae Prodromus seu Animalium Daniae et Norvegiae indigenarum characters, nomine, et synonyma imprimis popularium.* 1776.

Ugrappa Nagalakshmi, Zhong Wang, Karl Waern, Chong Shou, Debasish Raha, Mark Gerstein, and Michael Snyder. The transcriptional landscape of the yeast genome defined by RNA sequencing. *Science (New York, N.Y.)*, 320(5881):1344–1349, 2008.

Hiroaki Nakano, Taku Hibino, Tatsuo Oji, Yuko Hara, and Shonan Amemiya. Larval stages of a living sea lily (stalked crinoid echinoderm). *Nature*, 421(6919):158–160, 2003.

Hiroaki Nakano, Yoko Nakajima, and Shonan Amemiya. Nervous system development of two crinoid species, the sea lily Metacrinus rotundus and the feather star Oxycomanthus japonicus. *Development Genes and Evolution*, 219(11-12):565–576, 2009.

Andrew C Nelson and Fiona C Wardle. Conserved non-coding elements and cis regulation: actions speak louder than words. *Development*, 140(7):1385–1395, 2013.

TimothyD D O'Hara, AndrewF F Hugall, Ben Thuy, and Adnan Moussalli. Phylogenomic resolution of the class ophiuroidea unlocks a global microfossil record. *Current Biology*, 24(16): 1874–9, August 2014.

P Oliveri, E Davidson, and David R McClay. Activation of pmar1 controls specification of micromeres in the sea urchin embryo. *Developmental Biology*, 258:32–43, 2003.

Paola Oliveri and Eric H. Davidson. Gene regulatory network controlling embryonic specification in the sea urchin. *Current Opinions Genetic Development*, 14(4):351–360, 2004.

Paola Oliveri, Deanna M Carrick, and Eric H Davidson. A regulatory gene network that directs micromere specification in the sea urchin embryo. *Developmental Biology*, 246:209–228, 2002.

Paola Oliveri, Katherine D Walton, Eric H Davidson, and David R McClay. Repression of mesodermal fate by foxa, a key endoderm regulator of the sea urchin embryo. *Development (Cambridge, England)*, 133(21):4173–4181, 2006.

Paola Oliveri, Qiang Tu, and Eric H Davidson. Global regulatory logic for specification of an embryonic cell lineage. *Proceedings of the National Academy of Sciences of the United States of America*, 105(16):5955–5962, April 2008.

Silvan Oulion, Stephanie Bertrand, and Hector Escriva. Evolution of the FGF Gene Family. *International journal of evolutionary biology*, 2012:298147, 2012.

Fatih Ozsolak and Patrice M Milos. NIH Public Access. *Nature Reviews Genetics*, 12(2):87–98, 2011.

Hugo J Parker, Paul Piccinelli, Tatjana Sauka-Spengler, Marianne Bronner, and Greg Elgar. Ancient Pbx-Hox signatures define hundreds of vertebrate developmental enhancers. *BMC Genomics*, 12:637, 2011.

Genis Parra, Keith Bradnam, and Ian Korf. CEGMA: A pipeline to accurately annotate core genes in eukaryotic genomes. *Bioinformatics*, 23:1061–1067, 2007.

Romualdo Pastor-Satorras, Eric Smith, and Ricard V. Solé. Evolving protein interaction networks through gene duplication. *Journal of Theoretical Biology*, 222(2):199–210, 2003.

C R C Paul and A B Smith. The early radiation and phylogeny of echinoderms. *Biological Reviews of the Cambridge Philosophical Society*, 59:443–481, 1984.

Helen Pearson. Genetics: what is a gene? *Nature*, 441(7092):398–401, 2006.

Héctor Peinado, Francisco Portillo, and Amparo Cano. Transcriptional regulation of cadherins during development and carcinogenesis. *Int J Dev Biol.*, 48(5-6):365–375, 2004.

Yu Peng, Henry C M Leung, Siu Ming Yiu, Ming Ju Lv, Xin Guang Zhu, and Francis Y L Chin. IDBA-tran: A more robust de novo de Bruijn graph assembler for transcriptomes with uneven expression levels. volume 29, pages 326–334, 2013.

E Pennisi. ENCODE Project Writes Eulogy for Junk DNA. *Science*, 337(6099):1159–1161, 2012.

Marleen Perseke, Detlef Bernhard, Guido Fritzsch, Franz Brümmer, Peter F. Stadler, and Martin Schlegel. Mitochondrial genome evolution in Ophiuroidea, Echinoidea, and Holothuroidea: Insights in phylogenetic relationships of Echinodermata. *Molecular Phylogenetics and Evolution*, 56(1):201–211, 2010.

Isabelle S. Peter and Eric H. Davidson. Modularity and design principles in the sea urchin embryo gene regulatory network. *FEBS Letters*, 583(24):3948–3958, 2009.

Isabelle S Peter and Eric H Davidson. A gene regulatory network controlling the embryonic specification of endoderm. *Nature*, 474(7353):635–639, 2011.

Isabelle S Peter, Emmanuel Faure, and Eric H Davidson. Predictive computation of genomic logic processing functions in embryonic development. *PNAS*, 109(41):16434–16442, 2012.

Kevin J. Peterson, César Arenas-Mena, and Eric H. Davidson. The A/P axis in echinoderm ontogeny and evolution: Evidence from fossils and molecules. *Evolution and Development*, 2(2): 93–101, 2000.

M W Pfaffl and M W Pfaffl. A new mathematical model for relative quantification in real-time RT-PCR. *Nucleic acids research*, 29(9):e45, 2001.

Michael W Pfaffl, Ales Tichopad, Christian Prgomet, and Tanja P Neuvians. Determination of stable housekeeping genes, differentially regulated target genes and sample integrity: BestKeeper Excel-based tool using pair-wise correlations. *Biotechnology Letters*, 26(6):509–515, 2004.

Davide Pisani, Roberto Feuda, Kevin J. Peterson, and Andrew B. Smith. Resolving phylogenetic signal from noise when divergence is rapid: A new look at the old problem of echinoderm class relationships. *Molecular Phylogenetics and Evolution*, 62(1):27–34, 2012.

Chris P Ponting, Christoffer Nellå ker, and Stephen Meader. Rapid turnover of functional sequence in human and other genomes. *Annual review of genomics and human genetics*, 12: 275–299, 2011.

Alexander E. Primus. Regional specification in the early embryo of the brittle star Ophiopholis aculeata. *Developmental Biology*, 283(2):294–309, 2005.

Benjamin Prud'homme, Nicolas Gompel, Antonis Rokas, Victoria A Kassner, Thomas M Williams, Shu-Dan Yeh, John R True, and Sean B Carroll. Repeated morphological evolution through cis-regulatory changes in a pleiotropic gene. *Nature*, 440(7087):1050–1053, 2006.

Sruthi Purushothaman, Sandeep Saxena, Vuppalapaty Meghah, Cherukuvada V Brahmendra, Olga Ortega-martinez, Sam Dupont, and Mohammed Idris. Transcriptomic and proteomic analyses of Amphiura filiformis arm tissue-undergoing regeneration. *Journal of Proteomics*, 112: 113–124, 2014.

K. Rafiq, M. S. Cheers, and C. A. Ettensohn. The genomic regulatory control of skeletal morphogenesis in the sea urchin. *Development*, 139(3):579–590, 2012.

Kiran Rafiq, Tanvi Shashikant, C. Joel McManus, and Charles A. Ettensohn. Genome-wide analysis of the skeletogenic gene regulatory network of sea urchins. *Development*, 141(4):950–961, 2014.

Arjun Raj and Alexander van Oudenaarden. Stochastic gene expression and its consequences. *Cell*, 135(6):216–226, 2008.

A Ransick. ScienceDirect.com - Methods in Cell Biology - Detection of mRNA by In Situ Hybridization and RT-PCR. *Methods in cell biology*, 2004.

Andrew Ransick and Eric H. Davidson. cis-regulatory processing of Notch signaling input to the sea urchin glial cells missing gene during mesoderm specification. *Developmental Biology*, 297 (2):587–602, 2006.

J P Rast, G Amore, C Calestani, C B Livi, A Ransick, and E H Davidson. Recovery of developmentally defined gene sets from high-density cDNA macroarrays. *Developmental biology*, 228 (2):270–286, December 2000.

Adrian Reich, Casey Dunn, Koji Akasaka, and Gary Wessel. Phylogenomic Analyses of Echinodermata Support the Sister Groups of Asterozoa and Echinozoa. *PLOS One*, pages 1–11, 2015.

Philip L. Reno, Cory Y. McLean, Jasmine E. Hines, Terence D. Capellini, Gill Bejerano, and David M. Kingsley. A penile spine/vibrissa enhancer sequence is missing in modern and extinct humans but is retained in multiple primates with penile spines and sensory vibrissae. *PLoS ONE*, 8, 2013.

Roger Revilla-i Domingo, Paola Oliveri, and Eric H Davidson. A missing link in the sea urchin embryo gene regulatory network: hesC and the double-negative specification of micromeres. *Proceedings of the National Academy of Sciences of the United States of America*, 104(30): 12383–12388, 2007.

Francesca Rizzo, Montserrat Fernandez-Serra, Paola Squarzoni, Aristea Archimandritis, and Maria I. Arnone. Identification and developmental expression of the ets gene family in the sea urchin (Strongylocentrotus purpuratus). *Developmental Biology*, 300(1):35–48, 2006.

Gordon Robertson, Jacqueline Schein, Readman Chiu, Richard Corbett, Matthew Field, Shaun D Jackman, Karen Mungall, Sam Lee, Hisanaga Mark Okada, Jenny Q Qian, Malachi Griffith, Anthony Raymond, Nina Thiessen, Timothee Cezard, Yaron S Butterfield, Richard Newsome, Simon K Chan, Rong She, Richard Varhol, Baljit Kamoh, Anna-Liisa Prabhu, Angela Tam, YongJun Zhao, Richard a Moore, Martin Hirst, Marco A Marra, Steven J M Jones, Pamela a Hoodless, and Inanc Birol. De novo assembly and analysis of RNA-seq data. *Nature methods*, 7(11):909–912, 2010.

Matthew Ronshaugen, Nadine McGinnis, and William McGinnis. Hox protein mutation and macroevolution of the insect body plan. *Nature*, 415(6874):914–917, 2002.

Eric Röttinger, Alexandra Saudemont, Véronique Duboc, Lydia Besnardeau, David McClay, and Thierry Lepage. FGF signals guide migration of mesenchymal cells, control skeletal morphogenesis [corrected] and regulate gastrulation during sea urchin development. *Development (Cambridge, England)*, 135(2):353–365, 2008.

José Luis Royo, Ignacio Maeso, Manuel Irimia, Feng Gao, Isabelle S Peter, Carla S Lopes, Salvatore D'Aniello, Fernando Casares, Eric H Davidson, Jordi Garcia-Fernández, and José Luis Gómez-Skarmeta. Transphyletic conservation of developmental regulatory state in animal evolution. *Proceedings of the National Academy of Sciences of the United States of America*, 108 (34):14186–14191, 2011.

S Rozen and H Skaletsky. Primer3 on the WWW for general users and for biologist programmers. *Methods in molecular biology (Clifton, N.J.)*, 132:365–386, 2000.

Lindsay R Saunders and David R McClay. Sub-circuits of a gene regulatory network control a developmental epithelial-mesenchymal transition. *Development (Cambridge, England)*, 141(7): 1503–13, 2014.

Johannes Schindelin, Ignacio Arganda-Carreras, Erwin Frise, Verena Kaynig, Mark Longair, Tobias Pietzsch, Stephan Preibisch, Curtis Rueden, Stephan Saalfeld, Benjamin Schmid, Jean-Yves Tinevez, Daniel James White, Volker Hartenstein, Kevin Eliceiri, Pavel Tomancak, and Albert Cardona. Fiji: an open-source platform for biological-image analysis. *Nature Methods*, 9 (7):676–682, 2012.

Dominic Schmidt, Michael D Wilson, Benoit Ballester, Petra C Schwalie, Gordon D Brown, Aileen Marshall, Claudia Kutter, Stephen Watt, Celia P Martinez-jimenez, Sarah Mackay, Iannis Talianidis, Paul Flicek, and Duncan T Odom. Five-Vertebrate ChIP-seq Reveals the Evolutionary Dynamics of Transcription Factor Binding. *Science*, 1036(May):1036–1041, 2010.

Marcel H. Schulz, Daniel R. Zerbino, Martin Vingron, and Ewan Birney. Oases: Robust de novo RNA-seq assembly across the dynamic range of expression levels. *Bioinformatics*, 28(8): 1086–1092, 2012.

Sea Urchin Genome Consortium. The Genome of the Sea Urchin. *Science*, 314(February): 941–952, 2006.

Ryan W Seaver and Brian T Livingston. Examination of the skeletal proteome of the brittle star Ophiocoma wendtii reveals overall conservation of proteins but variation in spicule matrix proteins. *Proteome Science*, 13(1):1–12, 2015.

Arun Seetharam and Gary W Stuart. A study on the distribution of 37 well conserved families of C2H2 zinc finger genes in eukaryotes. *BMC genomics*, 14(1):420, 2013.

Shai S Shen-Orr, Ron Milo, Shmoolik Mangan, and Uri Alon. Network motifs in the transcriptional regulation network of Escherichia coli. *Nature genetics*, 31(1):64–68, 2002.

Oleg Simakov, Ferdinand Marletaz, Sung-Jin Cho, Eric Edsinger-Gonzales, Paul Havlak, Uffe Hellsten, Dian-Han Kuo, Tomas Larsson, Jie Lv, Detlev Arendt, Robert Savage, Kazutoyo Osoegawa, Pieter de Jong, Jane Grimwood, Jarrod a Chapman, Harris Shapiro, Andrea Aerts, Robert P Otillar, Astrid Y Terry, Jeffrey L Boore, Igor V Grigoriev, David R Lindberg, Elaine C Seaver, David a Weisblat, Nicholas H Putnam, and Daniel S Rokhsar. Insights into bilaterian evolution from three spiralian genomes. *Nature*, 493(7433):526–31, 2013.

Harinder Singh, Aly a. Khan, and Aaron R. Dinner. Gene regulatory networks in the immune system. *Trends in Immunology*, 35(5):211–218, 2014.

Mattias Skold, Lars-ove Loo, and Rutger Rosenberg. Amphiura filiformis population 1 L. *Marine Ecology Progress Series*, 103:81–90, 1994.

Andrew B. Smith. Echinoderm Larvae and Phylogeny. *Annual Review of Ecology and Systematics*, 28(1):219–241, 1997.

Andrew B Smith, Samuel Zamora, and J Javier Alvaro. The oldest echinoderm faunas from Gondwana show that echinoderm body plan diversification was rapid. *Nature communications*, 4:1385, 2013.

Joel Smith and Eric H Davidson. Gene regulatory network subcircuit controlling a dynamic spatial pattern of signaling in the sea urchin embryo. *Proceedings of the National Academy of Sciences of the United States of America*, 105:20089–20094, 2008.

Joel Smith and Eric H Davidson. Regulative recovery in the sea urchin embryo and the stabilizing role of fail-safe gene network wiring. *Proceedings of the National Academy of Sciences of the United States of America*, 106(43):18291–18296, 2009.

Joel Smith, Christina Theodoris, and Eric H Davidson. A gene regulatory network subcircuit drives a dynamic pattern of gene expression. *Science*, 318(5851):794–797, 2007.

K Tagawa, a Nishino, T Humphreys, and N Satoh. The Spawning and Early Development of the Hawaiian Acorn Worm (Hemichordate), Ptychodera flava. *Zoological science*, 15(1):85–91, 1998.

Gerard Talavera and Jose Castresana. Improvement of phylogenies after removing divergent and ambiguously aligned blocks from protein sequence alignments. *Systematic biology*, 56(4): 564–577, August 2007.

Koichiro Tamura, Daniel Peterson, Nicholas Peterson, Glen Stecher, Masatoshi Nei, and Sudhir Kumar. MEGA5: Molecular evolutionary genetics analysis using maximum likelihood, evolutionary distance, and maximum parsimony methods. *Molecular Biology and Evolution*, 28(10): 2731–2739, 2011.

M. J. Telford, C. J. Lowe, C. B. Cameron, O. Ortega-Martinez, J. Aronowicz, P. Oliveri, and R. R. Copley. Phylogenomic analysis of echinoderm class relationships supports Asterozoa. *Proceedings of the Royal Society B: Biological Sciences*, 281:20140479–20140479, 2014.

Julie D Thompson, Toby J Gibson, and Des G Higgins. Multiple sequence alignment using ClustalW and ClustalX. *Current Protocols in Bioinformatics*, Chapter 2:Unit 2.3, 2002.

Claire J Tomlin and Jeffrey D Axelrod. Biology by numbers: mathematical modelling in developmental biology. *Nature reviews. Genetics*, 8(5):331–340, 2007.

Qiang Tu, R. Andrew Cameron, Kim C. Worley, Richard a. Gibbs, and Eric H. Davidson. Gene structure in the sea urchin Strongylocentrotus purpuratus based on transcriptome analysis. *Genome Research*, 22:2079–2087, 2012.

Qiang Tu, R. Andrew Cameron, and Eric H. Davidson. Quantitative developmental transcriptomes of the sea urchin Strongylocentrotus purpuratus. *Developmental Biology*, 385(2):160–167, 2014.

Erik van Nimwegen. Scaling laws in the functional content of genomes. *Trends in Genetics*, 19 (9):479–484, 2003.

Roy Vaughn, Nancy Garnhardt, James R Garey, W. Kelley Thomas, and Brian T Livingston. Sequencing and analysis of the gastrula transcriptome of the brittle star Ophiocoma wendtii. *EvoDevo*, 3(1):19, 2012.

Nagarjun Vijay, Jelmer W. Poelstra, Axel Künstner, and Jochen B W Wolf. Challenges and strategies in transcriptome assembly and differential gene expression quantification. A comprehensive in silico assessment of RNA-seq experiments. *Molecular Ecology*, 22(3):620–634, 2013.

Nedumparambathmarath Vijesh. Modeling of gene regulatory networks: A review. *Journal of Biomedical Science and Engineering*, 06(February):223–231, 2013.

Oliver Voigt, Marcin Adamski, Kasia Sluzek, and Maja Adamska. Calcareous sponge genomes reveal complex evolution of α-carbonic anhydrases and two key biomineralization enzymes. *BMC Evolutionary Biology*, 14:1–18, 2014.

K E von Bear. *Entwicklungsgeschichte der Thiere: Beobachtung und Reflexion.* Bornträger: Königsberg., 1828.

Günter P. Wagner and Vincent J. Lynch. The gene regulatory logic of transcription factor evolution. *Trends in Ecology and Evolution*, 23(7):377–385, 2008.

Mary E. Wahl, Julie Hahn, Kasia Gora, Eric H. Davidson, and Paola Oliveri. The cis-regulatory system of the tbrain gene: Alternative use of multiple modules to promote skeletogenic expression in the sea urchin embryo. *Developmental Biology*, 335(2):428–441, 2009.

Xi Wang, Zhengpeng Wu, and Xuegong Zhang. Isoform abundance inference provides a more accurate estimation of gene expression levels in RNA-seq. *Journal of bioinformatics and computational biology*, 8 Suppl 1:177–192, 2010.

Zhipeng Wang and Qin Zhang. Genome-wide identification and evolutionary analysis of the animal specific ETS transcription factor family. *Evolutionary bioinformatics online*, 5:119–131, 2008.

Zhong Wang, Mark Gerstein, and Michael Snyder. RNA-Seq: a revolutionary tool for transcriptomics. *Nature reviews. Genetics*, 10(1):57–63, 2009.

Athula H. Wikramanayake, Robert Peterson, Jing Chen, Ling Huang, Joanna M. Bince, David R. McClay, and William H. Klein. Nuclear β-catenin-dependent Wnt8 signaling in vegetal cells of the early sea urchin embryo regulates gastrulation and differentiation of endoderm and mesodermal cell lineages. *Genesis*, 39:194–205, 2004.

Brian T. Wilhelm and J. R. Landry. RNA-Seq-quantitative measurement of expression through massively parallel RNA-sequencing. *Methods*, 48(3):249–257, 2009.

Fred Wilt, Christopher E. Killian, Lindsay Croker, and Patricia Hamilton. SM30 protein function during sea urchin larval spicule formation. *Journal of Structural Biology*, 183(2):199–204, 2013.

Gregory A Wray. The evolutionary significance of cis-regulatory mutations. *Nature reviews. Genetics*, 8:206–216, 2007.

Shu-Yu Wu and David R McClay. The Snail repressor is required for PMC ingression in the sea urchin embryo. *Development (Cambridge, England)*, 134(6):1061–1070, 2007.

Shu Yu Wu, Yu Ping Yang, and David R. McClay. Twist is an essential regulator of the skeletogenic gene regulatory network in the sea urchin embryo. *Developmental Biology*, 319(2): 406–415, 2008.

S Wuchty, Z N Oltvai, and a L Barabási. Evolutionary conservation of motif constituents in the yeast protein interaction network. *Nature genetics*, 35(2):176–179, 2003.

Yinlong Xie, Gengxiong Wu, Jingbo Tang, Ruibang Luo, Jordan Patterson, Shanlin Liu, Weihua Huang, Guangzhu He, Shengchang Gu, Shengkang Li, Xin Zhou, Tak Wah Lam, Yingrui Li, Xun Xu, Gane Ka Shu Wong, and Jun Wang. SOAPdenovo-Trans: De novo transcriptome assembly with short RNA-Seq reads. *Bioinformatics*, 30(12):1660–1666, 2014.

Masakane Yamashita. Embryonic development of the brittle star Amphipholis kochii in laboratory culture. *Biol Bull*, 169(1):131–142, 1985.

Atsuko Yamazaki, Yumi Kidachi, Masaaki Yamaguchi, and Takuya Minokawa. Larval mesenchyme cell specification in the primitive echinoid occurs independently of the double-negative gate. *Development*, 141:2669–79, 2014.

Jing Yang, Sendurai A. Mani, Joana Liu Donaher, Sridhar Ramaswamy, Raphael A. Itzykson, Christophe Come, Pierre Savagner, Inna Gitelman, Andrea Richardson, and Robert A. Weinberg. Twist, a master regulator of morphogenesis, plays an essential role in tumor metastasis. *Cell*, 117(7):927–939, 2004.

Aleksey Zimin, Kristian a. Stevens, Marc W. Crepeau, Ann Holtz-Morris, Maxim Koriabine, Guillaume Marçais, Daniela Puiu, Michael Roberts, Jill L. Wegrzyn, Pieter J. de Jong, David B. Neale, Steven L. Salzberg, James a. Yorke, and Charles H. Langley. Sequencing and assembly of the 22-Gb loblolly pine genome. *Genetics*, 196(3):875–890, 2014.